Transport through inhomogeneous interacting low-dimensional systems

Dennis Hank Schimmel

München 2017

Transport through inhomogeneous interacting low-dimensional systems

Dennis Hank Schimmel

Doktorarbeit
an der Fakultät für Physik
der Ludwig–Maximilians–Universität
München

vorgelegt von
Dennis Hank Schimmel
aus Stuttgart

München, den 06.11.2017

Erstgutachter: Professor Jan von Delft
Zweitgutachter: Professor Stefan Hofmann
Tag der mündlichen Prüfung: 10.01.2018

Contents

List of Figures

Zusammenfassung in deutscher Sprache

Diese Arbeit zielt darauf ab, auftretende Phänomene beim Transport von Elektronen durch inhomogene Systeme in niedriegen Dimensionen in zwei unterschiedlichen Fällen zu erklären: (i) Transport durch eine kurze Verengung (QPC), und (ii) Transport durch einen Quantendraht, welcher mit magnetischen Störstellen ausgestattet ist.

Während Fall (i), mit welchem wir uns vornehmlich befassen wollen, durch unerwartete experimentelle Signaturen getrieben wird, ist Fall (ii) bisher lediglich theoretisch erforscht.

Transport durch einen QPC ist – wenn der Transport durch den Leitwert G (d.h. die Ableitung des Stroms j bezügliche einer angelegten Quellspannung V_{sd}, $G = \partial_{V_{\mathrm{sd}}} j$) beschrieben wird – quantisiert in Einheiten von $G_Q = 2e^2/h$. Diese Quantisierung ist theoretisch verstanden [Lan57] und auf die Quantisierung des Impulses senkrecht zur Transportrichtung zurückzuführen. Die erste Leitwertstufe allerdings zeigt im Experiment ein Verhalten, welches nicht mit einem nicht-wechselwirkenden Modell erklärt werden kann: Wird das Experiment bei einem endlichen Magnetfeld oder einer endlichen Temperatur ausgeführt, so entwickelt die erste Leitwertstufe eine Asymmetrie. Diese Asymmetrie ist eine starke Unterdrückung des Leitwerts im sub-offenen Bereich (bei einem Leitwert von ca. $0.7G_Q$), wohingegen der Ansatz der Stufe (der geschlossene QPC) nahezu unverändert ist.

Aufgrund der reichhaltigen experimentellen Beobachtungen (eindeutig wechselwirkende Effekte werden in z.B. der Entwicklung des Leitwerts bei Veränderung der Temperatur, des angelegten Magnetfeldes, oder der Quellspannung gemessen; außerdem sind derartige Effekte u.a. in der Messung des thermoelektrischen Effekts oder den Streuphasen sichtbar; [Mic11] gewährt einen guten Überblick) gibt es eine Vielzahl theoretischer Erklärungsversuche, welche oftmals inkompatibel erscheinen. Auf demjenigen minimalen Modell aufbauend, welches in [BHS+13] dargelegt wurde, zeigen wir durch das Studium *dynamischer* Größen, dass verschiedene, scheinbar inkompatible Erklärungen tatsächlich aus einem zugrundeliegenden, mikrosokopischen Modell hervorgehen und lediglich auf verschiedenen Interpretationen der gleichen Daten beruhen. Das Modell enthält lediglich die minimalen Zutaten, über die Einigkeit unter Forschern in diesem Feld besteht: Es ist ein-dimensional (in der ersten Leitwertstufe ist nur eine transversale Mode angeregt), wechselwirkend, und enthält eine glatte Inhomogenität, welche zu Impuls-ändernden Streuprozessen führt. Die Berechnung der dynamischen Größen ist essentiell für diese Erklärungen, da wir eine zuverlässige Extraktion von Zeitskalen benötigen. Wir zeigen Resultate bei endlicher Temperatur, endlicher Energie, und – in einem geringeren

Maß – auch bei endlicher Quellspannung.

In einer anders gelagerten Fragestellung untersuchen wir geschützten Transport in einem Quantendraht mit magnetischen Störstellen. Mit "geschütztem Transport" meinen wir, dass die Ladungsträger nur schwach an lokale nicht-magnetische Störstellen koppeln, und der Quantendraht daher eine hohe Leitfähigkeit besitzt. Der geschützte Transport wird dadurch erreicht, dass die Niederenergie-Freiheitsgrade in einem Quantendraht mit zufälligen magnetischen Störstellen, an welche die Elektronen des Drahts anisotropisch koppeln, aus helikalen Moden besteht, was eine Rückstreuung an nicht-magnetischen Störstellen stark unterdrückt. Die helikalen Moden entstehen aus dem spontanen Brechen einer $\mathbb{Z}_2$-Symmetrie. Hierbei erweitern wir vorangegangene Arbeiten [TY15], indem wir kurzreichweitige Elektron-Elektron Wechselwirkungen hinzufügen. Außerdem bestimmen wir den Ordnungsparameter der $\mathbb{Z}_2$-Symmetriebrechung.

Abstract

This thesis aims to highlight transport phenomena in low dimensions through an inhomogeneous system in two different cases: (i) Transport through a narrow, short constriction (a QPC), and (ii) transport along a quantum wire functionalized with magnetic impurities (or – equivalently – transport along a quantum wire with magnetic disorder).

While case (i) – which will be the main focus of this work – is driven by anomalous signatures in experiment, case (ii) is not yet experimentally realized and thus a purely theoretical prediction.

Transport through a QPC, when characterized through the conductance G (i.e. the derivative of the current j with respect to an applied bias voltage V_{sd}, $G = \partial_{V_{\mathrm{sd}}} j$), is quantized in units of $G_Q = 2e^2/h$. This quantization is well understood theoretically [Lan57] and is simply due to the quantization of momenta orthogonal to the direction of transport in a narrow constriction. However, at finite but small temperature or magnetic field the very first conductance step experimentally shows behavior impossible to explain in a simple non-interacting model: The first step is skewed in a manner which may best be viewed as a strong suppression of the conductance in the subopen regime, which is to say at a conductance of about $0.7G_Q$, while the closed regime shows almost no change at the corresponding temperature or magnetic field.

The rich experimental features (phenomena in contradiction with a simple, non-interacting model are seen in almost all observables, e.g. the evolution of the conductance at finite temperature, source-drain bias voltage, or magnetic field; the thermo-power; the scattering phases at finite bias voltage, ...; for a review see [Mic11]) have led to a variety of seemingly mutually exclusive theoretical explanations. Based on the model put forward in [BHS+13], we show how different theoretical explanations may be seen to emerge from a common model and simply constitute different ways of interpreting the same data. The ingredients of the model are only the minimal ingredients researchers in the field agree on: It is one-dimensional (as we consider the first conductance step, only one transverse mode is occupied), interacting, and contains a smooth inhomogeneity, leading to momentum-changing scattering processes. In an extension of the methods used in [BHS+13], we obtain data on the real frequency axis, allowing us to compare physical timescales. This is essential to merge different explanations. We show results at finite temperature, finite energy, and – to a lesser extent – finite bias.

In a completely orthogonal problem, recently there has been a lot of excitement about the prospect of protected transport. By "protected transport" we mean transport that only very weakly couples to potential disorder, leading to a low resistivity. One candidate system is a one-dimensional quantum wire with magnetic impurites. If the coupling between the electrons in

the wire and the magnetic impurities is anisotropic, in the easy-plane scenario the low-energy sector is described by helical modes (a helical mode links the orientation of the spin to the direction of motion), which follow from the spontaneous breaking of a $\mathbb{Z}_2$ symmetry. Due to their helical nature, backscattering of the low-energy modes by potential impurites is reduced, leading to transport with low losses. We extend early studies of this system [TY15], by taking into account short-ranged electron-electron interactions and determining the order parameter of the $\mathbb{Z}_2$-breaking.

Chapter 1

Preliminaries

1.1 Introduction

With the progression of miniaturization, new, high-quality materials and fabrication methods have become available to build mesoscopic systems. Mesoscopic systems are characterized by their length-scale: It is sufficiently short that quantum effects become relevant, even in the absence of macroscopic quantum phenomena (as for example superconductivity). The length scale is also sufficiently large that atomic scales are not yet relevant, meaning that the physics is usually captured quite well by an electron gas (possibly with impurities). The details of atoms rarely enter beyond the band-structure induced by them.

Due to the difficulty in measuring local thermodynamic observables in systems whose extent is on the scale of hundreds of nanometers, such mesoscopic systems are often characterized by their transport properties. Experimentally, a mesoscopic system is exposed to an applied bias voltage and the current through the system is measured. By now, many phenomena of transport have been thoroughly understood, e.g. the quantization of conductance through a one-dimensional system [Lan57], the Aharonov-Bohm effect [AB59], or the integer quantum Hall effect [Lau81]. Nonetheless, there are still transport phenomena, where no consensus has been reached thus far, e.g. the 0.7 anomaly in quantum point contacts (QPCs) (which we will be concerned with), or – on a much larger scale – the fractional quantum Hall effect (away from $1/n$ plateaus, which are understood through the Laughlin wave function [Lau83]).

While the general form of the conductance through a QPC precisely shows the predicted quantization (e.g. [TNA+98]), the first conductance step shows anomalous behavior ("anomalous" in this case meaning "in disagreement with a non-interacting model"). In contrast to naïve expectations and the behavior of the other conductance steps, the first step shows a clear asymmetric skewing as finite temperature or a finite magnetic field is applied. This skewing is most prominent in the subopen region, corresponding to a conductance of about $0.7G_Q = 0.7\frac{2e^2}{h}$ (hence the name "0.7 anomaly"). So far, no non-interacting model has been able to reproduce this skewing (and it seems very likely that there is no non-interacting model explaining this behavior).

It has become consensus that the skewing is related to interaction effects within the QPC. Numerous experiments have been performed, finding anomalous behavior in almost all ob-

servables (see [Mic11] for a review), amongst them the evolution of the conductance as a function of temperature, magnetic field, or bias voltage, and the structure of shot-noise, compressibility, and thermo-power.

Corresponding to the large amount of experimental data, there is host of theories. The most prominent theoretical models involve various conceptual ideas, ranging from spontaneous spin polarization [TNS+96, WB98], over the Kondo effect of an emerging localized state [CLGG+02, ILK+13] and the onset of Wigner crystallization [Mat04], to inelastic scattering [SMS08]. While most of these models convincingly explain certain features, they often lack the ability to explain all features and are rarely supplemented by reliable calculations of the conductance.

Since the models are convincing for certain phenomena, it is hard to reject the corresponding intuition out of hand. In this thesis, we adopt a simple one-dimensional model [SMS08, BHS+13], and study the dynamical properties at finite energy, using fRG on the Keldysh contour. From the dynamical properties we are able to extract the merits of different explanations and we are able to show how seemingly disjoint explanations emerge from the same model. Thus, we can identify the large grains of truth found in each explanation, hopefully leading to a unified understanding of the 0.7 anomaly.

Apart from mesoscopic systems, which constitute possible building blocks of future electronic devices, significant effort is put into finding and understanding materials exhibiting low resistivity. One ansatz is provided by topological materials, which exhibit edge modes with peculiar properties, for example helical edge modes [KM05].[1] However, helical low-energy modes can be achieved even in a purely one-dimensional system [BSL09, TY15]: the anisotropic Kondo-chain.[2] Here, the $\mathbb{Z}_2$ helical symmetry is spontaneously broken in the easy-plane case.

We analyze the role of electron-electron interactions and forward-scattering, and compute the order parameter of the spontaneous symmetry breaking.

1.2 Other preliminaries

1.2.1 Conventions

Unless explicitly specified otherwise, we use the following conventions:

Constants:

Reduced Planck Constant:	$\hbar = 1$	(1.1a)
Boltzmann constant:	$k_B = 1$	(1.1b)

[1] In a one-dimensional helical mode, the direction of motion is in one-to-one correspondence with the spin of the particle. For example, in one helical sector, all particles travelling to the right would have spin up, while all particles travelling to the left would have spin down.

[2] The anisotropic Kondo chain consists of one-dimensional electrons, coupled to a random distribution of localized spins. The coupling between the electrons and the spins is anisotropic and explicitely breaks the $SU(2)$ spin symmetry.

Lattice spacing: $a = 1$ (1.1c)

Sign: $\xi = \begin{cases} +1 \text{ (bosons)} \\ -1 \text{ (fermions)} \end{cases}$ (1.1d)

Sources:

generic: J (1.1e)

fermionic: $\eta, \bar{\eta}$ (1.1f)

Fields and operators:

generic: Φ (1.1g)

fermionic: $\psi, \overline{\psi}$ (1.1h)

generic operator: $\mathcal{O}, \mathcal{P}$ (1.1i)

density matrix: ρ (1.1j)

Functionals:

generating functional: $Z[J]$ (1.1k)

normalized generating functional: $W[J] = Z[J]/Z_0[0]$ (1.1l)

connected generating functional: $W^c[J] = \log(Z[J]/Z_0[0])$ (1.1m)

1PI generating functional: $\Gamma[\overline{\Phi}] = -W^c[J] - (J, \overline{\Phi}) + (\overline{\Phi}^\dagger, G_0^{-1}\overline{\Phi}), \overline{\Phi} = \partial_J W^c[J]$ (1.1n)

Green's functions

Green's functions: $G^{a|a'}_{i|i'}(t|t') = (-i)^n \left\langle \mathcal{T}_c a^{a_1}_{i_1}(t_1) \dots a^{a_n}_{i_n}(t_n) a^{\dagger a'_n}_{i'_n}(t'_n) \dots a^{\dagger a'_1}_{i'_1}(t'_1) \right\rangle$ (1.1o)

Keldysh Green's functions:

$$G^R(\omega) = G^{cq}(\omega) = \frac{1}{\omega - H_0 - \Sigma^R(\omega)},$$
$$G^A(\omega) = G^{qc}(\omega) = \left(G^R(\omega)\right)^\dagger,$$
$$G^K(\omega) = G^{cc}(\omega) = G^R(\omega)\Sigma^K(\omega)G^A(\omega) \quad (1.1p)$$

1-particle S-matrix: $\mathcal{S}(\omega) = \mathbb{1} - 2\pi i \nu(\omega) \begin{pmatrix} G^R_{LL}(\omega) & G^R_{LR}(\omega) \\ G^R_{RL}(\omega) & G^R_{RR}(\omega) \end{pmatrix}$ (1.1q)

LDOS: $\mathcal{A}_i(\omega) = -\frac{1}{\pi}\mathrm{Im}G^R_{ii}(\omega)$ (1.1r)

local distribution function: $n_i(\omega); G^K_{ii}(\omega) = (1 - 2n_i(\omega)) \left(G^R_{ii}(\omega) - G^A_{ii}(\omega)\right)$ (1.1s)

Keldysh:

Field on the forward branch: Φ^- (1.1t)

Field on the backward branch: Φ^+ (1.1u)

Quantum component: $\Phi^q = \frac{1}{\sqrt{2}}\left(\Phi^- - \Phi^+\right)$ (1.1v)

Classic component: $\Phi^c = \frac{1}{\sqrt{2}}\left(\Phi^- + \Phi^+\right)$ (1.1w)

fRG:

Single Scale propagator: $S = G\dot{G}_0^{-1}G$ (1.1x)

Keldysh Single scale propagator:

$$\begin{aligned} S^R(\omega) &= G_\Lambda^R \cdot \left(-\frac{i}{2} + \partial_\Lambda \Sigma^R_{\text{lead}}(\omega,\Lambda)\right) \cdot G_\Lambda^R \\ S^A(\omega) &= \left(S^R(\omega)\right)^\dagger \\ S^K(\omega) &= -G^R\left(\partial_\Lambda G_0^{K-1}\right)G^A - G^K\left(\partial_\Lambda G_0^{A-1}\right)G^A \\ &\quad - G^R\left(\partial_\Lambda G_0^{R-1}\right)G^K \end{aligned} \tag{1.1y}$$

Self-energy, physical lead: $\Sigma_{\text{lead}\,ij}(\Lambda,\omega)$ (1.1z)

Self-energy, artificial lead: $\Sigma_{\text{art.lead}\,ij}(\Lambda,\omega)$ (1.1aa)

Self-energy, from interactions: $\Sigma_{\text{U}\,ij}(\Lambda,\omega)$ (1.1ab)

Self-energy, total: $\Sigma_{ij}(\Lambda,\omega) = \Sigma_{\text{U}\,ij}(\Lambda,\omega) + \Sigma_{\text{lead}\,ij}(\Lambda,\omega) + \Sigma_{\text{art.lead}\,ij}(\Lambda,\omega)$ (1.1ac)

Vertex: $\gamma^2(\omega_1',\omega_2';\omega_1,\omega_2) =$ (1.1ad)

Channels:

$$\begin{aligned} \gamma^{2,\sigma\tau|\sigma\tau}_{i'j'|ij}(\omega_1',\omega_2';\omega_1,\omega_2) \approx\ & \bar{v}^{\sigma\bar{\sigma}|\sigma\bar{\sigma}}_{ij|ij}\delta_{i'i}\delta_{ij}\delta_{j'j}\delta^{\bar{\sigma}\tau} \\ & + \varphi^{P\,\sigma\bar{\sigma}|\sigma\bar{\sigma}}_{i'i'|ii}(\omega_1+\omega_2)\delta_{i'j'}\delta_{ij}\delta^{\bar{\sigma}\tau} \\ & + \varphi^{X\,\sigma\bar{\sigma}|\sigma\bar{\sigma}}_{i'i|ii'}(\omega_2-\omega_1')\delta_{i'j}\delta_{j'i}\delta^{\bar{\sigma}\tau} \\ & + \varphi^{D\,\sigma\sigma|\sigma\sigma}_{i'j|i'j}(\omega_2-\omega_2')\delta_{i'i}\delta_{j'j}\delta^{\sigma\tau}, \end{aligned} \tag{1.1ae}$$

Channels, Keldysh structure:

$$\gamma^{\alpha\beta|\gamma\delta} = \begin{pmatrix} (qq|qq) & (qq|cq) & (qq|qc) & (qq|cc) \\ (cq|qq) & (cq|cq) & (cq|qc) & (cq|cc) \\ (qc|qq) & (qc|cq) & (qc|qc) & (qc|cc) \\ (cc|qq) & (cc|cq) & (cc|qc) & (cc|cc) \end{pmatrix} \tag{1.1af}$$

$$(\varphi^P)^{\uparrow\downarrow|\uparrow\downarrow}_{ii|jj}(\Pi) = \begin{pmatrix} 0 & a^{P*}_{ji} & a^{P*}_{ji} & 0 \\ a^P_{ij} & b^P_{ij} & b^P_{ij} & a^P_{ij} \\ a^P_{ij} & b^P_{ij} & b^P_{ij} & a^P_{ij} \\ 0 & a^{P*}_{ji} & a^{P*}_{ji} & 0 \end{pmatrix}(\Pi) \tag{1.1ag}$$

$$(\varphi^X)^{\uparrow\downarrow|\uparrow\downarrow}_{ji|ij}(X) = \begin{pmatrix} 0 & a^{X*}_{ji} & a^X_{ij} & b^X_{ij} \\ a^X_{ij} & b^X_{ij} & 0 & a^{X*}_{ji} \\ a^{X*}_{ji} & 0 & b^X_{ij} & a^X_{ij} \\ b^X_{ij} & a^X_{ij} & a^{X*}_{ji} & 0 \end{pmatrix} (X) \tag{1.1ah}$$

$$(\varphi^D)^{\sigma\sigma|\sigma\sigma}_{ij|ij}(\Delta) = \begin{pmatrix} 0 & a^D_{ij} & a^{D*}_{ji} & b^D_{ij} \\ a^D_{ij} & 0 & b^D_{ij} & a^{D*}_{ii} \\ a^{D*}_{ji} & b^D_{ij} & 0 & a^D_{ij} \\ b^D_{ij} & a^{D*}_{ji} & a^D_{ij} & 0 \end{pmatrix}^{\sigma\sigma} (\Delta) \tag{1.1ai}$$

Frequencies:

$$\Pi = \omega_1 + \omega_2 \tag{1.1aj}$$

$$X = \omega_2 - \omega_1' \tag{1.1ak}$$

$$\Delta = \omega_2 - \omega_2' \tag{1.1al}$$

Observables:

Current: j (1.1am)

Conductance: $G = \partial_{V_{\mathrm{sd}}} j = g \cdot G_Q = g \cdot 2e^2/h$ (1.1an)

Functions:

Fermi function: $$n_F(\omega) = \frac{1}{1 + \exp\left(\frac{\omega - \mu}{T}\right)} \tag{1.1ao}$$

Parametrization:

Position(sites, central region): $i, j, \cdots = 1, 2, \ldots, N$ (1.1ap)

Position(sites, central region): left-most site$L = 1$; right-most site$R = N$ (1.1aq)

Position(continuum, central region): $x \in \{-l, l\}$ (1.1ar)

Model:

Hamiltonian (continuous):

$$H = \int dx \sum_\sigma V_\sigma(x) \psi^\dagger_\sigma(x) \left(-\partial_x^2\right) \psi_\sigma(x) + U(x) \psi^\dagger_\uparrow(x) \psi_\uparrow(x) \psi^\dagger_\downarrow(x) \psi_\downarrow(x) \tag{1.1as}$$

Hamiltonian (discrete):

$$H = \sum_{\sigma,i,j} \psi^\dagger_{\sigma,i} H_{0,\sigma,ij} \psi_{\sigma,j} + \sum_i U_i \psi^\dagger_{\uparrow,i} \psi_{\uparrow,i} \psi^\dagger_{\downarrow,i} \psi_{\downarrow,i} \tag{1.1at}$$

bare Hamiltonian (discrete): $H_{0,\sigma,ij} = \tau_j \delta_{ji+1} + \tau_j \delta_{i+1j}$ (1.1au)

bare hopping (discrete): $$\tau_j = \tau - \tfrac{1}{2}\tilde{V}_\mathrm{g} \exp\left(-\frac{x_j^2}{1-x_j^2}\right);\ x_j = 2\frac{j-1}{N-2} - 1 \tag{1.1av}$$

bare interaction (discrete): $$U_i = U_0 \exp\left(-\frac{l_i^6}{1-l_i^2}\right);\ l_i = 2\frac{j-1}{N-1} - 1 \tag{1.1aw}$$

We note that for a central region of N sites, there are $N-1$ hopping elements within the central region and N on-site terms. The bare hopping and interaction are to be read accordingly. As an additional remark, we may write expression of the form $(-1)^q$ etc. In these expressions, q is to be interpreted as 1 and c as 2.

Unless otherwise noted, we use the following numerical values:

System:

Total number of sites:	$N = \begin{cases} 41 \text{ (Non-equilibrium)} \\ 61 \text{ (Equilibrium)} \end{cases}$	(1.2a)
Hopping:	$\tau = 1$	(1.2b)
Interaction:	$U_0 = \begin{cases} 0.9 \text{ (Non-equilibrium)} \\ 0.7 \text{ (Equilibrium)} \end{cases}$	(1.2c)
Gate-voltage:	$V_\mathrm{g} = 2\tilde{V}_\mathrm{g} \approx 0.22$ to 0.29	(1.2d)
Temperature:	$T \lesssim 0.01$	(1.2e)
Chemical potential:	$\mu = -1.475$	(1.2f)
Source-drain bias voltage:	$V_\mathrm{sd} \lesssim 0.04$	(1.2g)

Implementation:

Number of frequencies (self-energy):	$N_f \approx 1500$	(1.2h)
Number of frequencies (P-channel):	$N_{bp} \approx 1500$	(1.2i)
Number of frequencies (X,D-channel):	$N_{bx} \approx 1500$	(1.2j)
Number of frequencies (precomputed):	$N_{f;\mathrm{pre}} \approx 30000$	(1.2k)
Accuracy:	$\mathrm{err} \approx 10^{-4}$	(1.2l)
Distance to singular points:	$\Delta \approx 10^{-12}$	(1.2m)
Initial flow parameter:	$\Lambda_0 \approx 10^6$	(1.2n)
Final flow parameter:	$\Lambda_\mathrm{end} \approx 10^{-9}$	(1.2o)

1.2.2 How to use this thesis

This thesis is *not* a complete introduction to anything. While the thesis contains most relevant information, a certain set of elementary considerations will be reviewed only superficially, and

some basics are completely missing. The reader is assumed to be familiar with the following concepts, which we will not explain at all:

1. Path-integrals in quantum mechanics and functional integrals in quantum field theories. In particular, familiarity with the derivation of the integrals via time-slicing is assumed. Familiarity with Grassmann numbers is considered part of familiarity with functional integrals.

2. Conventional perturbation theory and Feynman diagrams. This includes the ability to derive Feynman diagrams from the functional integral.

3. The renormalization group (particularly in the Wilsonian sense). The reader should feel comfortable with statements of the form: "During the RG-flow, high-energy degrees of freedom are integrated out. This means that we consider only sources coupling to low-energy degrees of freedom. The dynamics of the low-energy degrees of freedom are captured by the effective action $\mathcal{S} = \ldots$."

4. The Matsubara formalism for quantum field theories at finite temperature.

5. Electrons as quasi-particle excitations in a metal.

6. Spins and their representation through angles.

7. Bosonization and Luttinger liquids.

We *will* introduce the bare basics for

1. The Keldysh formalism. For a good introduction, we recommend [Kam11, Jak10].

2. The functional renormalization group (fRG). For a good introduction, we recommend [MSH+12, AEKM08].

3. The physics of a quantum point contact (QPC). For an in-depth review of the experimental data and alternative attempts at explanations, we recommend [Mic11].

Regarding the basics, it is useful to complement this thesis by the works cited above. While we do cover the basics, and explain some subtle issues, we do not treat all of them. Sometimes, derivations are cumbersome and not necessary for our purpose, but nonetheless important to fully grasp the concepts. In such cases, we will usually refer the reader to some other literature.

When reading the sections on the basics, we recommend to first skip all the subtleties to get a rough idea of what is happening and to decide if more information is required. Once a sufficient understanding of the basics has been reached, there are some useful subtleties explained in the corresponding sections.

1.3 Outline

In chapter 2, we introduce the basics of QPCs and the 0.7 anomaly. In particular, some interesting experimental features are collected in Sec. 2.3. In order to obtain information at finite energy, we use the Keldysh formalism, which is briefly introduced in chapter 3. Chapter 4 introduces the functional renormalization group and contains the explicit flow equations used in the thesis. Thus far, the quality of the non-equilibrium data is insufficient to accurately analyze the QPC. One reason lies in the fact that fRG violates Ward identities. In order to explain this statement, we have included a short recap of Ward identities in chapter 5. In the same chapter, we also explain the concept of a local distribution function in the context of QPCs. This local distribution function is important to improve the quality of the non-equilibrium flow. Chapter 6 is the major result of this thesis and explains how different explanations of the 0.7 anomaly are just different ways of looking at the same thing. We explain some further physics on the QPC in more detail in chapter 7 and give all relevant details on the actual implementation in chapter 8.

Chapter 9 deals with a completely different system: A one-dimensional chain of electrons coupled to magnetic impurities. This model shows – in a wide range of parameters – interesting transport properties: The low-energy degrees of freedom are two helical sectors, with vastly different velocities. We show that these results are robust against electron-electron interactions and explain details of the helical phase, e.g. the order parameter.

Finally, we conclude with chapter 10, where we give a short outlook on other interesting observables within the QPC that require checking.

The results of chapter 6, 7, 8, and 9 are original work unless otherwise noted. The content of all other sections are previously known facts, unless explicitly specified otherwise.

Chapter 2

Physics of a QPC

2.1 Basic Setup

A QPC is a special link between two baths. One possible experimental realization is based on a potential imprinted on a two-dimensional electron gas (2DEG) through external gates (essentially a field-effect transistor). The most commonly used realization uses a heterostructure to generate the 2DEG (e.g. GaAs/AlGaAs). In such a heterostructure, the motion of electrons is effectively confined to a single plane (which we will consider to be horizontal). Within this plane, the electrons may scatter off of impurities or with phonons. At sufficiently low temperatures, we may neglect the impact of phonons. If the structure we consider is smaller than the mean free path induced by the impurities, we may also approximate the electrons as free particles with infinite lifetime.

If the heterostructure is equipped with spatially inhomogeneous top gates, then the application of a finite voltage leads to electric field lines penetrating into the 2DEG. Fig. 2.1(a) shows one possible schematic representation. Let us assume that the top gates are constructed such that the field lines split the 2DEG into two parts (which we call "source" and "drain"), with a narrow path between them (Fig. 2.1(b,c,d)). Depending on the form of the path, we would then call the system either a quantum dot (if the potential between the 2DEGs allows for localized states), a quantum point contact (if the potential is a saddle point), or a quantum wire (if the path is long and flat) (Fig. 2.1(f)).

By tuning the barrier (i.e. changing the voltage applied on the top gate), we may modulate the current flowing between the source and drain upon applying a source-drain bias voltage. If the barrier is very high, only a small current will flow at a given source-drain bias. If the barrier is very shallow, a comparatively large current will flow at the same source-drain bias. Of course, if there is no bias voltage applied between source and drain, no current will flow between source and drain. It thus seems useful to introduce the conductance G, which is the derivative of the current between source and drain with respect to the source-drain bias voltage.

The two most common representations of this behavior are:

1. *The linear conductance* shows the conductance at zero source-drain bias voltage as function of top gate voltage.

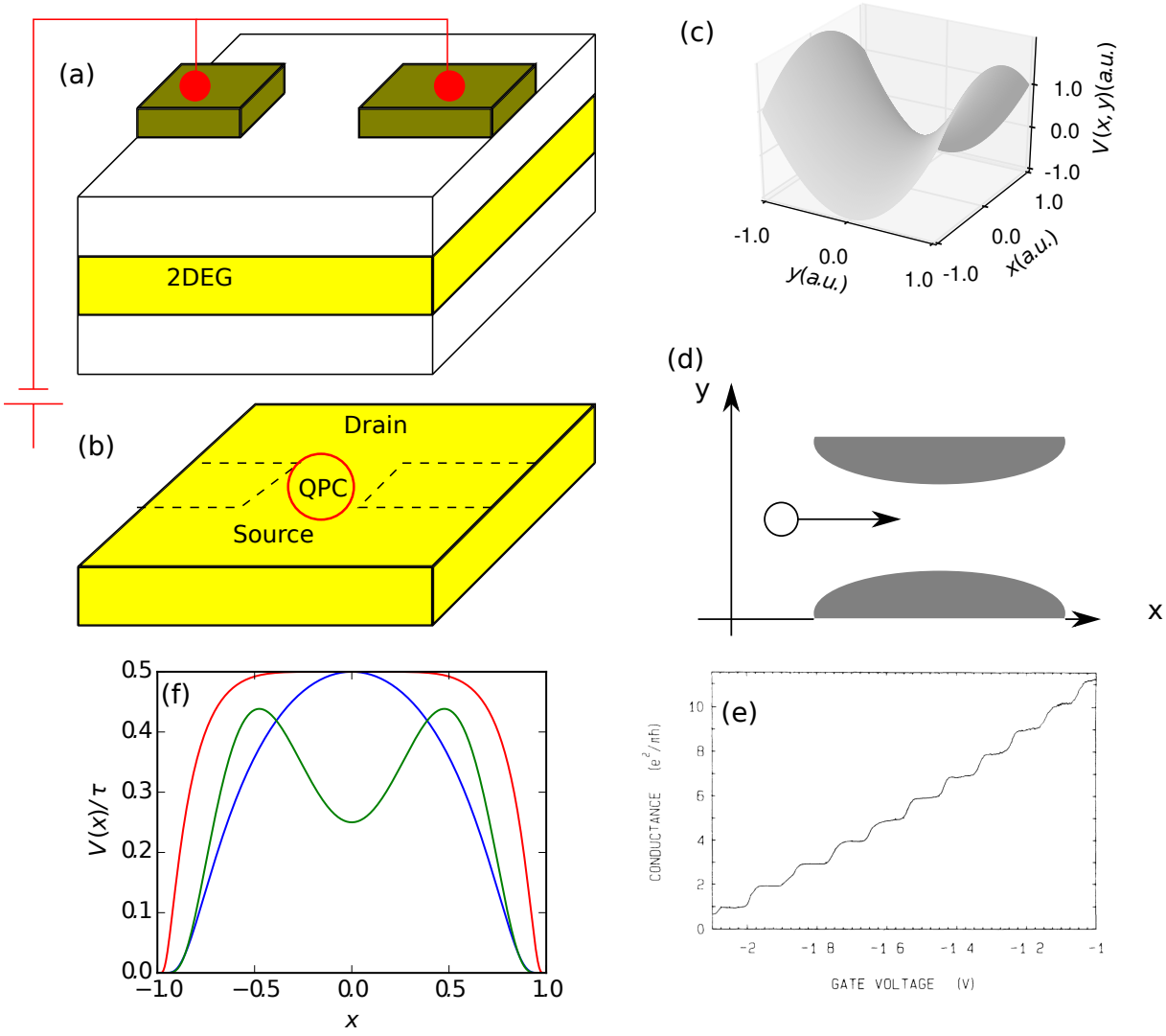

Figure 2.1: (a) Schematic representation of a QPC. The 2DEG (yellow) stems from one layer of the heterostructure (some of the other layers are shown in white). The green gates on top induce an effective potential in the 2DEG. (b) Contacts allow to inject/extract particles from the 2DEG (the regions where this happens are labeled by "source" and "drain"). The contacts are separated by the imprint of the central gate on the 2DEG (dashed). The imprint allows a confined region of transport between source and drain, labeled by "QPC". (c) The effective potential in the 2DEG belonging to a QPC. (d) In the 2DEG, electrons (white circle) traverse the potential (gray) in x-direction. The motion in y-direction is constrained throughout the constriction. (e) Experimental conductance as a function of gate voltage. Data is taken from [vWvHB+88]. The potential in y-direction leads to a quantization of modes. As the barrier is lowered (a lower barrier corresponds to a gate voltage of smaller modulus), more and more modes in y-direction can become occupied. Thus, at lower barriers, more channels contribute to transport, leading to a larger conductance. The conductance rises in steps of $2e^2/h$, each subsequent step corresponding to one additional mode in y-direction becoming available. (f) The effective one-dimensional potential of the lowest transmitting channel for a QPC (blue), a quantum dot (green), and a quantum wire (red).

2. *The differential conductance* shows the conductance as function of finite source-drain bias voltage at different (fixed) gate voltages.

Both the linear and differential conductance are then shown at different temperatures, magnetic fields, or orientation of the QPC relative to the crystal axes.

Typical scales of the experimental setup in GaAs we consider are: electron density $\sim 2 \cdot 10^{11}\mathrm{cm}^{-1}$; mean free path $\sim$ several microns; length of the QPC $\sim$ hundreds of nm; temperature $\sim$ K; central gate voltage $\sim$ hundreds of mV; source-drain bias voltage $\sim$ mV; magnetic field $\sim$ T.

2.2 Model and Experimental Data

Transport through the top-gate induced potential wall is constrained in y-direction, leading to a quantization of the corresponding momentum k_y (Fig. 2.1(c,d)). This quantization of k_y momentum leads to a quantization of the conductance (Fig. 2.1(e)). Essentially, the conductance (in units of e^2/h) counts the number of transmitting modes. This number increases by two each time an additional k_y momentum becomes occupied, due to the spin degeneracy of the 2DEG.

In this thesis, we want to focus on the behavior of the first conductance step, between $G = 0$ and $G = 2e^2/h$ (of which only the last part is shown in Fig. 2.1(e)).

All transmitting states within the first conductance step correspond to states within the space spanned by the lowest value of k_y. We may thus effectively eliminate the k_y quantum number (i.e. consider only states with the lowest value of k_y and take the effect of the other states into account via a renormalization of the parameters through virtual processes), yielding a one-dimensional model within the area of the constriction for the first step. Under the additional assumption that no relevant physics occurs in the large spaces of the 2DEG removed from the constriction, we may approximate these spaces as baths, whose only relevant property is the density of states close to the chemical potential. For the precise form of the leads' density of states we choose that of a one-dimensional tight-binding chain.[1] The model is spatially inhomogeneous, with the inhomogeneity representing the QPC. The electrons interact through Coulomb-repulsion, which we will assume to be short-ranged.[2] We will further assume that the temperature is sufficiently low such that we may neglect phonons.

[1] This choice is a matter of convenience, to avoid spurious non-adiabatic features in the effective model when the central region meets the baths.

[2] Let us examine this assumption somewhat more closely: We are interested in physics occurring at timescales much longer than $\frac{\text{length of the constriction}}{\text{speed of light}}$. We may thus neglect the photon's retardation and assume a static bare interaction of the form $\sim 1/r$, where r denotes the distance of the charge carriers. This $1/r$ potential is affected by two relevant effects: the top gates, which we may consider to be a metallic surface leading to a change of the electrostatic potential due to mirror-charges, and the screening of the Coulomb-interaction through a polarized "cloud" of electrons and holes. The strength of this screening depends on density, we expect the screening to be small if the density is low. During the conductance step, the electrons' density in the constriction is small. However, we will assume that the surrounding material can rearrange sufficiently to efficiently screen the Coulomb interaction. The extent to which this rearrangement actually does occur is by no means clear and a long-ranged interaction can have severe effects [WBvD17]. Here, we will assume short-range interactions and see how far we can get under this assumption.

2.2.1 Simple Intuition

An intuitive, single particle way to think about the conductance is in terms of *channels*. In our case, each channel corresponds to a different value of k_y. This way of thinking is at the heart of the Landauer-Büttiker equation for transport through a non-interacting system [Lan81, B̈88]:[3]

$$G = \frac{2e^2}{h} \sum_j \int d\omega \partial_\omega n_F(\omega) \mathcal{T}_j(\omega). \tag{2.1}$$

In Eq. (2.1), $\mathcal{T}_j$ denotes the *transmission probability through channel* j. Essentially, at a given energy ω, a particle in channel j contributes to the current $\sim \mathcal{T}_j$. The current is obtained by integrating over all occupied states (i.e. energies weighted with the Fermi function). The transmission probability can be read off from the single-particle $\mathcal{S}$-matrix connecting the two halves (left and right) of the system:

$$\mathcal{S}(\omega) = \mathbb{1} - 2\pi i \nu(\omega) \begin{pmatrix} G_{LL}(\omega) & G_{LR}(\omega) \\ G_{RL}(\omega) & G_{RR}(\omega) \end{pmatrix} = \begin{pmatrix} R_{LL}(\omega) & T_{LR}(\omega) \\ T_{RL}(\omega) & R_{RR}(\omega) \end{pmatrix}, \tag{2.2}$$

where $\nu(\omega)$ denotes the density of states at the lead site connected to the central region in the absence of the central region, and G is the (retarded) Green's function. The indices L and R denote the left- and right-most site of the central region. The variables T and R denote the transmission and reflection amplitude, respectively. The transmission probability is the modulus squared of the transmission amplitude. In equilibrium, the transmission from left to right is equal to the transmission from right to left, $|T_{RL}| = |T_{LR}|$. We will later on (Sec. 5.4) recast our expressions for the conductance in a form similar to Eq. (2.1).

At the first conductance step, only the lowest k_y states contribute to the transmission in a meaningful way. We thus consider a single channel. Clearly, the transmission probability should be bounded by zero and one. If we consider the simplest model of a smooth barrier at zero temperature, classically the transmission probability is a step function with the step occurring when the maximum of the barrier hits the chemical potential. Quantum-mechanically, this step is smeared out: At energies below the maximum of the barrier, we obtain a tunneling current, which decays as the exponential of the area enclosed by the potential above the considered energy. This tunneling current leads to a conductance greater than zero even for chemical potentials below the maximum of the barrier. At energies above the barrier, the wave nature of quantum-mechanics leads to a reduction of transmission as waves can be back-scattered by the potential. This is the reason for the finite width of the conductance steps in Fig. 2.1(e). At finite temperature, thermal broadening averages over different energies (in the non-interacting case this is the only effect of temperature). Physically, thermal broadening may be thought of as thermal activation (if the chemical potential is below the maximum of the barrier, finite temperature allows the occupation of states above the maximum, which transmit quite well), or thermal suppression (at energies above the maximum of the barrier, at finite temperature

[3] We emphasize that Eq. (2.1) is only valid for a non-interacting system. The generalization to an interacting system is given in [Ogu01, HBSvD17] for the linear conductance and in Sec. 5.4 for arbitrary bias. In general, a correction to Eq. (2.1) corresponding to the change of transmission within the bias window due to the changed occupation when the window is enlarged appears.

also states below the maximum of the barrier are relevant for transport. Since these states are mostly reflected, the total transmission is reduced).

2.2.2 Shape of the barrier

Before we proceed, a few short words on the choice of the barrier in the model are in order. We are interested in a barrier with no additional features, i.e. the non-interacting conductance should be fully described by the position and width of the step.

If we recall the conventional wisdom on resonances (e.g. [Tay12]), we expect additional features to appear in the transmission whenever the real part of a complex eigenvalue of the potential is close to the energy at which we probe the system. For the conductance to be featureless, we thus would like to consider a setup where the transmission peaks all lie at the same energy. It is straightforward to see that this is the case only for a quadratic barrier: We consider the Hamiltonian

$$H = -\frac{\partial_x^2}{2m} + \gamma|x|^\alpha, \alpha \in \mathbb{R}^+. \tag{2.3}$$

Here, γ is a positive number (times the correct units). The Hamiltonian Eq. (2.3) has a discrete spectrum. We obtain the resonances of a corresponding barrier by letting $\gamma \to -\gamma$. The spectrum of H is given by

$$\text{spectrum}(H) = f_\alpha^{(n)} \gamma^{2/(2+\alpha)} m^{-\alpha/(2+\alpha)}, \tag{2.4}$$

where $f_\alpha^{(n)}$ is a discrete set of real numbers labeled by n. For example, in the harmonic oscillator (where $\alpha = 2$), we have $f_2^{(n)} = n + \frac{1}{2}$. Eq. (2.4) is the only combination of γ and m that has the correct units of energy. If we now let $\gamma \to -\gamma$, we see that the resonances are determined by the points

$$f_\alpha^{(n)} \gamma^{2/(2+\alpha)} m^{-\alpha/(2+\alpha)} (-1)^{2/(2+\alpha)}. \tag{2.5}$$

Different eigenvalues will thus exhibit different real parts unless $\alpha = 2$. We thus expect to see additional structure in the transmission if $\alpha \neq 2$. Consequently, as we focus on QPC whose conductance steps do not exhibit resonance-like structures, it seems plausible to consider a model with an essentially quadratic potential.

We remark that the arguments just presented are easily circumvented by allowing for additional parameters. However, even if additional parameters are allowed, it turns out that significant fine-tuning is required to get rid of the resonances in the conductance. As a minimal model, which should be parametrized by as few parameters as possible, the quadratic barrier thus seems the best choice.[4] The model is thus given by

$$H = \sum_{\sigma=\uparrow,\downarrow} \int dx \psi_\sigma^\dagger \frac{-\partial_x^2}{2m} \psi_\sigma + V_\sigma(x) \psi_\sigma^\dagger \psi_\sigma + U(x) \psi_\uparrow^\dagger \psi_\uparrow \psi_\downarrow^\dagger \psi_\downarrow, \tag{2.6}$$

[4] While it is tempting to simply argue that we Taylor-expand the potential around its maximum and only keep the leading terms (yielding a quadratic barrier), it is by no means clear that the higher orders have to remain irrelevant on the scale set by the quadratic potential. Following the argument of the main text, if the higher orders enter, we will generically observe additional features in the conductance.

where $V_\sigma(x) = \tilde{V}(x) + \frac{1}{2}\mathrm{sgn}(\sigma)B$ is a function that is parabolic near the center of the QPC and contains the Zeemann-splitting (where we define $\mathrm{sgn}(\uparrow) = +1 = -\mathrm{sgn}(\downarrow)$, and denote the magnetic field by B). $U(x)$ is a phenomenological interaction, which is large in the center of the QPC and vanishes towards the leads. Physically, we would expect that the strength of U is determined predominantly by the spread of the density (in y-direction), which is large in the leads (leading to a small or vanishing U in the leads; in order to avoid Luttinger-liquid effects in the leads, which physically correspond to two-dimensional systems not exhibiting any of the peculiarities of one dimension, we pick the leads to be completely non-interacting). We will see later on (Sec. 8.2) how to best deal with this Hamiltonian on a computer.

2.3 Basic Phenomenology

Let us compare the naïve (non-interacting) intuition with experiment. To do so, we compare the conductance as we vary the magnetic field B, the temperature T, or the bias V_{sd}. The first conductance step shows anomalous behavior if either of these quantities is varied.[5]

Fig. 2.2 shows how the conductance as function of gate voltage changes as the magnetic field is varied. In the non-interacting model (Fig. 2.2(c)), a symmetric splitting of the conductance step occurs. This symmetric splitting is in clear contradiction with all experimental data (Fig. 2.2(a,b,d,e)), which exhibits a comparatively strong suppression of the conductance in the subopen regime, leading to significant skewing of the conductance step. The interacting model reproduces this behavior (Fig. 2.2(f)).

Fig. 2.3 shows how the conductance as function of gate voltage changes as the temperature is varied. In the non-interacting model (Fig. 2.3(f)), a symmetric flattening of the conductance step occurs. This symmetric flattening is in clear contradiction with all experimental data (Fig. 2.3(a-e)), which exhibits a comparatively strong suppression of the conductance in the subopen regime, leading to significant skewing of the conductance step. The interacting model qualitatively reproduces this behavior (Fig. 2.3(g)).

Fig. 2.4 shows how the conductance as function of source-drain bias voltage changes as the gate voltage is varied. In the non-interacting model (Fig. 2.4(h)), the conductance approaches $g = 0.5$ at large bias and the curvature at small bias is positive for conductances $g < 0.5$ and negative for conductances $g > 0.5$. This behavior at $g < 0.5$ is in clear contradiction with all experimental data (Fig. 2.4(a-g)), which exhibits a clear zero-bias peak, even down to $g \approx 10^{-3}$ (Fig. 2.4(f)). In Sec. 8.3, Fig. 8.2, we show the current status of the fRG results for the interacting model. So far, our fRG code is able to qualitatively show the presence of a zero-bias peak at conductances $g \approx 0.4$, but we cannot extract sufficiently reliable information about the curvature at small conductances ($g < 0.3$). Our fRG results also give no indication of the side-peaks clearly visible at bias voltages of about $0.5mV$.

While more advanced experiments exist, attempting to measure e.g. the transmission phase through scanning tip microscopy [BMF+16], these results are more difficult to interpret, as the scanning tip (and the disorder in the bulk) have significant impact on the results of a single QPC.

[5] In this context, "anomalous behavior" should be understood as "behavior disagreeing with a non-interacting model".

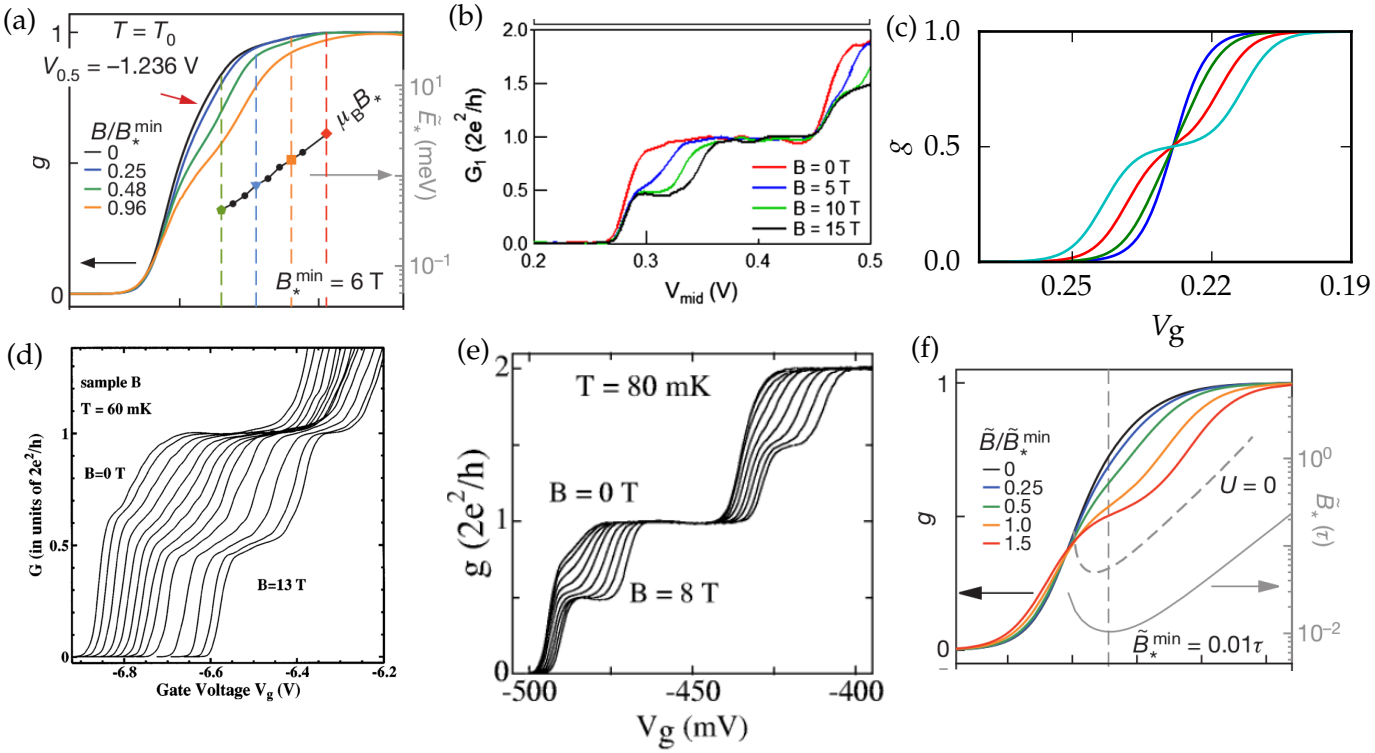

Figure 2.2: Conductance as function of gate voltage as the magnetic field is tuned. (a,b,d,e) Experimental data, reproduced from (a) [BHS+13], (b) [SHT+11], (d) [CLGG+02], (e) [TNS+96]; (c,f) theoretical predictions: (c) non-interacting and (f) interacting model [BHS+13]. The precise form of the conductance shoulder and its evolution with magnetic field vary from one experiment to the next. All experiments show the common generic feature, that the conductance decreases significantly with the increasing magnetic field in the subopen regime. This feature is well captured by the fRG results in (g).

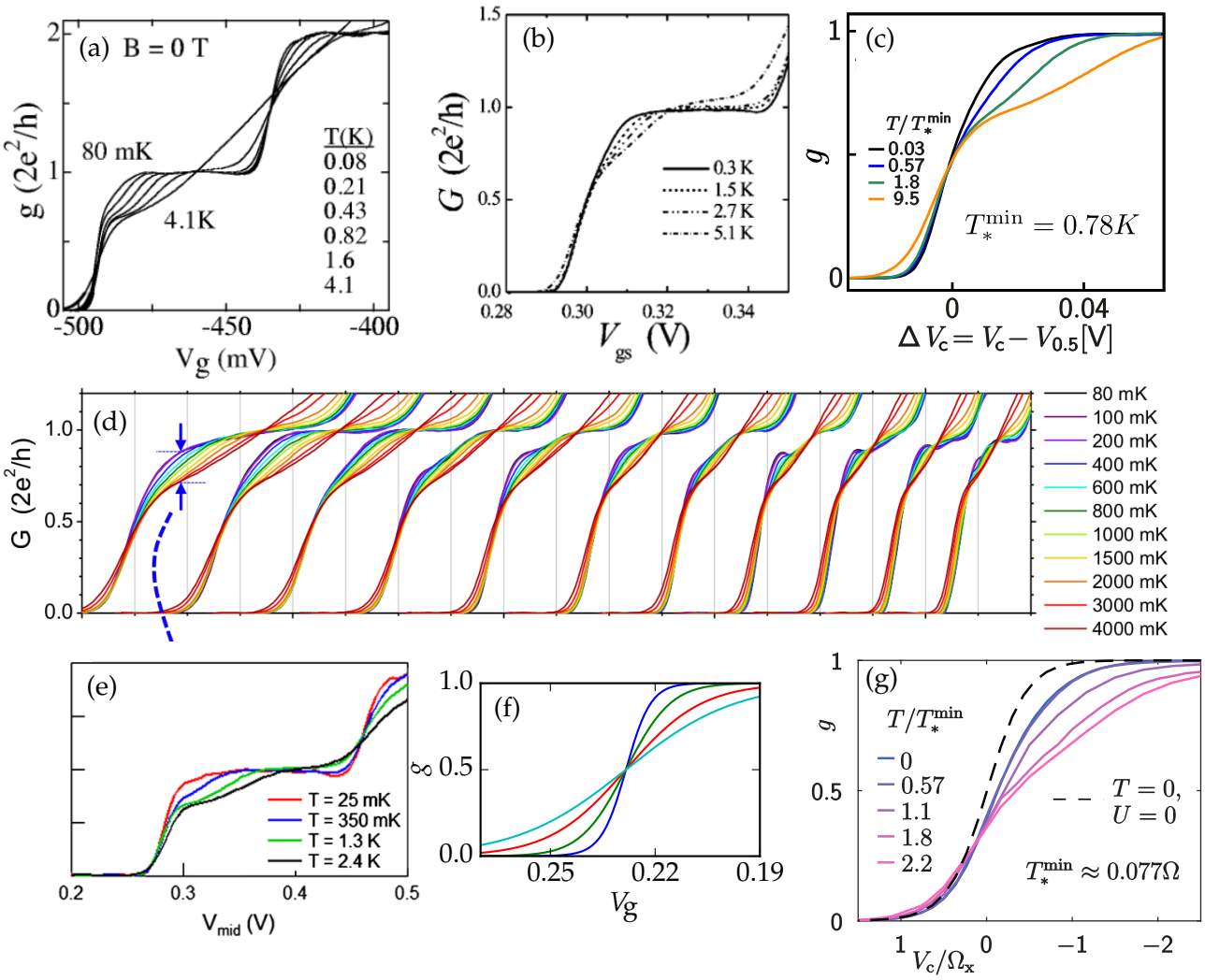

Figure 2.3: Conductance as function of gate voltage as the temperature is tuned. (a)-(e) Experimental data, reproduced from (a) [CLGG+02], (b) [KBH+00], (c) [BHS+13], (d) [ILK+13] (e) [SHT+11]; (f,g) theoretical predictions: (f) non-interacting model, and (g) interacting model[SBv17]. The precise form of the conductance shoulder and its evolution with temperature vary from one experiment to the next. All experiments show the common generic feature, that the conductance decreases significantly with the increasing temperature in the subopen regime. This feature is well captured by our fRG results in (g) (the black dashed line in (g) corresponds to the non-interacting conductance at zero temperature and is plotted for reference). In (d), the different curves show QPCs of increasing lengths, from a short QPC on the left to a short quantum wire on the right. Our model is used for short QPCs, corresponding to the curves on the left of (d). In (e), $T = 350$ mK, 1.3 K, and 2.4 K data are shifted horizontally by 2.5, 5, and -3.5 mV, respectively, to align with 25 mK data.

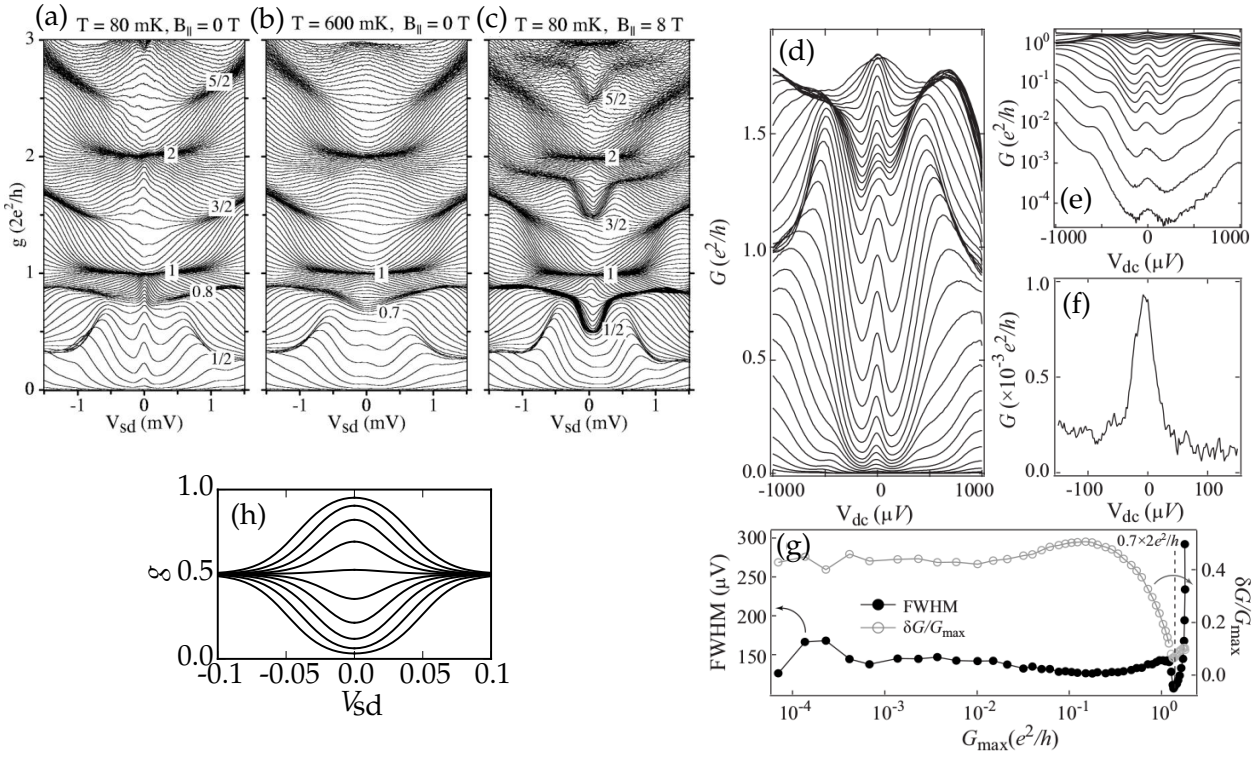

Figure 2.4: Conductance as function of bias voltage as the gate voltage is tuned. (a)-(g) Experimental data, reproduced from (a-c) [CLGG+02], (d-g) [RYF+10]; (h) theoretical expectations from the non-interacting model. (a-c) Conductance as function of source-drain bias voltage. Different lines correspond to different gate voltage. In (a) a clear zero-bias peak is visible. (b,c) show how this peak vanishes as (b) temperature or (c) magnetic field is increased. (d) Conductance as function of source-drain bias voltage. The zero-bias peak is clearly visible. (e) Conductance as function of source-drain bias voltage in the low-conductance regime. The zero-bias peak persists to very small values of the conductance, even down to $g \approx 10^{-3}$ (f). (g) The evolution of the relative height of the peak (grey) and width of the peak (black) as a function of the conductance at zero bias. Each dot corresponds to a different gate voltage; $G_{\max}$ is the conductance at zero bias, while δG denotes the difference in height between the conductance-peak at zero bias and the bottom of the valley. (h) The non-interacting model clearly does not exhibit a zero-bias peak (the curvature of the conductance at $g < .5$ is positive, in contrast to experiment).

In this thesis, we will show the behaviour of the conductance at finite temperature and show the first steps towards a reliable calculation of the differential conductance at finite bias.

Chapter 3

Keldysh

Throughout this work, we will use the (Schwinger-)Keldysh formalism [Kam11, Kel64], which is able to treat arbitrary out-of-equilibrium situations. For the explanations in the following, we will use the Heisenberg picture, i.e. the operators are time-dependent, while the states are not.

3.1 Basic idea

In general, we are interested in correlation functions of the following form:

$$\langle \mathcal{O}(t_1, t_2, \ldots, t_n) \rangle = \mathrm{Tr}\left[\mathcal{O}(t_1, t_2, \ldots, t_n)\rho\right], \tag{3.1}$$

where ρ is some initial density matrix, and $\mathcal{O}$ is some operator expressed in terms of creation and annihilation operators acting at the times $\{t_i\}$. In the following, we will focus on correlation functions satisfying an internal ordering of the form

$$\mathcal{O}(t_1, t_2, \ldots, t_n) = \mathcal{O}_{\tilde{T}}(\{t_i\})\mathcal{O}_T(\{t_i\}), \tag{3.2}$$

where $\mathcal{O}_T$ ($\mathcal{O}_{\tilde{T}}$) is some internally (anti-)time-ordered operator, i.e. the earlier in time the action of a creation or annihilation operator occurs, the further to the right (left) this operator stands. Note that the definition of $\mathcal{O}_T$ is not necessarily unique.

For example, assuming $t_1 > t_2 > t_3 > t_4$, the operator

$$\mathcal{O}_1(t_1, t_2, t_3, t_4) = a^\dagger(t_1)a(t_3)a^\dagger(t_2)a(t_4) \tag{3.3}$$

is not of the form Eq. (3.2), while the operator

$$\mathcal{O}_2(t_1, t_2, t_3, t_4) = a^\dagger(t_3)a(t_1)a^\dagger(t_2)a(t_4) \tag{3.4}$$

is, with $\mathcal{O}_{2T} = a(t_1)a^\dagger(t_2)a(t_4)$ and $\mathcal{O}_{2\tilde{T}} = a^\dagger(t_3)$, or $\mathcal{O}_{2T} = a^\dagger(t_2)a(t_4)$ and $\mathcal{O}_{2\tilde{T}} = a^\dagger(t_3)a(t_1)$. The reason for the restriction Eq. (3.2) lies in the way we will construct the Keldysh contour.

As a first step, we consider time-ordered correlation functions of the form (assuming for simplicity that $t_1 > t_2 > \cdots > t_n$)

$$\begin{aligned}\langle \mathcal{T}\mathcal{O}(t_1, t_2, \ldots, t_n)\rangle &= \xi^\sigma \mathrm{Tr}\left[\mathcal{O}_1(t_1)\mathcal{O}_2(t_2)\ldots\mathcal{O}_n(t_n)\rho\right] \\ &= \xi^\sigma \mathrm{Tr}\left[U_{-\infty,t_1}\mathcal{O}_1 U_{t_1,t_2}\mathcal{O}_2 U_{t_2,t_3}\ldots U_{t_{n-1},t_n}\mathcal{O}_n U_{t_n,-\infty}\rho\right], \end{aligned} \tag{3.5}$$

where we introduced $\mathcal{T}$ to denote time-ordering and split up the operator $\mathcal{O}$ into operators at various times before making the time-dependence explicit by writing the time-evolution operator U. ξ^σ denotes the sign obtained from re-ordering the operator $\mathcal{O}$ into the form $\mathcal{O}_1 \ldots \mathcal{O}_n$. We have assumed that the initial state, determined by the density matrix ρ, is prepared at $t = -\infty$. If ρ corresponds to a thermal distribution of the non-interacting system, we may write

$$\rho = \exp\left(-\beta H_{\mathrm{eff}}\right), \tag{3.6}$$

where $\beta = 1/T$ is the inverse temperature, and H_{eff} depends on the ensemble we consider (for the canonical ensemble, $H_{\mathrm{eff}} = H_0$; for the grand-canonical ensemble, $H_{\mathrm{eff}} = H_0 + \mu N$, where N is the particle number). We will now assume that interactions are switched on adiabatically at some time $t_{\mathrm{int}} \ll t_n$, and that otherwise the Hamiltonian is time-dependent only for times much later than t_{int}. We may then formally write

$$\rho = U^{\mathrm{eff}}_{-\infty-i\beta,-\infty}, \tag{3.7}$$

where U^{eff} is the time-evolution using the Hamiltonian H_{eff}. Eq. (3.5) thus becomes

$$\begin{aligned}\langle \mathcal{T}\mathcal{O}(t_1, t_2, \ldots, t_n)\rangle &= \xi^\sigma \mathrm{Tr}\left[U_{-\infty,t_1}\mathcal{O}_1 U_{t_1,t_2}\mathcal{O}_2(t_2)\ldots\mathcal{O}_n(t_n)U_{t_n,-\infty}U^{\mathrm{eff}}_{-\infty-i\beta,-\infty}\right] \\ &= \xi^\sigma \mathrm{Tr}\left[U^{\mathrm{eff}}_{-\infty-i\beta,-\infty}U_{-\infty,t_1}\mathcal{O}_1 U_{t_1,t_2}\mathcal{O}_2 U_{t_2,t_3}\ldots U_{t_{n-1},t_n}\mathcal{O}_n U_{t_n,-\infty}\right], \end{aligned} \tag{3.8}$$

where we have used cyclicity of the trace.

A way to represent Eq. (3.8) is shown in Fig. 3.1: Starting out at $t = -\infty$, we evolve up to time t_n, where we insert the operator $\mathcal{O}_n$. From there, we evolve to time t_{n-1}, where we insert the operator $\mathcal{O}_{n-1}$, and so on until we insert the operator $\mathcal{O}_1$ at time t_1. From there, we evolve back to $t = -\infty$, and then move in the complex time plane to $t = -\infty - i\beta$. To represent the trace, we require a closed contour: the contour used here is closed because we may identify the time $t = t_0$ with the time $t = t_0 - i\beta$, due to the (anti-)periodicity of correlation functions in equilibrium [NO88].

Schematically, we have replaced the expression Eq. (3.5) by the expectation value of some operators while performing time-evolution along a somewhat complicated contour $\mathcal{C}$ in the complex time plane. A close look at the contour reveals that we can represent any ordering in Eq. (3.2) by this contour, by placing the operators either on $\mathcal{C}_-$ or $\mathcal{C}_+$. The fact that we intend to use this type of contour is the reason for the restriction Eq. (3.2). On the contour, we may define a generating functional of the form

$$Z[J] = \int \mathcal{D}\Phi \exp\left(iS_{\mathcal{C}}[\Phi] + i\int_{\mathcal{C}} J\Phi\right), \tag{3.9}$$

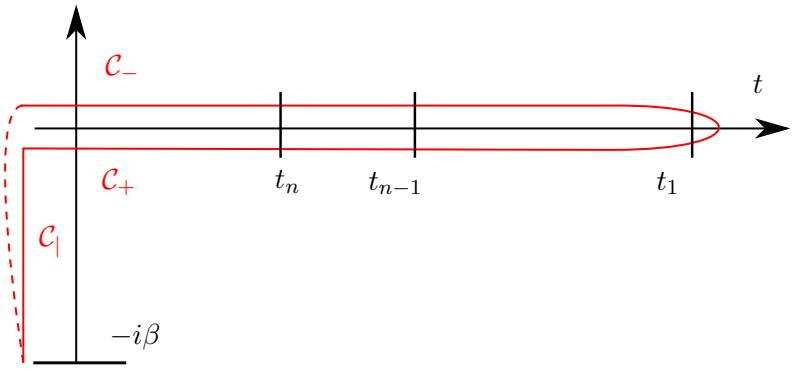

Figure 3.1: The Keldysh-contour (solid red line) in equilibrium in the complex time (t) plane. The dashed line represents the (anti-)periodicity of the generating functional under $t \to t - i\beta$ for bosons (fermions), allowing us to identify the points t and $t - i\beta$. Usually, the contour is traversed as follows: start at the upper left point, follow $\mathcal{C}_-$, go down to $\mathcal{C}_+$ and follow it to the left, before going down along $\mathcal{C}_|$. However, cyclicity of the trace implies that we may also traverse the contour by starting at any arbitrary point (Note however that starting at a different point is not necessarily useful: If we start at a different point, the initial state, whose density matrix corresponds to the part $\mathcal{C}_|$ of the contour is inserted somewhere in the middle of the operators we consider). Operators are inserted at times t_i.

where $S_\mathcal{C}$ is the action evaluated along the contour $\mathcal{C}$.

In the usual Keldysh formalism, we are not interested in placing additional operators on the part of the contour parallel to the imaginary axis, which determines the initial state.[1] On the level of a generating functional, in this case it is sufficient to introduce sources on the lines parallel to the real axis (i.e. on $\mathcal{C}_-$ and $\mathcal{C}_+$). We parametrize points on $\mathcal{C}_-$ and $\mathcal{C}_+$ by a real time t and an additional contour-index j via (s is a general parametrization of $\mathcal{C}_- + \mathcal{C}_+$, s_- (s_+) is some parametrization of $\mathcal{C}_-$ ($\mathcal{C}_+$) [we impose that the parametrizations are the same in the sense that both branches are traversed with the same velocity]; we absorb any nontrivial measure in the ds):

$$\begin{aligned}\int_{\mathcal{C}_-+\mathcal{C}_+} ds\tilde{f}(s) &= \int_{\mathcal{C}_-} ds_-\tilde{f}(s_-) + \int_{\mathcal{C}_+} ds_+\tilde{f}(s_+) \\ &= \int_{-\infty}^{\infty} dt f(t) + \int_{\infty}^{-\infty} dt f(t), \quad f(t) = \tilde{f}(s(t)) \\ &= \int_{-\infty}^{\infty} dt f(t) - \int_{-\infty}^{\infty} dt f(t) \\ &= -\sum_{j=\pm}\int_{-\infty}^{\infty} dt j f^j(t),\end{aligned} \tag{3.10}$$

where we have defined $f^\pm(t) = f(t)$. To exemplify matters, consider the one-particle Green's

[1] Note that in the Matsubara formalism, we consider operators *only* on the contour parallel to the imaginary axis.

function parametrized by the contour-indices j_i and the times t_i (for now, we omit other labels)

$$G^{j_1 j_2}(t_1, t_2) = -i\langle \mathcal{T}_\mathcal{C} a^{j_1}(t_1) a^{\dagger j_2}(t_2)\rangle, \tag{3.11}$$

where we have introduced contour-ordering $\mathcal{T}_\mathcal{C}$. Under $\mathcal{T}_\mathcal{C}$ operators are ordered according to the sequence in which they are encountered when traversing the contour $\mathcal{C}_- + \mathcal{C}_+ + \mathcal{C}_|$. Explicitly,

$$G^T(t_1, t_2) = G^{++}(t_1, t_2) = -i\langle \mathcal{T}_\mathcal{C} a^+(t_1) a^{\dagger +}(t_2)\rangle = -i\langle \tilde{\mathcal{T}} a(t_1) a^\dagger(t_2)\rangle \tag{3.12a}$$

$$G^>(t_1, t_2) = G^{+-}(t_1, t_2) = -i\langle \mathcal{T}_\mathcal{C} a^+(t_1) a^{\dagger -}(t_2)\rangle = -i\langle a(t_1) a^\dagger(t_2)\rangle \tag{3.12b}$$

$$G^<(t_1, t_2) = G^{-+}(t_1, t_2) = -i\langle \mathcal{T}_\mathcal{C} a^-(t_1) a^{\dagger +}(t_2)\rangle = -i\xi\langle a^\dagger(t_2) a(t_1)\rangle \tag{3.12c}$$

$$G^{\tilde{T}}(t_1, t_2) = G^{--}(t_1, t_2) = -i\langle \mathcal{T}_\mathcal{C} a^-(t_1) a^{\dagger -}(t_2)\rangle = -i\langle \mathcal{T} a(t_1) a^\dagger(t_2)\rangle, \tag{3.12d}$$

where $\mathcal{T}$ ($\tilde{\mathcal{T}}$) denotes (anti-)time-ordering. We see that these Green's functions satisfy the *linear* identity

$$+ G^{++}(t_1, t_2) - G^{+-}(t_1, t_2) - G^{-+}(t_1, t_2) + G^{--}(t_1, t_2) = 0. \tag{3.13}$$

We may make use of this identity by rotating to a different basis in $\pm$-space and define quantum (q) and classic (c) components:[2]

$$\Phi^q = \frac{1}{\sqrt{2}}\left(\Phi^- - \Phi^+\right), \quad \Phi^c = \frac{1}{\sqrt{2}}\left(\Phi^- + \Phi^+\right).^{3} \tag{3.14}$$

We thus aim to express the action in terms of $\Phi^{q/c}$. Before we can work with the Keldysh-action, one further step is customarily performed: Instead of integrating over the whole contour $\mathcal{C} = \mathcal{C}_- + \mathcal{C}_+ + \mathcal{C}_|$, we find a representation where we only need to integrate over the contour $\mathcal{C}_- + \mathcal{C}_+$. This is useful because we have excluded sources on $\mathcal{C}_|$, and as such we should be able to perform the integral along $\mathcal{C}_|$ and achieve an effective representation on $\mathcal{C}_- + \mathcal{C}_+$. Here, we just state the result (in [Kam11] this is performed explicitly) of the following construction: Construct an effective action along the path $\mathcal{C}_- + \mathcal{C}_+$ whose generating functional has the same moments as the generating functional Eq. (3.9). We note that in perturbative models, it is sufficient to consider a non-interacting Hamiltonian on the contour $\mathcal{C}_|$ by the following argument:[4] A thermal state determined by the interacting density matrix may be achieved by starting with a thermal state of the non-interacting Hamiltonian and then time-evolving this state through an adiabatic switching-on of the interaction. So, if we consider a thermal state determined by the interacting Hamiltonian at some time t after the interaction has been switched on, we can accommodate this state in the contour-formalism by considering a $\mathcal{C}_|$ contour with the Hamiltonian *at that time*, i.e. the non-interacting Hamiltonian. If one goes through the derivation of a

[2] The names "quantum" and "classic" refer to the following fact: If we expand the action to first order in the quantum component and perform the integral over the quantum component, we obtain a constraint enforcing the classical equation of motion for the classic component.

[3] Note the normalization. This normalization ensures that terms quadratic in Φ do not pick up any additional factors of 2. However, terms that are e.g. quartic in Φ pick up additional factors.

[4] We emphasize that the term "perturbative model" implies the absence of interaction-induced phase transitions.

non-interacting model, it turns out that we need to consider the action

$$S_{\mathrm{K}}[\phi] = \int dt \phi^T G^{-1} \phi + S_{\mathrm{int}}[\phi], \tag{3.15}$$

where $\phi = (\Phi^q, \Phi^c)^T$ and S_{int} is the interacting part of the action, obtained in a "naïve" manner by performing the Keldysh-rotation Eq. (3.14) on $S_{\mathrm{int}}[\Phi^+, \Phi^-] = S_{\mathrm{int}}[\Phi^+] - S_{\mathrm{int}}[\Phi^-]$. In frequency-space, G is a 2 by 2 matrix with entries $G^{qq} = 0$ (due to Eq. (3.13)), $G^{cq}(\omega) = \frac{1}{\omega - H_0 + i\eta} = G^R(\omega)$, $G^{qc}(\omega) = G^{cq\dagger}(\omega) = G^A(\omega)$, and $G^{cc}(\omega) = G^K(\omega) = (1 - 2n_F(\omega))(G^R(\omega) - G^A(\omega))$ (in equilibrium; in general: $G^{cc}(\omega) = G^R(\omega)F(\omega) - F(\omega)G^A(\omega)$, with an anti-Hermitian matrix F). We have introduced an infinitesimal level-broadening $\eta > 0$.

Before we consider possible subtleties involved (equal times, Feynman $i\eta$), let us turn to an open system, where some of these issues disappear automatically.

Comment 1: The derivation can also be performed as a limiting procedure of some time $T \to -\infty$ instead of using $t = -\infty$. However, we avoid this, because it just clutters up the notation.

Comment 2: Unfortunately, the labeling conventions in the Keldysh formalism are manifold: Some authors swap $+$ and $-$ relative to this work, others denote $\pm$ by 1 and 2. c and q are sometimes referred to as 2 and 1, or even as r and a.

Comment 3: The subtleties in the Keldysh formalism we alluded to just before the first comment are the following:

(a) Equal times: If a creation and an annihilation operator share the same time, there is an ordering ambiguity. In a formalism containing discrete times (which is used to derive the functional integral), it is customary to order annihilation operators to the right of creation operators, for both time-ordering and anti-time-ordering (if both operators occur at the same time). However, the continuous time formalism does not order in this way. Rather, it corresponds to $\mathcal{T} c^\dagger(t)c(t) = \frac{1}{2}c^\dagger(t)c(t) + \frac{1}{2}\xi c(t)c^\dagger(t)$ (in [Kam11], this is called "democratic"). This issue can be avoided somewhat by considering different times and a limiting procedure, excluding the single point of coinciding times.[5] However, the issue arises again when considering the Keldysh-rotation of the single-particle Green's function (where equal times correspond to an integral over all frequencies): Consider e.g. the Hartree-correction: It is proportional to the density, which is $\int d\omega G^<$. However, the naïve Keldysh-formalism after the rotation suggests a Hartree-term of the form $\int d\omega G^K$, which differs from the correct result by terms of the form $\int d\omega G^R$.[6] Since G^R decays only as $1/\omega$, the integral over it may be finite (and great caution has to be employed when attempting to compute it e.g.

[5] In the discrete time formalism, $\mathcal{T} c^\dagger(t)c(t) = c^\dagger(t)c(t) = \lim_{\epsilon \searrow 0} c^\dagger(t+\epsilon)c(t)$. The discrete and the continuous time formalism agree for all times except for equal times. We may thus compute the correlation function $\langle \tilde{\mathcal{O}}(\tilde{t} > t) c^\dagger(t)c(t)\mathcal{O}(t' < t)\rangle = \lim_{\epsilon \searrow 0} \langle \tilde{\mathcal{O}}(\tilde{t} > t) \mathcal{T}\left(c^\dagger(t+\epsilon)c(t)\right)\mathcal{O}(t' < t)\rangle$ in the continuous time formalism, where $\mathcal{O}$ is some internally time-ordered operator. Note that this footnote becomes relevant only if $\tilde{\mathcal{O}} \neq 1$, as otherwise we could enforce the ordering by attributing different contour-indices to c and $c^\dagger$, as $\langle \mathcal{T}_C c_+^\dagger(t)c_-(t)\rangle = \langle c^\dagger(t)c(t)\rangle$.

[6] The Hartree-term is obtained in first order in perturbation theory from a diagram with a single bare vertex and a single loop. The bare vertex is non-vanishing only for indices $cqqq$ and $cccq$. The external indices are cq (we are interested in a contribution to the retarded or advanced self-energy), such that the internal indices are cc or qq. Since $G^{qq} = 0$, and $G^{cc} = G^K$, the term naïvely contains as internal line a G^K.

by some clever tricks of deforming contours in the complex plane; in fact, we know that $-\frac{1}{\pi}\int d\omega \mathrm{Im}G^R(\omega) = 1$). We will however avoid this issue to a certain degree during the fRG-flow as we will be focused on the behavior of the single-scale propagator, which decays as $1/\omega^2$.

(b) Feynman $i\eta$: In closed systems, one introduces a regularization of the Fourier-transform to make all integrals well-defined. However, in equilibrium we have $G^K \sim \mathrm{Im}G^R$, which in the case of a discrete spectrum causes all sorts of unpleasantness. We will avoid this issue by going to an open system, where all states have a finite decay-width.[7]

Comment 4: We have considered only a generating functional $Z[J]$ with sources coupling to creation or annihilation operators. While in principle we could write a generating functional with sources also for other operators, it can be shown that any operator can be decomposed as a sum of products of creation and annihilation operators [Wei95]. Thus, it is sufficient to consider only source coupling to creation and annihilation operators, as the corresponding generating functional can be used to compute the expectation value of any product of creation and annihilation operators. It might be useful to introduce additional sources, e.g. a source for $c_i c_j^\dagger$ (i and j are arbitrary indices). These sources then lead to self-consistency equations when the source J of a creation or annihilation operator is included as well. For example, if we include the source term $A_i c_i c_{i+1}$ and the source term $J_i c_i$ in a generating functional $\tilde{Z}[J, A]$, then the derivative of the generating functional $\tilde{Z}$ with respect to A_1 and the derivative of the generating functional $\tilde{Z}$ with respect to J_2 and J_1 are related, i.e. $\delta_{A_1}\tilde{Z} \sim \delta_{J_1}\delta_{J_2}\tilde{Z}$ (depending on the precise way the sources are introduced, there may occur factors of i or additional minus signs). The introduction of additional sources is a key element of the Luttinger-Ward-functional [LW60].[8]

Comment 5: In some situations it may be useful to consider an extension of the Keldysh formalism to a more complicated contour. For example, if we take a "double contour", which has two time-ordered and two anti-time-ordered parts (essentially we add another copy of a path similar to $\mathcal{C}_- \cup \mathcal{C}_+$ after $\mathcal{C}_+$, but before $\mathcal{C}_|$), we can represent all possible orderings of four creation or annihilation operators as contour-ordering. While this new contour drastically increases the number of components, the extension might become necessary when attempting to link the Keldysh and Matsubara formalism (c.f. Sec. 3.6.4).

3.2 General Green's functions

The generating functional $Z[J]$ (Eq. (3.9)) can be used to compute correlation functions where creation or annihilation operators are ordered along the Keldysh-contour (Fig. 3.1). It is useful to give short names to certain sets of correlation functions. We introduce the contour-ordered

[7] A priori, not all states in an open system are required to have finite lifetime. For example, any state not coupling to lead-states will have infinite lifetime. However, we will construct our open system in such a manner that all states have finite lifetime (c.f. Sec. 8.2).

[8] The Luttinger-Ward functional can be used to determine if a given approximation respects certain conservation laws (continuity equations obtained from a global continuous symmetry).

multi-particle Green's functions

$$G^{j|j'}_{q|q'}(t|t') = (-i)^n \left\langle \mathcal{T}_c c^{j_1}_{q_1}(t_1)\dots c^{j_n}_{q_n}(t_n) c^{\dagger j'_n}_{q'_n}(t'_n)\dots c^{\dagger j'_1}_{q'_1}(t'_1)\right\rangle, \tag{3.16}$$

where j (j') is an n-component vector whose entries are either $+$ or $-$ (determining the part of the contour the annihilation (creation) operator is inserted on), q (q') is an n-component vector whose entries are all the quantum numbers necessary to specify an annihilation (creation) operator, and t (t') is an n-component vector whose entries are the times at which the annihilation (creation) operators act. In the case considered in the following (the QPC), it is sufficient to consider the Green's functions where there is an equal number of creation and annihilation operators. In general, there are of course additional Green's functions that have to be considered, e.g. containing three operators (for bosons) or where the number of creation and annihilation operators differs by an integer multiple of two (superconductivity). If we change to the Keldysh basis of q and c (c.f. Eq. (3.14)), we see that the Green's function vanishes if the index associated with the largest time is q(uantum).[9] From this follow two generic, and highly relevant properties of the multi-particle Green's function:

(i) $G^{q\dots q|q\dots q} = 0$, by which we mean: If all Keldysh-indices are q(uantum), the Green's function vanishes regardless of the values of the other arguments/indices. Since all Keldysh-indices are q(uantum), clearly the largest time is associated with a q(uantum) index. Thus, $G^{q|q}$ vanishes.

(ii) $G^{cq\dots q|qq\dots q}$ is retarded, i.e. it is non-zero only if the time t_1 is the largest time. In particular, this implies that the Fourier-transform $(G^{cq\dots q|qq\dots q}(t_1,\omega_2,\dots\omega_n|\omega'_1,\dots,\omega'_n)$ in frequency space as function of $\omega_2,\dots\omega_n$, $\omega'_1,\dots\omega'_n$) is analytic in the upper half plane (for the frequencies ω'_i) or the lower half plane (for the frequencies ω_i). This retarded component may be continued analytically and coincides with the Matsubara Green's function in the corresponding analytic region [Hao81, CSHY85].

3.3 Open Systems

We now consider the generating functional of an open system. To be specific, we consider the generating functional for correlation functions where all operators act on a spatially confined region $\mathcal{A}$ within an infinitely large system (c.f. Fig. 3.2(a)). We are interested in the generating functional where the only remaining integration over fields is to be performed over fields within the region $\mathcal{A}$ (c.f. Fig. 3.2(b)). To get there, in the generating functional of the full system we integrate out the the fields with support outside of $\mathcal{A}$. We will assume that outside of $\mathcal{A}$ the system is non-interacting, and that the coupling between the region $\mathcal{A}$ and the rest of the system is linear in creation/annihilation operators within $\mathcal{A}$ and outside of $\mathcal{A}$ (for example, the coupling could be of the form $a^\dagger_i a_j + H.c.$, where i lies within $\mathcal{A}$, and j lies outside of $\mathcal{A}$,

[9] The ordering of the operators does not change when the operator corresponding to the largest time is moved between plus- and minus-contour. Since the q(uantum) component takes the difference between plus- and minus-contour, G vanishes if the largest time is q(uantum).

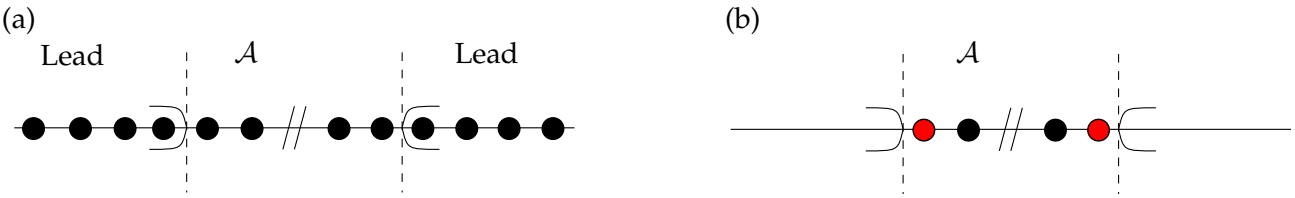

Figure 3.2: Schematic of the open system we have in mind. (a) The region $\mathcal{A}$ is interacting, while the leads are non-interacting. The leads extend to infinity. (b) After integrating out the leads, we only deal with the central region $\mathcal{A}$. The effect of the leads is fully absorbed in a lead self-energy modifying the sites coupling to leads (these sites are shown in red).

but not of the form $a_i^\dagger a_i a_j^\dagger a_j$).[10] Physically, this means that the region outside of $\mathcal{A}$ acts as a non-interacting bath for the region $\mathcal{A}$.

Because the system is non-interacting outside of $\mathcal{A}$, we can perform the field-integrals outside of $\mathcal{A}$ exactly (e.g. [FV63]). One way of performing the integration is through the projection method ([Kar10, Tay12]): First, we note that upon integrating non-interacting degrees of freedom ψ_{lead} coupled linearly to some operators $\mathcal{O}_{\text{center}}$ (which in the current case are the operators within $\mathcal{A}$), the new effective action (without the degrees of freedom ψ_{lead}) is quadratic in the operators $\mathcal{O}_{\text{center}}$. This is a direct consequence of the fact that we have excluded interactions outside of $\mathcal{A}$. If there were interactions outside of $\mathcal{A}$, the effective action would generically contain all (symmetry-allowed) powers of the operators $\mathcal{O}_{\text{center}}$ (with various integral-kernels). So, what remains to be done is to determine the contribution to the quadratic part of the effective action. Before we do so, let us collect some intuition:

1. Since the region $\mathcal{A}$ is open (equivalently: we have a bath), some states within $\mathcal{A}$ should decay at finite times by escaping into the bath. Of course, only states that couple to the bath-states are eligible to decay. Since decay (equivalently: finite lifetime) is modeled by a finite imaginary contribution to the inverse Green's function, we expect a finite imaginary part in the quadratic part of the action at energies where bath-states exist. Equivalently, in frequency space, states coupling to the leads are smeared out.

2. The contributions from the bath mix the coupled operators only, i.e. after integrating out the bath, we obtain non-trivial contributions to the quadratic part of the action only for operators coupling to the bath.

3. If we have multiple, disconnected baths, then only operators coupling to the same bath are mixed.

[10] This definition of the coupling and the absence of interactions outside of $\mathcal{A}$ depends on the choice of basis in field space. The statements made here refer to basis that is being integrated over with the usual functional integral measure. For example, in a situation where bosonization is applicable, the bosonic degrees of freedom might fall within the range of our assumptions, while the fermionic degrees of freedom do not. In the applications of this work, where we consider systems perturbatively related to free fermions and where it is important that the dispersion is non-linear and spatially dependent, the relevant degrees of freedom are free fermions in a (discretized) position basis.

In order to integrate out the regions outside of $\mathcal{A}$, consider the schematic action

$$S = \int dt \left(\sum_{i,j \notin \mathcal{A}} \Phi_i G^{-1}_{\mathrm{lead},ij} \Phi_j + \mathcal{L}_\mathrm{c}[\Phi_i] + \sum_{i \in \mathcal{A}, j \notin \mathcal{A}} \Phi_i \tau_{ij} \Phi_j \right), \tag{3.17}$$

where $\mathcal{L}_\mathrm{c}$ is the Lagrangian of the central region ($\mathcal{A}$) in the absence of coupling between $\mathcal{A}$ and the rest of the system. G_lead is the Green's function of the leads at $\tau_{ij} = 0$. i and j are multi-indices containing all necessary labels in addition to the one distinguishing $\mathcal{A}$ from the rest of the system. Note that the indices outside of $\mathcal{A}$ do not contain interactions (the action is quadratic in these degrees of freedom) and the coupling between $\mathcal{A}$ and the rest of the system (parametrized by τ) is linear. To integrate out the system outside of $\mathcal{A}$, we consider τ as a perturbation and expand around $\tau = 0$. We will also assume for now that we can expand $\mathcal{L}_\mathrm{c}$ in some diagrammatic series, following conventional perturbation theory.

Diagrams are built of the following blocks: A Green's function $G_\mathcal{A}$ within $\mathcal{A}$, a Green's function G_lead outside of $\mathcal{A}$, the coupling τ, and some interaction vertices within $\mathcal{A}$. Since we aim to integrate out the parts outside of $\mathcal{A}$, no external legs are allowed to have indices outside of $\mathcal{A}$. We may schematically construct all diagrams corresponding to a correlation function purely within $\mathcal{A}$ by proceeding as follows (classification in powers of τ):

1. Draw all corresponding diagrams *without* τ.
2. At first order in τ, there is no allowed diagram (a single τ converts one index within $\mathcal{A}$ to one index outside of $\mathcal{A}$. The only way to get back to indices within $\mathcal{A}$ is through τ).
3. At second order in τ, we change one Green's function within $\mathcal{A}$ to $G_\mathcal{A} \tau G_\mathrm{lead} \tau G_\mathcal{A}$.
4. All orders in τ are achieved by exchanging all $G_\mathcal{A}$ for $\sum_n G_\mathcal{A} \left(\tau G_\mathrm{lead} \tau G_\mathcal{A}\right)^n$.[11]
5. The sum may be performed by Dyson's equation (or by noting that it is a geometric series). We thus replace $G_\mathcal{A}$ by $\left(G_\mathcal{A}^{-1} - \tau G_\mathrm{lead} \tau\right)^{-1}$. This replacements suggests the definition of the lead self-energy $\Sigma_\mathrm{lead} \sim \tau G_\mathrm{lead} \tau$.

We note that the Dyson resummation with respect to the interaction is fully compatible with this resummation of the coupling to the leads.

As we will see explicitly in Sec. 3.4.1, this structure yields an expression consistent with our prior intuition. Also, if we assume that all states within $\mathcal{A}$ couple to the degrees of freedom outside of $\mathcal{A}$, there is no need to use the infinitesimal level broadening η.

3.4 The specific setup

After these general considerations, let us now turn to some peculiarities of the system at hand (and our implementation of it).

[11] Here the assumptions enter: Due to the linear coupling between $\mathcal{A}$ and the rest of the system, τ always comes with exactly two lines. Thus, it can only be attached to the G's. Since the system outside of $\mathcal{A}$ is non-interacting, we cannot combine multiple lines that have left the region $\mathcal{A}$. We need even powers of τ, as an odd number of τ's implies that certain lines have left $\mathcal{A}$, but not returned, which is not a viable diagram with all external lines within $\mathcal{A}$.

3.4.1 General considerations concerning the leads

Let us now integrate out the leads with the corresponding details. To be specific, we will assume the following setup: We consider a system of fermions on a lattice in the position basis. We spatially split the system into a finite central region ($\mathcal{A}$) and the rest (the leads). The leads need not be connected, e.g. in a one-dimensional system, we could have a lead to the right and a lead to the left of the central region. Each lead has its own Green's function and is assumed to always be in equilibrium, i.e. for any two sites i, j within the same lead, we have

$$G^K_{\text{lead},ij}(\omega) = (1 - 2n_{F,\text{lead}}(\omega))(G^R_{\text{lead},ij} - G^A_{\text{lead},ij}), \tag{3.18}$$

with the Fermi-Dirac-distribution function $n_{F,\text{lead}}$. We remark that G_{lead} is computed in the lead only, i.e. it is the Green's function of a single, *isolated* lead.[12] We do not impose that all leads are in the "same" equilibrium, i.e. have the same distribution function. So, in particular, we still allow for thermal or voltage bias across the central region. We assume that all states within the central region couple to at least one lead.[13]

Before we delve into the details, let us make a short remark: Since we aim to integrate out a non-interacting part of the system, which couples linearly to the interacting part of the system, we might as well use a non-interacting system overall. As a non-interacting system leads to additional simplifications, we will do so for the rest of this section. Note that in a non-interacting system we may formally still introduce self-energies, which we take to be infinitesimal.

As a first step, we integrate out a single lead: The coupling between the central region and the lead is

$$S_{cl} = \int dt \sum_{i\in\mathcal{A}, i'\notin\mathcal{A}} \tau_{ii'} c_i^\dagger c_{i'} + H.c. \tag{3.19}$$

which becomes on the Keldysh contour

$$S_{cl} = \int dt \sum_{i\in\mathcal{A}, i'\notin\mathcal{A}} \tau^{--}_{ii'} c_i^{-\dagger} c^-_{i'} + H.c. - \int dt \sum_{i\in\mathcal{A}, i'\notin\mathcal{A}} \tau^{++}_{ii'} c_i^{+\dagger} c^+_{i'} + H.c., \tag{3.20}$$

[12] We note that for non-interacting systems distributions other than the usual thermodynamic Fermi-Dirac- or Bose-functions are valid equilibrium distribution functions (in the sense that they are stationary under time-evolution). However, for any physical lead, there will be weak interactions. While we may in some expansion attempt to neglect these interactions, the long-time distribution function will typically approach the usual thermodynamic distribution (we consider only bosons or fermions and exclude anyons or hard-core bosons, whose distribution functions may differ). Since the results are much more sensitive to the distribution function than to some small renormalization of energy levels, or some weak scattering within the leads, it makes sense to restrict the distribution function of a physical lead to the thermodynamic one. In other words, we neglect the interactions within the leads, but we expand around the distribution stable under the inclusion of weak interactions.

It is furthermore worthwhile to note that our leads actually simulate two-dimensional baths. While weak interaction effects in two-dimensional systems are well captured by renormalized parameters in the fermionic action, this is not the case in one-dimensional systems (in a one-dimensional system, there is no irrelevant interaction, as the particles cannot avoid each other [Gia03]). By using non-interacting leads, we thus also avoid purely one-dimensional effects spoiling our results.

[13] To be precise: We impose that all eigenstates of the Hamiltonian of the isolated central region $\mathcal{A}$ couple to at least one lead.

where we have introduced $\tau^{\pm} = \tau$ for later convenience. Upon the Keldysh-rotation (Eq. (3.14)) the coupling becomes

$$S_{cl} = \int dt \sum_{i\in\mathcal{A}, i'\notin\mathcal{A}} \tau^{cq}_{ii'} c^{\dagger}_i c^q_{i'} + H.c. + \int dt \sum_{i\in\mathcal{A}, i'\notin\mathcal{A}} \tau^{qc}_{ii'} c^{q\dagger}_i c^c_{i'} + H.c., \tag{3.21}$$

where we have introduced $\tau^{qc} = \tau^{cq} = \tau$ to emphasize that the coupling is between q and c components. It is convenient to extend τ to a matrix in Keldysh space via the additional entries $\tau^{cc} = 0 = \tau^{qq}$. Following the steps outlined previously, the Dyson equation for the single-particle Green's function in the central region is

$$G_{ij} = G_{ij}|_{t=0} + G_{ik}|_{t=0}\tau_{kk'}G_{\text{lead},k'l'}\tau_{l'l}G_{lj} \tag{3.22}$$

Explicitly, using Keldysh-indices, we obtain

$$\begin{aligned} G^R_{ij} &= G^R_{ij}|_{\tau=0} + G^{c\alpha}_{ik}|_{\tau=0}\tau^{\alpha\bar{\alpha}}_{kk'}G^{\bar{\alpha}\beta}_{\text{lead},k'l'}\tau^{\beta\bar{\beta}}_{l'l}G^{\bar{\beta}q}_{lj}, \\ G^K_{ij} &= G^K_{ij}|_{\tau=0} + G^{c\alpha}_{ik}|_{\tau=0}\tau^{\alpha\bar{\alpha}}_{kk'}G^{\bar{\alpha}\beta}_{\text{lead},k'l'}\tau^{\beta\bar{\beta}}_{l'l}G^{\bar{\beta}c}_{lj}, \end{aligned} \tag{3.23}$$

where $\alpha, \beta \in \{c, q\}$ and a bar over α, β denotes exchanging c and q (i.e. if α is q, then $\bar{\alpha}$ is c). We do not write the expression for G^A explicitly, as we know that $G^A = G^{R\dagger}$. Using that $G^{qq} = 0$, we may simplify

$$G^R_{ij} = G^R_{ij}|_{\tau=0} + G^{cq}_{ik}|_{\tau=0}\tau^{qc}_{kk'}G^{cq}_{\text{lead},k'l'}\tau^{qc}_{l'l}G^{cq}_{lj} = G^R_{ij}|_{t=0} + G^R_{ik}|_{t=0}\tau_{kk'}G^R_{\text{lead},k'l'}\tau_{l'l}G^R_{lj}, \tag{3.24}$$

$$\begin{aligned} G^K_{ij} &= G^K_{ij}|_{\tau=0} + G^{cc}_{ik}|_{\tau=0}t^{cq}_{kk'}G^{qc}_{\text{lead},k'l'}\tau^{cq}_{l'l}G^{qc}_{lj} + G^{cq}_{ik}|_{\tau=0}\tau^{qc}_{kk'}G^{cq}_{\text{lead},k'l'}\tau^{qc}_{l'l}G^{cc}_{lj} + G^{cq}_{ik}|_{\tau=0}\tau^{qc}_{kk'}G^{cc}_{\text{lead},k'l'}\tau^{cq}_{l'l}G^{qc}_{lj} \\ &= G^K_{ij}|_{\tau=0} + G^K_{ik}|_{\tau=0}\tau_{kk'}G^A_{\text{lead},k'l'}\tau_{l'l}G^A_{lj} + G^R_{ik}|_{\tau=0}\tau_{kk'}G^R_{\text{lead},k'l'}\tau_{l'l}G^K_{lj} + G^R_{ik}|_{\tau=0}\tau_{kk'}G^K_{\text{lead},k'l'}\tau_{l'l}G^A_{lj}. \end{aligned} \tag{3.25}$$

Solving for G^R, we obtain for indices within the central region

$$G^R_{ij} = \left(G^{R^{-1}}|_{\tau=0} - \underbrace{\tau G^R_{\text{lead}}\tau}_{=\Sigma^R_{\text{lead}}} \right)^{-1} \tag{3.26}$$

Note that $G^{R^{-1}}|_{\tau=0}$ contains an infinitesimal self-energy $i\eta$. If we assume that all states within the central region couple to the leads, this infinitesimal part does not matter, as there is a finite Σ^R_{lead} added to the infinitesimal part. It is slightly more subtle to determine G^K: We first introduce the *Keldysh self-energy* Σ^K via[14]

$$G^K = G^R\Sigma^K G^A. \tag{3.27}$$

[14] The expression Eq. (3.27) may be obtained by inverting the Dyson equation $G = G_0 + G_0\Sigma G$, where G is the full Green's function and G_0 is the Green's function in absence of some perturbation. Note that in this notation, Σ is a matrix in Keldysh-space. We call Σ^{qq} the Keldysh self-energy.

If we now consider the Eq. (3.25), we obtain (omitting spatial indices)

$$\begin{aligned} G^K &= G^R|_{\tau=0}\Sigma^K|_{\tau=0}G^A|_{\tau=0} + G^R|_{\tau=0}\Sigma^K|_{\tau=0}G^A|_{\tau=0}\tau G^A_{\text{lead}}\tau G^A \\ &\quad + G^R|_{\tau=0}\tau G^R_{\text{lead}}\tau G^R\Sigma^K G^A + G^R|_{\tau=0}\tau G^R_{\text{lead}}G^K_{\text{lead}}G^A_{\text{lead}}\tau G^A \\ &= G^R|_{\tau=0}\Sigma^K|_{\tau=0}G^A + G^R|_{\tau=0}\tau G^R_{\text{lead}}\tau G^R\Sigma^K G^A + G^R|_{\tau=0}\tau G^R_{\text{lead}}G^K_{\text{lead}}G^A_{\text{lead}}\tau G^A \\ &\quad + G^R|_{\tau=0}\Sigma^K G^A - G^R|_{\tau=0}\Sigma^K G^A \\ &= G^R|_{\tau=0}\left(\Sigma^K|_{\tau=0} + \tau G^R_{\text{lead}}G^K_{\text{lead}}G^A_{\text{lead}}\tau - \Sigma^K\right)G^A + G^R\Sigma^K G^A, \end{aligned} \tag{3.28}$$

where we have used Eq. (3.26) and its Hermitian conjugate. With the definition of the Keldysh self-energy Eq. (3.27), we thus see that

$$\Sigma^K = \Sigma^K|_{\tau=0} + \underbrace{\tau G^R_{\text{lead}}G^K_{\text{lead}}G^A_{\text{lead}}\tau}_{=\Sigma^K_{\text{lead}}}. \tag{3.29}$$

As a direct consequence of Eq. (3.18), $\Sigma^K_{\text{lead}} = (1-2n_{F,\text{lead}}(\omega))(\Sigma^R_{\text{lead}}-\Sigma^A_{\text{lead}})$. In a non-interacting closed system Σ^K is infinitesimal, i.e. in a non-interacting system we may neglect the first summand in Eq. (3.29) if all states in the central region couple to lead-states.

If we go to an interacting region, the contribution from the leads has to have precisely the same form as for an overall non-interacting system, provided the leads remain non-interacting.

3.4.2 The tight-binding chain as lead

We have seen that we may model leads by considering a generating functional determined by a Hamiltonian in a finite region and a lead contribution to a self-energy. The lead contribution to the self-energy Σ_{lead} depends on the coupling t between the system and the lead and the Green's function between the lead-sites coupling to the system *in the absence of the system*, i.e. of the lead only. Thus, to fully determine the generating functional in the present setup, where only one site of each lead couples to only one site of the central region, we require the Green's function of a semi-infinite tight-binding chain (which we use as lead) at the last site. We thus consider the system

$$\mathcal{H}_{\text{lead}} = \sum_{i=-\infty}^{n} \tau c_i^\dagger c_{i-1} + H.c., \tag{3.30}$$

where we have fixed the origin of the energy to lie at the center of the band. The simplest way to obtain the self-energy induced by this type of lead is through the following consideration [NO88]:

1. A semi-infinite chain ending on site $n = 0$ is physically equivalent to a semi-infinite chain ending on site $n = 1$.

2. Assuming that the retarded Green's function at the end of the semi-infinite chain is $f(\omega)$, we have $G^R_{00}(\omega) = f(\omega)$ for the chain ending at 0, and $G^R_{11}(\omega) = \frac{1}{\omega-\tau^2 f(\omega)}$ (c.f. Eq. (3.26)) for the chain ending at 1.

3. We thus obtain the defining equation $f(\omega) = \frac{1}{\omega - \tau^2 f(\omega)}$, which has the two solutions $f(\omega) = \frac{1}{2\tau^2}\left(\omega \pm \sqrt{\omega^2 - 4\tau^2}\right)$.

4. We fix the sign by imposing $\lim_{\omega\to\pm\infty} f = 0$, and $\mathrm{Im} f < 0$.[15]

The Keldysh self-energy is determined by a fluctuation-dissipation theorem, i.e. we assume that the isolated lead is in equilibrium. We thus obtain for a lead simulated by a semi-infinite tight-binding chain:

$$\Sigma^R_{\mathrm{lead}}(\omega) = \begin{cases} \frac{1}{2}\left(\omega - \sqrt{\omega^2 - 4\tau^2}\right) & \text{for } |\omega| < 2|\tau| \\ \frac{1}{2}\left(\omega - i\sqrt{4\tau^2 - \omega^2}\right) & \text{else,} \end{cases} \tag{3.31a}$$

$$\Sigma^A_{\mathrm{lead}}(\omega) = \Sigma^R_{\mathrm{lead}}(\omega)^\dagger, \tag{3.31b}$$

$$\Sigma^K_{\mathrm{lead}}(\omega) = (1 - 2n_{F,\mathrm{lead}}(\omega))\left(\Sigma^R_{\mathrm{lead}}(\omega) - \Sigma^A_{\mathrm{lead}}(\omega)\right). \tag{3.31c}$$

We note that Σ^R is purely real if $|\omega| > 2|\tau|$. Physically, this is eminently reasonable: the band-width of a tight-binding chain is $4|\tau|$, i.e. the states in the lead occur at energies in the interval $[-2|\tau|, 2|\tau|]$. The imaginary part of the self-energy corresponds to a life-time of the single-particle excitation at the given energy. Since only particles with an energy within the spectrum of the lead states can directly decay into lead states (i.e. escape into lead), only states with energies within the lead's band should acquire a finite lifetime due to the lead. Thus, the lead-induced self-energy can only have an imaginary contribution for energies within the lead's band, which we observe.

Let us also reiterate that - since the lead is a non-interacting system - n_F is in principle an arbitrary function. However, for an actual, physical lead, which has weak interactions and equilibrates, n_F will be the Fermi-Dirac function.

3.5 Properties of the single-particle Green's function

Finally, let us take a closer look at some single-particle properties which we will use extensively throughout.

3.5.1 Analyticity

The retarded component of the Green's function, $G^R(t_1, t_2)$, is non-vanishing only if $t_1 > t_2$. We prove this by inserting the definition

$$G^R(t_1, t_2) = G^{cq}(t_1, t_2) \sim G^{--}(t_1, t_2) - G^{-+}(t_1, t_2) + G^{+-}(t_1, t_2) - G^{++}(t_1, t_2)$$

[15] Physically, at large energies, the relevance of the lead (which has a finite band-width) should vanish, thus $\lim_{\omega\to\pm\infty} \Sigma_{\mathrm{lead}} = 0$, which implies for constant coupling between system and lead $\lim_{\omega\to\pm\infty} f = 0$. If the imaginary part of a self-energy is negative, this means that over time probability is lost, i.e. the norm of wave-functions taken only over the considered region shrinks over time, which corresponds to particles decaying/escaping. Conversely, if the imaginary part of a self-energy is positive, this means that over time probability is gained, i.e. the norm of wave-functions taken only over the considered region grows over time, which corresponds to particles being created/moving into the system. In either case, the probability for a particle to remain within a finite part of the system is not 1. The physically relevant case for us is the case of escaping particles, i.e. the case of $\mathrm{Im} f < 0$.

$$\sim \langle \mathcal{T}\Phi(t_1)\Phi(t_2)\rangle - \xi\langle\Phi(t_2)\Phi(t_1)\rangle + \langle\Phi(t_1)\Phi(t_2)\rangle - \langle\tilde{\mathcal{T}}\Phi(t_1)\Phi(t_2)\rangle, \tag{3.32}$$

which trivially vanishes if $t_1 < t_2$. If we are interested only in the behavior of G^R multiplied by smooth functions, we may write $G^R(t,0) = G^R(t,0)\Theta(t)$, with the Heaviside Θ-function. The Fourier-transform is thus

$$G^R(\omega) = \int dt \exp(i\omega t) G^R(t,0) = \int_0^\infty dt \exp(i\omega t) G^R(t,0). \tag{3.33}$$

The integral converges absolutely for any complex ω in the upper half plane.[16] We thus say: $G^R(\omega)$ is analytic in the upper half plane. However, we remark that since $G^R(\omega) \sim 1/\omega$ for large ω, we obtain that $\int d\omega G^R(\omega) \neq 0$.

$G^A(\omega)$, being the Hermitian conjugate of $G^R(\omega)$ is analytic in the lower half plane. $G^K(\omega)$, which in equilibrium may be obtain through the FDT, $G^K = (1-2n_F)(G^R - G^A)$, has poles in both the upper and lower half plane, due to n_F.

3.5.2 The local density of states

From the retarded component of the single-particle Green's function we may read off the density of states $\mathcal{A}$, which we define through the spectral representation:

$$G^R(\omega) = \int d\bar{\omega} \frac{\mathcal{A}(\bar{\omega})}{\omega - \bar{\omega} + i\epsilon}. \tag{3.34}$$

Since $G^R(\omega)$ is analytic in the upper half plane, we may use the Kramers-Kronig relations to find

$$\mathcal{A}(\omega) = -\frac{1}{\pi}\mathrm{Im}G^R(\omega). \tag{3.35}$$

So far, the density of states $\mathcal{A}$ has the same labels as the single-particle basis we use to describe G^R. If these labels are position labels (e.g. on a lattice), we may define the *local density of states* (LDOS) as

$$\mathcal{A}_i(\omega) = -\frac{1}{\pi}\mathrm{Im}G^R_{ii}(\omega), \tag{3.36}$$

with some site-index i.[17] To get some idea why $\mathcal{A}$ is called density of states, we consider a homogeneous system with dispersion ϵ_k:

$$\mathrm{Im}G^R(\omega) = \mathrm{Im}\frac{1}{\omega - \epsilon_k + i\epsilon} \sim \delta(\omega - \epsilon_k) = \frac{\delta(k-k_\omega)}{|\partial_k \epsilon_k|} = \underbrace{|\partial_\epsilon k|}_{\nu}\delta(k-k_\omega), \tag{3.37}$$

[16] Mathematically, the convergence requires that $G^R(t,0)$ grows slower than exponentially in time t. Physically, this is always the case. In fact, for the systems considered here, $G^R(t,0)$ *decays* at least algebraically in time t.

[17] We note that the local density of states (or rather: the equal-time, equal position Green's function) is only well-defined in a model with a sensible UV behavior. A spatial lattice guarantees this sensible UV behavior by serving as an effective UV cut-off (as the lattice yields a finite band-width). However, if the system had a linear dispersion (in a spatial continuum), the local density of states could be problematic. This is directly related to the fact that relativistic QFTs need to be regularized in the UV.

with $\omega = \epsilon_{k_\omega}$ and the "usual" density of states ν. In a homogeneous system, the density of states ν is proportional to the inverse group velocity v of a wave-packet with energies centered on ω. In an inhomogeneous system, where the inhomogeneity is adiabatically turned on/off (on the scale of the local Fermi wave-length), we retain the semi-classical relation $\mathcal{A} \sim 1/v_F$.

In a one-dimensional system, we have the following useful properties of the LDOS:

1. At the sharp band edges (at energy ω_0), where the dispersion is quadratic, the LDOS exhibits a $1/\sqrt{|\omega - \omega_0|}$ singularity when approaching the band edge from within the band.
2. In an inhomogeneous system, a potential barrier will smooth out this behavior (c.f. chapter 6). We may interpret the LDOS below the classical minimum of the potential as tunneling states.
3. In a fermionic system, the LDOS is normalized, even with interactions:

$$\int d\omega \mathcal{A}_i(\omega) = 1. \tag{3.38}$$

3.5.3 The local distribution function

Another useful concept is the *local distribution function* n_i, which we extract from the Keldysh- and the retarded Green's functions. If we define n_i through

$$G^K_{ii}(\omega) = (1 - 2n_i(\omega)) \left(G^R_{ii}(\omega) - G^A_{ii}(\omega) \right), \tag{3.39}$$

we see that the density ρ at site i is

$$\rho_i = \int \frac{d\omega}{2\pi} G^<_{ii}(\omega) = \int \frac{d\omega}{2\pi} \left(G^K_{ii}(\omega) - G^R_{ii}(\omega) + G^A_{ii}(\omega) \right) = \int d\omega n_i \mathcal{A}_i(\omega). \tag{3.40}$$

In equilibrium, we have as an FDT

$$G^K(\omega) = (1 - 2n_F(\omega)) \left(G^R(\omega) - G^A(\omega) \right), \tag{3.41}$$

such that the local distribution function is identical to the Fermi-Dirac function n_F, as it should be. We will see later (Sec. 5.3) that this definition of the local distribution function is fully consistent with the local distribution used to determine the current.

For a system attached to two leads at different chemical potentials, the local distribution function interpolates between the distribution functions in the leads. Usually, this means that a single step function is turned (roughly) into a function with two steps, one at each chemical potential. We explain this in more detail later (Sec. 7.5).

3.6 Symmetries

Symmetries play a crucial role in reducing the effort required to solve a given system. In this thesis, we use the transformation under particle exchange and complex conjugation to reduce the complexity of the problem [JPS10b]. In equilibrium, we can also use the KMS conditions (fluctuation-dissipation theorems) [Kub57, Kub66, MS59] and a parity-symmetry of the model [BHS+13] to further reduce the number of independent components.

3.6.1 Particle exchange

Essentially, for fermions, exchanging two particles yields one additional minus-sign. Of course, this statement is only true if the fermions are commuted under a prescribed ordering, i.e.

$$\langle \mathcal{T}\mathcal{O}\psi_1\bar{\psi}_2\mathcal{O}'\rangle = -\langle \mathcal{T}\mathcal{O}\bar{\psi}_2\psi_1\mathcal{O}'\rangle, \tag{3.42}$$

where the indices 1, 2 are multi-indices encompassing position, spin, time, etc., and $\mathcal{T}$ denotes an ordering prescription, e.g. normal-ordering or contour-ordering, whereas in general

$$\langle \mathcal{O}\psi_1\bar{\psi}_2\mathcal{O}'\rangle \neq -\langle \mathcal{O}\bar{\psi}_2\psi_1\mathcal{O}'\rangle, \tag{3.43}$$

because the fermions satisfy an anti-commutation relation

$$\{\psi_1, \bar{\psi}_2\}|_{t_1=t_2} = \delta_{12}. \tag{3.44}$$

Note that we explicitly distinguish between creation and annihilation operators, such that we do not obtain any symmetry for the single-particle Green's function. However, the two-particle Green's function satisfies

$$G_{12|34} = -G_{21|34} = -G_{12|43} = G_{21|43}, \tag{3.45}$$

where 1 etc. are multi indices encompassing spin, position, time, contour etc.

Since the two-particle vertex can be obtained directly from the Green's functions, it has the same property:

$$\gamma_{12|34} = -\gamma_{21|34} = -\gamma_{12|43} = \gamma_{21|43}. \tag{3.46}$$

This property remains unaffected by the Keldysh-rotation, in other words, Eq. (3.46) is valid also if the multi-index 1, 2, etc. contains Keldysh-indices after the rotation, i.e. if 1 contains an index taking the value c or q.

3.6.2 Complex conjugation

Another fundamental property of correlation functions is encoded in the behavior under complex conjugation. First, we note that

$$\langle \mathcal{O}\mathcal{P}\rangle^* = \langle \mathcal{P}^\dagger\mathcal{O}^\dagger\rangle, \tag{3.47}$$

for arbitrary operators $\mathcal{O}$ and $\mathcal{P}$. While it is obvious that the Hermitian conjugate of a creation operator $c^\dagger$ is the corresponding annihilation operator c, what it is not necessarily obvious what happens with the contour indices. As seen from Eq. (3.47), complex conjugation exchanges the order of operators. If we recall that complex conjugation does not change the time at which an operator is evaluated in the interaction picture, we see that upon complex conjugation a time-ordered arrangement of operators turns into an anti-time-ordered sequence.[18] If we work on

[18] Consider the operator $\mathcal{O}$ at time t: $\mathcal{O}(t) = \exp(iHt)\mathcal{O}\exp(-iHt)$. We obtain $(\mathcal{O}(t))^\dagger = (\exp(-iHt))^\dagger\,\mathcal{O}^\dagger\,(\exp(iHt))^\dagger = \exp(iHt)\mathcal{O}^\dagger\exp(-iHt) = \mathcal{O}^\dagger(t)$, where we used that the Hamiltonian is Hermitian.

the level of correlation functions, we see more generally that a contour-ordering becomes 'anti-contour-ordering'. However, this anti-contour-ordering can again be represented as contour-ordering, if we exchange the $+$ and $-$ indices, i.e.

$$G^*_{12|34} = (-)^2 G_{\bar{3}\bar{4}|\bar{1}\bar{2}}, \tag{3.48}$$

where a bar over the multi-index signifies exchanging $+$ and $-$ on the contour-index. The minus in front is due to the factors of $-i$ in the definition of the Green's functions.

As complex conjugation exchanges $+$ and $-$, after the rotation it exchanges c with c and q with $-q$, i.e.

$$G^*_{12|34} = (-)^m G_{34|12}, \tag{3.49}$$

where m is number of q(uantum) indices.

Since the two-particle vertex can be obtained directly from the Green's functions, it has the same property after the Keldysh-rotation:

$$\gamma^*_{12|34} = (-)^m \gamma_{34|12}. \tag{3.50}$$

3.6.3 Equilibrium: KMS conditions and time-reversal symmetry

In equilibrium, correlation functions satisfy the so-called Kubo-Martin-Schwinger conditions [Kub57, Kub66, MS59]. These conditions stem from the fact that the thermal distribution and the time-evolution can both be generated by the microscopic Hamiltonian. We have already seen in Sec. 3.1 that we may think of the density matrix as time-evolution along the imaginary time axis. If we take the idea of complexified time to its logical conclusion, we see that for any operator $\mathcal{O}$ in the Heisenberg picture

$$\begin{aligned}
\mathcal{O}(t) &= \exp(iHt)\mathcal{O}\exp(-iHt) \\
&= \exp(+\beta H - \beta\mu N - \beta H + \beta\mu N)\exp(iHt)\mathcal{O}\exp(-iHt)\exp(+\beta H - \beta\mu N - \beta H + \beta\mu N) \\
&= \rho_{\mathrm{gc}}\exp(-\beta\mu N)\exp(iH(t-i\beta))\mathcal{O}\exp(-iH(t-i\beta))\exp(\beta\mu N)\rho_{\mathrm{gc}}^{-1} \\
&= \rho_{\mathrm{gc}}\exp(-\beta\mu N)\mathcal{O}(t-i\beta)\exp(\beta\mu N)\rho_{\mathrm{gc}}^{-1},
\end{aligned} \tag{3.51}$$

where we have introduced the grand-canonical density matrix $\rho_{gc} = \exp(+\beta H - \beta\mu N)$, with the number operator N, the chemical potential μ and the inverse temperature $\beta = 1/k_B T$, and the complex time evolution $\mathcal{O}(\tau) = \exp(-iH\tau)\mathcal{O}\exp(iH\tau)$, $\tau \in \mathbb{C}$.[19] We have assumed that the number operator N and the Hamiltonian H commute (which is the case for the system we consider). For correlation functions, we thus have the KMS condition

$$\mathrm{Tr}\left(\mathcal{O}_1(t_1)\mathcal{O}_2(t_2)\rho_{\mathrm{gc}}\right) = \mathrm{Tr}\left(\exp(-\beta\mu N)\mathcal{O}_2(t_2 - i\beta)\exp(\beta\mu N)\mathcal{O}_1(t_1)\rho_{\mathrm{gc}}\right), \tag{3.52}$$

where we have used cyclicity of the trace. The KMS condition Eq. (3.52), when applied to operators on the Keldysh contour yields [CSHY85, Jak10]

$$\exp\left(\beta\Delta^{j|j'}(\omega|\omega')\right) G^{j|j'}_{q|q'}(\omega|\omega') = \xi^{m^{j|j'}}\tilde{G}^{\bar{j}|\bar{j}'}_{q|q'}(\omega|\omega'), \tag{3.53}$$

[19] We note that the complex time evolution is not a unitary operation.

where the bar over j denotes "swapping plus and minus" (i.e. if $j = +$, then $\bar{j} = -$),

$$\Delta^{j|j'}(\omega|\omega') = \sum_{k:j'_k=+} (\omega'_k - \mu) - \sum_{k:j_k=+} (\omega_k - \mu), \tag{3.54}$$

$$m^{j|j'} = \sum_{k:j'_k=+} 1 - \sum_{k:j_k=+} 1, \tag{3.55}$$

and $\tilde{G}$ is the Green's function with a different contour-ordering: On the right, we have operators on the minus contour anti-time-ordered, then – further left – operators on the plus-contour time-ordered. So, in $\tilde{G}$, we simply change the ordering on each branch compared to G, while keeping the ordering between the branches the same. In general, for most components, there is no relation between $\tilde{G}$ and G.[20] To get optimal use out of Eq. (3.53), we would like to have a relation between $\tilde{G}$ and G.

If the system under consideration has a special anti-unitary symmetry (which we call "time-reversal"), such a relation between $\tilde{G}$ and G can indeed be found. We emphasize that the nomenclature "time-reversal" is only loosely related to the physical symmetry of inverting the direction of time.[21] In the context of the KMS condition, what we mean by "systems with time-reversal symmetry" is the following statement: There exists an anti-unitary operator Θ, which we associate with time-reversal. We may define tilded operators $\tilde{A} = \Theta A \Theta^\dagger$. Systems with time-reversal symmetry satisfy for the number operator $\tilde{N} = N$ and for the Green's function

$$G^{j|j'}_{q|q'}(t|t') = G^{j|j'}_{\tilde{q}|\tilde{q}'}(t|t')|_{\tilde{H}}, \tag{3.56}$$

where $\tilde{q}$ is the time-reversed quantum number q (i.e. $\tilde{q}$ corresponds to Θq) and the right-hand side is time-evolved with the time-reversed Hamiltonian $\tilde{H}$. One can further show that

$$\tilde{G}^{j|j'}_{q|q'}(t|t') = G^{\bar{j}'|\bar{j}}_{\tilde{q}'|\tilde{q}}(-t'|-t)|_{\tilde{H}}, \tag{3.57}$$

such that the KMS condition Eq. (3.53) becomes

$$\exp\left(\beta\Delta^{j|j'}(\omega|\omega')\right) G^{j|j'}_{q|q'}(\omega|\omega') = \xi^{m^{j|j'}} G^{j'|j}_{\tilde{q}'|\tilde{q}}(\omega'|\omega)|_{\tilde{H}} = \xi^{m^{j|j'}} G^{j'|j}_{q'|q}(\omega'|\omega). \tag{3.58}$$

For a single-particle Green's function, Eq. (3.58) leads to the well-known FDT $G^K = (1 - 2n_F)(G^R - G^A)$. So, in equilibrium, on the single particle level there is only one independent Keldysh component, G^R (recall that $G^A = (G^R)^\dagger$).

What happens in the two-particle case? First, let us note that in the two-particle case there are in principle $2^4 = 16$ Keldysh components. One combination ($G^{qq|qq}$) vanishes (c.f. Sec. 3.2).

[20] Some components, e.g. $\tilde{G}$ with only plus indices and G with only minus indices are trivially the same. On the one-particle level, we can identify each Keldysh component of $\tilde{G}$ with a Keldysh component of G. For an arbitrary number of particles this is no longer the case.

[21] Systems exhibiting "physical" time-reversal invariance possess the anti-unitary symmetry we require. Systems that do not exhibit physical time-reversal invariance (e.g. electrons in a finite magnetic field) may still exhibit the symmetry we require.

Of the remaining 15 components, 8 can be extracted through KMS conditions out of the remaining 7 components ([WH02] gives the explicit relations for bosons; in their notation, an index a roughly corresponds to our index q, while r roughly corresponds to c; We say "roughly" because the normalization of the Keldysh-rotation differs; the calculation for fermions may be performed in a similar manner). If we further use the transformation rules under complex conjugation and particle exchange, of the 7 components only 3 independent components remain, e.g. $G^{cq|qq}$, $G^{cc|qq}$ and $G^{cq|cq}$.

As far as we can tell, it is not possible to further reduce the number of components without additional symmetries. However, within certain approximations, we may have additional constraints reducing the number of independent components. For example, in the coupled ladder approximation of fRG (channel decomposition; see Sec. 4.4) in equilibrium each channel is characterized completely by a single component.

As a final remark on the KMS conditions, we note that the KMS conditions may also be derived from a symmetry of the generating functional [SCG+15].

3.6.4 Relation between Keldysh and Matsubara Correlation Functions

Let us briefly consider the relation between the Keldysh and the Matsubara formalism. Clearly, we have to restrict the comparison to the equilibrium setup (as the Matsubara formalism is only applicable in equilibrium). In equilibrium, the single-particle Green's function on the Keldysh contour is fully determined by G^R through either Hermitian conjugation (to obtain G^A) or a fluctuation-dissipation theorem (yielding G^K). $G^R(\omega)$ is analytic in the upper half plane and in fact related to the Matsubara single-particle Green's function $G(i\omega_n)$.[22] Is a similar statement true for multi-particle Green's functions?

This question has been answered in part by [AB92, Wel05]: If there are only three or less times appearing in the Green's function (in the sense that the single-particle Green's function depends on two times or the two-particle Green's function on four times), there is a unique identification between Matsubara and Keldysh correlation functions. If there are four or more times, one Keldysh component can readily be identified with a region in complex frequency space: $G^{cq\ldots q|q\ldots q}$.[23] Unfortunately, every other analytically continued expression but the one identified with $G^{cq\ldots q|q\ldots q}$ contains a correlation function that cannot be expressed through the Keldysh Green's functions ([Wel05] gives the explicit expression for all other correlation functions computed from analytically continuing the Matsubara frequencies; the correlation functions appearing are of the type exemplified in Eq. (3.3)). There does not appear to exist a linear combination of these analytical continuations that can be represented as a two-particle Keldysh Green's function.

Note that if we use an extension of the contour to a double-contour (which extends from $t = -\infty$ to $t = \infty$, then winds back to $t = -\infty$, and then repeats this process before going down to $t = -\infty - \beta$), then we can of course represent all possible two-particle orderings. In this double-contour, the analytical continuation is thus clear. However, the naïve number of

[22] If we analytically continue the single-particle Matsubara Green's function $G(i\omega_n)$ to the real axis from positive ω_n, we obtain $G^R(\omega)$.

[23] c.f. (ii) at the end of Sec. 3.2.

Keldysh components of the two-particle vertex grows from $2^4 = 16$ to $4^4 = 256$.

If we were required to perform the analytical continuation, we would recommend to write down all 256 components, and then use exchange of particles, complex conjugation, trivial identification (e.g. the correlation function between all operators on the first forward contour and all operators on the second forward contour are obviously identical), and the KMS condidtions to reduce the number of components as far as possible, keeping the components obtained from analytical continuation as given functions. It is in principle straightforward but tedious to check if the resulting set of equations is solvable for all components not obtained through analytical continuation.

Chapter 4

The Functional Renormalization Group

The functional Renormalization Group (fRG) is a powerful method to compute correlation functions in quantum systems. Since a large number of excellent reviews and derivations exist in the context of condensed matter theory [JPS10a, JPS10b, KEM06, MSH+12, AEKM08], here we will keep the derivation short and emphasize the aspects related to the details we need here as they appear. We will also emphasize specific points of view, which are useful to better understand the objects we are dealing with, but are not discussed in the reviews treating systems most similar to the QPC we consider.

Before we start with the basic idea of fRG, let us briefly examine *why* we even want to use Keldysh-fRG:

1. Analytics is almost impossible for our system of interest. While it is known how to solve fermionic systems in one dimension with short-ranged interactions and linear dispersion through bosonization, we are interested in the physics occuring as the potential barrier intersects the chemical potential. Thus, approximating the dispersion as linear would neglect essential physics, namely that of slow electrons, while for a quadratic dispersion an exact solution is not known. Futhermore, the two conventional approximations to inhomogenuities – adiabatic and point-like – fail as the relevant physics occurs at the intrinsic length scale of the impurity.

2. We desire real frequency information. Once we have consigned ourselves to using a computer, analytical continuation becomes challenging, if not impossible. However, in order to give a new and meaningful contribution to the ongoing discussion, information at real frequencies is necessary. This means that we require a scheme which directly works on either the real axis or at real times.

3. The system is large. We solve an open system of about 40 to 60 sites (and two semi-infinite leads). If we use less sites, artifacts of the discretization start to appear and the barrier is no longer smooth (recall that we intend to resolve a parabola).

4. Ultimately, we would like to obtain information at finite source-drain bias voltage. The Keldysh-formalism naturally allows for an inclusion of finite source-drain bias voltage, directly yielding the steady state.

These issues put severe demands on any method attempting to solve the problem. Since fRG is a comparatively cheap method (when compared to exact methods like DMRG or Monte-Carlo) and previous studies clearly indicated that we were in a regime where fRG could be expected to work reasonably well [BHS+13], Keldysh-fRG seems a natural path to pursue. Now, let us start by briefly explaining the basic idea of fRG.

4.1 Basic Idea

Consider a quantum system described by a generating functional

$$Z[J] = \langle \mathcal{T} \exp\left((J,\Phi)\right)\rangle = \int \mathcal{D}\{\Phi\} \exp\left[iS[\Phi] + (J,\Phi)\right], \tag{4.1}$$

where we call J a "source", Φ stands for arbitrary fields (in this first part, we omit any sign factors related to fermionic statistics as they distract from the underlying ideas), S is the action and we use the shorthand

$$(J,\Phi) = i \int dt \sum_{\alpha} J_\alpha(t)\Phi_\alpha(t). \tag{4.2}$$

α is a multi-index, denoting e.g. spin, position, contour, particle species, etc. Time-ordered correlation functions are obtained by taking functional derivatives of Z w.r.t. J and then setting $J = 0$, e.g.

$$\langle \mathcal{T}\Phi_\uparrow(t_1,x_1)\Phi_\downarrow(t_2,x_2)\rangle = \frac{1}{i^2}\delta_{J_\uparrow(t_1,x_1)}\delta_{J_\downarrow(t_2,x_2)}Z[J]|_{J=0}. \tag{4.3}$$

We note that most of the physically interesting correlation functions can be represented in this way.[1] We will call correlation functions with n field operators "n-point correlation functions" (note that there are different conventions regarding this nomenclature: sometimes "n-point correlation function" refers not to the number of field operators, but rather to the number of different space and time arguments appearing). The generating functional is generically difficult to compute. Instead of attempting to directly evaluate $Z[J]$, we may approach the problem by inserting an artificial parameter Λ in the action

$$Z[\Lambda, J] = \int \mathcal{D}\{\Phi\} \exp\left[iS[\Lambda,\Phi] + (J,\Phi)\right], \tag{4.4}$$

such that for some value of Λ, say $\Lambda = 0$, we recover the generating functional $Z[J] = Z[\Lambda = 0, J]$. If we are able to solve the model for some other value of Lambda, i.e. if e.g. $Z[\Lambda \to \infty, J]$ is known, and we can compute $\partial_\Lambda Z[\Lambda, J]$ in terms of quantities evaluated only at Λ, then we

[1] Actually, *all* correlation functions may be represented in this manner, if we perform a trick similar to the doubling of the contour when we introduced the Keldysh-indices: Consider a non-time-ordered correlation function $\langle \mathcal{O}_1(t_1)\dots\mathcal{O}_n(t_n)\rangle$. We now introduce one contour that goes back and forth along the real axis $n/2$ times (for the usual Keldysh-contour, $n = 1$). We may attribute a specific part of the contour with each operator $\mathcal{O}_i$ in such a manner that the correlation function we are interested in is ordered with respect to the contour. $\mathcal{T}$ then has to be changed to ordering along this contour, and the action actually contains n time integrals.

However, for most applications, it is sufficient to consider either purely retarded correlation functions, or time-ordered correlation functions, both of which can be represented in the usual Keldysh formalism.

may recover $Z[0, J]$ by integrating the derivative starting from the solvable initial condition. This is the essential idea of fRG.

Of course, in practice, there are some useful tricks in the application of this idea, which we will explain in more detail later:

1. It turns out that it is better to consider not the generating functional of correlation functions $Z[J]$, but rather the generating functional of 1-particle irreducible vertices $W[\bar{\Phi}]$.

2. A convenient way of implementing Λ is to have it appear only in the quadratic part of the action, in such a way that the bare Green's function vanishes for $\Lambda \to \infty$.

4.1.1 The 1PI generating functional

It is useful to split the action S appearing in the generating functional $Z[J]$ into two parts,

$$S[\Phi] = S_0[\Phi] + S_{\text{int}}[\Phi], \tag{4.5}$$

and expanding $\exp[iS] = \exp[iS_0] \sum_n S_{\text{int}}^n/n! = \exp[i\Phi G_0^{-1}\Phi] \sum_n S_{\text{int}}^n/n!$ (note that we are working with functional integrals, such that the Φs appearing are numbers [possibly Grassmann-valued], *not* operators). If S_0 is a quadratic function of Φ, then Wick's theorem applies and we may derive the usual diagrammatic representation of the generating functional [Wei95, Sre07, NO88]. Note that a truncation in the sum makes sense if S_0 already captures the main physics (i.e. if the bare degrees of freedom coincide with the degrees of freedom at the energy scale at which we probe the system). If the low-energy degrees of freedom are contained already in S_0, we will call the system "perturbative". fermions in high dimensions (three or larger) with weak repulsive interactions are a perturbative system in this sense, while non-charged superconductors at energies below the single-particle gap are not (assuming S_0 denotes the action of free electrons; below the gap, the relevant degrees of freedom in the bulk are Cooper-pairs). In particular, perturbative systems do not exhibit a spontaneous breaking of a continuous symmetry relative to the quadratic part of the action. For a perturbative system, it makes sense to normalize the generating functional with respect to the non-interacting (i.e. $S_{\text{int}} = 0$) generating functional in the absence of sources, which we call $Z_0[0]$. We thus define

$$W[J] = Z[J]/Z_0[0]. \tag{4.6}$$

We may define the generating functional of *connected* diagrams as:

$$W^c[J] = \log(Z[J]/Z_0[0]). \tag{4.7}$$

The Legendre transformation of W^c, which in the fRG context usually is defined as

$$\Gamma[\bar{\Phi}] = -W^c[J] - (J, \bar{\Phi}) + (\bar{\Phi}^\dagger, G_0^{-1}\bar{\Phi}), \tag{4.8}$$

with

$$\bar{\Phi} = \partial_J W^c \tag{4.9}$$

as the expectation value of Φ, is the 1PI generating functional.[2] Since the fields $\overline{\Phi}$ are numbers, the $\dagger$ appearing in the the Legendre transformation is a purely formal expression. It should be read as complex conjugation, which for fermions includes a conjugation in the Grassmann basis. In a perturbative theory, it makes sense to expand Γ around $\overline{\Phi} = 0$ to obtain a set of vertices $\{\gamma_p\}$:

$$\Gamma[\overline{\Phi}] = \sum_n \frac{(-i)^{n/2}}{n!} \gamma_p^n \overline{\Phi}^n. \tag{4.10}$$

To see why this is useful, let us consider some correlation function. It may be computed from the generating functional $Z[J]$. $Z[J]$ is given by the inverse Legendre transformation of Γ. To determine $Z[J]$, we thus need to find the saddle-points of Γ. If we think of Γ as an action, we are looking for the (semi-)classical solutions, which are given by adding all tree-level diagrams generated by γ. We thus identify the γ_p^n with full, amputated 1PI vertices. Note that we usually would identify γ_p^2 with the inverse full Green's function. However, because the way we defined the Legendre-transformation, γ_p^2 is actually only the negative self-energy.

Comment 1: In the case of spontaneous symmetry breaking, we may of course still perform all of the above steps to arrive at a set of γ_p^n's. However, there are some subtleties involved ([Wei96], chapter 16): If a symmetry is spontaneously broken, the generating functional is usually not a convex function of the source. The Legendre-transformation thus yields the Legendre-transform of the convex hull of the generating functional. In the context of spontaneous symmetry breaking, we may exemplify the meaning of this by considering a typical Mexican hat potential. The convex hull is obtained by a Maxwell construction. The Legendre-transform minimizes the energy given an expectation value $\overline{\Phi}$. In a Mexican hat potential, if $\overline{\Phi} = 0$, we may consider a superposition of the different vacua which has minimal energy (i.e. the energy of the vacua) and yet averages to an expectation value of zero. This is precisely the form obtained by a Maxwell construction. It is then clear that in the case of spontaneous symmetry breaking, an expansion of the 1PI generating functional around $\overline{\Phi} = 0$ is not necessarily as useful as in the perturbative case. In this work, however, we remain firmly in the perturbative regime.

Comment 2: In a model with the unbroken $\mathbb{Z}_2$-symmetry $\Phi \to -\Phi$ we have $\gamma_p^{2n+1} = 0$.[3] [4]

Comment 3: Once we leave the perturbative regime, the expansion Eq. (4.10) is usually a bad idea. Thankfully, in most cases, the expansion itself clearly indicates this by having the full vertex γ_p^4 become large compared to the bare vertex. We may use the size of γ_p^4 as an indication for the "perturbativity" of our system.

[2] At this stage, we start to be somewhat imprecise, as the precise statements distract from the essential ideas. We will clean up the details in Sec. 4.3.1

[3] This $\mathbb{Z}_2$-symmetry is usually present for fermions; in relativistic systems this may be related to a super-selection rule [WWW52]. Since the super-selection rule can be traced to the behavior of fermions under time-reversal (a state with an odd number of fermions picks up an additional minus sign), we will assume the same super-selection rule here.

[4] In fact, linearly realized symmetries of the action that are not anomalous also appear in the 1PI generating functional [ZJ02].

4.2 Simplifications for the model at hand

Before we derive the fRG equations as used in this work, let us specify some properties of our system, which are important when deriving the fRG equations:

1. We describe only fermionic degrees of freedom, no bosons appear as explicit degrees of freedom, i.e. Φ is a Grassmann field. To distinguish the specific case considered here from general statements, we will call the fermionic field ψ.
2. ψ will be labeled by either frequency ω or time t, site i, spin σ, and Keldysh index α. We group all labels into a multi-index ρ. To distinguish between particles and holes, we use ψ (which annihilates a particle or creates a hole) and $\bar{\psi}$ (which creates a particle or annihilates a hole).
3. The model has an unbroken global $U(1)$-symmetry $\psi_\rho \to \exp(i\gamma)\psi_\rho$. It is an actual symmetry of the full quantum system (i.e. not anomalous).
4. While we may explicitly break the spin $SU(2)$ symmetry by including a magnetic field, this symmetry is not broken spontaneously.
5. We work with a reduced generating functional, where some degrees of freedom (the leads) have been integrated out (c.f. Sec. 3.3), and only effective degrees of freedom with finite lifetime remain in the system.

In the case considered here it is useful to expand in the n-particle vertex γ^n instead of the $2n$-vertex γ_p^{2n}:

$$\Gamma[\bar{\Phi}] = \sum_n \frac{(-i)^n}{(n!)^2} \sum_{j'_1,\dots,j'_n} \sum_{j_1,\dots,j_n} \gamma^n(j'_1,\dots,j'_n;j_1,\dots j_n)\bar{\psi}_{j'_1}\dots\bar{\psi}_{j'_n}\psi_{j_n}\dots\psi_{j_1}, \tag{4.11}$$

where $j_k^{(\prime)}$ contains all relevant quantum numbers.

4.3 fRG on the level of the connected generating functional: flow equations

In order to derive the flow equations, we first consider the derivative of the normalized generating functional:

$$\dot{W}[\eta,\bar{\eta}] = \frac{d}{d\Lambda}W = \frac{d}{d\Lambda}\left[\frac{1}{Z_0}\int \mathcal{D}\{\tilde{\psi}\}\exp\left(S_0 + iS_{\text{int}} - (\bar{\tilde{\psi}},\eta) - (\bar{\eta},\tilde{\psi})\right)\right], \tag{4.12}$$

where we have labeled the sources for $\tilde{\psi}$ ($\bar{\tilde{\psi}}$) with $\bar{\eta}$ (η).[5] The dot denotes a derivative with respect to the flow parameter Λ. We write

$$S_0 = (\bar{\tilde{\psi}}, G_0^{-1}\tilde{\psi}) \tag{4.13}$$

[5] Throughout this section, we will use tildes to denote the field we integrate over (i.e. the name of the integration-variable). The expectation value of a field (or better: the new variable introduced in the Legendre-transform) we denote without tildes. We use bars to distinguish between creation and annihilation of particles.

and assume that G_0 is the only quantity in the exponent of Eq. (4.12) that explicitly depends on Λ. We thus obtain

$$\dot{W}[\eta,\bar{\eta}] = -\frac{\dot{Z}_0}{Z_0}W[\eta] + i\partial_\Lambda\left(G_0^{-1}\right)\partial_\eta\partial_{\bar{\eta}}W \tag{4.14}$$

$$\Rightarrow \dot{W}^c = \frac{d}{d\Lambda}\log W = -\frac{\dot{Z}_0}{Z_0} + \frac{1}{W}i\partial_\Lambda\left(G_0^{-1}\right)\partial_\eta\partial_{\bar{\eta}}W \tag{4.15}$$

Our first goal is to re-express $\dot{W}^c$ in terms of its "natural" quantities: W^c and G. To this end, we note that $\dot{Z}_0 = Tr\left(G_0\dot{G}_0^{-1}\right)$ and $W = e^{W^c}$. Eq. (4.15) may thus be written as

$$\dot{W}^c = -Tr\left(G_0\dot{G}_0^{-1} - i\dot{G}_0^{-1}\partial_{\bar{\eta}}W^c\partial_\eta W^c - i\dot{G}_0^{-1}\partial_{\bar{\eta}}\partial_\eta W^c\right), \tag{4.16}$$

where we have used the trick $x_iA_{ij}y_j = \mathrm{Tr}\left(A(yx^T)\right)$ for normal numbers and $x_iA_{ij}y_j = -Tr\left(A(yx^T)\right)$ if x and y are Grassmann-odd numbers.

To obtain the flow of the 1PI generating functional, we need to perform the Legendre transformation, Eqs. (4.8) and (4.9), of Eq. (4.16). Note that the Legendre transformation entails a change of coordinates. With the introduction of Λ, there are two simple choices: (i) have $\overline{\psi}$ depend on Λ, or (ii) have η depend on Λ. We will go with option (ii), i.e. we fix the same value of ψ for each Λ. With this in mind, we actually have to change Eq. (4.16) to

$$\dot{W}^c\left[\bar{\eta},\eta\right] = -Tr\left(G_0\dot{G}_0^{-1} - i\dot{G}_0^{-1}\partial_{\bar{\eta}}W^c\partial_\eta W^c - i\dot{G}_0^{-1}\partial_{\bar{\eta}}\partial_\eta W^c\right) + \dot{\bar{\eta}}\partial_{\bar{\eta}}W^c + \dot{\eta}\partial_\eta W^c. \tag{4.17}$$

Inserting into the Legendre transformation and using Eq. (4.9) we obtain

$$\begin{aligned}\dot{\Gamma}\left[\overline{\psi},\psi\right] &= -\dot{W}^c - \left(\overline{\psi},\dot{\eta}\right) - \left(\dot{\bar{\eta}},\psi\right) + \left(\overline{\psi},\dot{G}_0^{-1}\psi\right)\\ &= Tr\left[G_0\dot{G}_0^{-1} + i\dot{G}_0^{-1}\partial_{\bar{\eta}}\partial_\eta W^c\right]|_{\overline{\psi}=-i\partial_\eta W^c,\psi=i\partial_{\bar{\eta}}W^c}.\end{aligned} \tag{4.18}$$

The next step is to figure out if there is a convenient way of expressing $\partial_{\bar{\eta}}\partial_\eta W^c$ in terms of Γ and ψ. Naively, $\partial_{\bar{\eta}}\partial_\eta W^c$ is related to the single-particle Green's function (however, note that it is not directly proportional to the Green's functions, as the sources are not necessarily put to zero). It is however reasonable to expect some relation between $\partial_{\bar{\eta}}\partial_\eta W^c$ and the self-energy type term $\partial_\psi\partial_{\overline{\psi}}\Gamma$ (if ψ is not put to zero, this is unrelated to the self-energy). We thus compute

$$\begin{aligned}\partial_\psi\Gamma &= -\partial_\psi\eta\underbrace{\partial_\eta W^c}_{i\overline{\psi}} - \partial_\psi\bar{\eta}\underbrace{\partial_{\bar{\eta}}W^c}_{-i\psi} + \left(\overline{\psi},\partial_\psi\eta\right) - \left(\partial_\psi\bar{\eta},\psi\right) + i\bar{\eta} - i\overline{\psi}G_0^{-1}\\ &= i\bar{\eta} - i\overline{\psi}G_0^{-1},\\ \partial_{\overline{\psi}}\Gamma &= -\partial_{\overline{\psi}}\eta\underbrace{\partial_\eta W^c}_{i\overline{\psi}} - \partial_{\overline{\psi}}\bar{\eta}\underbrace{\partial_{\bar{\eta}}W^c}_{-i\psi} - i\eta + \left(\overline{\psi},\partial_{\overline{\psi}}\eta\right) - \left(\partial_{\overline{\psi}}\bar{\eta},\psi\right) + iG_0^{-1}\psi\\ &= -i\eta + iG_0^{-1}\psi,\end{aligned} \tag{4.19}$$

which implies

$$\begin{pmatrix} \partial_{\bar\psi}\partial_\psi\Gamma & \partial_{\bar\psi}\partial_{\bar\psi}\Gamma \\ \partial_\psi\partial_\psi\Gamma & \partial_\psi\partial_{\bar\psi}\Gamma \end{pmatrix} = \begin{pmatrix} i\partial_{\bar\psi}\bar\eta - iG_0^{-1} & -i\partial_{\bar\psi}\eta \\ i\partial_\psi\bar\eta & -i\partial_\psi\eta + iG_0^{-1T} \end{pmatrix}. \tag{4.20}$$

While Eq. (4.20) does not yet constitute the relation we are looking for, we may in addition consider the (trivial) equations

$$\begin{aligned} \begin{pmatrix} 1 & 0 \\ 0 & 1 \end{pmatrix} &= \begin{pmatrix} \partial_{\bar\psi}\bar\psi & \partial_{\bar\psi}\psi \\ \partial_\psi\bar\psi & \partial_\psi\psi \end{pmatrix} = \begin{pmatrix} -i\partial_{\bar\psi}\partial_\eta W^c & i\partial_{\bar\psi}\partial_{\bar\eta}W^c \\ -i\partial_\psi\partial_\eta W^c & i\partial_\psi\partial_{\bar\eta}W^c \end{pmatrix} \\ &= \begin{pmatrix} -i\partial_{\bar\psi}\eta\partial_\eta\partial_\eta W^c - i\partial_{\bar\psi}\bar\eta\partial_{\bar\eta}\partial_\eta W^c & i\partial_{\bar\psi}\eta\partial_\eta\partial_{\bar\eta}W^c + i\partial_{\bar\psi}\bar\eta\partial_{\bar\eta}\partial_{\bar\eta}W^c \\ -i\partial_\psi\eta\partial_\eta\partial_\eta W^c - i\partial_\psi\bar\eta\partial_{\bar\eta}\partial_\eta W^c & i\partial_\psi\eta\partial_\eta\partial_{\bar\eta}W^c + i\partial_\psi\bar\eta\partial_{\bar\eta}\partial_{\bar\eta}W^c \end{pmatrix} \\ &= \begin{pmatrix} \partial_{\bar\psi}\bar\eta & -\partial_{\bar\psi}\eta \\ \partial_\psi\bar\eta & -\partial_\psi\eta \end{pmatrix} \begin{pmatrix} -i\partial_{\bar\eta}\partial_\eta W^c & i\partial_{\bar\eta}\partial_{\bar\eta}W^c \\ i\partial_\eta\partial_\eta W^c & -i\partial_\eta\partial_{\bar\eta}W^c \end{pmatrix} \\ &\overset{4.20}{=} \underbrace{\begin{pmatrix} -i\partial_{\bar\psi}\partial_\psi\Gamma + iG_0^{-1} & -i\partial_{\bar\psi}\partial_{\bar\psi}\Gamma \\ -i\partial_\psi\partial_\psi\Gamma & -i\partial_\psi\partial_{\bar\psi}\Gamma - iG_0^{-1T} \end{pmatrix}}_{=:A_\Gamma} \underbrace{\begin{pmatrix} -i\partial_{\bar\eta}\partial_\eta W^c & i\partial_{\bar\eta}\partial_{\bar\eta}W^c \\ i\partial_\eta\partial_\eta W^c & -i\partial_\eta\partial_{\bar\eta}W^c \end{pmatrix}}_{=:A_W} \end{aligned} \tag{4.21}$$

If we read Eq. (4.21) as matrix equation, we see that

$$\partial_{\bar\eta}\partial_\eta W^c = i\left(A_\Gamma^{-1}\right)_{1,1}. \tag{4.22}$$

Inserting into Eq. (4.18), we obtain the flow

$$\dot\Gamma\left[\bar\psi,\psi\right] = Tr\left[G_0\dot G_0^{-1} - \dot G_0^{-1}\left(A_\Gamma^{-1}\right)_{1,1}\right]. \tag{4.23}$$

In order to get a handle on A_Γ^{-1}, it is useful to write it as

$$\begin{aligned} \left(A_\Gamma^{-1}\right)_{11} &= \begin{pmatrix} -i\partial_{\bar\psi}\partial_\psi\Gamma + iG_0^{-1} & -i\partial_{\bar\psi}\partial_{\bar\psi}\Gamma \\ -i\partial_\psi\partial_\psi\Gamma & -i\partial_\psi\partial_{\bar\psi}\Gamma - iG_0^{-1T} \end{pmatrix}_{11} \\ &= \left(\left[\begin{pmatrix} G^{-1} & 0 \\ 0 & -G^{-1T} \end{pmatrix} + \begin{pmatrix} U & -i\partial_{\bar\psi}\partial_{\bar\psi}\Gamma \\ -i\partial_\psi\partial_\psi\Gamma & -U^T \end{pmatrix}\right]^{-1}\right)_{11}, \; U = -i\partial_{\bar\psi}\partial_\psi\Gamma - G^{-1} + iG_0^{-1} \\ &= \left(\left[\begin{pmatrix} 1 & 0 \\ 0 & 1 \end{pmatrix} + \begin{pmatrix} G & 0 \\ 0 & -G^T \end{pmatrix}\begin{pmatrix} U & -i\partial_{\bar\psi}\partial_{\bar\psi}\Gamma \\ -i\partial_\psi\partial_\psi\Gamma & -U^T \end{pmatrix}\right]^{-1}\begin{pmatrix} G & 0 \\ 0 & -G^T \end{pmatrix}\right)_{11} \\ &= G - GUG + GUGUG + G\partial_{\bar\psi}\partial_{\bar\psi}\Gamma G^T\partial_\psi\partial_\psi\Gamma G + \dots. \end{aligned} \tag{4.24}$$

If we expand the flow Eq. (4.23), using the definition Eq. (4.11) and the expansion Eq. (4.24), by comparing coefficients of powers of ψ, we obtain the equations

$$\dot\gamma^1_{1'1} = S_{22'}\gamma^2_{1'2';12}, \tag{4.25}$$

$$\begin{aligned} \dot\gamma^2_{1'2';12} = S_{33'}\big(&\gamma^3_{1'2'3';123} - \gamma^2_{3'4;12}G_{4'4}\gamma^2_{1'2';4'3} - \gamma^2_{1'3';14}G_{44'}\gamma^2_{2'4';23} \\ &+\gamma^2_{2'3';14}G_{44'}\gamma^2_{1'4';23} + \gamma^2_{1'3';24}G_{44'}\gamma^2_{2'4';13} - \gamma^2_{2'3';24}G_{44'}\gamma^2_{1'4';13}\big). \end{aligned} \tag{4.26}$$

Here, we have introduced the *single-scale propagator*

$$S = G\dot{G}_0^{-1}G. \tag{4.27}$$

Upon inspection, we see that Eqs. (4.25) and (4.26) do not constitute a closed set of equations, as we require input from γ^3. This is actually a generic feature of the expansion: The flow of γ^n will require input of γ^{n+1}. Before we delve into the approximations used in this work, let us briefly mention some properties of the flow equations Eqs. (4.25) and (4.26) and the objects therein:

1. The flow of γ^n can be obtained by drawing all 1PI diagrams containing the available vertices γ^m with a single loop and then substituting one Green's function within the loop by S. We sum over all possible diagrams and all ways of substituting a Green's function by S. In particular, this implies that the flow of the n-particle vertex contains the $n+1$-particle vertex. We thus obtain an infinite hierarchy of flow equations.
2. If the interacting part of the bare model contains only a two-particle interaction of strength u, then $\gamma^n \sim u^n$ for $n > 2$.

4.3.1 Minor correction

We have cheated somewhat when introducing the 1PI generating functional. Let us clean this up: The Legendre transformation L is actually defined for *real* functions f as

$$L(f)(p) = \sup_x \left(xp - f(x)\right). \tag{4.28}$$

If the function f is convex, then $xp - f$ is concave and the supremum coincides with the extremum of $xp - f$, which is determined by $\partial_x(xp - f) = 0$, yielding $p = \partial_x f$ (assuming f is sufficiently nice). With this in mind, for differentiable, convex, real functions f we might as well define the Legendre transformation as

$$L(f)(p) = xp - f(x),\ p = \partial_x f, \tag{4.29}$$

as is usually done in physics.[6] In the case discussed above, we would like to identify f as the generating functional of connected diagrams W^c, x as the source J, and p as the new field $\overline{\Phi}$.

Comment: The generating functional is usually a complex function. In fact, for a non-interacting model, we have

$$Z[J] = \exp\left((J, G_0 J)\right) \tag{4.30}$$

(recall that the brackets are defined with a factor of i, Eq. (4.2)). For complex functions, we may use the definition Eq. (4.29), but we need to keep in mind that it now refers to stationary points, not necessarily minima of the function. However, this is perfectly fine, as in a perturbative model stationary points are unique, and we can invert the Legendre transformation as defined in Eq. (4.29). After a Wick-rotation (in a Euclidean space-time) the non-interacting model actually has a convex generating functional. This follows from the fact that we impose stability (a lower bound on the spectrum of the Hamiltonian).

[6] Note that we have to be able to invert the relation $p = \partial_x f$ to obtain $x(p)$, which we then use in $L(f)(p) = xp - f(x)$ to make the right-hand-side a function of p.

4.4 Truncating the flow; Channel decomposition

In practice, the flow Eq. (4.23) is approximated. While different approximation schemes are possible, in this work we use a perturbative scheme: We expand the flow equations in terms of the vertices and set the 3-particle vertex (and all higher vertices) to zero throughout the flow. At weak interaction strength u, this means that we keep all terms of order u^2, but neglect some terms of order u^3. Note that due to the resummation occurring by solving the flow we still take into account some diagrams of arbitrary order.

We also note that such a truncation violates the symmetries of the underlying action: For a given global, continuous symmetry, we may derive Ward-identities, which usually relate vertices of different particle numbers (c.f. Sec. 5.2, or [ZJ02, Kat04]). Any approximation which simply neglects one vertex thus usually violates at least some Ward-identities, i.e. symmetries.

As further approximation, we decompose the 2-particle vertex into channels as

$$\gamma^2 \approx \bar{v} + \gamma_P^2 + \gamma_X^2 + \gamma_D^2, \tag{4.31}$$

where $\bar{v}$ is the bare interaction.

At this stage, additional details are required: While we may associate each of the channels with a possible two-particle pairing, depending on how the quantum numbers are introduced, the labeling of the channels may differ, as they usually are related through symmetries (e.g. exchange of external legs). In general, the vertex γ^2 depends on three frequencies (assuming temporal translational invariance), four positions (provided we break spatial translational invariance), four Keldysh indices, and two spins (provided spin [in the $U(1)$, not necessarily the $SU(2)$ sense, i.e. the number of up spins and the number of down spins is conserved] is conserved). In the leading order (i.e. second order in the on-site interactions), each channel corresponds to one possible type of contraction. Restricting to the structure obtained already in second order, each channel depends only on one frequency, two positions, one Keldysh index, and one spin (in the X- and P-Channel, the spins of the in-going particles have to be different, in the D-Channel they have to be the same). Using the symmetries (see Sec. 3.6), we may restrict to vertices where the spins are arranged according to the scheme $\sigma\tau|\sigma\tau$. For the spatial indices, the spin indices, and the frequency dependence (which is that of Ref. [BHS+13]) we use:

$$\begin{aligned}\gamma^{\sigma\tau|\sigma\tau}_{i'j'|ij}(\omega_1', \omega_2'; \omega_1, \omega_2) \approx{}& \bar{v}^{\sigma\bar{\sigma}|\sigma\bar{\sigma}}_{ij|ij}\delta_{i'i}\delta_{ij}\delta_{j'j}\delta^{\bar{\sigma}\tau} + \varphi^{P\,\sigma\bar{\sigma}|\sigma\bar{\sigma}}_{i'i'|ii}(\omega_1+\omega_2)\delta_{i'j'}\delta_{ij}\delta^{\bar{\sigma}\tau} \\ &+ \varphi^{X\,\sigma\bar{\sigma}|\sigma\bar{\sigma}}_{i'i|ii'}(\omega_2-\omega_1')\delta_{i'j}\delta_{j'i}\delta^{\bar{\sigma}\tau} + \varphi^{D\,\sigma\sigma|\sigma\sigma}_{i'j|i'j}(\omega_2-\omega_2')\delta_{i'i}\delta_{j'j}\delta^{\sigma\tau},\end{aligned} \tag{4.32}$$

We arrange the Keldysh structure according to the convention

$$\gamma^{\alpha\beta|\gamma\delta} = \begin{pmatrix} (qq|qq) & (qq|cq) & (qq|qc) & (qq|cc) \\ (cq|qq) & (cq|cq) & (cq|qc) & (cq|cc) \\ (qc|qq) & (qc|cq) & (qc|qc) & (qc|cc) \\ (cc|qq) & (cc|cq) & (cc|qc) & (cc|cc) \end{pmatrix}. \tag{4.33}$$

The channels are labeled as (the Keldysh structure corresponds to Eqs. (A8,A11,A17) of Ref. [JPS10a])

$$(\varphi^P)^{\uparrow\downarrow|\uparrow\downarrow}_{ii|jj}(\Pi) = \begin{pmatrix} 0 & a^{P*}_{ji} & a^{P*}_{ji} & 0 \\ a^P_{ij} & b^P_{ij} & b^P_{ij} & a^P_{ij} \\ a^P_{ij} & b^P_{ij} & b^P_{ij} & a^P_{ij} \\ 0 & a^{P*}_{ji} & a^{P*}_{ji} & 0 \end{pmatrix} (\Pi), \tag{4.34a}$$

$$(\varphi^X)^{\uparrow\downarrow|\uparrow\downarrow}_{ji|ij}(X) = \begin{pmatrix} 0 & a^{X*}_{ji} & a^X_{ij} & b^X_{ij} \\ a^X_{ij} & b^X_{ij} & 0 & a^{X*}_{ji} \\ a^{X*}_{ji} & 0 & b^X_{ij} & a^X_{ij} \\ b^X_{ij} & a^X_{ij} & a^{X*}_{ji} & 0 \end{pmatrix} (X), \tag{4.34b}$$

$$(\varphi^D)^{\sigma\sigma|\sigma\sigma}_{ij|ij}(\Delta) = \begin{pmatrix} 0 & a^D_{ij} & a^{D*}_{ji} & b^D_{ij} \\ a^D_{ij} & 0 & b^D_{ij} & a^{D*}_{ii} \\ a^{D*}_{ji} & b^D_{ij} & 0 & a^D_{ij} \\ b^D_{ij} & a^{D*}_{ji} & a^D_{ij} & 0 \end{pmatrix}^{\sigma\sigma} (\Delta). \tag{4.34c}$$

Each channel is labeled by only two spatial indices and one frequency. Conceptually, it can be thought of as the propagator of a Hubbard-Stratonovitch particle of the corresponding channel with retarded (a^P, a^D, and a^{X*}) and Keldysh (b^P, b^D, and b^X) components. From this point of view it is not surprising that in equilibrium the channels satisfy the fluctuation-dissipation theorems (c.f. Eqs. (A10,A13,A19) of Ref. [JPS10a], or section 3.6.3):

$$b^{P\,(\sigma\bar{\sigma})}_{(ij)}(\Pi) = 2i \coth\left[\beta\left(\frac{\Pi}{2} - \mu\right)\right] \operatorname{Im} a^{P\,(\sigma\bar{\sigma})}_{(ij)}(\Pi) \tag{4.35a}$$

$$b^{X\,(\sigma\bar{\sigma})}_{(ij)}(X) = -2i \coth\left[\frac{\beta X}{2}\right] \operatorname{Im} a^{X\,(\sigma\bar{\sigma})}_{(ij)}(X) \tag{4.35b}$$

$$b^{D\,(\sigma\sigma)}_{(ij)}(\Delta) = 2i \coth\left[\frac{\beta\Delta}{2}\right] \operatorname{Im} a^{D\,(\sigma\sigma)}_{(ij)}(\Delta) \tag{4.35c}$$

We note that – due to the symmetries of complex conjugation and particle exchange – there are no more independent components. Consider e.g. $(\varphi^P)^{\downarrow\uparrow|\uparrow\downarrow}_{ii|jj}(\Pi)$. Using particle exchange we have $(\varphi^P)^{\downarrow\uparrow|\uparrow\downarrow}_{ii|jj}(\Pi) = -(\varphi^P)^{\uparrow\downarrow|\uparrow\downarrow}_{ii|jj}(\Pi)$. Similarly all other components may be eliminated.

While the representation Eq. (4.34) is not the most general representation, it is the most general representation obtainable by the approximated flow we use (c.f. Ref. [JPS10a]).[7]

[7] In Sec. 3.6.3, we stated that it is possible in equilibrium to reduce the vertex to three Keldysh components. Here, each channel is – in equilibrium – determined by a single Keldysh component. This makes sense on a simple, physical level: Each channel may be thought of as some quasi-particle excitation (associate each channel with a Hubbard-Stratonovitch field). In the channel decomposition, the vertex determines the propagation of one channel-particle (the corresponding Hubbard-Stratonovitch field). On a single particle level, one Keldysh component is sufficient to capture the physics. So, one Keldysh component should suffice to describe the propagation of a single Hubbard-Stratonovitch field. In the same spirit, we will call the a's "retarded" (for the P- and $D-$channel) or "advanced" (for the X-channel).

4.4.1 The Flow Equations

When all vertices higher than the 2-particle vertex are set to zero, the resulting truncated flow equations are (c.f. Eqs. (27,28) of Ref. [JPS10a])

$$\begin{aligned}
\frac{d}{d\Lambda}\Sigma^{\Lambda}_{1'1} &= -\sum\!\!\!\!\!\!\int_{2'2} \frac{i}{2\pi}\gamma^{\Lambda}_{1'2'12}S^{\Lambda}_{22'} \\
\frac{d}{d\Lambda}\gamma^{\Lambda}_{1'2'12} &= +\sum\!\!\!\!\!\!\int_{3'4'34} \frac{i}{2\pi}\gamma^{\Lambda}_{1'2'34}S^{\Lambda}_{33'}G^{\Lambda}_{44'}\gamma^{\Lambda}_{3'4'12} \\
&\quad +\sum\!\!\!\!\!\!\int_{3'4'34} \frac{i}{2\pi}\gamma^{\Lambda}_{1'4'32}\left[S^{\Lambda}_{33'}G^{\Lambda}_{44'} + S^{\Lambda}_{44'}G^{\Lambda}_{33'}\right]\gamma^{\Lambda}_{3'2'14} \\
&\quad -\sum\!\!\!\!\!\!\int_{3'4'34} \frac{i}{2\pi}\gamma^{\Lambda}_{1'3'14}\left[S^{\Lambda}_{33'}G^{\Lambda}_{44'} + S^{\Lambda}_{44'}G^{\Lambda}_{33'}\right]\gamma^{\Lambda}_{4'2'32}.
\end{aligned} \tag{4.36}$$

Here, 1, $1'$ etc. are multi-indices encompassing spin, site and frequency. In the flow of the vertex, each summand corresponds to a single channel. The vertex of each summand will be approximated by the contribution of the corresponding channel for all frequencies and the feedback of the other channels at a specific frequency ($\mu_L + \mu_R$ for the P-channel, 0 for the X- and D-channels). Inserting the channel decomposition with the above notations into the flow equations, the flow of the self-energy is given by [compare Eqs. (B3,B4) of Ref. [JPS10a]; For illustration purposes, we will give the detailed steps for the derivation of the flow of the P-Channel in the appendix 10]:

$$\begin{aligned}
\partial_\Lambda \Sigma^{q|c(\sigma)}_{(kl)}(\omega) = -\frac{i}{2\pi}\int d\omega' \Big[& S^{c|c(\bar\sigma)}_{(lk)}(\omega')a^{P\,(\sigma\bar\sigma)}_{(kl)}(\omega+\omega') + S^{c|c(\bar\sigma)}_{(kl)}(\omega')a^{X\,(\sigma\bar\sigma)}_{(lk)}(\omega'-\omega) \\
& - S^{c|c(\sigma)}_{(kl)}(\omega')a^{D\,(\sigma\sigma)}_{(kl)}(\omega-\omega') + S^{q|c(\bar\sigma)}_{(lk)}(\omega')b^{P\,(\sigma\bar\sigma)}_{(kl)}(\omega+\omega') \\
& + S^{c|q(\bar\sigma)}_{(kl)}(\omega')b^{X\,(\sigma\bar\sigma)}_{(lk)}(\omega'-\omega) - S^{c|q(\sigma)}_{(kl)}(\omega')b^{D\,(\sigma\sigma)}_{(kl)}(\omega-\omega') \\
& + S^{c|c(\bar\sigma)}_{(lk)}(\omega')U_k/2\delta_{kl} + \sum_m S^{c|c(\sigma)}_{(mm)}(\omega')a^{D\,(\sigma\sigma)}_{(km)}(0)\delta_{kl}\Big]
\end{aligned} \tag{4.37a}$$

and

$$\begin{aligned}
\partial_\Lambda \Sigma^{q|q(\sigma)}_{(kl)}(\omega) = -\frac{i}{2\pi}\int d\omega' \Big[& S^{c|q(\bar\sigma)}_{(kl)}(\omega')a^{X\,(\sigma\bar\sigma)}_{(lk)}(\omega'-\omega) - S^{c|q(\sigma)}_{(kl)}(\omega')a^{D\,(\sigma\sigma)}_{(kl)}(\omega-\omega') \\
& + S^{q|c(\bar\sigma)}_{(lk)}(\omega')a^{P\,(\sigma\bar\sigma)}_{(kl)}(\omega+\omega') + S^{c|q(\bar\sigma)}_{(lk)}(\omega')a^{P*\,(\sigma\bar\sigma)}_{(lk)}(\omega'+\omega) \\
& + S^{q|c(\bar\sigma)}_{(kl)}(\omega')a^{X*\,(\sigma\bar\sigma)}_{(kl)}(\omega'-\omega) - S^{q|c(\sigma)}_{(kl)}(\omega')a^{D*\,(\sigma\sigma)}_{(lk)}(\omega-\omega') \\
& + S^{c|c(\bar\sigma)}_{(lk)}(\omega')b^{P\,(\sigma\bar\sigma)}_{(kl)}(\omega+\omega') + S^{c|c(\bar\sigma)}_{(kl)}(\omega')b^{X\,(\sigma\bar\sigma)}_{(lk)}(\omega'-\omega)
\end{aligned}$$

$$- S^{c|c(\sigma)}_{(kl)}(\omega') b^{D\,(\sigma\sigma)}_{(kl)}(\omega-\omega') + \left(S^{c|q(\bar\sigma)}_{(lk)}(\omega') + S^{q|c(\bar\sigma)}_{(lk)}(\omega')\right) U_k/2\delta_{kl}\Big]. \tag{4.37b}$$

The flow of the vertex contains two bubbles

$$I^{pp}_{ab|a'b'}(\omega)^{(\sigma_1\sigma_2)}_{(ij|kl)} = \frac{i}{2\pi}\int d\omega' \Big[G^{a|a'(\sigma_1)}_{(i|k)}(\omega/2+\omega') S^{b|b'(\sigma_2)}_{(j|l)}(\omega/2-\omega') + S^{a|a'(\sigma_1)}_{(i|k)}(\omega/2+\omega') G^{b|b'(\sigma_2)}_{(j|l)}(\omega/2-\omega')\Big], \tag{4.38}$$

$$I^{ph}_{ab|a'b'}(\omega)^{(\sigma_1\sigma_2)}_{(ij|kl)} = \frac{i}{2\pi}\int d\omega' \Big[G^{a|a'(\sigma_1)}_{(i|k)}(-\omega/2+\omega') S^{b|b'(\sigma_2)}_{(j|l)}(\omega/2+\omega') + S^{a|a'(\sigma_1)}_{(i|k)}(-\omega/2+\omega') G^{b|b'(\sigma_2)}_{(j|l)}(\omega/2+\omega')\Big], \tag{4.39}$$

and is given by (compare Eqs. (C3,C6,C9) of Ref. [JPS10a])

$$\begin{aligned}
&\partial_\Lambda (\varphi^P)^{qq|cq}_{(\sigma\bar\sigma|\sigma\bar\sigma)(ii|jj)}(\Pi) = \partial_\Lambda a^{P*\,(\sigma\bar\sigma)}_{(ij)}(\Pi)\\
&= \sum_{km}\left(\tfrac{1}{2}U_k\delta_{kj} + a^{P*}(\Pi)^{(\sigma\bar\sigma)}_{(kj)} + \tfrac{1}{2}U^{X\,(\sigma\bar\sigma)}_{(kj)}\right)\left(I^{pp}_{cq|cc}(\Pi)^{(\sigma\bar\sigma|\sigma\bar\sigma)}_{(kk|mm)} + I^{pp}_{qc|cc}(\Pi)^{(\sigma\bar\sigma|\sigma\bar\sigma)}_{(kk|mm)}\right)\\
&\quad\times\left(\tfrac{1}{2}U_m\delta_{im} + a^{P*}(\Pi)^{(\sigma\bar\sigma)}_{(im)} + \tfrac{1}{2}U^{X\,(\sigma\bar\sigma)}_{(im)}\right)
\end{aligned} \tag{4.40a}$$

$$\begin{aligned}
&\partial_\Lambda (\varphi^X)^{qq|cq}_{(\sigma\bar\sigma|\sigma\bar\sigma)(ji|ij)}(X) = \partial_\Lambda a^{X*}(X)^{(\sigma\bar\sigma)}_{(ji)}\\
&= \sum_{kl}\left(\tfrac{1}{2}U_j\delta_{jk} + \tfrac{1}{2}U^{P\,(\sigma\bar\sigma)}_{(jk)} + a^{X*}(X)^{(\sigma\bar\sigma)}_{(jk)}\right)\left(I^{ph}_{qc|cc}(X)^{(\sigma\bar\sigma|\sigma\bar\sigma)}_{lk|kl} + I^{ph}_{cc|cq}(X)^{(\sigma\bar\sigma|\sigma\bar\sigma)}_{lk|kl}\right)\\
&\quad\times\left(\tfrac{1}{2}U_i\delta_{il} + \tfrac{1}{2}U^{P\,(\sigma\bar\sigma)}_{(li)} + a^{X*}(X)^{(\sigma\bar\sigma)}_{(li)}\right)
\end{aligned} \tag{4.40b}$$

$$\begin{aligned}
&\partial_\Lambda (\varphi^D)^{cq|qq}_{(\sigma\sigma)(ij|ij)}(\Delta) = \partial_\Lambda a^D(\Delta)^{(\sigma\sigma)}_{(ij)}\\
&= -\sum_{kl}\Big[\left(-\tfrac{1}{2}W^{D\,(\sigma\sigma)}_{(ik)} + a^D(\Delta)^{(\sigma\sigma)}_{(ik)}\right)\left(I^{ph}_{qc|cc}(\Delta)^{(\sigma\sigma|\sigma\sigma)}_{(lk|kl)} + I^{ph}_{cc|cq}(\Delta)^{(\sigma\sigma|\sigma\sigma)}_{(lk|kl)}\right)\\
&\qquad\times\left(-\tfrac{1}{2}W^{D\,(\sigma\sigma)}_{(lj)} + a^D(\Delta)^{(\sigma\sigma)}_{(lj)}\right)\\
&\quad + \left(\tfrac{1}{2}U_i + \tfrac{1}{2}U^{P\,(\sigma\bar\sigma)}_{(ik)} + \tfrac{1}{2}U^{X\,(\sigma\bar\sigma)}_{(ik)}\right)\delta_{ik}\left(I^{ph}_{qc|cc}(\Delta)^{(\bar\sigma\bar\sigma|\bar\sigma\bar\sigma)}_{(lk|kl)} + I^{ph}_{cc|cq}(\Delta)^{(\bar\sigma\bar\sigma|\bar\sigma\bar\sigma)}_{(lk|kl)}\right)\delta_{jl}\\
&\qquad\times\left(\tfrac{1}{2}U_j + \tfrac{1}{2}U^{P\,(\bar\sigma\sigma)}_{(jl)} + \tfrac{1}{2}U^{X\,(\bar\sigma\sigma)}_{(jl)}\right)\Big]
\end{aligned} \tag{4.40c}$$

$$\begin{aligned}
&\partial_\Lambda (\varphi^P)^{cq|cq}_{(\sigma\bar\sigma)(ii|jj)}(\Pi) = \partial_\Lambda b^P(\Pi)^{(\sigma\bar\sigma)}_{(ij)}\\
&= \sum_{km}\Big[\left(\tfrac{1}{2}U_i\delta_{ik} + a^P(\Pi)^{(\sigma\bar\sigma)}_{(ik)} + \tfrac{1}{2}U^{X\,(\sigma\bar\sigma)}_{(ik)}\right)\left(I^{pp}_{cc|cc}(\Pi)^{(\sigma\bar\sigma|\sigma\bar\sigma)}_{(kk|mm)} + I^{pp}_{qq|cc}(\Pi)^{(\sigma\bar\sigma|\sigma\bar\sigma)}_{(kk|mm)} + I^{pp}_{cc|qq}(\Pi)^{(\sigma\bar\sigma|\sigma\bar\sigma)}_{(kk|mm)}\right)
\end{aligned}$$

$$
\begin{aligned}
&\times \left(\tfrac{1}{2}U_j\delta_{jm} + a^{P*}(\Pi)^{(\sigma\bar{\sigma})}_{(jm)} + \tfrac{1}{2}U^{X\,(\sigma\bar{\sigma})}_{(jm)}\right) \\
&+ b^P(\Pi)^{(\sigma\bar{\sigma})}_{(ik)} \left(I^{pp}_{qc|cc}(\Pi)^{(\sigma\bar{\sigma}|\sigma\bar{\sigma})}_{(kk|mm)} + I^{pp}_{cq|cc}(\Pi)^{(\sigma\bar{\sigma}|\sigma\bar{\sigma})}_{(kk|mm)}\right) \left(\tfrac{1}{2}U_j\delta_{jm} + a^{P*}(\Pi)^{(\sigma\bar{\sigma})}_{(jm)} + \tfrac{1}{2}U^{X\,(\sigma\bar{\sigma})}_{(jm)}\right) \\
&+ \left(\tfrac{1}{2}U_i\delta_{ik} + a^{P}(\Pi)^{(\sigma\bar{\sigma})}_{(ik)} + \tfrac{1}{2}U^{X\,(\sigma\bar{\sigma})}_{(ik)}\right) \left(I^{pp}_{cc|qc}(\Pi)^{(\sigma\bar{\sigma}|\sigma\bar{\sigma})}_{(kk|mm)} + I^{pp}_{cc|cq}(\Pi)^{(\sigma\bar{\sigma}|\sigma\bar{\sigma})}_{(kk|mm)}\right) b^P(\Pi)^{(\sigma\bar{\sigma})}_{(mj)}\Big]
\end{aligned}
\tag{4.40d}
$$

$$
\begin{aligned}
&\partial_\Lambda(\varphi^X)^{qq|cc}_{ji|ij}(X) = \partial_\Lambda b^X(X)^{(\sigma\bar{\sigma})}_{(ij)} \\
&= \sum_{kl}\Big[\left(\tfrac{1}{2}U_k\delta_{kj} + \tfrac{1}{2}U^{P\,(\sigma\bar{\sigma})}_{(jk)} + a^X(X)^{(\sigma\bar{\sigma})}_{(kj)}\right) \left(I^{ph}_{cc|cc}(X)^{(\sigma\bar{\sigma}|\sigma\bar{\sigma})}_{kl|lk} + I^{ph}_{qc|cq}(X)^{(\sigma\bar{\sigma}|\sigma\bar{\sigma})}_{kl|lk} + I^{ph}_{cq|qc}(X)^{(\sigma\bar{\sigma}|\sigma\bar{\sigma})}_{kl|lk}\right) \\
&\quad \times \left(\tfrac{1}{2}U_l\delta_{il} + \tfrac{1}{2}U^{P\,(\sigma\bar{\sigma})}_{(il)} + a^{X*}(X)^{\sigma\bar{\sigma}}_{(li)}\right) \\
&\quad + b^X(X)^{(\sigma\bar{\sigma})}_{(kj)} \left(I^{ph}_{qc|cc}(X)^{(\sigma\bar{\sigma}|\sigma\bar{\sigma})}_{kl|lk} + I^{ph}_{cc|cq}(X)^{(\sigma\bar{\sigma}|\sigma\bar{\sigma})}_{kl|lk}\right) \left(\tfrac{1}{2}U_l\delta_{il} + \tfrac{1}{2}U^{P\,(\sigma\bar{\sigma})}_{(li)} + a^{X*}(X)^{\sigma\bar{\sigma}}_{li}\right) \\
&\quad + \left(\tfrac{1}{2}U_j\delta_{jk} + \tfrac{1}{2}U^{P\,(\sigma\bar{\sigma})}_{(jk)} + a^X(X)^{(\sigma\bar{\sigma})}_{(kj)}\right) \left(I^{ph}_{cq|cc}(X)^{(\sigma\bar{\sigma}|\sigma\bar{\sigma})}_{kl|lk} + I^{ph}_{cc|qc}(X)^{(\sigma\bar{\sigma}|\sigma\bar{\sigma})}_{kl|lk}\right) b^X(X)^{(\sigma\bar{\sigma})}_{(il)}\Big]
\end{aligned}
\tag{4.40e}
$$

$$
\begin{aligned}
&\partial_\Lambda(\varphi^D)^{cc|qq}_{(\sigma\sigma)(ij|ij)}(\Delta) = \partial_\Lambda b^D(\Delta)^{(\sigma\sigma)}_{(ij)} \\
&= -\sum_{kl}\Big[\left(-\tfrac{1}{2}W^{D\,\sigma\sigma}_{ik} + a^D(\Delta)^{(\sigma\sigma)}_{(ik)}\right) \cdot \left(I^{ph}_{cc|cc}(\Delta)^{(\sigma\sigma|\sigma\sigma)}_{(lk|kl)} + I^{ph}_{qc|cq}(\Delta)^{(\sigma\sigma|\sigma\sigma)}_{(lk|kl)} + I^{ph}_{cq|qc}(\Delta)^{(\sigma\sigma|\sigma\sigma)}_{(lk|kl)}\right) \\
&\quad \times \left(-\tfrac{1}{2}W^{D\,(\sigma\sigma)}_{(lj)} + a^{D*}(\Delta)^{(\sigma\sigma)}_{(jl)}\right) \\
&\quad + \left(-\tfrac{1}{2}W^{D\,(\sigma\sigma)}_{(ik)} + a^D(\Delta)^{(\sigma\sigma)}_{(ik)}\right) \left(I^{ph}_{qc|cc}(\Delta)^{(\sigma\sigma|\sigma\sigma)}_{(lk|kl)} + I^{ph}_{cc|cq}(\Delta)^{(\sigma\sigma|\sigma\sigma)}_{(lk|kl)}\right) b^D(\Delta)^{(\sigma\sigma)}_{(lj)} \\
&\quad + b^D(\Delta)^{(\sigma\sigma)}_{(ik)} \left(I^{ph}_{cq|cc}(\Delta)^{(\sigma\sigma|\sigma\sigma)}_{(lk|kl)} + I^{ph}_{cc|qc}(\Delta)^{(\sigma\sigma|\sigma\sigma)}_{(lk|kl)}\right) \left(-\tfrac{1}{2}W^{D\,(\sigma\sigma)}_{(jl)} + a^{D*}(\Delta)^{(\sigma\sigma)}_{(jl)}\right) \\
&\quad + \left(\tfrac{1}{2}U_i\delta_{ik} + \tfrac{1}{2}U^{P\,\sigma\bar{\sigma}}_{(ik)} + \tfrac{1}{2}U^{X\,\sigma\bar{\sigma}}_{(ik)}\right) \left(I^{ph}_{cc|cc}(\Delta)^{(\bar{\sigma}\bar{\sigma}|\bar{\sigma}\bar{\sigma})}_{(lk|kl)} + I^{ph}_{qc|cq}(\Delta)^{(\bar{\sigma}\bar{\sigma}|\bar{\sigma}\bar{\sigma})}_{(lk|kl)} + I^{ph}_{cq|qc}(\Delta)^{(\bar{\sigma}\bar{\sigma}|\bar{\sigma}\bar{\sigma})}_{(lk|kl)}\right) \\
&\quad \times \left(\tfrac{1}{2}U_l\delta_{lj} + \tfrac{1}{2}U^{P\,(\bar{\sigma}\sigma)}_{(lj)} + \tfrac{1}{2}U^{X\,(\bar{\sigma}\sigma)}_{(lj)}\right)\Big]
\end{aligned}
\tag{4.40f}
$$

The relative signs between the X- and the D-channel stem from the fact that they are related through exchange of two fermionic legs.

4.4.2 The Feedback

Since we introduced a decomposition of the two-particle vertex into channels, Eq. (4.32), we have to specify the mixing (or feedback) of the channels. In other words, we have to determine the quantities U^X, U^P, and W^D. We fix them by the following consideration: The feedback should be such, that the properties visible in second order in the interaction (which is the "natural" order when determining the channels) remain valid. The simplest way to ensure this is if the feedback is of the same structure as the bare interaction. In this case, the Keldysh-structure,

the analytical properties and the spatial and spin structure of the channels are conserved even with the feedback. This is clear because we know that these properties are conserved in the absence of feedback, and the feedback – if it has the structure of the bare interaction – only changes the value, but not the properties of the flow equation.

How can we construct a feedback that is of the same form as the bare interaction? First, let us recall the main properties of the bare interaction:

1. The bare interaction is purely local in space (i.e. the bare interaction is non-zero only if all four spatial indices take the same value).
2. The bare interaction conserves spin and charge (i.e. it contains the same number of creation and annihilation operators for each spin species).
3. The bare interaction is purely local in time (i.e. it is non-zero only if all times are equal).
4. The bare interaction is non-zero only if an odd number of Keldysh-indices are q(uantum).
5. The bare interaction is real.

These properties may be satisfied by the following choice:

1. We consider the diagonal part in space of the channels only.
2. Conservation of spin and charge was used during the definition of the channels to constrain the available indices.
3. The feedback is the same for all frequencies.
4. The feedback is completely determined by the "a" components of the channels, while we neglect the "b" components.
5. We may take the real part of the combination of the "a" that we choose.

So, what remains to be done is to fix a way of obtaining a frequency-independent number from the frequency-dependent diagonal part of the "a"s. In equilibrium, we know from the fluctuation-dissipation theorems that $a^P(2\mu)$, $a^X(0)$, and $a^D(0)$ are all real. It thus seems natural to use these numbers for the feedback, as they automatically satisfy the last condition. In non-equilibrium, the feedback is less clear, as these numbers are no longer real in a general setting. However, in the case of proportional coupling, $a^P(\mu_L+\mu_R)$, $a^X(0)$, and $a^D(0)$ are all real. We use this as justification to use the real part of the "a"s at these frequencies for the feedback, i.e. the interchannel feedback we use is given by

$$U^P = 2\mathrm{Re}a^P(\mu_L+\mu_R); \quad U^X = 2\mathrm{Re}a^X(0); \quad W^D_\sigma = 2\mathrm{Re}a^D_{\sigma\sigma}(0). \tag{4.41}$$

Since in our approximation the feedback has the same form as the bare vertex, there is a small trick we may use: If we consider the flow equations in the channel decomposition Eq. (4.37a) to (4.40f), and insert the specific feedback Eq. (4.41), we see that the bare vertex U never enters on its own. Rather, it always enters in the combination $U/2+a^P+a^X$ (diagonal in

real space). If we introduce $\tilde{a}^P = U/4 + a^P$, $\tilde{a}^X = U/4 + a^X$, we see that the flow-equations retain their form, but without the explicit bare vertex. In other words, the flow for Σ, $\tilde{a}^P$, $\tilde{a}^X$, and a^D, with a flow where we set $U = 0$ in the flow equations and $\tilde{a}^X = U/4 = \tilde{a}^P$ as initial condition yields the same result as the flow for Σ, a^P, a^X, and a^D, with the equations as written here and the initial condition $a^X = 0 = a^P$. By introducing the tilde quantities, we have absorbed the bare interaction in the P- and X-channels.

4.5 The choice of flow parameter

We choose the flow parameter following the considerations in Ref. [Jak10]: We want to ensure that the Green's function satisfies as many exact properties as possible. The flow parameter chosen here satisfies: Analytic properties ($G^R(\omega)$ is analytic in the upper half plane), fluctuation-dissipation-theorems in equilibrium, Fermi-liquid relations (e.g. $\Sigma^R(\omega = \mu)$ is real). The way to achieve this is to pick a "physical" flow parameter, where the relations are satisfied at each step of the flow. Note that we will usually not be able to satisfy Ward-identities in the truncation used.[8]

Here, we use as flow parameter a set of artificial leads. Heuristically, to each site we couple a flat lead, which at the beginning of the flow dominates the physics and is removed through the flow. In order to avoid artifacts due to a sharp transition between the physical leads and the central region, we couple the artificial leads to all sites, including the physical leads.

Mathematically, the flow parameter is determined by the bare retarded Green's function of the full system

$$\tilde{G}^R_{0,\Lambda,\sigma}(\omega) = \frac{1}{\omega \mathbb{1} - \tilde{H}^\sigma + i\left(\frac{1}{2}\Lambda\right)\mathbb{1}}, \tag{4.42}$$

where $\tilde{H}^\sigma$ is the non-interacting Hamiltonian matrix. Λ is the flow parameter, ranging from ∞ (start of flow) to 0 (end of flow). $\mathbb{1}$ is the unit matrix in the space of the sites, which we will omit from now on. The tilde denotes that we deal with the full system, not only the reduced system with an effective generating functional (c.f. Sec. 3.3).

Once the leads have been projected out, we drop the tilde on the restricted Hamiltonian matrix H^σ and the spatial indices then only run from $-N'$ to N'. We use the artificial on-site broadening for all sites (including the leads) to avoid artifacts at the transition from the lead to the central region.

The retarded single-scale propagator $\tilde{S}^R$ is

$$\tilde{S}^R(\omega) = \left(\tilde{G}\tilde{G}_0^{-1}\partial_\Lambda \tilde{G}_0 \tilde{G}_0^{-1}\tilde{G}\right)^R = -\frac{i}{2}\tilde{G}^R_\Lambda \cdot \tilde{G}^R_\Lambda, \tag{4.43}$$

where we omit the site and spin labels.

[8] While it is possible to interpret fluctuation-dissipation-theorems as Ward-Identities of a symmetry of the Keldysh action [SCG+15], the Ward-identities corresponding to this symmetry do not link vertices of different particle number. Thus, it is in fact not necessarily impossible to respect that symmetry even in a truncated flow (the flow parameter chosen here does in fact respect that symmetry).

After the integration over the leads' degrees of freedom has been performed, the Green's function projected onto the central part acquires an additional self-energy term

$$G_0^{R(\sigma)}(\omega) = \frac{1}{\omega^{(\sigma)} - \mathcal{H}^{(\sigma)} - \Sigma_{\text{lead}}^{(\sigma)R}(\omega, \Lambda) + i\Lambda/2}, \tag{4.44}$$

where $\omega^{(\sigma)} = \omega + \frac{\sigma}{2}B$ and

$$\begin{aligned}\Sigma_{\text{lead}\ ij}^{(\sigma)R}(\omega, \Lambda) = \frac{1}{2}\left(\omega^{(\sigma)} + i\tfrac{\Lambda}{2} - i\sqrt{4\tau^2 - \left(\omega^{(\sigma)} + i\tfrac{\Lambda}{2}\right)^2}\right) \\ \times \left(\delta_{i,-N'}\delta_{j,-N'} + \delta_{i,N'}\delta_{j,N'}\right).\end{aligned} \tag{4.45}$$

This self-energy is also reflected in the projected single-scale propagator, which now takes the form

$$\begin{aligned}S^R(\omega) &= \left(GG_0^{-1}\partial_\Lambda G_0 G_0^{-1} G\right)^R \\ &= G_\Lambda^R \cdot \left(-\frac{i}{2} + \partial_\Lambda \Sigma_{\text{lead}}^R(\omega, \Lambda)\right) \cdot G_\Lambda^R.\end{aligned} \tag{4.46}$$

For $\Lambda \to \infty$ the model is exactly solvable and the irreducible part of the full vertex is simply the bare vertex [JPS10b]. The Keldysh-components are determined via the relations

$$G^K = G^R\left(\Sigma^K + \Sigma_{\text{lead}}^K\right) G^A, \tag{4.47}$$

and

$$S^K(\omega) = \left(GG_0^{-1}\partial_\Lambda G_0 G_0^{-1} G\right)^K. \tag{4.48}$$

In equilibrium, G^K and S^K are determined through the FDT.

4.5.1 Initial conditions

In order to solve the flow Eqs. (4.37) and (4.40), we need to know the initial conditions, i.e. the value of the self-energy and the vertex at the beginning of the flow. If we start at some finite, but large value Λ_0, we have [JPS10b]

$$\Sigma(\Lambda_0) = U/2; \quad \gamma^2(\Lambda_0) = U/2. \tag{4.49}$$

The initial conditions are obtained by approximately solving the system at this large value of Λ_0: At large Λ, the physics is clearly dominated by the artificial leads. On each site, there is a number of electrons in accordance with the filling of the artificial leads, and hopping between sites is suppressed quite strongly. Since the artificial leads have infinite band-width, irrespective of the chemical potential and temperature the artificial leads are at half-filling. Thus, on each site we have one particle (the density of up- and down-electrons is one half each). The only contribution to the self-energy in this scenario stems from the first-order Hartree term, each other diagram is suppressed by positive powers of $1/\Lambda_0$. The Hartree term yields $\Sigma^\sigma = Un^{\bar{\sigma}}$, where n^τ is the filling of the species with spin τ. All loop-diagrams contributing to the vertex are suppressed by positive powers of $1/\Lambda_0$. To accuracy $\mathcal{O}(1/\Lambda_0)$, Eq. (4.49) thus yields the initial condition of the flow.

Chapter 5

The local current density

In field theory, any global, continuous symmetry leads to a local conservation equation. On the classical level, this conservation equation is a continuity equation. On the quantum level, two subtleties enter:

1. Anomalies: It is possible that a symmetry of the bare action is not a symmetry of the generating functional. This is the case if – in a functional integral – the measure is not invariant under the symmetry. In this case the symmetry is called anomalous and is not a real symmetry of the theory. A famous example is the chiral anomaly.

2. The continuity equation only holds in the weak sense, i.e. it is a relation for expectation values with certain operator insertions, not an operator identity. Furthermore, the continuity acquires a new name: The weak equations are called "Ward identities".

The classical continuity equation following from a continuous global symmetry is of the form

$$\partial_t q + \partial_x j = 0. \tag{5.1}$$

We will call q the *(Noether) charge* and j the *(Noether) current*. For the purpose of this section, we restrict ourselves to Abelian symmetries (we will be interested in the electric current, which is associated with a $U(1)$ symmetry).

5.1 Classical Field Theory

Before we go into the derivation of the Ward-identities, let us recall Noether's procedure for a classical field theory [ZJ02]. We will use the derivation which most easily generalizes to the quantum case: Let us consider the action of a complex bosonic scalar field in $d = \tilde{d} + 1$ total dimensions (of which $\tilde{d}$ are spatial dimensions)

$$\mathcal{S}_{\text{classical}}[\Phi] = \int d^d x \overline{\Phi} G^{-1} \Phi + \mathcal{S}_{\text{classical;int}}[\overline{\Phi}\Phi]. \tag{5.2}$$

For simplicity, we will assume that the interactions depend only on the combination $\overline{\Phi}\Phi$. This action has the global symmetry

$$\Phi \to \exp(i\alpha)\Phi; \quad \overline{\Phi} \to \exp(-i\alpha)\overline{\Phi} \tag{5.3}$$

A solution Φ_s to the equations of motion is obtained through a variational principle:

$$\delta\mathcal{S}_{\text{classical}}[\Phi_s] = 0. \tag{5.4}$$

The idea of Noether's theorem is to consider a variational direction which corresponds to a symmetry transformation, i.e. we consider the variation (for infinitesimal α)

$$\Phi(x) \to \Phi(x) + \delta\Phi(x) = \exp(i\alpha(x))\Phi(x) = \Phi(x) + i\alpha(x)\Phi(x) + \dots. \tag{5.5}$$

If Φ_s is a solution of the equations of motion, the action does not change under *any* infinitesimal change of Φ_s, so – in particular – the action does not change under the variation (5.5). Since the variation Eq. (5.5) is a symmetry-transformation for $\alpha = \text{const.}$, the change of the action under the variation must be proportional to derivatives of α. We thus obtain for the variation Eq. (5.5)

$$\delta\mathcal{S} \sim \int d^dx \partial_x\alpha \left(A(x)\right) = -\int d^dx \alpha\partial_x \left(A(x)\right) \overset{!}{=} 0. \tag{5.6}$$

We thus observe that the quantity $\partial_x \left(A(x)\right)$ vanishes for solutions of the equations of motion, i.e. A satisfies a continuity equation. We note that the continuity equation is only satisfied for fields solving the equations of motion (for fields not satisfying the equations of motion we cannot impose $\delta\mathcal{S} = 0$).

Let us turn to the specific example, Eq. (5.2): If we perform the transformation Eq. (5.5), we see that

$$\delta\mathcal{S} = \int d^dx \left(-i\alpha\overline{\Phi}G^{-1}\Phi + i\overline{\Phi}G^{-1}\left(\alpha\Phi\right)\right). \tag{5.7}$$

We note that $\mathcal{S}_{\text{classical;int}}$ does not contribute as it only depends on the combination $\overline{\Phi}\Phi$, which is invariant even under the gauged (local) variation Eq. (5.5). Further, we note that usually G^{-1} contains one or more derivatives (e.g. $G^{-1} = \Box$ (where $\Box$ denotes the d'Alembert operator) for a relativistic, massless field). As an example (which is almost relevant here), consider a non-relativistic field with quadratic dispersion $G^{-1} = i\partial_t - av\partial_x^2$, where a is a length and v a velocity:

$$G^{-1}\left(\alpha\Phi\right) = \left(i\partial_t - av\partial_x^2\right)\left(\alpha\Phi\right) = i\alpha\partial_t\Phi + i\partial_t\alpha\Phi - 2av\partial_x\alpha\partial_x\Phi - av\partial_x^2\alpha\Phi - av\alpha\partial_x^2\Phi. \tag{5.8}$$

Thus,

$$\begin{aligned}
\delta\mathcal{S} &= \int d^dx \left(-i\alpha\overline{\Phi}\left(i\partial_t - av\partial_x^2\right)\Phi + i\overline{\Phi}\left(i\alpha\partial_t\Phi + i\partial_t\alpha\Phi - 2av\partial_x\alpha\partial_x\Phi - av\partial_x^2\alpha\Phi - av\alpha\partial_x^2\Phi\right)\right) \\
&= \int d^dx \left(+i\overline{\Phi}\left(+i\partial_t\alpha\Phi - 2av\partial_x\alpha\partial_x\Phi - av\partial_x^2\alpha\Phi\right)\right) \\
&\overset{IP}{=} \int d^dx\alpha \underbrace{\left(\partial_t\left(\overline{\Phi}\Phi\right) + 2iav\partial_x\left(\overline{\Phi}\partial_x\Phi\right) - iav\partial_x^2\left(\overline{\Phi}\Phi\right)\right)}_{=A},
\end{aligned} \tag{5.9}$$

where we have integrated by parts in the last step. If we now write the equation $A = 0$, and interpret this equation as a continuity equation, we may identify the charge and current densities

$$0 = \partial_t \left(\bar{\Phi}\Phi\right) + \partial_x \left(2iav\bar{\Phi}\partial_x\Phi - iav\partial_x\left(\bar{\Phi}\Phi\right)\right) = \partial_t \underbrace{\left(\bar{\Phi}\Phi\right)}_{=\rho} + \partial_x \underbrace{\left(iav\bar{\Phi}\partial_x\Phi - iav\left(\partial_x\bar{\Phi}\right)\Phi\right)}_{=j}. \quad (5.10)$$

As generally expected, the charge looks like the overall density, while the current depends on the spatial change of the field.

In the following, we will essentially redo the above steps for the fermionic quantum system we are actually attempting to solve.

5.2 Ward Identities

We now turn to the quantum case and specify to the action (we now focus on the QPC at zero magnetic field; the derivation at finite magnetic field is perfectly analogous)

$$\mathcal{S} = \int dt \int dx \sum_\sigma \bar{\psi}_\sigma(x,t) G_0^{-1} \psi_\sigma(x,t) + U\bar{\psi}_\uparrow(x,t)\bar{\psi}_\downarrow(x,t)\psi_\uparrow(x,t)\psi_\downarrow(x,t). \quad (5.11)$$

Considering the generating functional

$$\mathcal{Z}[J] = \int \mathcal{D}\psi \exp\left(i\mathcal{S} + i\int dt \int dx \bar{J}\psi + i\int dt \int dx \bar{\psi}J\right), \quad (5.12)$$

we observe that we integrate over all configurations of ψ. Following [ZJ02] we consider the global change of coordinates in field space

$$\bar{\psi}(x,t) \to \exp\left[-i\alpha(x,t)\right]\bar{\psi}(x,t),\ \psi(x,t) \to \exp\left[i\alpha(x,t)\right]\psi(x,t), \quad (5.13)$$

where α is some smooth function of x, t. Clearly, $\mathcal{Z}[J]$ must be invariant under any valid reparametrization of the integration manifold, i.e. $\mathcal{Z}[J] \to \mathcal{Z}[J]$ for any $\alpha(x,t)$. Expanding the change of $\mathcal{Z}[J]$ in powers of α thus leads to a set of equations, of which we will use the linear order. We remark that the measure contains $\bar{\psi}$ and ψ at the same position in equal powers and is invariant under the change of coordinates Eq. (5.13).[1] We thus obtain for the change of the generating functional $\delta\mathcal{Z}$ to first order in α

$$\begin{aligned}\delta\mathcal{Z}[J] = \int \mathcal{D}\psi \exp\left(i\mathcal{S} + i\int dt \int dx \bar{J}\psi + i\int dt \int dx \bar{\psi}J\right) \\ \times \left(i\delta\mathcal{S} + i\int dt \int dx \bar{J}\psi(i\alpha) + i\int dt \int dx \bar{\psi}J(-i\alpha)\right) \stackrel{!}{=} 0,\end{aligned} \quad (5.14)$$

[1] For general symmetries, it is non-trivial to prove the absence of an anomaly. For the symmetry at hand, the absence of an anomaly is a well-known fact (e.g. [Wei96]).

Now, since for $\alpha = \text{const.}$ the action $\mathcal{S}$ is invariant, we know that $\delta\mathcal{S}$ is proportional to

$$\delta\mathcal{S} \sim \int dt \int dx \alpha \left(\partial_t q + \partial_x j\right). \tag{5.15}$$

Note that this expression for $\delta\mathcal{S}$ actually defines q and j.[2] It coincides with the classical expressions for q and j obtained by the Noether procedure. To proceed, we expand Eq. (5.14) in powers of J and obtain

$$J^0: \quad 0 = \langle \mathcal{T}\delta\mathcal{S}\rangle, \tag{5.16a}$$

$$\bar{J}_1 J_2: \quad 0 = \left\langle \mathcal{T}\left(-i\delta\mathcal{S}\psi_1\bar{\psi}_2 - i\psi_1\alpha_1\bar{\psi}_2 + i\psi_1\alpha_2\bar{\psi}_2\right)\right\rangle, \tag{5.16b}$$

where we have introduced the index 1, 2 to denote the arguments (x_1, t_1), (x_2, t_2).

Before proceeding with the Ward identities, let us take a closer look at $\delta\mathcal{S}$: The interaction part of $\mathcal{S}$ is of the density-density type. Since the density is invariant under the transformation Eq. (5.13), the interaction part of $\mathcal{S}$ does not contribute to the continuity equation. We are thus left with the quadratic part $\mathcal{S}_0$ of $\mathcal{S}$. For the model under consideration (we now go to discrete positions), we have

$$\mathcal{S}_0 = \int dt \sum_{ij} \bar{\psi}_i(t)\left(i\partial_t\delta_{ij} - H_{ij}\right)\psi_j(t), \tag{5.17}$$

where the matrix H is symmetric and only has non-vanishing entries $H_{ij} \neq 0$ for $|i-j| = 1$. Under the transformation Eq. (5.13) we obtain

$$\begin{aligned}
\delta\mathcal{S} = \delta\mathcal{S}_0 &= i\int dt \sum_{ij}\left[\left(\bar{\psi}_i(t)\left(i\partial_t\delta_{ij} - H_{ij}\right)\psi_j(t)\right)\left(-\alpha_i + \alpha_j\right) - \partial_t\alpha_j\bar{\psi}_i\psi_j\delta_{ij}\right] \\
&= i\int dt \sum_{ij}\left[\left(\bar{\psi}_i(t)\left(-H_{ij}\right)\psi_j(t)\right)\left(-\alpha_i + \alpha_j\right) - \partial_t\alpha_j\bar{\psi}_i\psi_j\delta_{ij}\right] \\
&= i\int dt \sum_{ij}\alpha_i(t)\left[-\left(\bar{\psi}_i(t)\left(-H_{ij}\right)\psi_j(t)\right) + \left(\bar{\psi}_j(t)\left(-H_{ji}\right)\psi_i(t)\right) + \partial_t\left(\bar{\psi}_i\psi_j\delta_{ij}\right)\right].
\end{aligned} \tag{5.18}$$

To get a better understanding of the expression Eq. (5.18), let us assume $\alpha_i(t) = \delta_{i0}\delta(t)$. Then:

$$\delta\mathcal{S} \sim +\bar{\psi}_0(t)H_{01}\psi_1(t) - \bar{\psi}_1(t)H_{10}\psi_0(t) + \bar{\psi}_0(t)H_{0-1}\psi_{-1}(t) - \bar{\psi}_{-1}(t)H_{-10}\psi_0(t) - \partial_t\left(\bar{\psi}_0\psi_0\right), \tag{5.19}$$

where we assumed that H only contains short-range hopping. Comparing Eq. (5.19) with Eq. (5.15), we identify the charge and current as

$$q_0(t) = -\bar{\psi}_0(t)\psi_0(t), \quad j_0(t) = +\bar{\psi}_0(t)H_{01}\psi_1(t) - \bar{\psi}_1(t)H_{10}\psi_0(t), \tag{5.20}$$

which have the physical interpretation as counting the number of charged particles on site 0 to obtain the charge and counting the number of charged particles moving between site 0 and site 1 to obtain the current. Note that the Noether procedure does not fix the overall scale of

[2] A unique identification of q and j is possible because G_0^{-1} does not mix space and time.

the current or the charge. However, the Noether procedure does fix the relative scale between charge and current.

Now that we have an expression for the current, we could proceed with the Ward identities. However, it is useful to first consider these expressions on the Keldysh-contour.

Upon instating the contour-indices, we obtain as Ward identities

$$J^0: \quad 0 = \langle \mathcal{T}_c \delta\mathcal{S} \rangle \,, \tag{5.21a}$$

$$\bar{J}_1 J_2: \quad 0 = \left\langle \mathcal{T}_c \left(-i\delta\mathcal{S} \psi_1^{a'} \bar{\psi}_2^{a''} - (-a') i \psi_1^{a'} \alpha_1^{a'} \bar{\psi}_2^{a''} + (-a'') i \psi_1^{a'} \alpha_2^{a''} \bar{\psi}_2^{a''} \right) \right\rangle , \tag{5.21b}$$

where

$$\delta\mathcal{S} = i \int dt \sum_{ij} \sum_{a=\pm} (-a) \alpha_i^a(t) \left[- \left(\bar{\psi}_i^a(t) \left(-H_{ij} \right) \psi_j^a(t) \right) + \left(\bar{\psi}_j^a(t) \left(-H_{ji} \right) \psi_i^a(t) \right) + \partial_t \left(\bar{\psi}_i^a \psi_j^a \delta_{ij} \right) \right] . \tag{5.22}$$

When introducing the contour-indices for α, we have made the choice $\alpha \to (-a)\alpha^a$. If we now redo the previous example, i.e. we set e.g. $\alpha_i^a(t) = \delta_{i0}\delta(t)\delta^{a-}$, we obtain:

$$\delta\mathcal{S} \sim + \bar{\psi}_0^-(t) H_{01} \psi_1^-(t) - \bar{\psi}_1^-(t) H_{10} \psi_0^-(t) + \bar{\psi}_0^-(t) H_{0-1} \psi_{-1}^-(t) - \bar{\psi}_{-1}^-(t) H_{-10} \psi_0^-(t) - \partial_t \left(\bar{\psi}_0^- \psi_0^- \right) . \tag{5.23}$$

As before, we would like to identify the density as $\bar{\psi}_0^- \psi_0^-$. However, this term is proportional to $G^{--} \sim G^K - G^R - G^A$. But we know that the particle density is proportional to $G^< \sim G^K + G^A - G^R$. The two results differ by $2G^A$ evaluated at equal times. The reason lies in the ordering of operators at equal times in the continuum and discrete time representation of the Keldysh action. We note that in the steady-state setup pursued here, on the level of the Ward identity, this difference does not matter, as the charge only enters via the the temporal derivative (which vanishes in a steady state) and the current does not suffer from this problem, as the ordering issues of operators at equal times on different sites do not arise. For now, we will proceed by ignoring the ordering subtlety.

We thus proceed naïvely and consider the term $\sim J^2$:

$$\begin{aligned}
0 = & \left\langle \mathcal{T}_c \left(\int dt \sum_{ij} \sum_{a=\pm} (-a) \alpha_i^a(t) \left[\bar{\psi}_i^a(t) H_{ij} \psi_j^a(t) - \bar{\psi}_j^a(t) H_{ji} \psi_i^a(t) + \partial_t \left(\bar{\psi}_i^a \psi_j^a \delta_{ij} \right) \right] \psi_1^{a'} \bar{\psi}_2^{a''} \right) \right\rangle \\
& + \left\langle \mathcal{T}_c \left(-(-a') i \psi_1^{a'} \alpha_1^{a'} \bar{\psi}_2^{a''} + (-a'') i \psi_1^{a'} \alpha_2^{a''} \bar{\psi}_2^{a''} \right) \right\rangle \\
= & \int dt \sum_{ij} \sum_{a=\pm} (-a) \alpha_i^a(t) \left\{ \left\langle \mathcal{T}_c \left(\left[\bar{\psi}_i^a(t) H_{ij} \psi_j^a(t) - \bar{\psi}_j^a(t) H_{ji} \psi_i^a(t) + \partial_t \left(\bar{\psi}_i^a \psi_j^a \delta_{ij} \right) \right] \psi_l^{a'}(t') \bar{\psi}_k^{a''}(t'') \right) \right\rangle \right. \\
& \qquad \left. + \left\langle \mathcal{T}_c \left(-\delta^{aa'} \delta(t-t') \delta_{il} i \psi_l^{a'}(t') \bar{\psi}_k^{a''}(t'') + \delta^{aa''} \delta(t-t'') \delta_{ik} i \psi_l^{a'}(t') \bar{\psi}_k^{a''}(t'') \right) \right\rangle \right\} \\
= & \int dt \sum_{ij} \sum_{a=\pm} (-a) \alpha_i^a(t) \left\{ -G^{aa'|a''a}_{jl|ki}(t,t'|t'',t) H_{ij} + G^{aa'|a''a}_{il|kj}(t,t'|t'',t) H_{ji} - \partial_t G^{aa'|a''a}_{jl|ki}(t,t'|t'',t) \delta_{ij} \right. \\
& \qquad \left. + \delta^{aa'} \delta(t-t') \delta_{ij} G^{a'|a''}_{j|k}(t'|t'') - \delta^{aa''} \delta(t-t'') \delta_{ik} G^{a'|a''}_{j|k}(t'|t'') \right\}
\end{aligned} \tag{5.24}$$

where we have used the definition of the Green's function and reinstated the labels $i, j, \ldots$ and $t, t', \ldots$ instead of 1 or 2. As Eq. (5.24) should hold for all $\alpha_i^a(t)$, we obtain

$$\begin{aligned} 0 = &- G^{aa'|a''a}_{jl|ki}(t,t'|t'',t)H_{ij} + G^{aa'|a''a}_{il|kj}(t,t'|t'',t)H_{ji} - \partial_t G^{aa'|a''a}_{jl|ki}(t,t'|t'',t)\delta_{ij} \\ &+ \delta^{aa'}\delta(t-t')\delta_{ij}G^{a'|a''}_{j|k}(t'|t'') - \delta^{aa''}\delta(t-t'')\delta_{ik}G^{a'|a''}_{j|k}(t'|t''). \end{aligned} \tag{5.25}$$

We see that we obtain a relation between one- and two-particle correlation functions.

If we had considered the term $\sim J^3$, we would have obtained a relation between one-, two-, and three-particle correlation functions. It is to be expected that an approximation of the flow corresponding to a truncation of any n-particle vertex will violate the Ward-identity linking the corresponding n-particle correlation function to other correlation functions (this violation does indeed appear).

5.3 Derivation of the local distribution function

We now have obtained an expression for the current flowing between the neighboring sites j and k (c.f. Eqs. (5.18) and (5.20)):[3]

$$\begin{aligned} j_{jk} &= -\frac{e}{\hbar}H_{jk}\left(G^{-+}_{jk}(t,t) - G^{-+}_{kj}(t,t)\right) \\ &= -\frac{e}{\hbar}H_{jk}\int\frac{d\omega}{2\pi}\left(G^{-+}_{jk}(\omega) - G^{-+}_{kj}(\omega)\right) \\ &= -\frac{e}{\hbar}H_{jk}\int\frac{d\omega}{2\pi}\left(G^K_{jk}(\omega) + G^A_{jk}(\omega) - G^R_{jk}(\omega) - G^K_{kj}(\omega) - G^A_{kj}(\omega) + G^R_{kj}(\omega)\right). \end{aligned} \tag{5.26}$$

We may now study the current between the system and an artificial lead coupling infinitesimally to a single site. To do so, let us assume that j is an index within the system and k is an index describing the site in the official lead coupled to j. For simplicity, we set the hopping between j and k to τ, i.e. $H_{jk} = \tau$, and control the importance of the artificial lead through its (decoupled) density of states on site k, i.e. the LDOS of the lead at site k if we set H_{jk} to zero. In order to eliminate the lead, we consider the Dyson equations

$$G^R_{jk} = \tau G^R_{jj}g^R_{kk}, \quad G^A_{jk} = \tau G^A_{jj}g^A_{kk}, \quad G^K_{jk} = \tau G^R_{jj}g^K_{kk} + \tau G^K_{jj}g^A_{kk}, \tag{5.27}$$

where g denotes the lead's Green's function in the absence of coupling between system and lead. Inserting the Dyson Eqs. (5.27) into the expression for the current Eq. (5.26), we obtain

$$\begin{aligned} j_{jk} = -\frac{e}{\hbar}\tau^2\int\frac{d\omega}{2\pi}&\left(G^R_{jj}(\omega)g^K_{kk}(\omega) + G^K_{jj}(\omega)g^A_{kk}(\omega) + G^A_{jj}(\omega)g^A_{kk}(\omega) - G^R_{jj}(\omega)g^R_{kk}(\omega)\right. \\ &\left. - g^R_{kk}(\omega)G^K_{jj}(\omega) - g^K_{kk}(\omega)G^A_{jj}(\omega) - g^A_{kk}(\omega)G^A_{jj}(\omega) + g^R_{kk}(\omega)G^R_{jj}(\omega)\right). \end{aligned} \tag{5.28}$$

In the artificial leads, we assume some distribution function $f_k(\omega)$, such that a generalized fluctuation-dissipation theorem is satisfied:

$$g^K = (1 - 2f_k)\left(g^R - g^A\right). \tag{5.29}$$

[3] Recall that we assume that the bare non-interacting Hamiltonian H is a real, symmetric matrix.

Inserting the generalized fluctuation-dissipation theorem Eq. (5.29) into Eq. (5.28), and defining

$$\Gamma_k(\omega) = \tau^2 \left(g^R_{kk}(\omega) - g^A_{kk}(\omega)\right), \tag{5.30}$$

the current into the artificial lead can be written as

$$j_{jk} = \frac{e}{\hbar}\tau^2 \int \frac{d\omega}{2\pi} \left[G^K_{jj}(\omega) - (1-2f_k(\omega))\left(G^R_{jj}(\omega) - G^A_{jj}(\omega)\right)\right] \Gamma_k(\omega). \tag{5.31}$$

We introduce the *local distribution function* $n_j(\omega)$ through the relation

$$G^K_{jj}(\omega) = (1-2n_j(\omega))\left(G^R_{jj}(\omega) - G^A_{jj}(\omega)\right), \tag{5.32}$$

and assume the existence of a solution for $n_j(\omega)$[4]. Inserting Eq. (5.32) into the current Eq. (5.31), we obtain

$$j_{jk} = \frac{e}{\hbar}\tau^2 \int \frac{d\omega}{2\pi} \left[-2n_j(\omega) + 2f_k(\omega)\right]\left(G^R_{jj}(\omega) - G^A_{jj}(\omega)\right) \Gamma_k(\omega). \tag{5.33}$$

We see that no current flows if $f_k(\omega) = n_j(\omega)$. This motivates the use of $n_j(\omega)$ as local distribution function: Instead of an artificial lead, we might have coupled an actual probing lead to the system. If we apply an ac-bias, the current through this probing lead would measure the frequency-dependent integrand of the current. If the states of the probing lead are occupied according to the local distribution function, the probing lead and the system are in local equilibrium and no current flows.

Later on, in Sec. 8.3, we will use the current into an artificial lead Eq. (5.33), to determine a flow where no electrons flow between the artificial leads and the system, thus improving the fRG-flow.

5.4 The local conductance

Once we have an expression for the local current (Eq. (5.26)), we may obtain an expression for the conductance as the derivative of the current with respect to the bias voltage $\mu_L - \mu_R$. We will assume that the voltage drops symmetrically, i.e. $\mu_L = \bar{\mu} + \frac{1}{2}\delta\mu$, $\mu_R = \bar{\mu} - \frac{1}{2}\delta\mu$. Thus, we need to compute[5]

$$\begin{aligned}
\mathfrak{G}_{jk} &= \partial_{V_{\mathrm{sd}}} j_{jk} \\
&= -\frac{e^2}{\hbar} H_{jk} \partial_{V_{\mathrm{sd}}} \int \frac{d\omega}{2\pi} \left(G^K_{jk}(\omega) + G^A_{jk}(\omega) - G^R_{jk}(\omega) - G^K_{kj}(\omega) - G^A_{kj}(\omega) + G^R_{kj}(\omega)\right) \\
&= -\frac{e^2}{\hbar} H_{jk} \partial_{V_{\mathrm{sd}}} \int \frac{d\omega}{2\pi} \left(G^R_{jl}\Sigma^K_{lm}G^A_{mk} + G^A_{jk} - G^R_{jk} - G^R_{kl}\Sigma^K_{lm}G^A_{mj} - G^A_{kj} + G^R_{kj}\right) \\
&= -\frac{e^2}{\hbar} H_{jk} \int \frac{d\omega}{2\pi} \Big(G^{R\prime}_{jl}\Sigma^K_{lm}G^A_{mk} + G^R_{jl}\Sigma^{K\prime}_{lm}G^A_{mk} + G^R_{jl}\Sigma^K_{lm}G^{A\prime}_{mk} + G^{A\prime}_{jk} - G^{R\prime}_{jk}
\end{aligned}$$

[4] Clearly, no unique solution for $n_j(\omega)$ can exist if $\mathrm{Im}G^R_{jj}(\omega) = 0$. In our setup, we have $\mathrm{Im}G^R_{jj}(|\omega| > 2\tau) = 0$ to a very good approximation. Unless indicated otherwise, we pick $n_j(\omega < -2\tau) = 1$ and $n_j(\omega > 2\tau) = 0$.

[5] To avoid confusion, in this section only, we will label the conductance by a gothic $\mathfrak{G}$.

$$-G^{R\prime}_{kl}\Sigma^{K}_{lm}G^{A}_{mj} - G^{R}_{kl}\Sigma^{K\prime}_{lm}G^{A}_{mj} - G^{R}_{kl}\Sigma^{K}_{lm}G^{A\prime}_{mj} - G^{A\prime}_{kj} + G^{R\prime}_{kj}\Big)\,, \tag{5.34}$$

where a prime denotes a derivative w.r.t. the bias voltage. We observe that

$$G^{R\prime} = \partial_{V_{\mathrm{sd}}}\frac{1}{\omega - H - \Sigma^{R}} = G^{R}\Sigma^{R\prime}G^{R}, \tag{5.35}$$

as the Hamiltonian H does not contain any information on the distribution functions.

We recall that the bias enters only in the distribution function of the leads in the absence of the central system. Thus, the bias enters only in the quadratic part of the generating action. However, we already know how to take derivatives of the self-energy with respect to a parameter appearing only in the quadratic part of the action: the fRG-equations (chapter 4).[6] Before we apply the fRG-equations, we remark that the self-energy Σ has two contributions: the lead contribution Σ_{lead} and the interaction-induced contribution Σ_{U}. The fRG-equations apply for the interaction-induced contribution, *not* the lead contribution. We thus have to write $\Sigma' = \Sigma_{\mathrm{lead}}{}' + \Sigma_{\mathrm{U}}{}'$, where only $\Sigma_{\mathrm{U}}{}'$ is determined by the fRG-equations, and $\Sigma_{\mathrm{lead}}{}'$ is "trivial". Since we intend to vary the distribution functions only and the leads are assumed to be in equilibrium,

$$\Sigma_{\mathrm{lead}}{}^{R\prime} = 0 = \Sigma_{\mathrm{lead}}{}^{A\prime}, \text{ and } \Sigma_{\mathrm{lead}}{}^{K\prime} = -2n'(\Sigma_{\mathrm{lead}}{}^{R} - \Sigma_{\mathrm{lead}}{}^{A}). \tag{5.36}$$

To determine $\Sigma_{\mathrm{U}}{}'$, we require the appropriate single-scale propagator S. S^K is the only non-vanishing component, as the Hamiltonian does not change as we vary the bias $\delta\mu$, and is given by

$$S^{K} = -\left(G\partial_{V_{\mathrm{sd}}}G_0^{-1}G\right)^{K} = G^{R}\partial_{V_{\mathrm{sd}}}\Sigma_{\mathrm{lead}}{}^{K}G^{A}. \tag{5.37}$$

If we insert Eqs. (5.35), (5.36), and (5.37) into Eq. (5.34), we obtain the schematic answer

$$\mathfrak{G}_{jk} = -\frac{e^2}{\hbar}H_{jk}\int\frac{d\omega}{2\pi}\left(+G^{R}_{jl}\Sigma_{\mathrm{lead}}{}^{K\prime}_{lm}G^{A}_{mk} - G^{R}_{kl}\Sigma_{\mathrm{lead}}{}^{K\prime}_{lm}G^{A}_{mj} + F[n, n', G, \gamma^{(2)}]\right), \tag{5.38}$$

where F depends on the leads' distribution functions n, its derivative n', the Green's functions G and the two-particle vertex γ.[7] F vanishes if the two-particle vertex is zero (e.g. in a non-interacting system).

Eq. (5.38), when read in the spirit of Eq. (5.33), has a simple physical interpretation: For simplicity, let us first consider a system at zero temperature. If the system is non-interacting, the current is determined by the number of particles that traverse the system within the bias window. If we infinitesimally increase the bias window, more particles traverse the system. These particles have energies at the edges of the old bias window and are fully responsible for the conductance. This type of physics corresponds to the first two summands in Eq. (5.38). If we now turn on interactions, we introduce two additional effects: The transmission probability of particles at the edges of the bias window is different (which is still modeled by the first two summands of Eq. (5.38), which contain the full Green's functions), and the transmission

[6] Note that the fRG-equations are in principle exact, i.e. the (schematic) equation $\partial_\Lambda\Sigma = \gamma^2 S$ is always satisfied, provided we have computed the two-particle vertex γ^2 and the Green's function exactly.

[7] Eq. (5.38) constitutes a straightforward extension of the conductance equations proposed in [Ogu01, HBSvD17].

of particles within the bias window is different (naïvely, a larger bias window may lead to a larger density, which induces a higher potential barrier; this change of transmission probability within the bias window is modeled by the last term in Eq. (5.38)). At finite temperature, this interpretation is enriched by a smearing of the distribution functions.

Finally, we note that if an fRG implementation that can deal with arbitrary single-scale propagators already exists, it is most useful to employ this implementation to determine Σ' and insert Σ' into the Eqs. (5.35) and (5.34), directly yielding the conductance.

Chapter 6

Publication: Spin fluctuations in the 0.7-anomaly in quantum point contacts

Now that we have introduced the physical system and model (chapter 2), and the method (chapter 4 and chapter 3), let us take a closer look at what we can learn about the model. This closer look was performed in the publication [SBv17].[1] The dynamical properties of the model Eq. (2.6) are analyzed in detail. It is found that a parabolic barrier in a one-dimensional model is able to qualitatively reproduce the universal behavior of the 0.7 anomaly as a function of temperature. The 0.7 anomaly goes hand in hand with a pinning of the maximum of the LDOS to the chemical potential, leading to an enhancement of interaction effects throughout the whole subopen region. As the temperature is increased, the large LDOS at the chemical potential opens up a large phase-space for (back-)scattering, leading to a suppression of the conductance throughout the whole subopen region. In order to connect different attempts at explaining the 0.7 anomaly, we have compared the characteristic time scales of spin excitations and the single-particle traversal time. While we find no indication of truly static spin configurations, we do find that the time scale of spin excitations is of the same size as the single-particle traversal time. Since the spin excitations are spatially aligned over the range of the QPC, we may interpret the findings as follows: If there is some finite excitation energy within the system (we need finite energy to activate the spin excitations), the electrons traversing the QPC experience a quasi-static, spatially extended spin polarized background. While this background does fluctuate as function of time and space, on the length scale of the QPC ($\sim l_{\mathrm{x}}$) and the time scale of traversing the QPC, the background changes only little.

The supplement of [SBv17] gives more details and the technical aspects, explains the form of the spin excitations, and compares the fRG results to DMRG computations.

The DMRG computations were performed by Benedikt Bruognolo, while the supervision and conception of the project were due to Jan von Delft. The rest of the publication was due to Dennis Schimmel.

In the following chapters we will explain more on the frequency (dynamical) structure of

[1] In this chapter, this copy of the thesis differs from the copy handed in by the fact that the publication itself is used instead of the preprint.

the QPC (chapter 7) and the technical details (chapter 8).

Spin Fluctuations in the 0.7 Anomaly in Quantum Point Contacts

Dennis H. Schimmel,[1] Benedikt Bruognolo,[1,2] and Jan von Delft[1]
[1]*Physics Department, Arnold Sommerfeld Center for Theoretical Physics, and Center for NanoScience, Ludwig-Maximilians-Universität, Theresienstraße 37, 80333 Munich, Germany*
[2]*Max-Planck-Institut für Quantenoptik, Hans-Kopfermann-Straße 1, 85748 Garching, Germany*
(Received 9 March 2017; revised manuscript received 1 June 2017; published 7 November 2017)

It has been argued that the 0.7 anomaly in quantum point contacts (QPCs) is due to an enhanced density of states at the top of the QPC barrier (the van Hove ridge), which strongly enhances the effects of interactions. Here, we analyze their effect on dynamical quantities. We find that they pin the van Hove ridge to the chemical potential when the QPC is subopen, cause a temperature dependence for the linear conductance that qualitatively agrees with experiments, strongly enhance the magnitude of the dynamical spin susceptibility, and significantly lengthen the QPC traversal time. We conclude that electrons traverse the QPC via a slowly fluctuating spin structure of finite spatial extent.

DOI: 10.1103/PhysRevLett.119.196401

Quantum point contacts are narrow, one-dimensional (1D) constrictions usually patterned in a two-dimensional electron system by applying voltages to local gates. As quantum point contacts (QPCs) are the ultimate building blocks for controlling nanoscale electron transport, much effort has been devoted to understanding their behavior at a fundamental level. Nevertheless, in spite of a quarter of a century of intensive research into the subject, some aspects of their behavior still remain puzzling.

When a QPC is opened up by sweeping the gate voltage, V_g, that controls its width, its linear conductance famously rises in integer steps of the conductance quantum, $G_Q = 2e^2/h$ [1,2]. This conductance quantization is well understood [3] and constitutes one of the foundations of mesoscopic physics. However, during the first conductance step, where the dimensionless conductance $g = G/G_Q$ changes from 0 to 1 (from a "closed" to an "open" QPC), an unexpected shoulder is generically observed near $g \simeq 0.7$. More generally, the conductance shows anomalous behavior as a function of temperature (T), magnetic field (B), and source-drain voltage (V_{sd}) throughout the regime $0.5 \lesssim g \lesssim 0.9$, where the QPC is "subopen." The source of this behavior, collectively known as the "0.7 anomaly," has been controversially discussed [4–23] ever since it was first systematically described in 1996 [4]. Though no consensus has yet been reached regarding its detailed microscopic origin [10,22], general agreement exists that it involves electron spin dynamics and geometrically enhanced interaction effects.

In this Letter, we further explore the van Hove ridge scenario proposed in Ref. [22]. It asserts that the 0.7 anomaly is a direct consequence of a "van Hove ridge," i.e., a smeared van Hove peak in the energy-resolved local density of states (LDOS) $\mathcal{A}_i(\omega)$ at the bottom of the lowest 1D subband of the QPC. Its shape follows that of the QPC barrier [22–24] and, in the subopen regime, where the barrier top lies just below the chemical potential μ, it causes the LDOS *at* μ to be strongly enhanced. This reflects the fact that electrons slow down while crossing the QPC barrier [since the semiclassical velocity of an electron with energy ω at position i is inversely proportional to the LDOS, $\mathcal{A}_i(\omega) \sim v^{-1}$]. The slow electrons experience strongly enhanced mutual interactions, with striking consequences for various physical properties.

In this Letter, we elucidate their effect on various *dynamical* quantities, which govern those aspects of the 0.7 anomaly that probe finite-energy excitations. To this end, we compute real-frequency correlation functions computed using the functional renormalization group (FRG) on the Keldysh contour [25–28]. We compute (i) the energy dependence of the LDOS, finding that its maximum is pinned to μ in the subopen regime due to a Hartree increase in the barrier height with increasing density, (ii) the temperature dependence of the linear conductance, finding qualitative agreement with experiments, (iii) the dynamical spin susceptibility $\chi(\omega)$, from which we extract a characteristic time scale t_{spin} for spin fluctuations, and (iv) the time t_{trav} for a quasiparticle to traverse the QPC, which we extract from the single-particle scattering matrix $S(\omega)$. Intermediate interaction strengths suffice to obtain the characteristic 0.7 shoulder at finite temperatures. We find strong links among the ω dependence of the spin susceptibility, the one-particle S matrix, and the form of the LDOS. As long as the van Hove ridge is pinned to μ, interactions cause relevant degrees of freedom to slow down, inducing significant increases in both t_{trav} and t_{spin}. Moreover, these two times are comparable in magnitude, implying that a quasiparticle traversing the QPC encounters a quasistatic spin background. This provides links to other proposed explanations of the 0.7 anomaly [4–18].

Model.—Focusing on the first subband, we model the QPC by a smooth potential barrier describing the effective

1D potential along the transport direction. After discretizing the longitudinal position coordinate as $x = ai$, with site index i and lattice spacing a, the model Hamiltonian has the form [22]

$$\mathcal{H} = -\sum_{\sigma,i} \tau_i (c^\dagger_{i+1,\sigma} c_{i,\sigma} + \text{H.c.}) + \sum_i U_i c^\dagger_{i\uparrow} c_{i\uparrow} c^\dagger_{i\downarrow} c_{i\downarrow}. \quad (1)$$

It describes an infinite tight-binding chain with nearest-neighbor hopping τ_i of quasiparticles with spin $\sigma = \uparrow, \downarrow$ and short-range interactions U_i. The hopping amplitude τ_i varies smoothly with i, thus creating an effective potential barrier $V_i = -(\tau_i + \tau_{i+1}) + 2\tau$ measured with respect to the leads' band bottom -2τ. We choose $U_i \neq 0$ and $\tau_i \neq \tau$ for $N = 2N' + 1$ sites only, symmetric around $i = 0$, that define the extent of the QPC (central region). U_i is constant in the center of the QPC with $U_0 = U$ and drops smoothly to zero as i approaches the edges of the central region at sites $\pm N'$. We tune the hopping such that the effective barrier is symmetric and parabolic near the top, $V_i = \tilde{V}_c - i^2\Omega_x^2/(2\tau)$, where the barrier height $\tilde{V}_c$ mimics the role of gate voltage from an experiment, and the curvature Ω_x sets the characteristic length scale $l_x = a\sqrt{\tau/\Omega_x}$ of the QPC. We sweep $\tilde{V}_c$ such that the barrier crosses the chemical potential μ. The precise form of U_i and τ_i is given in Sec. S-I of the Supplemental Material [29]. The model is solved with the perturbatively truncated Keldysh FRG in equilibrium (see Sec. S-II of the Supplemental Material [29]). We use $\tau = 1$, $U = 0.7\tau$, $\mu = -1.475\tau$, $V_c = \tilde{V}_c - \mu - 2\tau \in [-2.83, 1.83]\Omega_x$, and $\Omega_x \approx 0.03\tau$ (with $\hbar = 1$).

Local density of states.—It was argued in Ref. [22] that the physics of the QPC is governed by the LDOS, $\mathcal{A}_i(\omega) = -(1/\pi)\text{Im}G^R_{ii}(\omega)$, where G^R_{ij} is the retarded single-particle Green's function between sites i and j. Figures 1(a)–1(c) show the bare LDOS $\mathcal{A}_i^{U=0}(\omega)$ of the QPC as a function of site i and energy ω at three values of the barrier height V_c. The bare LDOS has a maximum just above the band bottom, visible as a red structure, that follows the shape of the effective potential (the thick white line). This structure is the bare van Hove ridge discussed in Ref. [22], the apex of which has a maximum value $\sim(\Omega_x\tau)^{-1/2}$, and occurs at an energy $\omega_{\max}(V_c)$ that lies slightly higher than the bare potential maximum V_0, by an amount $\sim\Omega_x$.

Upon adding interactions, we obtain Figs. 1(d)–1(f), which shows two striking differences to the noninteracting case: In the (sub)open regime, the renormalized van Hove ridge is shifted upward in energy ($\omega_{\max}$ is larger) and becomes flatter spatially. Both of these effects may *qualitatively* be understood by a mean field argument [37,38]: The slope of the van Hove ridge may be interpreted as reflecting the shape of an effective, renormalized potential barrier, which is shifted upward relative to the bare barrier

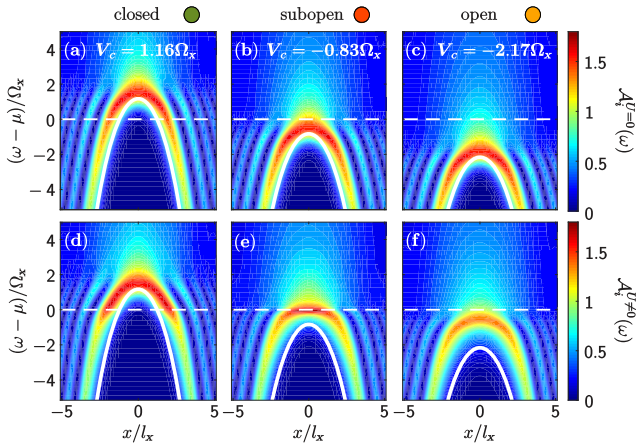

FIG. 1. van Hove ridge in the LDOS $\mathcal{A}_i(\omega)$ (color scale) of (a,b,c) a noninteracting and (d,e,f) an interacting QPC, plotted as a function of energy $\omega - \mu$ and position $x = ai$. The thick solid white line depicts the effective bare potential barrier V_i, the thin dashed white line, and the chemical potential μ. Closed (a,d), subopen (b,e), and open (c,f) regimes are shown from left to right. With interactions, the van Hove ridge is shifted upward and flattened in the (sub)open regime [compare (b) and (e) to (c) and (f)].

by a Hartree shift proportional to the local electron density. Away from the center, the density is higher, such that the shift is larger, causing the van Hove ridge to become flatter as a function of x near its apex, while becoming narrower and higher as a function of ω. This is also seen clearly in Fig. 2(a), which shows the interacting (solid lines) and bare (dashed lines) LDOS $\mathcal{A}_0(\omega)$. The x flattening and ω sharpening is most striking in the subopen regime, where the van Hove ridge apex intersects the chemical potential [Fig. 1(e)], because the interaction-induced effects are largest there. We have checked our Keldysh-FRG results against density matrix renormalization group (DMRG) computations of the system with somewhat different parameters, finding good qualitative agreement and, specifically, the same values for $\omega_{\max}$ (see Sec. S-III of the Supplemental Material [29]).

The evolution of $\mathcal{A}_0(\omega)$ as V_c is varied is shown in Fig. 2(c). As V_c is lowered, the energy $\omega_{\max}$ of the van Hove ridge maximum follows the bare barrier top (the solid white line) as long as the QPC is closed, then remains *pinned* at the chemical potential throughout the subopen regime to form a plateaulike structure, and finally decreases again only deep in the open regime [compare this to Fig. 1(d) of Ref. [37]]. The plateaulike structure sets in once the bare barrier top V_0 drops below the chemical potential because then the electron density near the QPC center begins to increase, leading to an upward Hartree shift of the barrier height that almost compensates for the decrease in V_c [37]. This pinning is the reason why the conductance step at zero temperature is asymmetric [compared to the noninteracting case, the dashed line in Fig. 2(d)],

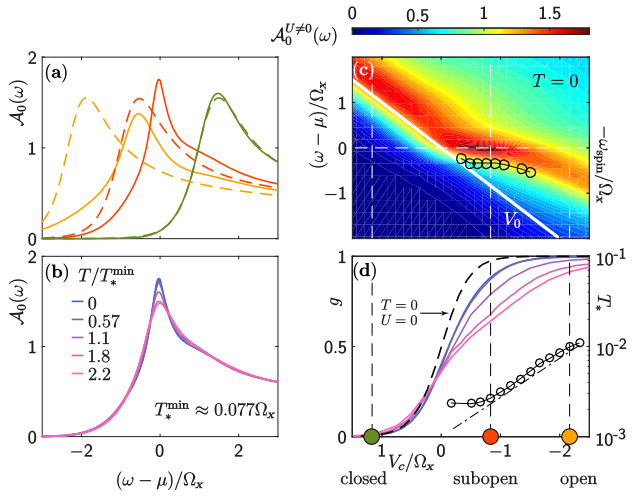

FIG. 2. (a) The interacting LDOS (the solid lines) and bare LDOS (the dashed lines), plotted as a function of energy ω for three values of V_c, indicated by dots of corresponding color in (c), (d). In the subopen (red) and open (orange) regimes, interactions shift the van Hove peak to larger energies, as the barrier height is renormalized. Moreover, in the subopen regime, flattening of the van Hove ridge causes the peak to become sharper and higher. (b) $\mathcal{A}_0(\omega)$ in the subopen regime for several different temperatures. At larger temperatures, the maximum is lower as weight is shifted into the flanks of the van Hove ridge and redistributed in the band. (c) $\mathcal{A}_0(\omega)$, the interacting LDOS (color scale) at the central site, as a function of ω and V_c. The solid white line shows the bare barrier height, V_0. In the subopen regime, the energy of the van Hove ridge maximum, $\omega_{\max}$, is pinned to the chemical potential. The black circles show the characteristic energy ω_{spin} of the spin susceptibility χ. They clearly follow the LDOS maximum. (d) Conductance g (left axis) for different temperatures (the dashed curve, g for $T = U = 0$), and T_* (the circles), extracted via Eq. (2), shown on a logarithmic scale (right axis). Temperature is measured in units of $T_*^{\min} = \min T_*(V_c)$. As a guide for the eye, $0.001\exp(-V_c/\Omega_x)$ (the dashed-dotted line). Our FRG results qualitatively reproduce the generic feature common to numerous experiments [29], namely, a strong reduction of g with increasing T in the subopen regime, causing an increasing asymmetry in the conductance step.

changing much more slowly with V_c for $g \gtrsim 0.5$ than for $g \lesssim 0.5$.

Finite temperature.—This structure sheds new light on the temperature dependence of the linear conductance on temperature. When the temperature, T, is increased, the van Hove peak in the LDOS retains its overall shape and is broadened only slightly (for $T \lesssim \Omega_x/10$) [Fig. 2(b)]. At the same time, the first conductance step is flattened out in a characteristic, asymmetric fashion [Fig. 2(d)], in qualitative agreement with experiments (see Sec. S-IV of the Supplemental Material [29]). This can be understood as follows [22]: Increasing T increases the available phase space for inelastic scattering, thus enhancing interaction effects. Their strength is governed by the LDOS near the chemical potential, which is particularly large *throughout the subopen region* due to the pinning of $\omega_{\max}$ to the chemical potential. Accordingly, interaction-induced backscattering is large in the whole subopen regime, leading to a strong suppression of the conductance [Fig. 2(d)] even into the open regime. At pinch-off, the conductance is slightly increased due to thermal activation.

To quantify the strength of the temperature dependence as a function of V_c, we expand the conductance as

$$g(T, V_c) = g(0, V_c) - T^2/T_*^2(V_c) + \mathcal{O}(T^3), \qquad (2)$$

as appropriate for a Fermi liquid [22]. The $T_*(V_c)$ values extracted from our finite-T data [see Fig. 2(d), the circles] depend roughly exponentially on gate voltage $T_*(V_c) \sim \exp(-V_c/\Omega_x)$ [Fig. 2(d), the dashed-dotted line], when the QPC is tuned from subopen to open, reflecting the V_c dependence of the bare QPC transmission rate [22].

Spin susceptibility.—In the van Hove ridge scenario, a key property of a subopen QPC is the presence of "slow spin fluctuations" [22], as advocated for also in Ref. [39]. To explore this, we have computed the dynamical equilibrium spin susceptibility,

$$\chi_{ij}(\omega) = \int dt \langle \mathcal{T} S_i^z(t) S_j^z(0) \rangle \exp(i\omega t), \qquad (3)$$

where $\mathcal{T}$ denotes time ordering. In a Fermi liquid, the spin susceptibility is determined by the particle-hole bubble and thus governed by single-particle properties. However, due to the inhomogeneity of the QPC, both the energy and the position dependence of the spin susceptibility are nontrivial. For now, we focus on χ_{0j}, shown in Fig. 3, which has the following salient features.

(i) χ_{0j} oscillates with a spatially varying wavelength which becomes shorter as the QPC is opened or the energy is increased. For small energies ω, the wavelength of these oscillations is determined by the "local Fermi wavelength" λ_F, which can be extracted from $|\mathrm{Im}G_{0j}^R(\mu)|$ (the blue line in Fig. 3). In the subopen regime, λ_F is large in the center, where the density is small, such that the sign of the spin susceptibility changes only far away from the center. Thus, an excited spin in the center leads to a rather large cloud (covering a region of $\sim 3l_x$) of co-oriented spins. Away from the QPC, the oscillations in χ_{0j} simply follow the Friedel oscillations.

(ii) On the central site, $\chi_{00}(\omega)$ shows a clear characteristic at an energy $\omega_{\text{spin}}(V_c)$, whose dependence on V_c follows that of $\omega_{\max}$ [$-\omega_{\text{spin}}$ is indicated by black circles in Fig. 2(c)]. In general, for small energies, ω_{spin} is set by the distance between the chemical potential and the nearest peak in the LDOS (see Sec. S-V of the Supplemental Material [29]).

(iii) The spin susceptibility $\chi_{0i}(\omega)$ is amplified by interactions (Stoner physics) [compare Figs. 3(a)–3(c) to Figs. 3(d)–3(f), and also Fig. 4(a) to Fig. 4(b)]. Interactions

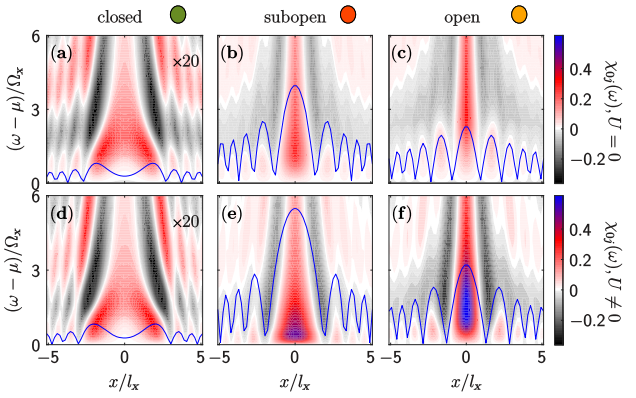

FIG. 3. (a)–(c) Noninteracting and (d)–(f) interacting dynamical spin susceptibility [multiplied by a factor of 20 in order to be visible in (a) and (d)] for a closed, a subopen, and an open QPC. The blue line shows $|\mathrm{Im}[G_{0i}(\omega=\mu)]|$ (arbitrary units).

also amplify the temperature-induced reduction of the spin susceptibility at ω_{spin} [Figs. 4(a) and 4(b)]. This effect is of a similar strength as the decrease of the LDOS at ω_{max} [Fig. 2(b)].

Traversal time.—The traversal time t_{trav} for a single incident quasiparticle with energy ω to traverse a scattering region can be obtained by a procedure attributed to Wigner [40], which relates it to the scattering-induced dispersion of the incident wave packet: It is given by

$$t_{\mathrm{trav}}(\omega)=t_0(\omega)+t_{\mathrm{delay}}(\omega), \quad t_{\mathrm{delay}}(\omega)=2\partial_\omega\phi(\omega), \quad (4)$$

where $t_0(\omega)$ is the traversal time through the central region with the potential and interactions being turned off, t_{delay} and $\phi(\omega)$ are the delay time and the scattering phase shift due to the potential- and interaction-induced slowdown of the quasiparticles. In our setup, $\phi(\omega)$ is the phase of the left-right component of the zero-temperature single-particle S matrix,

$$S_{l,r}(\omega) = -2\pi i\tau\rho(\omega)G^R_{-N',N'}(\omega), \quad (5)$$

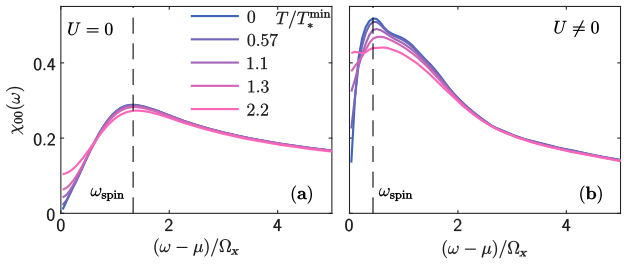

FIG. 4. (a) Noninteracting and (b) interacting spin-spin correlations on the central site in the subopen regime at different temperatures; i.e., the blue lines are vertical cuts of Figs. 3(b) and 3(e) through $x=0$. The dashed black line is at $\omega=\omega_{\mathrm{spin}}$. The shoulder in (b) is due to the LDOS-dependent enhancement of the spin susceptibility due to interactions.

where $\rho(\omega)$ is the lead density of states at the sites $\pm(N'+1)$ in the absence of the central region and τ is the hopping amplitude there. $|S_{l,r}(\omega)|^2$ yields the transmission probability. Figures 5(a) and 5(b) show the traversal time. Though calculated from a nonlocal correlation function, its behavior is strikingly similar to that of the LDOS at the central site, Fig. 2(c). This is consistent with the semiclassical interpretation $\mathcal{A}\sim v^{-1}$: Whenever the LDOS is large, quasiparticles are slow, and thus a large time is required to traverse the QPC.

Interestingly, we find that in the subopen regime the traversal time t_{trav} is of the same order as the characteristic time scale, $t_{\mathrm{spin}}=(2\pi/\omega_{\mathrm{spin}})$, associated with spin fluctuations, namely, $t_{\mathrm{trav}}\lesssim 8/\Omega_x$ and $t_{\mathrm{spin}}\lesssim 10/\Omega_x$. We note that, with our parameters, $t_0\approx 1.3/\Omega_x$; thus, t_{trav} is dominated by the delay time. That t_{trav} and t_{spin} are comparable in magnitude is consistent with a Fermi-liquid description of the system (which underlies the FRG method used here): The only stable degrees of freedom in a Fermi liquid are dressed electron- and holelike quasiparticles, and spin fluctuations arise via electron-hole–like excitations. Near the QPC center ($x\lesssim l_x$), the lifetime of spin fluctuations is thus governed by the quasiparticle decay time. Heuristically, this roughly corresponds to t_{trav}, as the region where interaction effects are strongest extends over only a few λ_F oscillations. Though we find no static contributions to the dynamical spin susceptibility at zero magnetic field, the fact that $t_{\mathrm{spin}}\simeq t_{\mathrm{trav}}$, together with the extended spatial structure of the spin susceptibility in the subopen regime, suggests the heuristic view that a quasiparticle traversing the QPC encounters a quasistatic, spatially coherent spin environment.

Discussion.—Our results allow us to establish contact with two other prominent scenarios that have been proposed to explain the 0.7 anomaly. (i) According to the

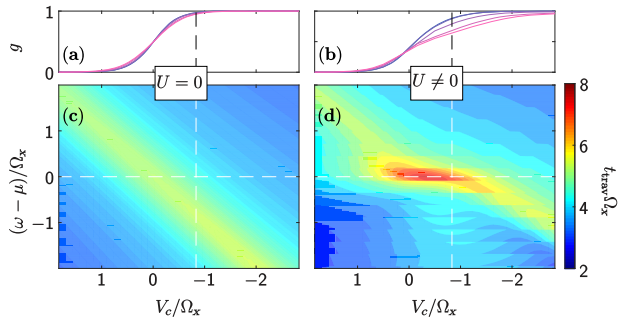

FIG. 5. Comparison of (a), (c) noninteracting and (b), (d) interacting traversal time. (a), (b) Conductance g, as a function of gate voltage V_c, to identify the closed, subopen, and open regimes. The color code is identical to Fig. 2. (c), (d) Traversal time [Eq. (4)] as a function of energy ω and gate voltage V_c. While the traversal time of modes below the barrier is small, these modes have a low transmission probability and are irrelevant when determining the time scale of transport.

"spin-polarization scenario," interactions cause the spin degree of freedom in the QPC to spontaneously polarize, giving rise to a nonzero magnetization even at vanishing magnetic field, $B = 0$ [4–9,14–18]. (ii) According to the "quasilocalized spin scenario" proposed by Meir *et al.* [13], a subopen QPC hosts a quasilocalized state involving a spin-1/2 magnetic moment, causing Kondo-like conductance anomalies [10–13]. At low energies, a quasilocalized spin would be screened, giving rise to Fermi-liquid behavior that includes slow spin fluctuations. These two scenarios thus seem to offer starkly contrasting views of the spin structure in a QPC: (i) spatially extended but static in time vs (ii) spatially localized but fluctuating in time. Our work suggests that a view that entails elements of both: The spin structure fluctuates in time, in accord with (ii), but *slowly*—which is compatible with (i) if one is willing to reinterpret "spontaneous polarization" as "slowly fluctuating polarization." Also, the spin structure is spatially coherent, in accord with (i), over a region of *finite extent*—which is compatible with (ii) if one is willing to associate a nonzero spatial extent and a finite lifetime with the quasilocalized state evoked there. We thus suggest that the controversy between the opposing views (i) and (ii) can be resolved by associating the quasilocalized state evoked in (ii) with the slow electrons of the van Hove ridge, and by realizing that these constitute a quasistatic, spatially coherent spin environment, in the spirit of (i), for electrons traversing the QPC. Thus, though the various scenarios differ substantially in their details (and if one insists on comparing these details, the controversy will never be put to rest), they can be argued to have a common core: a slowly fluctuating spin structure of finite spatial extent in the center of the QPC. Moreover, our work shows that this spin structure originates naturally from the same interplay of interactions and QPC barrier geometry, encoded in the van Hove ridge, that causes transport properties to be anomalous.

We thank F. Bauer, J. Heyder, Y. Meir, S. Ludwig, and L. Weidinger for the useful discussions. B. B. thanks S. R. White for the discussions on the DMRG setup. The authors acknowledge support from the Deutsche Forschungsgemeinschaft (DFG) through the Excellence Cluster "Nanosystems Initiative Munich."

[1] D. A. Wharam, T. J. Thornton, R. Newbury, M. Pepper, H. Ahmed, J. E. F. Frost, D. G. Hasko, D. C. Peacock, D. A. Ritchie, and G. A. C. Jones, J. Phys. C **21**, L209 (1988).
[2] B. J. van Wees, H. van Houten, C. W. J. Beenakker, J. G. Williamson, L. P. Kouwenhoven, D. van der Marel, and C. T. Foxon, Phys. Rev. Lett. **60**, 848 (1988).
[3] M. Büttiker, Phys. Rev. B **41**, 7906 (1990).
[4] K. J. Thomas, J. T. Nicholls, M. Y. Simmons, M. Pepper, D. R. Mace, and D. A. Ritchie, Phys. Rev. Lett. **77**, 135 (1996); K. J. Thomas, J. T. Nicholls, N. J. Appleyard, M. Y. Simmons, M. Pepper, D. R. Mace, W. R. Tribe, and D. A. Ritchie, Phys. Rev. B **58**, 4846 (1998).
[5] D. J. Reilly, T. M. Buehler, J. L. O'Brien, A. R. Hamilton, A. S. Dzurak, R. G. Clark, B. E. Kane, L. N. Pfeiffer, and K. W. West, Phys. Rev. Lett. **89**, 246801 (2002).
[6] D. J. Reilly, Phys. Rev. B **72**, 033309 (2005).
[7] P. Jaksch, I. Yakimenko, and K.-F. Berggren, Phys. Rev. B **74**, 235320 (2006).
[8] E. Koop, A. Lerescu, J. Liu, B. van Wees, D. Reuter, A. D. Wieck, and C. van der Wal, J. Supercond. Novel Magn. **20**, 433 (2007).
[9] L. W. Smith, A. R. Hamilton, K. J. Thomas, M. Pepper, I. Farrer, J. P. Griffiths, G. A. C. Jones, and D. A. Ritchie, Phys. Rev. Lett. **107**, 126801 (2011).
[10] M. J. Iqbal, R. Levy, E. J. Koop, J. B. Dekker, J. P. de Jong, J. H. M. van der Velde, D. Reuter, A. D. Wieck, R. Aguado, Y. Meir, and C. H. van der Wal, Nature (London) **501**, 79 (2013).
[11] B. Brun, F. Martins, S. Faniel, B. Hackens, G. Bachelier, A. Cavanna, C. Ulysse, A. Ouerghi, U. Gennser, D. Mailly, S. Huant, V. Bayot, M. Sanquer, and H. Sellier, Nat. Commun. **5**, 4290 (2014).
[12] S. M. Cronenwett, H. J. Lynch, D. Goldhaber-Gordon, L. P. Kouwenhoven, C. M. Marcus, K. Hirose, N. S. Wingreen, and V. Umansky, Phys. Rev. Lett. **88**, 226805 (2002).
[13] Y. Meir, K. Hirose, and N. S. Wingreen, Phys. Rev. Lett. **89**, 196802 (2002); K. Hirose, Y. Meir, and N. S. Wingreen, Phys. Rev. Lett. **90**, 026804 (2003); A. Golub, T. Aono, and Y. Meir, Phys. Rev. Lett. **97**, 186801 (2006); T. Rejec and Y. Meir, Nature (London) **442**, 900 (2006).
[14] T.-M. Chen, A. C. Graham, M. Pepper, I. Farrer, and D. A. Ritchie, Appl. Phys. Lett. **93**, 032102 (2008).
[15] T.-M. Chen, A. C. Graham, M. Pepper, I. Farrer, D. Anderson, G. A. C. Jones, and D. A. Ritchie, Nano Lett. **10**, 2330 (2010).
[16] T.-M. Chen, M. Pepper, I. Farrer, G. A. C. Jones, and D. A. Ritchie, Phys. Rev. Lett. **109**, 177202 (2012).
[17] R. M. Potok, J. A. Folk, C. M. Marcus, and V. Umansky, Phys. Rev. Lett. **89**, 266602 (2002).
[18] C.-K. Wang and K.-F. Berggren, Phys. Rev. B **54**, R14257 (1996); **57**, 4552 (1998).
[19] A. P. Micolich, J. Phys. Condens. Matter **23**, 443201 (2011).
[20] Y. Komijani, M. Csontos, I. Shorubalko, T. Ihn, K. Ensslin, Y. Meir, D. Reuter, and A. D. Wieck, Europhys. Lett. **91**, 67010 (2010).
[21] Y. Chung, S. Jo, D.-I. Chang, H.-J. Lee, M. Zaffalon, V. Umansky, and M. Heiblum, Phys. Rev. B **76**, 035316 (2007).
[22] F. Bauer, J. Heyder, E. Schubert, D. Borowsky, D. Taubert, B. Bruognolo, D. Schuh, W. Wegscheider, J. von Delft, and S. Ludwig, Nature (London) **501**, 73 (2013).
[23] J. Heyder, F. Bauer, D. Schimmel, and J. von Delft, Phys. Rev. B **96**, 125141 (2017).
[24] F. Bauer, J. Heyder, and J. von Delft, Phys. Rev. B **89**, 045128 (2014); J. Heyder, F. Bauer, E. Schubert, D. Borowsky, D. Schuh, W. Wegscheider, J. von Delft, and S. Ludwig, Phys. Rev. B **92**, 195401 (2015).
[25] S. G. Jakobs, M. Pletyukhov, and H. Schoeller, Phys. Rev. B **81**, 195109 (2010).
[26] S. G. Jakobs, M. Pletyukhov, and H. Schoeller, J. Phys. A **43**, 103001 (2010).

[27] C. Karrasch, T. Enss, and V. Meden, Phys. Rev. B **73**, 235337 (2006).
[28] W. Metzner, M. Salmhofer, C. Honerkamp, V. Meden, and K. Schönhammer, Rev. Mod. Phys. **84**, 299 (2012).
[29] See Supplemental Material at http://link.aps.org/supplemental/10.1103/PhysRevLett.119.196401, which includes Refs. [30–36], for technical details pertaining to our calculations.
[30] U. Schollwöck, Rev. Mod. Phys. **77**, 259 (2005); Ann. Phys. (Amsterdam) **326**, 96 (2011); S. R. White, Phys. Rev. Lett. **69**, 2863 (1992); Phys. Rev. B **48**, 10345 (1993).
[31] M. Vekić and S. R. White, Phys. Rev. B **53**, 14552 (1996); Phys. Rev. Lett. **71**, 4283 (1993).
[32] G. Vidal, Phys. Rev. Lett. **93**, 040502 (2004); A. J. Daley, C. Kollath, U. Schollwöck, and G. Vidal, J. Stat. Mech. (2004) P04005; S. R. White and A. E. Feiguin, Phys. Rev. Lett. **93**, 076401 (2004).
[33] S. R. White and I. Affleck, Phys. Rev. B **77**, 134437 (2008); T. Barthel, U. Schollwöck, and S. R. White, Phys. Rev. B **79**, 245101 (2009).
[34] A. Weichselbaum, Ann. Phys. (Amsterdam) **327**, 2972 (2012).
[35] A. Kristensen, H. Bruus, A. E. Hansen, J. B. Jensen, P. E. Lindelof, C. J. Marckmann, J. Nygård, C. B. Sørensen, F. Beuscher, A. Forchel, and M. Michel, Phys. Rev. B **62**, 10950 (2000).
[36] F. B. Kugler and J. von Delft, arXiv:1703.06505; arXiv:1707.04536.
[37] S. Ihnatsenka and I. V. Zozoulenko, Phys. Rev. B **79**, 235313 (2009).
[38] A. X. Sánchez and J.-P. Leburton, Phys. Rev. B **88**, 075305 (2013).
[39] K. Aryanpour and J. E. Han, Phys. Rev. Lett. **102**, 056805 (2009).
[40] E. P. Wigner, Phys. Rev. **98**, 145 (1955).

Supplementary material

This supplement consists of two parts. In the first, we give the technical details on the model, the fRG- flow equations and the numerics involved. We also argue that the characteristic energy for spin fluctuations, ω_{spin}, is governed by the distance between the chemical potential and the effective lower band edge, $\omega_{\text{spin}} \simeq \mu - \omega_{\max}$. In the second part, we report on DMRG calculations of the LDOS that we have performed to as an independent check of our fRG predictions. We find good qualitative agreement between both methods.

S-I. MODEL

We use a modified version of Model II of Ref. [22]: In the central region, described by $N = 2N' + 1$ sites, with $i = -N', \ldots, N'$, the on-site potential is zero, and the hopping elements vary from site to site according to

$$\tau_j = \tau - \tfrac{1}{2}\tilde{V}_{\text{c}} \exp\left(-\frac{x_j^2}{1-x_j^2}\right);\ x_j = \frac{2j+1}{N-1}, \tag{S1}$$

where j runs from $-N'$ to $N'-1$. In Ref. [22, 23], it was shown that such a spatially varying hopping may be used to mimick an inhomogenous on-site potential, which has the advantage that no long-lived states appear above the upper band edge (see Sec. V of [23] for a detailed discussion). The on-site interaction in the central region is given by

$$U_i = U_0 \exp\left(-\frac{l_i^6}{1-l_i^2}\right);\ l_i = \frac{i}{N' + \frac{1}{2}}, \tag{S2}$$

The hopping and interaction Eqs. (S1),(S2) lead to a Hamiltonian

$$\begin{aligned}\mathcal{H} &= -\sum_{\sigma,i} \tau_i \left(c^\dagger_{i+1,\sigma} c_{i,\sigma} + \text{h.c.}\right) + \sum_i \left(U_i c^\dagger_{i\uparrow} c_{i\uparrow} c^\dagger_{i\downarrow} c_{i\downarrow}\right), \\ &=: \sum_{\sigma,i,j} \left(\tilde{H}^\sigma_{ji} c^\dagger_{j,\sigma} c_{i,\sigma} + \text{h.c.}\right) + \sum_i \left(U_i c^\dagger_{i\uparrow} c_{i\uparrow} c^\dagger_{i\downarrow} c_{i\downarrow}\right),\end{aligned} \tag{S3}$$

where we use the tilde to indicate that the indices of the Hamiltonian matrix $\tilde{H}^\sigma$ run over $\mathbb{Z}$. $\tilde{H}^\sigma_{ij}$ is invariant under transposition and parity $\mathcal{P}$, which we implement as $\mathcal{P} : i \mapsto -i$. We will explicitly assume the presence of these symmetries in the following. Note that for our description of the central region, the effect of the tight-binding leads with hopping τ coupling to sites $-N'$ and N' is fully included in the self-energy contribution

$$\begin{aligned}\Sigma^R_{\text{lead}\,ij}(\omega) =& (\delta_{i,-N'}\delta_{j,-N'} + \delta_{i,N'}\delta_{j,N'}) \\ &\times \begin{cases} \frac{\omega}{2}\left(1 - \sqrt{1 - \left(\frac{2\tau}{\omega}\right)^2}\right), & |\omega| > 2\tau \\ \frac{\omega}{2} - i\tau\sqrt{1 - \left(\frac{\omega}{2\tau}\right)^2}, & |\omega| < 2\tau, \end{cases}\end{aligned} \tag{S4}$$

$$\Sigma^K_{\text{lead}\,ij}(\omega) = (1 - 2n_F(\omega))(\Sigma^R_{\text{lead}\,ij} - \Sigma^A_{\text{lead}\,ij}). \tag{S5}$$

Here, the superscript $R(K,A)$ denotes the retarded (Keldysh, advanced) component of the self energy and n_F is the Fermi distribution function.

As stated in the main text, we use $U_0 = 0.7\tau$ and $\tilde{V}_{\text{c}} \in [0.44, 0.58]\tau$.

S-II. KELDYSH FRG

The model is solved by employing the functional renormalization group (fRG) [25–28] on the Keldysh-contour to obtain real-frequency information. The flow is truncated perturbatively, i.e. we set the three-particle vertex (and all higher vertices) to zero during the flow and approximate the two-particle vertex by the three usual channels (P, X, and D) [22, 25], assuming a local and static inter-channel mixing (coupled-ladder-approximation). The computation is then exact to second order in the interaction. It may be viewed as extension of the flow used in Ref. [26] to multiple sites (neglecting the $D^{\sigma\bar{\sigma}}$-channel, which in our case is of order U_0^3) or an extension of the flow used in Ref. [22] to real frequencies. As flow parameter we use an artificial, on-site broadening of the spectrum (c.f. Eq. (S6), and Ref. [25]). This flow parameter respects fluctuation-dissipation theorems, so that in equilibrium it is unnecessary to compute the Keldysh components of the self energy (Σ^K) and the channels (b^P, b^X, b^D).

Once the model has been solved using Keldysh fRG, we use the two-particle vertex and the self-energy to compute the conductance, using Eq. (23) of Ref. [23].

The conventions on the Keldysh-contour used are those of Ref. [26], with the difference that after the Keldysh rotation we use the labels c(lassical) and q(uantum), instead of 2 and 1. In particular, this means that the Keldysh rotation used for the fermions is the same as the one usually used for bosons. We use $\sigma = \uparrow, \downarrow$ to denote spin, and $\bar{\sigma}$ to denote the spin opposite to σ. Letters from the middle of the roman alphabet (i,j) refer to spatial sites, while letters from the beginning of the Greek alphabet (α, β) refer to the Keldysh indices.

A. The Single-Scale Propagator

The flow parameter is determined by the bare retarded Green's function

$$\tilde{G}^R_{0,\Lambda,\sigma}(\omega) = \frac{1}{\omega \mathbb{1} - \tilde{H}^\sigma + i\left(\frac{1}{2}\Lambda\right)\mathbb{1}}, \tag{S6}$$

where $\tilde{H}^\sigma$ is the non-interacting Hamiltonian matrix extracted from Eq. (S3). Λ is the flow parameter, ranging from ∞ (start of flow) to 0 (end of flow). $\mathbb{1}$ is the unit matrix in the space of the sites, which we will omit from now on. Once the leads have been projected out, we drop the tilde on the restricted Hamiltonian matrix H^σ and the spatial indices then only run from $-N'$ to N'. We use the artificial on-site broadening for all sites (including the leads) to avoid artifacts at the transition from the lead to the central region.

The retarded single-scale propagator $\tilde{S}^R$ is

$$\tilde{S}^R(\omega) = \left(\tilde{G}\tilde{G}_0^{-1}\partial_\Lambda \tilde{G}_0 \tilde{G}_0^{-1}\tilde{G}\right)^R = -\frac{i}{2}\tilde{G}^R_\Lambda \cdot \tilde{G}^R_\Lambda, \tag{S7}$$

where we omit the site and spin labels.

After the integration over the leads' degrees of freedom has been performed, the Green's function projected onto the central part acquires an additional self-energy term

$$G_0^{R(\sigma)}(\omega) = \frac{1}{\omega^{(\sigma)} - \mathcal{H}^{(\sigma)} - \Sigma^{(\sigma)}_{\text{lead}}(\omega,\Lambda) + i\Lambda/2}, \tag{S8}$$

where $\omega^{(\sigma)} = \omega + \frac{\sigma}{2}B$ and

$$\Sigma^{(\sigma)}_{\text{lead}\,ij}(\omega,\Lambda) = \frac{1}{2}\left(\omega^{(\sigma)} + i\tfrac{\Lambda}{2} - i\sqrt{4\tau^2 - \left(\omega^{(\sigma)} + i\tfrac{\Lambda}{2}\right)^2}\right) \times (\delta_{i,-N'}\delta_{j,-N'} + \delta_{i,N'}\delta_{j,N'}). \tag{S9}$$

This self-energy is also reflected in the projected single-scale propagator, which now takes the form

$$\begin{aligned} S^R(\omega) &= \left(GG_0^{-1}\partial_\Lambda G_0 G_0^{-1} G\right)^R \\ &= G^R_\Lambda \cdot \left(-\frac{i}{2} + \partial_\Lambda \Sigma_{\text{lead}}(\omega,\Lambda)\right)\cdot G^R_\Lambda. \end{aligned} \tag{S10}$$

For $\Lambda \to \infty$ the model is exactly solvable and the irreducible part of the full vertex is simply the bare vertex [26]. Since we only consider equilibrium situations in this paper and the flow parameter respects fluctuation-dissipation theorems, the Keldysh Green's function G^K [and single scale S^K] is determined simply via the fluctuation-dissipation theorem

$$G^K = (1-2n_F)(G^R - G^A),\ S^K = (1-2n_F)(S^R - S^A). \tag{S11}$$

B. The Vertex

The vertex is assumed to consist *only* of a two-particle contribution. This contribution is approximated by a structure compatible with a decomposition into three channels (with only static and local interchannel feedback). This approximation yields a consistent set of flow equations. We use the following parametrization:

We decompose the 2-particle vertex into three channels, according to

$$\gamma(\omega_1',\omega_2';\omega_1,\omega_2) \approx \bar{v} + \varphi^P(\omega_1+\omega_2) + \varphi^X(\omega_2-\omega_1') + \varphi^D(\omega_2-\omega_2'), \tag{S12}$$

where we have suppressed all indices other than energy, and primed quantities denote outgoing legs. $\bar{v}$ denotes the bare vertex. The Keldsh structure is arranged according to the convention

$$\gamma^{\alpha\beta|\gamma\delta} = \begin{pmatrix} (qq|qq) & (qq|cq) & (qq|qc) & (qq|cc) \\ (cq|qq) & (cq|cq) & (cq|qc) & (cq|cc) \\ (qc|qq) & (qc|cq) & (qc|qc) & (qc|cc) \\ (cc|qq) & (cc|cq) & (cc|qc) & (cc|cc) \end{pmatrix}. \tag{S13}$$

The channels are labelled as (the Keldysh structure corresponds to Eqs. (A8,A11,A17) of Ref. [25], while the spatial structure is that of Eq. (S48) of Ref. [22])

$$(\varphi^P)_{(\sigma\bar{\sigma}|\sigma\bar{\sigma}),(ii|jj)}(\Pi) = \begin{pmatrix} 0 & a^{P*}_{ji} & a^{P*}_{ji} & 0 \\ a^P_{ij} & b^P_{ij} & b^P_{ij} & a^P_{ij} \\ a^P_{ij} & b^P_{ij} & b^P_{ij} & a^P_{ij} \\ 0 & a^{P*}_{ji} & a^{P*}_{ji} & 0 \end{pmatrix}^{(\sigma\bar{\sigma})} (\Pi), \tag{S14}$$

$$(\varphi^X)_{(\sigma\bar{\sigma}|\sigma\bar{\sigma}),(ji|ij)}(X) = \begin{pmatrix} 0 & a^{X*}_{ji} & a^X_{ij} & b^X_{ij} \\ a^X_{ij} & b^X_{ij} & 0 & a^{X*}_{ji} \\ a^{X*}_{ji} & 0 & b^X_{ij} & a^X_{ij} \\ b^X_{ij} & a^X_{ij} & a^{X*}_{ji} & 0 \end{pmatrix}^{(\sigma\bar{\sigma})} (X), \tag{S15}$$

$$(\varphi^D)_{(\sigma\sigma|\sigma\sigma),(ij|ij)}(\Delta) = \begin{pmatrix} 0 & a^D_{ij} & a^{D*}_{ji} & b^D_{ij} \\ a^D_{ij} & 0 & b^D_{ij} & a^{D*}_{ii} \\ a^{D*}_{ji} & b^D_{ij} & 0 & a^D_{ij} \\ b^D_{ij} & a^{D*}_{ji} & a^D_{ij} & 0 \end{pmatrix}^{(\sigma\sigma)} (\Delta). \tag{S16}$$

Each channel is labelled by only two spatial indices and one energy. Conceptually, it can be thought of as the propagator of a Hubbard-Stratonovitch particle of the corresponding channel with retarded (a^P, a^D, and a^{X*}) and Keldysh (b^P, b^D, and b^X) components. From this point of view it is not surprising that in equilibrium the channels satisfy the fluctuation-dissipation theorems (c.f.

Eqs. (A10,A13,A19) of Ref. [25]:

$$b^{P\,(\sigma\bar{\sigma})}_{(ij)}(\Pi) = 2i\coth\left[\beta\left(\frac{\Pi}{2}-\mu\right)\right]\mathrm{Im}\,a^{P\,(\sigma\bar{\sigma})}_{(ij)}(\Pi) \tag{S17a}$$

$$b^{X\,(\sigma\bar{\sigma})}_{(ij)}(X) = -2i\coth\left[\frac{\beta X}{2}\right]\mathrm{Im}\,a^{X\,(\sigma\bar{\sigma})}_{(ij)}(X) \tag{S17b}$$

$$b^{D\,(\sigma\sigma)}_{(ij)}(\Delta) = 2i\coth\left[\frac{\beta\Delta}{2}\right]\mathrm{Im}\,a^{D\,(\sigma\sigma)}_{(ij)}(\Delta) \tag{S17c}$$

C. The Flow Equations

When all vertices higher than the 2-particle vertex are set to zero, the resulting truncated flow equations are (c.f. Eqs. (27,28) of Ref. [25])

$$\begin{aligned}\frac{d}{d\Lambda}\Sigma^{\Lambda}_{1'1} &= -\sum\!\!\!\!\!\!\int_{2'2}\frac{i}{2\pi}\gamma^{\Lambda}_{1'2'12}S^{\Lambda}_{22'}\\ \frac{d}{d\Lambda}\gamma^{\Lambda}_{1'2'12} &= +\sum\!\!\!\!\!\!\int_{3'4'34}\frac{i}{2\pi}\gamma^{\Lambda}_{1'2'34}S^{\Lambda}_{33'}G^{\Lambda}_{44'}\gamma^{\Lambda}_{3'4'12}\\ &\quad+\sum\!\!\!\!\!\!\int_{3'4'34}\frac{i}{2\pi}\gamma^{\Lambda}_{1'4'32}\left[S^{\Lambda}_{33'}G^{\Lambda}_{44'}+S^{\Lambda}_{44'}G^{\Lambda}_{33'}\right]\gamma^{\Lambda}_{3'2'14}\\ &\quad-\sum\!\!\!\!\!\!\int_{3'4'34}\frac{i}{2\pi}\gamma^{\Lambda}_{1'3'14}\left[S^{\Lambda}_{33'}G^{\Lambda}_{44'}+S^{\Lambda}_{44'}G^{\Lambda}_{33'}\right]\gamma^{\Lambda}_{4'2'32}.\end{aligned} \tag{S18}$$

Here, 1, $1'$ etc. are multi-indices encompassing spin, site and energy. In the flow of the vertex, each summand corresponds to a single channel. The vertex of each summand will be approximated by the contribution of the corresponding channel for all energies and the feedback of the other channels at a specific energy (2μ for the P-channel, 0 for the X- and D-channels). Inserting the channel decomposition with the above notations into the flow equations, the flow of the self-energy is given by [compare Eqs. (B3,B4) of Ref. [25]]:

$$\begin{aligned}\partial_\Lambda\Sigma^{q|c(\sigma)}_{(kl)}(\omega) = -\frac{i}{2\pi}\int d\omega'\Big[&S^{c|c(\bar{\sigma})}_{(lk)}(\omega')a^{P\,(\sigma\bar{\sigma})}_{(kl)}(\omega+\omega') + S^{c|c(\bar{\sigma})}_{(kl)}(\omega')a^{X\,(\sigma\bar{\sigma})}_{(lk)}(\omega'-\omega) - S^{c|c(\sigma)}_{(kl)}(\omega')a^{D\,(\sigma\sigma)}_{(kl)}(\omega-\omega')\\ &+ S^{q|c(\bar{\sigma})}_{(lk)}(\omega')b^{P\,(\sigma\bar{\sigma})}_{(kl)}(\omega+\omega') + S^{c|q(\bar{\sigma})}_{(kl)}(\omega')b^{X\,(\sigma\bar{\sigma})}_{(lk)}(\omega'-\omega) - S^{c|q(\sigma)}_{(kl)}(\omega')b^{D\,(\sigma\sigma)}_{(lk)}(\omega-\omega')\\ &+ S^{c|c(\bar{\sigma})}_{(lk)}(\omega')U_k/2\delta_{kl} + \sum_m S^{c|c(\sigma)}_{(mm)}(\omega')a^{D\,(\sigma\sigma)}_{(km)}(0)\delta_{kl}\Big]\end{aligned} \tag{S19}$$

and

$$\begin{aligned}\partial_\Lambda\Sigma^{q|q(\sigma)}_{(kl)}(\omega) = -\frac{i}{2\pi}\int d\omega'\Big[&S^{c|q(\bar{\sigma})}_{(kl)}(\omega')a^{X\,(\sigma\bar{\sigma})}_{(lk)}(\omega'-\omega) - S^{c|q(\sigma)}_{(kl)}(\omega')a^{D\,(\sigma\sigma)}_{(kl)}(\omega-\omega') + S^{q|c(\bar{\sigma})}_{(lk)}(\omega')a^{P\,(\sigma\bar{\sigma})}_{(kl)}(\omega+\omega')\\ &+ S^{c|q(\bar{\sigma})}_{(lk)}(\omega')a^{P*\,(\sigma\bar{\sigma})}_{(lk)}(\omega'+\omega) + S^{q|c(\bar{\sigma})}_{(kl)}(\omega')a^{X*\,(\sigma\bar{\sigma})}_{(kl)}(\omega'-\omega) - S^{q|c(\sigma)}_{(kl)}(\omega')a^{D*\,(\sigma\sigma)}_{(lk)}(\omega-\omega')\\ &+ S^{c|c(\bar{\sigma})}_{(lk)}(\omega')b^{P\,(\sigma\bar{\sigma})}_{(kl)}(\omega+\omega') + S^{c|c(\bar{\sigma})}_{(kl)}(\omega')b^{X\,(\sigma\bar{\sigma})}_{(lk)}(\omega'-\omega) - S^{c|c(\sigma)}_{(kl)}(\omega')b^{D\,(\sigma\sigma)}_{(kl)}(\omega-\omega')\\ &+ \left(S^{c|q(\bar{\sigma})}_{(lk)}(\omega') + S^{q|c(\bar{\sigma})}_{(lk)}(\omega')\right)U_k/2\delta_{kl}\Big].\end{aligned} \tag{S20}$$

The flow of the vertex contains two bubbles

$$I^{pp}_{ab|a'b'}(\omega)^{(\sigma_1\sigma_2)}_{(ij|kl)} = \frac{i}{2\pi}\int d\omega'\left[G^{a|a'(\sigma_1)}_{(i|k)}(\omega/2+\omega')S^{b|b'(\sigma_2)}_{(j|l)}(\omega/2-\omega') + S^{a|a'(\sigma_1)}_{(i|k)}(\omega/2+\omega')G^{b|b'(\sigma_2)}_{(j|l)}(\omega/2-\omega')\right], \tag{S21}$$

$$I^{ph}_{ab|a'b'}(\omega)^{(\sigma_1\sigma_2)}_{(ij|kl)} = \frac{i}{2\pi}\int d\omega'\left[G^{a|a'(\sigma_1)}_{(i|k)}(-\omega/2+\omega')S^{b|b'(\sigma_2)}_{(j|l)}(\omega/2+\omega') + S^{a|a'(\sigma_1)}_{(i|k)}(-\omega/2+\omega')G^{b|b'(\sigma_2)}_{(j|l)}(\omega/2+\omega')\right], \tag{S22}$$

and is given by (compare Eqs. (C3,C6,C9) of Ref. [25])

$$\begin{aligned}
&\partial_\Lambda (\varphi^P)^{qq|cq}_{(\sigma\bar\sigma|\sigma\bar\sigma)(ii|jj)}(\Pi) = \partial_\Lambda a^{P*}{}^{(\bar\sigma\sigma)}_{(ij)}(\Pi) \\
&= \sum_{km} \left(\tfrac{1}{2}U_k\delta_{ki} + a^{P*}(\Pi)^{(\bar\sigma\sigma)}_{(ki)} + \tfrac{1}{2}U^{X\,(\bar\sigma\sigma)}_{(ki)}\right) \left(I^{pp}_{cq|cc}(\Pi)^{(\sigma\bar\sigma|\sigma\bar\sigma)}_{(kk|mm)} + I^{pp}_{qc|cc}(\Pi)^{(\sigma\bar\sigma|\sigma\bar\sigma)}_{(kk|mm)}\right) \left(\tfrac{1}{2}U_j\delta_{jm} + a^{P*}(\Pi)^{(\bar\sigma\sigma)}_{(jm)} + \tfrac{1}{2}U^{X\,(\bar\sigma\sigma)}_{(jm)}\right)
\end{aligned} \tag{S23}$$

$$\begin{aligned}
&\partial_\Lambda (\varphi^X)^{qq|cq}_{(\sigma\bar\sigma|\sigma\bar\sigma)(ji|ij)}(X) = \partial_\Lambda a^{X*}(X)^{(\bar\sigma\sigma)}_{(ji)} \\
&= \sum_{kl} \left(\tfrac{1}{2}U_j\delta_{jk} + \tfrac{1}{2}U^{P\,(\bar\sigma\sigma)}_{(jk)} + a^{X*}(X)^{(\bar\sigma\sigma)}_{(jk)}\right) \left(I^{ph}_{qc|cc}(X)^{(\sigma\bar\sigma|\sigma\bar\sigma)}_{kl|lk} + I^{ph}_{cc|cq}(X)^{(\sigma\bar\sigma|\sigma\bar\sigma)}_{kl|lk}\right) \left(\tfrac{1}{2}U_i\delta_{il} + \tfrac{1}{2}U^{P\,(\bar\sigma\sigma)}_{(li)} + a^{X*}(X)^{(\bar\sigma\sigma)}_{(li)}\right)
\end{aligned} \tag{S24}$$

$$\begin{aligned}
&\partial_\Lambda (\varphi^D)^{cq|qq}_{(\sigma\sigma)(ij|ij)}(\Delta) = \partial_\Lambda a^D(\Delta)^{(\sigma\sigma)}_{(ij)} \\
&= -\sum_{kl} \Big[\left(-\tfrac{1}{2}W^{D\,(\sigma\sigma)}_{(ik)} + a^D(\Delta)^{(\sigma\sigma)}_{(ik)}\right) \left(I^{ph}_{qc|cc}(\Delta)^{(\sigma\sigma|\sigma\sigma)}_{(lk|kl)} + I^{ph}_{cc|cq}(\Delta)^{(\sigma\sigma|\sigma\sigma)}_{(lk|kl)}\right) \left(-\tfrac{1}{2}W^{D\,(\sigma\sigma)}_{(lj)} + a^D(\Delta)^{(\sigma\sigma)}_{(lj)}\right) \\
&\quad + \left(\tfrac{1}{2}U_i + \tfrac{1}{2}U^{P\,(\sigma\bar\sigma)}_{(ik)} + \tfrac{1}{2}U^{X\,(\sigma\bar\sigma)}_{(ik)}\right)\delta_{ik} \left(I^{ph}_{qc|cc}(\Delta)^{(\bar\sigma\bar\sigma|\bar\sigma\bar\sigma)}_{(lk|kl)} + I^{ph}_{cc|cq}(\Delta)^{(\bar\sigma\bar\sigma|\bar\sigma\bar\sigma)}_{(lk|kl)}\right)\delta_{jl} \left(\tfrac{1}{2}U_j + \tfrac{1}{2}U^{P\,(\bar\sigma\sigma)}_{(jl)} + \tfrac{1}{2}U^{X\,(\bar\sigma\sigma)}_{(jl)}\right)\Big]
\end{aligned} \tag{S25}$$

$$\begin{aligned}
&\partial_\Lambda (\varphi^P)^{cq|cq}_{(\sigma\bar\sigma)(ii|jj)}(\Pi) = \partial_\Lambda b^P(\Pi)^{(\sigma\bar\sigma)}_{(ij)} \\
&= \sum_{km} \Big[\left(\tfrac{1}{2}U_i\delta_{ik} + a^P(\Pi)^{(\sigma\bar\sigma)}_{(ik)} + \tfrac{1}{2}U^{X\,(\sigma\bar\sigma)}_{(ik)}\right) \left(I^{pp}_{cc|cc}(\Pi)^{(\sigma\bar\sigma|\sigma\bar\sigma)}_{(kk|mm)} + I^{pp}_{qq|cc}(\Pi)^{(\sigma\bar\sigma|\sigma\bar\sigma)}_{(kk|mm)} + I^{pp}_{cc|qq}(\Pi)^{(\sigma\bar\sigma|\sigma\bar\sigma)}_{(kk|mm)}\right) \\
&\quad \times \left(\tfrac{1}{2}U_j\delta_{jm} + a^{P*}(\Pi)^{(\sigma\bar\sigma)}_{(jm)} + \tfrac{1}{2}U^{X\,(\sigma\bar\sigma)}_{(jm)}\right) \\
&\quad + b^P(\Pi)^{(\sigma\bar\sigma)}_{(ik)} \left(I^{pp}_{qc|cc}(\Pi)^{(\sigma\bar\sigma|\sigma\bar\sigma)}_{(kk|mm)} + I^{pp}_{cq|cc}(\Pi)^{(\sigma\bar\sigma|\sigma\bar\sigma)}_{(kk|mm)}\right) \left(\tfrac{1}{2}U_j\delta_{jm} + a^{P*}(\Pi)^{(\sigma\bar\sigma)}_{(jm)} + \tfrac{1}{2}U^{X\,(\sigma\bar\sigma)}_{(jm)}\right) \\
&\quad + \left(\tfrac{1}{2}U_i\delta_{ik} + a^P(\Pi)^{(\sigma\bar\sigma)}_{(ik)} + \tfrac{1}{2}U^{X\,(\sigma\bar\sigma)}_{(ik)}\right) \left(I^{pp}_{cc|qc}(\Pi)^{(\sigma\bar\sigma|\sigma\bar\sigma)}_{(kk|mm)} + I^{pp}_{cc|cq}(\Pi)^{(\sigma\bar\sigma|\sigma\bar\sigma)}_{(kk|mm)}\right) b^P(\Pi)^{(\sigma\bar\sigma)}_{(mj)}\Big]
\end{aligned} \tag{S26}$$

$$\begin{aligned}
&\partial_\Lambda (\varphi^X)^{qq|cc}_{ji|ij}(X) = \partial_\Lambda b^X(X)^{(\sigma\bar\sigma)}_{(ij)} \\
&= \sum_{kl} \Big[\left(\tfrac{1}{2}U_k\delta_{kj} + \tfrac{1}{2}U^{P\,(\sigma\bar\sigma)}_{(kj)} + a^X(X)^{(\sigma\bar\sigma)}_{(kj)}\right) \left(I^{ph}_{cc|cc}(X)^{(\sigma\bar\sigma|\sigma\bar\sigma)}_{kl|lk} + I^{ph}_{qc|cq}(X)^{(\sigma\bar\sigma|\sigma\bar\sigma)}_{kl|lk} + I^{ph}_{cq|qc}(X)^{(\sigma\bar\sigma|\sigma\bar\sigma)}_{kl|lk}\right) \\
&\quad \times \left(\tfrac{1}{2}U_l\delta_{il} + \tfrac{1}{2}U^{P\,(\sigma\bar\sigma)}_{(il)} + a^{X*}(X)^{\sigma\bar\sigma}_{(li)}\right) \\
&\quad + b^X(X)^{(\sigma\bar\sigma)}_{(kj)} \left(I^{ph}_{qc|cc}(X)^{(\sigma\bar\sigma|\sigma\bar\sigma)}_{kl|lk} + I^{ph}_{cc|cq}(X)^{(\sigma\bar\sigma|\sigma\bar\sigma)}_{kl|lk}\right) \left(\tfrac{1}{2}U_l\delta_{il} + \tfrac{1}{2}U^{P\,(\sigma\bar\sigma)}_{(li)} + a^{X*}(X)^{\sigma\bar\sigma}_{li}\right) \\
&\quad + \left(\tfrac{1}{2}U_j\delta_{jk} + \tfrac{1}{2}U^{P\,(\sigma\bar\sigma)}_{(jk)} + a^X(X)^{(\sigma\bar\sigma)}_{(kj)}\right) \left(I^{ph}_{cq|cc}(X)^{(\sigma\bar\sigma|\sigma\bar\sigma)}_{kl|lk} + I^{ph}_{cc|qc}(X)^{(\sigma\bar\sigma|\sigma\bar\sigma)}_{kl|lk}\right) b^X(X)^{(\sigma\bar\sigma)}_{(il)}\Big]
\end{aligned} \tag{S27}$$

$$\begin{aligned}
&\partial_\Lambda (\varphi^D)^{cc|qq}_{(\sigma\sigma)(ij|ij)}(\Delta) = \partial_\Lambda b^D(\Delta)^{(\sigma\sigma)}_{(ij)} \\
&= -\sum_{kl} \Big[\left(-\tfrac{1}{2}W^{D\,\sigma\sigma}_{ik} + a^D(\Delta)^{(\sigma\sigma)}_{(ik)}\right) \cdot \left(I^{ph}_{cc|cc}(\Delta)^{(\sigma\sigma|\sigma\sigma)}_{(lk|kl)} + I^{ph}_{qc|cq}(\Delta)^{(\sigma\sigma|\sigma\sigma)}_{(lk|kl)} + I^{ph}_{cq|qc}(\Delta)^{(\sigma\sigma|\sigma\sigma)}_{(lk|kl)}\right) \left(-\tfrac{1}{2}W^{D\,(\sigma\sigma)}_{(lj)} + a^{D*}(\Delta)^{(\sigma\sigma)}_{(jl)}\right) \\
&\quad + \left(-\tfrac{1}{2}W^{D\,(\sigma\sigma)}_{(ik)} + a^D(\Delta)^{(\sigma\sigma)}_{(ik)}\right) \left(I^{ph}_{qc|cc}(\Delta)^{(\sigma\sigma|\sigma\sigma)}_{(lk|kl)} + I^{ph}_{cc|cq}(\Delta)^{(\sigma\sigma|\sigma\sigma)}_{(lk|kl)}\right) b^D(\Delta)^{(\sigma\sigma)}_{(lj)} \\
&\quad + b^D(\Delta)^{(\sigma\sigma)}_{(ik)} \left(I^{ph}_{cq|cc}(\Delta)^{(\sigma\sigma|\sigma\sigma)}_{(lk|kl)} + I^{ph}_{cc|qc}(\Delta)^{(\sigma\sigma|\sigma\sigma)}_{(lk|kl)}\right) \left(-\tfrac{1}{2}W^{D\,(\sigma\sigma)}_{(lj)} + a^{D*}(\Delta)^{(\sigma\sigma)}_{(jl)}\right) \\
&\quad + \left(\tfrac{1}{2}U_i\delta_{ik} + \tfrac{1}{2}U^{P\,\sigma\bar\sigma}_{(ik)} + \tfrac{1}{2}U^{X\,\sigma\bar\sigma}_{(ik)}\right) \left(I^{ph}_{cc|cc}(\Delta)^{(\bar\sigma\bar\sigma|\bar\sigma\bar\sigma)}_{(lk|kl)} + I^{ph}_{qc|cq}(\Delta)^{(\bar\sigma\bar\sigma|\bar\sigma\bar\sigma)}_{(lk|kl)} + I^{ph}_{cq|qc}(\Delta)^{(\bar\sigma\bar\sigma|\bar\sigma\bar\sigma)}_{(lk|kl)}\right) \\
&\quad \times \left(\tfrac{1}{2}U_l\delta_{lj} + \tfrac{1}{2}U^{P\,(\bar\sigma\sigma)}_{(lj)} + \tfrac{1}{2}U^{X\,(\bar\sigma\sigma)}_{(lj)}\right)\Big]
\end{aligned} \tag{S28}$$

The relative signs between the X- and the D-channel stem from the fact that they are related through ex-

change of two fermionic legs.

In equilibrium, we set

$$U^{P}{}_{ij}^{(\sigma\bar{\sigma})} = 2\mathrm{Re}\, a^{P}(2\mu)_{(ij)}^{(\sigma\bar{\sigma})}\delta_{ij},$$
$$U^{X}{}_{(ij)}^{(\sigma\bar{\sigma})} = 2\mathrm{Re}\, a^{X}(0)_{(ij)}^{(\sigma\bar{\sigma})}\delta_{ij},$$
$$W^{D}{}_{(ij)}^{(\sigma\sigma)} = 2\mathrm{Re}\, a^{D}(0)_{(ij)}^{(\sigma\sigma)}\delta_{ij}. \quad \text{(S29)}$$

Note that in equilibrium, $a^P(2\mu)$, $a^X(0)$, and $a^D(0)$ are all real matrices.

In order to fully specify the flow, it remains to fix the initial conditions at large but finite Lambda:

$$\Sigma_{ij} = \delta_{ij}U_i/2, \quad \text{(S30)}$$
$$\phi^X = \phi^P = \phi^D = 0. \quad \text{(S31)}$$

D. Implementational Details

The central region consists of $N = 61$ sites. We use $\sim$ 1500 frequencies to sample the real frequency axis. One third of the frequencies is sampled exponentially in the region $|\omega| > 4\tau$, the rest is sampled homogeneously in the region $\omega \in [-4\tau, 4\tau]$. An additional 100 frequencies are included in windows of size $4T$ around μ and 2μ. In order to numerically perform the integrals, it is useful to map the real axis to a finite region. We thus represent $\omega \in \mathbb{R}$ in terms of the variable $\tilde{y} = y/\tau \in (-7, 7)$ via

$$\omega = \begin{cases} -2\tau\frac{(\tilde{y}+6)(1+\Lambda)}{(\tilde{y}+6)^2-1} - 6\tau, & \text{for } (\tilde{y} < -6) \\ -2\tau - \tau(\tilde{y}+2)^2/4, & \text{for } (-6 < \tilde{y} < -2) \\ \tau\tilde{y}\sqrt{\frac{4}{\tilde{y}^2} - \frac{(\tilde{y}^2-4)^2}{4\tilde{y}^2}}, & \text{for } (-2 < \tilde{y} < 2) \\ 2\tau + \tau(\tilde{y}-2)^2/4, & \text{for } (2 < \tilde{y} < 6) \\ -2\tau\frac{(\tilde{y}-6)(1+\Lambda)}{(\tilde{y}-6)^2-1} + 6\tau, & \text{for } (6 < \tilde{y}). \end{cases} \quad \text{(S32)}$$

The structure of this substitution is chosen such that the van Hove divergence at the band edges is trivially integrated (i.e. the integral $\int d\omega(\omega \pm 2\tau)^{-1/2}$ is mapped to the integral const. $\times \int d\tilde{y}1$ for ω close to the band edges), while the large-frequency region is scaled with the flow parameter Λ and substituted such that the integral $\int d\omega\omega^{-2}$ (the most diverging integral that occurs) is mapped to the integral const. $\times \int d\tilde{y}1$ for $\omega \gg \Lambda$. For convenience, $y = \pm 2\tau, \pm 6\tau$ is mapped to $\omega = \pm 2\tau, \pm 6\tau$. Continuous frequency information is obtained by linearly interpolating in y-space.

The flow equation is solved with a 6th-order Runge-Kutta ODE solver with adaptive step size, while the integrals over internal frequencies are computed using Patterson sets. The integrals over internal frequencies are split into multiple intervals, such that a strong dependence on the internal frequency occurs near the integration boundaries, as the sampling is more dense there. The boundaries are determined by either the unsubstituted frequency of a Green's function or single scale propagator taking the value $\pm 2\tau$, μ, $\mu \pm 10T$, $\pm(-2\tau + V_c)$ or $\pm 2\tau \pm \Lambda$, or by the argument of the P-channel (X-channel, D-channel) taking the value 2μ (0). The flow parameter used is not Λ, but rather $u := \log\left(\frac{\Lambda}{1+\Lambda}\right)$. This improves the dynamic choice of step size within the ODE-solver. The flow starts at $\Lambda \approx 10^5$ and goes down to $\Lambda \approx 10^{-9}$. To minimize runtime, the Green's function and single scale propagator are computed at $\sim$ 30000 frequencies, and a linear interpolation in y-space is used when either of them is required in an integrand. In equilibrium, the matrices appearing are symmetric under an exchange of sites. Further, the model considered here has a left-right parity symmetry. Both symmetries are exploited by using symmetric matrices to store the self-energy and the vertex, and by using a parity basis in the computation of the Green's function and the single scale propagator.

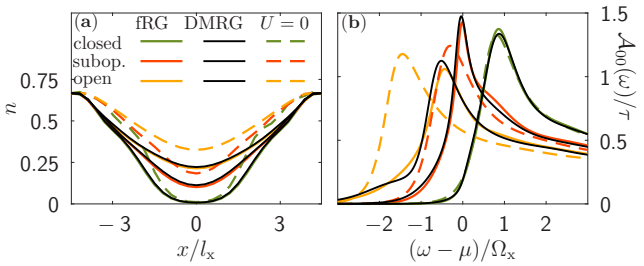

Figure S1. Comparison between Keldysh-fRG and DMRG results. (a) The local density as a function of position and (b) the LDOS as a function of energy of a closed (green), subopen (red), and open (orange) QPC, computed without interactions (dashed lines), and with interactions (solid lines), using Keldysh-fRG (colored) and DMRG (black), respectively.

S-III. DMRG CALCULATIONS

The results in the main text are obtained using Keldysh-fRG, which is based on a perturbative ansatz. To verify the validity of the fRG data, we also employ density-matrix-renormalization-group (DMRG) calculations [30]. DMRG represents one of the most powerful quasi-exact numerical method for describing one-dimensional quantum many-body systems regarding their static ground-state, dynamic, as well as thermodynamic properties. In particular, DMRG can treat fermionic systems with arbitrary interaction strength due to its non-perturbative character. Specifically, we have used DMRG to compute the local density n [Fig. S1(a)] and the LDOS [Fig. S1(b)], obtaining good qualitative agreement between our DMRG (black) and Keldysh-fRG (colored) results.

Below, we first elaborate on some peculiarities of our matrix-product-state (MPS) implementation [30], which could be of interest to practitioners, and then discuss the choice of model parameters used for this comparison.

A. DMRG details

The QPC model in Eq. (1) poses a particular challenge to DMRG since, in contrast to fRG, it is not possible to incorporate the non-interacting leads to the left and right of the interacting region by an additional term in the self-energy. Instead, a finite-size chain representation of both leads is necessary as a prerequisite to make the model accessible for DMRG. The simplest ansatz is to replace the semi-infinite leads by a finite-length tight-binding chain with open boundary conditions (OBC). However, this setup is not practicable as it requires to go to very large system sizes in order to avoid strong finite-size artefacts in physical properties in the interacting part of the QPC. Instead, we here employ the concept of smooth boundary conditions (SBC) [31], which enable us to minimize finite-size effects in the interacting region of the QPC. Implementing SBC, the parameters of the non-interacting tight-binding chains are smoothly decreased to zero towards both ends of the chain to avoid having a sharp and rigid boundary as in the OBC setup. Thus for the interacting region of the QPC, the system's size is no longer fully determinable. SBC enable us to mimic very large leads with only $\mathcal{O}(10)$ sites.

In practice, we scale the Hamiltonian parameters in the non-interacting regions (which we label symmetrically by $I = 1, \ldots, N_L$ for both the left and right lead; $I = 1$ corresponds to the left- or rightmost boundary, $I = N_L$ to the lead sites closest to the central region) with a smoothing function f_I such that $\tau_I = \frac{\tau}{2}(f_I + f_{I+1})$ and $\mu_I = \mu f_I$. Following Ref. [31], we choose $f_I = y(1 - I/[N_L + 1]])$, and the smoothing function $y(x) = \frac{1}{2}\big(1 - \tanh \frac{x-1/2}{x(1-x)}\big)$ for $0 < x < 1$, which interpolates between 1 at the edge of the central region and 0 and the boundary.

In this setup, we first determine the ground state of the QPC using standard DMRG formulated in terms of MPS. The LDOS $\mathcal{A}_i(\omega) = -\frac{1}{\pi}\mathrm{Im}G^R_{ii}(\omega)$ is then determined using time-dependent DMRG [32]. To this end, we carry out two independent tDMRG runs to determine the retarded correlator in the time domain, $G^R_{ii}(t) = -i[\langle c_i^\dagger(t)c_i\rangle + \langle c_i(t)c_i^\dagger\rangle^*]$. The entanglement in the MPS increases linearly during the real-time evolution, thus the number of states D kept in simulation needs to be continuously increased to kept the numerical error constant. This implies that the simulation is bound to some maximum time $T_{\max}$ at which the simulation is no longer numerically feasible. A finite-time cutoff typically introduces artificial oscillations in the Fourier transform, requiring some artificial broadening to obtain a smooth and positive definite LDOS. However, we can avoid incorporating a broadening function by extending $T_{\max}$ to much larger times by means of linear prediction [33]. The extrapolation scheme is expected to work for the present model since the correlator $G^R_{ii}(t)$ decreases exponentially over time scales smaller than the inverse mean level spacing and larger than the lifetime of excitations in the central region.

We end this section with some technical notes. All DMRG calculations in this work are performed with the QSpace tensor library of A. Weichselbaum [34]. We studied a QPC with an interacting region consisting of $N = 31$ sites and two non-interacting regions to the left and right containing $N_L = 50$ sites each, yielding a total of $N_{\mathrm{tot}}^{\mathrm{DMRG}} = 131$ sites, whose parameters are tuned in terms of SBCs (see above). The DMRG ground-state calculation employs a two-site update keeping up to $D = 1600$ states. Convergence was typically reached after 10 to 40 sweeps, 40 being required particularly for an almost closed QPC, where the low particle density slows down convergence and the algorithm can get stuck in local minima during early iterations. In the tDMRG simulations we use a second-order Trotter-Suzuki decomposition with a time step $\Delta t = 0.05/\tau$ and adapt the number of states in the MPS dynamically by truncating all singular values smaller than $\epsilon_{\mathrm{SVD}} = 5 \cdot 10^{-5}$. We stop the simulation when the number of kept states in the MPS exceeds $D = 4000$. In this setting, we typically reach time scales $T_{\max} \cdot \tau = 60 - 65$ before applying linear prediction.

B. Choice of model parameters

Since DMRG solves a finite system, we need a way to estimate the 'optimal' system size: We extract the LDOS as a Fourier-transform of the real time Green's function, computed by DMRG. However, the resulting LDOS is only reliable if the Green's function is evolved up to time scales of the order of the traversal time t_{trav}, as at shorter times the low-energy quasi-particles have yet to leave the central region. This means that the system size must be chosen sufficiently large, such that the reflection time $t_{\mathrm{refl}} \sim N_{\mathrm{tot}}^{\mathrm{DMRG}}/(2\tau)$ (the time until the first quasi-particles reflected at the boundary return to the center) is larger than the traversal time: $t_{\mathrm{refl}} \gtrsim t_{\mathrm{trav}}$. For the setup of the main text this yields $N_{\mathrm{tot}}^{\mathrm{DMRG}} \gtrsim 500$. Combined with the fact that we need to perform time-evolution up to the traversal time $t_{\mathrm{trav}} \approx 250/\tau$, this would have required an unfeasible amount of resources in DMRG.

In order to reduce the traversal time, we shrink the system (i.e. reduce N) and make the QPC potential steeper (i.e. increase the curvature Ω_{x}): If the curvature is larger, a larger interaction is necessary to observe the same physics, as the LDOS is smeared out more. We have tried to compensate for this by choosing an appropriately larger interaction. Comparing Figs. 2(a) and S1(b), we see that the qualitative features of the fRG-LDOS are the same: There is a roughly constant energy-shift of the LDOS in the open region, in the sub-open region the LDOS peak is sharpened (the effective potential is

flatter) and pinned to the chemical potential, while the LDOS in the closed region is almost unaffected by interactions. Since the new parameters yield results that exhibit the same qualitative features as those shown in the main text, we consider them a reasonable proxy for a direct comparison between DMRG and Keldysh-fRG.

To be specific, the set of parameters used for this comparison is: $N^{\mathrm{DMRG}} = 31$, $U^{\mathrm{DMRG}} = 0.94\tau$, $V_c^{\mathrm{DMRG}} = \{-1.69, -0.56, 0.56\}\Omega_{\mathrm{x}}^{\mathrm{DMRG}}$, $\mu^{\mathrm{DMRG}} = -\tau$, and $\Omega_{\mathrm{x}}^{\mathrm{DMRG}} \approx 0.9\tau$. Since Ω_{x} is 3 times larger than in the main text, the traversal time should be reduced by a factor of roughly 3. We find $t_{\mathrm{trav}} \approx 70/\tau$, and thus estimate $N_{\mathrm{DMRG}}^{\mathrm{tot}} \gtrsim 140$ (we use $N_{\mathrm{DMRG}}^{\mathrm{tot}} = 131$), which is still viable.

Finally, we remark that the choice of time t_{lp}, after which linear prediction is applied, is a subtle issue: The linear prediction method does not capture any physics that happens at time scales $t \gg t_{\mathrm{lp}}$ (this is an intended feature of the method, e.g. to mask finite-size effects). However, this implies that for $t_{\mathrm{trav}} \gg t_{\mathrm{lp}}$ there may exist times at which linear prediction appears stable (i.e. robust against variation of parameters used in linear prediction), while missing the finer details of the LDOS. This happens in our system for times $t_{\mathrm{lp}} \sim 30/\tau$, and is generically to be expected in a system with multiple time scales. Once the largest time scale surviving the limit of infinite leads is reached (which in our case is t_{trav}), and provided that time scale is still much shorter than the inverse level spacing, linear prediction appears to yield reasonable long-time results.

S-IV. COMPARISON TO EXPERIMENT

Numerous experiments have been performed on the 0.7 anomaly. Fig. S2 (a)-(e) displays some representative data sets from the literature for the first conductance step, showing how the step shape evolves with increasing temperature. The data shows multiple features, some of which are more robust than others:

1. When the temperature is increased, the conductance in the lower part of the conductance step ($g \lesssim 0.5$, the "pinch-off" regime), increases only weakly, whereas the conductance in the upper part of the conductance step ($0.5 \lesssim g \lesssim 0.9$, the "subopen regime") is strongly reduced. This causes the conductance step to become strongly asymmetric with increasing temperature. All data sets show this feature.

2. At the lowest temperature, a shoulder near $g \simeq 0.7$ is seen quite clearly in some data sets, e.g. (a), (e), but less clearly in (b), (c). Moreover the position of the shoulder is known to vary from sample to sample, with values in the range of 0.6 to 0.9 having been observed. Clearly, the shape of the conductance step is not universal, even at the lowest temperatures. This non-universality is exemplified by the data from [10], shown in Fig. S2(d), where the length of the QPC is varied, interpolating between a short QPC on the left and a long QPC (i.e. a short quantum wire) on the right.

3. With increasing temperatures, the asymmetry in the conductance step becomes so strong that a distinct plateau-like feature develops in some samples (a,c,e), though not in all (b,d).

To summarize, the temperature dependence of $g(T)$ shows a generic trend described in point 1 (strengthening asymmetry), but is not characterized by a set of curves $g(V_{\mathrm{c}}, T)$ of universal shape (points 2 and 3). Our data, shown in Fig. S2(f), clearly exhibits the strengthening asymmetry of point 1, while lacking the plateau at large temperatures mentioned in point 3. The absence of the plateau may be due to the fact that our Keldysh-fRG method was not able to reliably deal with a QPC at temperatures larger than the ones shown in Fig. S2(f). We suspect that the reduced reliability of our fRG method at finite temperature is due to the growing importance of multi-particle processess (recall that we neglect the three-particle vertex, and approximate the two-particle vertex through a channel decomposition). Improved fRG schemes which either do not approximate the two-particle vertex and/or strive to incorporate effects of the three-particle vertex [36] might be able to reach larger temperatures and determine if the model yields a plateau-like structure at these temperatures.

S-V. THE ENERGY STRUCTURE OF THE SPIN-SUSCEPTIBILITY

In this section, we substantiate the claim of the main text that the characteristic energy ω_{spin} of spin fluctuations is given by the distance between the chemical potential, μ, and the lower effective band edge, ω_{max}. To do so, we consider the local non-interacting spin-susceptibility, defined in Eq. (3), which at zero temperature can be written as

$$\chi_{ii}^{U=0}(\omega) = 2\pi^2 \int_{\mu}^{\mu+\omega} d\Omega \mathcal{A}_i(\Omega)\mathcal{A}_i(\Omega-\omega). \qquad \text{(S33)}$$

Let us begin by analyzing its properties for a homogenous tight-binding model with hopping τ and Fermi energy ϵ_{F} close to the lower band edge, i.e. $\epsilon_{\mathrm{F}} = \mu + 2\tau \ll D, \omega \ll D$, where $D = 4\tau$ is the band width. This choice of ϵ_{F} most closely resembles the situation in the center of a QPC. $\mathcal{A}_i(\Omega)$ is zero for energies below the band edge, shows a divergence at the band edge and subsequently decreases monotonically with increasing energies [Fig. S3 (a,b)]. $\chi_{ii}^{U=0}$ essentially counts the number of available electron-hole excitations, where the electrons have an energy of $\Omega \in [\mu, \mu+\omega]$ and the holes an energy $\Omega - \omega \in [\mu-\omega, \mu]$ [Fig. S3 (a,b)].

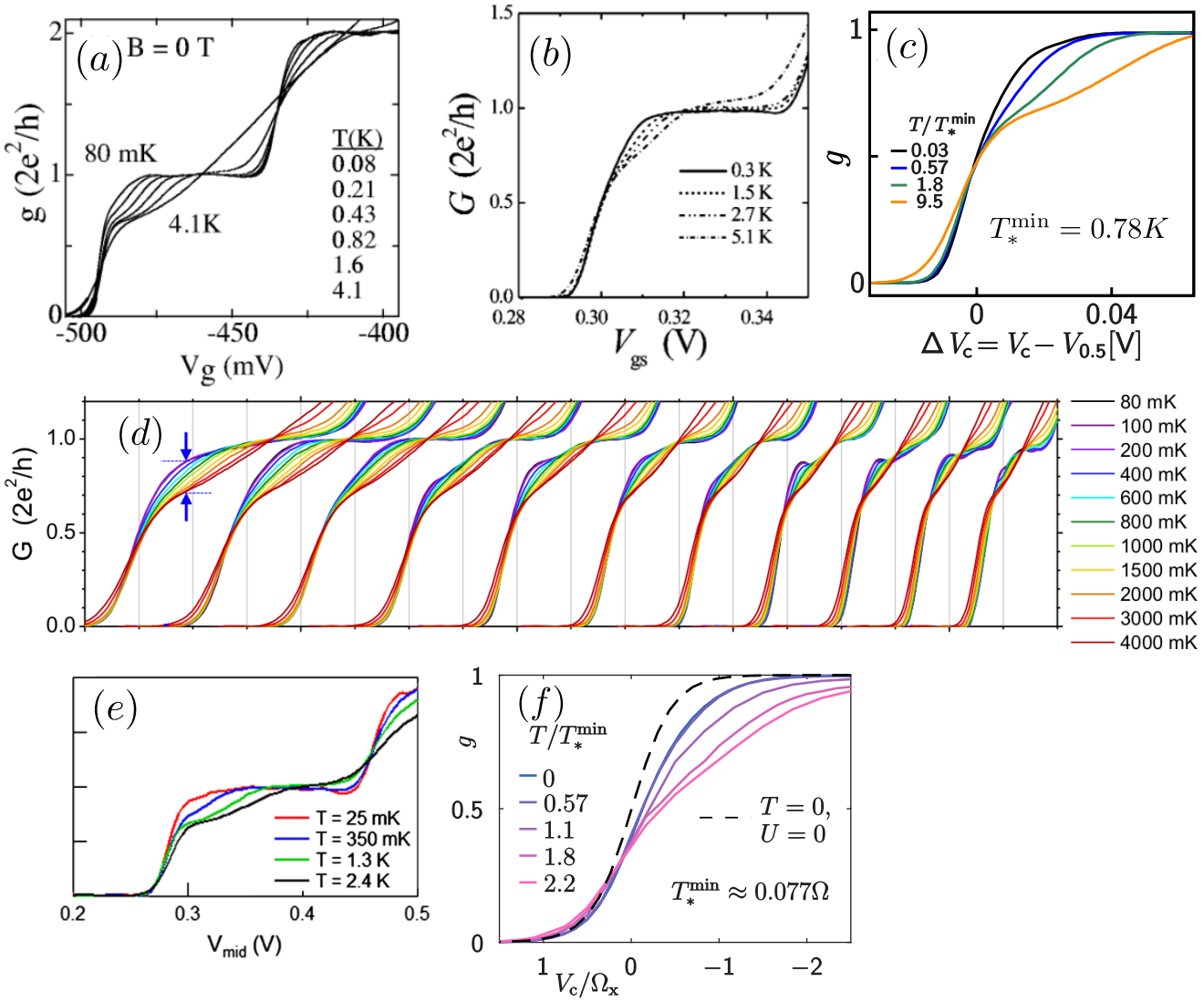

Figure S2. (a)-(e) Experimental data, reproduced from (a) [12], (b) [35], (c) [22], (d) [10] (e) [9], and (f) our data [Fig. 2(d) of the main text, with an additional curve (black, dashed) showing the conductance step for the non-interacting model ($U = 0$) at $T = 0$]. The precise form of the conductance shoulder and its evolution with temperature vary from one experiment to the next. All experiments show the common generic feature, that the conductance decreases significantly with the increasing temperature in the subopen regime. This feature is well captured by our fRG results in (f). In (d), the different curves show QPCs of increasing lengths, from a short QPC on the left to a short quantum wire on the right. Our model is used for short QPCs, corresponding to the curves on the left of (d). In (e), $T = 350$ mK, 1.3 K, and 2.4 K data are shifted horizontally by 2.5, 5, and -3.5 mV, respectively, to align with 25 mK data.

Consider $\omega < \epsilon_F$ [Fig. S3(a)]. Then

$$\partial_\omega \chi_{ii}^{U=0}(\omega) = -2\pi^2 \int_\mu^{\mu+\omega} d\Omega \mathcal{A}_i(\Omega)\mathcal{A}_i'(\Omega-\omega) + 2\pi^2 \mathcal{A}_i(\mu+\omega)\mathcal{A}_i(\mu) > 0. \quad \text{(S34)}$$

Here, the prime denotes a derivative. Thus $\chi_{ii}^{U=0}(\omega)$ increases monotonically with ω for $\omega < \epsilon_F$. This can be understood intuitively by considering the effects of an infinitesimal increase in ω: The first term in Eq. (S34) describes how, if the *electron* remains at energy Ω, the weight of the hole at energy $\Omega - \omega$ increases $[\mathcal{A}_i'(\Omega-\omega)]$. The second term in Eq. (S34) describes the appearance of additional electron-hole pairs.

For $\epsilon_F < \omega$ [Fig. S3(b)] Eq. (S34) is not useful, as the derivative of $\mathcal{A}$ is ill-defined at the band edge. We thus rewrite Eq. (S33) as

$$\chi_{ii}^{U=0}(\omega) = 2\pi^2 \int_{\mu-\epsilon_F}^{\mu} d\Omega \mathcal{A}_i(\Omega+\omega)\mathcal{A}_i(\Omega), \quad \text{(S35)}$$

where we have used the fact that $\mathcal{A}$ vanishes for arguments below the band edge to restrict the range of inte-

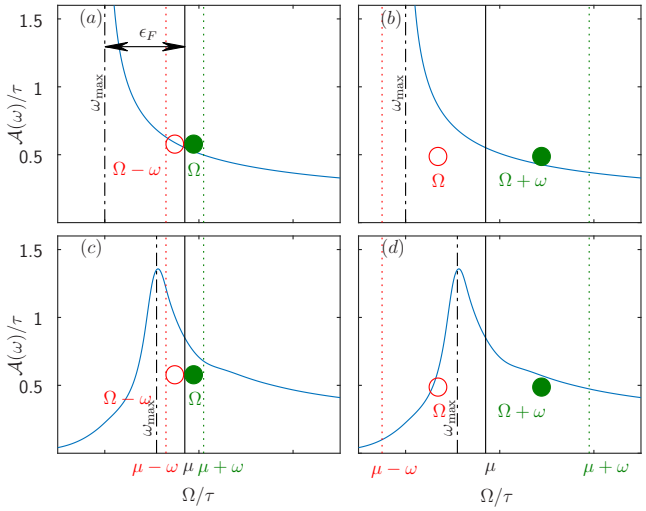

Figure S3. (a,b) LDOS of a non-interacting homogenous system and (c,d) LDOS at the central site of an interacting QPC in the open regime. The filled (empty) circles show electrons (holes) of an electron-hole pair contributing to the spin susceptibility Eq. (S33), (a,c) for $\omega < \epsilon_F$ and (b,d) for $\omega > \epsilon_F$. Electron (or hole) energies lie between the chemical potential μ (solid black line) and $\mu+\omega$ (or $\mu-\omega$), indicated by the dotted green (or red) line. The energy $\omega_{\max}$, at which the LDOS is maximal, is indicated by the black dashed-dotted line.

gration. Using Eq. (S35) we obtain

$$\partial_\omega \chi_{ii}^{U=0}(\omega) = 2\pi^2 \int_{\mu-\epsilon_F}^{\mu} d\Omega \mathcal{A}_i'(\Omega+\omega)\mathcal{A}_i(\Omega) < 0. \quad \text{(S36)}$$

For $\epsilon_F < \omega$, $\chi_{ii}^{U=0}(\omega)$ thus decreases monotonically with ω. This can again be understood intuitively by considering the effects of an infinitesimal increase in ω: consider an electron-hole pair with fixed *hole* energy Ω. The weight of the electron states near $\Omega+\omega$ [described by $\mathcal{A}_i'(\Omega+\omega)$] diminishes, reducing the spin susceptibility.

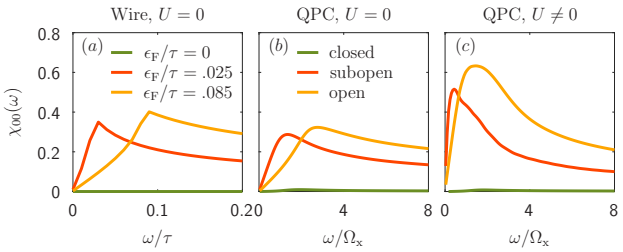

Figure S4. Local spin susceptibility as function of energy ω for (a) a non-interacting homogenous system (wire), (b) a non-interacting QPC, and (c) an interacting QPC. For the QPCs, the spin susceptibility is taken at the central site. The position of the maximum, ω_{spin}, is set by the energy difference from the lower band edge [at the central site, for (b,c)] and the chemical potential.

The above analysis and Eqs. (S34) and (S36), together, lead to the following important conclusion: For the homogenous system considered so far, $\chi_{ii}^{U=0}(\omega)$ exhibits a local maximum at an energy, ω_{spin}, that corresponds to the Fermi energy, i.e. to the distance between the chemical potential μ and the lower band edge $\omega_{\max}$, $\omega_{\text{spin}} = \mu - \omega_{\max}$. The function $\chi_{ii}^{U=0}(\omega)$ for a non-interacting homogenous system is shown in Fig. S4(a).

We now switch to a QPC geometry in the presence of interactions. The inhomogenuity of the QPC potential changes the divergence of the bare LDOS at the band bottom into a broadened peak, but leaves the other features of the LDOS qualitatively unchanged [compare Figs. S3(a) and (c), or Figs. S3 (b) and (d)]. The geometric effect of a smeared LDOS on $\chi_{ii}(\omega)$ can already be seen for a non-interacting QPC [Fig. S4(b)]: The sharp maximum gets smeared out, but the qualitative shape of $\chi_{ii}(\omega)$ remains the same as in Fig. S4(a).

For an interacting QPC, all of the above arguments still apply within a Fermi liquid picture, albeit with renormalized parameters. We thus expect in the interacting QPC that $\omega_{\text{spin}} \simeq \mu - \omega_{\max}$, where both ω_{spin} and $\omega_{\max}$ are renormalized quantities. This situation is shown in Fig. S4(c): Compared to the non-interacting QPC, the effective barrier is higher, reducing ω_{spin}. Moreover, there is an additional overall enhancement of the spin susceptibility in the interacting system due to Stoner physics.

Chapter 7

The frequency-resolved QPC

In this chapter, we will analyze the workings of a QPC from a dynamical perspective, i.e. we will look at frequency-resolved correlation functions. This chapter is intended as a an addendum to chapter 6. We will repeat the most important insights from chapter 6 and add some further concepts (the local distribution function is explained in Sec. 7.5, the S-matrix is considered in more detail in Sec. 7.4).

In order to emphasize the left-right symmetry of the problem and to connect to chapter 6, throughout this chapter we use the convention that the central site of the QPC is labelled by zero, and the left-most site has a negative index.

7.1 Local density of states

The main quantity we consider is the local density of states[1]

$$\mathcal{A}_i(\omega) = -\frac{1}{\pi}\mathrm{Im}G^R_{ii}(\omega). \tag{7.1}$$

Before we delve into the shape of the LDOS in a QPC, let us first as warm-up consider a one-dimensional homogeneous system. The LDOS is then given by

$$\mathcal{A}_i(\omega) = -\frac{1}{\pi}\int dk \mathrm{Im}\frac{1}{\omega - \epsilon(k) + i\eta} = \partial_\epsilon k(\epsilon)|_{\epsilon=\omega}, \tag{7.2}$$

where we have introduced the dispersion $\epsilon(k)$, its inverse $k(\epsilon)$, and an infinitesimal regularizer $\eta > 0$.[2] If we recall that the group velocity for a given dispersion is given by $v_{\mathrm{group}} \sim \partial_k \epsilon$, we see that the LDOS is proportional to the inverse velocity of a wave-packet centered at the corresponding energy $\mathcal{A}_i(\omega) \sim \frac{1}{v_{\mathrm{group}}}$.

[1] We remark that the definition Eq. (7.1) is for a system with a spatial lattice. In relativistic QFTs in continuum we usually cannot sensibly define a local density of states, due to divergences in the UV (the equal position correlation function is generically problematic in these theories).

[2] In a homogeneous system, the momentum k is a good quantum number and may be used to label eigenstates and eigenenergies $\epsilon(k)$.

If instead of a homogeneous system we now consider an inhomogeneous system where the inhomogeneity is adiabatically turned on, we may view the system as basically homogeneous, but with a weakly position-dependent momentum. We then expect to obtain $\mathcal{A}_i(\omega) \sim \frac{1}{v_{\mathrm{group}}(i)}$, where $v_{\mathrm{group}}(i)$ is the group velocity at site i. We may compute $v_{\mathrm{group}}(i)$ from the dispersion $\epsilon(k)$ of the homogeneous system and the local momentum $k(i)$.

Before we consider actual data of a QPC, let us formulate our expectations:

(a) Our model is one-dimensional and – in the leads – describes particles with a quadratic dispersion $\epsilon(k) = \frac{k^2}{2m}$. We obtain the group velocity $v_{\mathrm{group}}(\epsilon) = \sqrt{\frac{2\epsilon}{m}}$. Intuitively speaking, particles at low energy are slow. If we consider the LDOS, we see that this dispersion yields a $1/\sqrt{\epsilon}$-divergence if the momentum approaches zero (the kinetic energy becomes minimal). The LDOS should thus be large whenever the momentum is small.

(b) Since we think of a QPC as a barrier, there are tunneling states. This means that for a barrier of finite length, the LDOS underneath the barrier should not be zero. However, since tunneling is exponentially suppressed in a semi-classical approximation, we expect the LDOS below the barrier to vanish quickly the deeper we penetrate into the barrier.

(c) If we have states with a long lifetime (e.g. because these states couple only very weakly to the leads), these states should appear as narrow strips in frequency space at the sites where they are mainly localized. Candidates for such states are states outside of the leads' bandwidth, or states localized by a potential (e.g. between two barriers).

(d) At positions somewhat removed from the inhomogeneity we expect to see Friedel oscillations, i.e. peaks in the LDOS with a distance of $\lambda_F/2$ because the eigenfunctions are standing waves.

(e) Actually, our spatial direction is discretized, leading to a dispersion of the form $\epsilon(k) = -2\tau\cos(ka)$, with the hopping τ and the lattice spacing a. The corresponding group velocity $v_{\mathrm{group}}(\epsilon) = 2\tau a\sqrt{1 - \frac{\epsilon^2}{4\tau^2}}$ goes to zero for $\epsilon \to \pm 2\tau$. We thus expect a large LDOS not only at the lower band edge, where the dispersion is approximately quadratic, but also at the upper band edge (where the dispersion is quadratic as well, although with the opposite curvature and a different offset).

Since all of the above expectations hold for both interacting and non-interacting systems, we first consider the LDOS of non-interacting systems. Fig. 7.1(a-c) shows the LDOS of a non-interacting QPC (zoomed in on the barrier) at three different gate voltages V_{g}. To check the veracity of our expectations, we observe:

(a) The LDOS is large just above the barrier. At energies only slightly above the barrier, most of the energy is used as potential energy and the kinetic energy (and thus the momentum) is small.

(b) The LDOS underneath the barrier is very small. However, we can see that some of the LDOS leaks underneath the bare barrier (the bare barrier is indicated by the black curve).

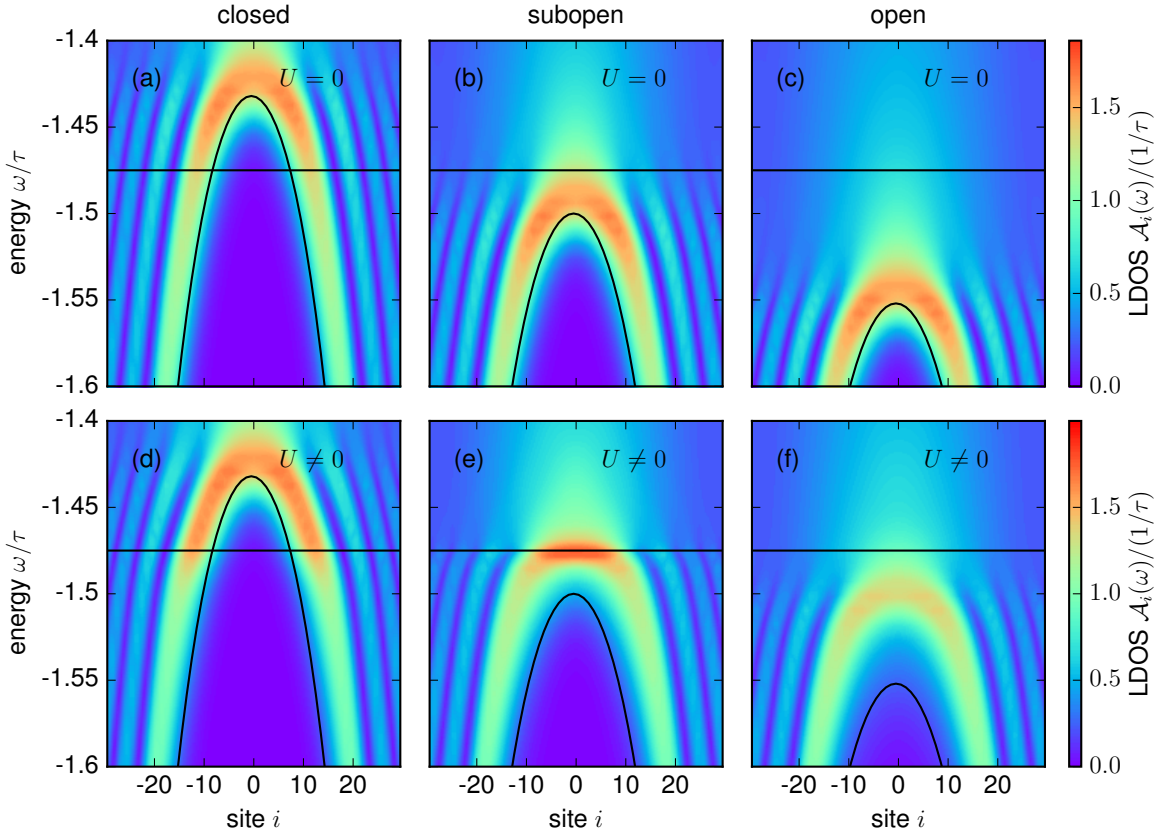

Figure 7.1: The local density of states (color scale) of a QPC with 61 sites as function of position (site) and energy ω at zero temperature. The maximum of the QPC potential is at site $i = 31$. Upper row: non-interacting ($U = 0$); lower row: interacting. From left to right: closed, subopen, and open QPC. The black horizontal line indicates the chemical potential and the black curve indicates the effective *bare* barrier. We clearly observe *flattening* and overall *growth* of the renormalized effective barrier due to interactions.

(c) (Quasi-)bound states do not appear in a QPC.

(d) Away from the center, there are clear stripes visible in the LDOS.

(e) In the non-interacting system, a change of chemical potential would have no influence whatsoever on the LDOS. We see that our choice of varying the gate voltage V_g instead of the chemical potential μ does not deform the barrier in a significant way throughout the range of parameters we consider. Therefore the LDOS of the closed QPC in a window around the chemical potential (the LDOS for low-energy excitations) looks just like the LDOS of the open QPC, only the window is shifted to a different energy.

Upon turning on interactions, we arrive at Fig. 7.1(d-f). In the closed QPC [Fig. 7.1(a,d)], we observe very little change in the LDOS. As soon as we reach the (sub-)open region however [Fig. 7.1(b,c,e,f)], we observe two clear effects:

(i) The peak of the LDOS is shifted to higher energies, i.e. the renormalized effective barrier is higher.

(ii) The peak of the LDOS is spatially broader, i.e. the renormalized effective barrier is flatter.

Both of these effects can qualitatively be understood as a Hartree-shift: To first order in the interaction U, the renormalized barrier $V_{\mathrm{ren,eff}}$ is

$$V_{\mathrm{ren,eff}}(x) = V_{\mathrm{bare,eff}}(x) + U(x)n(x), \tag{7.3}$$

where $n(x)$ is the local density. The density is small in the center of the QPC, and grows towards the QPC's edges. We thus expect the effective renormalized barrier to be higher than the bare effective barrier (once there is some density of electrons within the QPC's center). The growth should be larger away from the center, as the density there is higher than in the QPC's center. Thus, the barrier is shifted up in the (sub-)open region, and the effective renormalized barrier is flattened. We remark that a flatter barrier leads to a higher peak in the LDOS.

It is important to note that the first-order Hartree-shift can only yield a qualitative understanding of the new effective potential. While studies using the self-consistent Hartree approximation have found the same qualitative behavior, the effective renormalized barrier obtained in these studies leads to a conductance that disagrees with the experimental observations [SL13] (which the authors of [SL13] attribute to their choice of a smooth potential; in our view, the self-consistent Hartree approximation is simply not sufficiently powerful to capture all the relevant physics of the system).

It is also necessary to take into account the non-local parts of the self-energy and their effect on the renormalized effective barrier, as neglecting long-range parts of the self-energy leads to a wrong conductance and a wrong LDOS.[3]

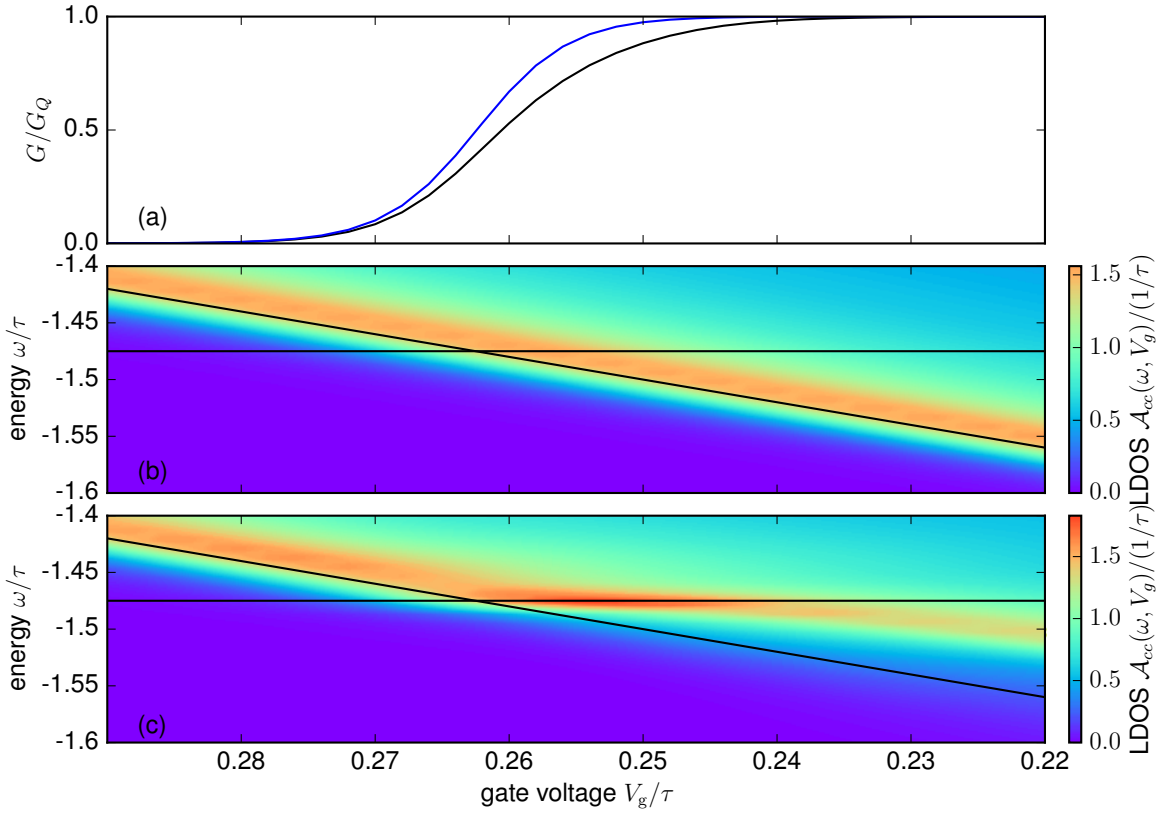

Figure 7.2: The local density of states (color scale) of a QPC at the central site as function of gate voltage V_g and energy ω at zero temperature [(b) non-interacting, and (c) interacting]. The black horizontal line indicates the chemical potential and the black diagonal line indicates the top of the effective *bare* barrier. For better identification of the relevant regions, we show the conductance [(a): the non-interacting conductance is shown in blue, the interacting conductance in black]. Throughout the subopen region, we clearly see that the maximum of the LDOS (i.e. the top of the renormalized effective barrier) is *pinned* to the chemical potential. Once the QPC is open, the maximum of the LDOS follows the gate voltage, although with a slightly different slope.

7.2 Resonant energy structure

Now that we have seen the structure of the LDOS at some given gate voltages V_g, let us consider the evolution of the LDOS as we vary V_g. If we want to see how the frequency-resolved LDOS changes as we vary V_g, we either have to take a lot of snapshots or decide on either a single site or the average of some sites. One possible choice is to view the LDOS at the central site as function of V_g and frequency ω. Following [IZ09], we call $\mathcal{A}_{\text{central site}}(\omega, V_\mathrm{g})$ the "resonant energy structure".[4] The result is shown in Fig. 7.2 (b,c). Fig. 7.2 shows the non-interacting LDOS at the central site as function of gate voltage V_g and energy ω. The solid black diagonal is the nominal barrier top (the maximum of the bare effective barrier). As can be clearly seen, the non-interacting resonant energy structure simply follows the nominal barrier top.

Upon adding interactions, we obtain Fig. 7.2(c). As long as the QPC is closed [we have plotted the conductance in Fig. 7.2(a) to allow for an easy identification of the different regimes], there is no significant difference in the resonant energy structure between the interacting and the non-interacting case. We have made the same observation for the LDOS in Fig. 7.1(a,d). As we reach the sub-open regime, we observe a pinning of the peak in the LDOS to the chemical potential (the chemical potential is indicated as a horizontal black line). Only once the QPC is open, the peak in the LDOS leaves the chemical potential and once again roughly follows the nominal barrier top (with an additional offset, and a slightly modified slope). The offset and the slightly slower growth of the energy of the peak in the LDOS can qualitatively be understood through the same Hartree-term we used earlier (c.f. Eq. (7.3)): Once the QPC is open, there is non-vanishing electron-density in the center which increases the effective renormalized barrier height. This electron density grows slowly as the QPC is opened further, thus reducing the effect of lowering the barrier, leading to a less steep slope of the peak of the LDOS.

For now, let us focus on the pinning of the peak of the LDOS to the chemical potential throughout the sub-open region. It is this pinning that sets apart the sub-open region from all other points in the conductance curve. When the peak of the LDOS is at the chemical potential, interaction effects are enhanced. We thus expect a strong reaction of the system to external stimulus (magnetic field or temperature) in and throughout the sub-open region. This strong reaction is in fact the common feature of all experimental data on the 0.7 anomaly (we note that the 0.7 anomaly occurs in exactly the region where we observe pinning of the peak of the LDOS to the chemical potential).

As a sanity check of our claims, we may estimate the interaction strength required to observe pinning: If we infinitesimally reduce the bare barrier height from V_0 to $V_0 - \delta V_0$, we increase the electron density n at the center to $n + \mathcal{A}_c(\omega = \mu)\delta V_0$. The renormalized effective barrier height changes from $V_0 + Un$ to approximately $V_0 - \delta V_0 + n + U\mathcal{A}_c(\omega = \delta)\delta V_0$. "Pinning"

[3] By "barrier" we denote the structure that pushes the maximum of the LDOS upwards. Note that we do not construct an on-site potential in the sense of a Kohn-Sham potential. "Barrier" in our context is thus slightly fuzzy, but attempts at more precise definitions are not necessary for a qualitative understanding.

[4] In [IZ09] the resonant energy structure is the position of the LDOS peak averaged over the QPC area. While the averaged position contains less information than the frequency-resolved LDOS, the idea behind the object considered is sufficiently close that we feel justified in using their term.

means that the new height of the barrier is the same as the old height of the barrier:

$$V_0 + Un \stackrel{!}{=} V_0 - \delta V_0 + Un + U\mathcal{A}_c(\omega = \delta)\delta V_0 \Rightarrow \mathcal{A}_c(\omega = \delta)U = 1. \tag{7.4}$$

Since we have used only the most naïve, first order in U, arguments, we cannot expect the relation $\mathcal{A}_c(\omega = \delta)U = 1$ to be satisfied exactly. However, it should yield the correct order of magnitude. For the plots shown in Fig. 7.2, we have $\mathcal{A}_c(\omega = \delta) \approx 1.4/\tau$, $U = 0.7\tau$, and thus $\mathcal{A}_c(\omega = \delta)U \approx 1$.

7.3 Local Fermi wavelength

In an inhomogeneous system, there is usually at least one intrinsic length-scale to the problem (the length scale(s) of the inhomogeneity). Before we turn to the QPC, let us take a short look at the quantum mechanical harmonic oscillator $H = \frac{p^2}{2m} + \frac{k}{2}x^2$. The eigenfunctions (polynomial times a Gaussian) contain the characteristic length $l_\mathrm{x} = (mk)^{-1/4}$.[5] The parabolic QPC-potential we use may be thought of as the continuation of the harmonic oscillator when sending $k \to -k$. After the continuation $k \to -k$, the eigenfunctions retain the same characteristic length scale.[6]

On a lattice, we use the length

$$l_\mathrm{x} = a\sqrt{\tau/\Omega_\mathrm{x}} \tag{7.5}$$

as characteristic of the potential. If there is a significant deviation from a parabolic potential at lengths smaller than l_x, we should not think of the potential as parabolic.

Is l_x the length scale associated with low-energy excitations in the center of the QPC (in other words: is l_x a relevant scale)? Yes, but we can do better: If the low-energy degrees of freedom are electrons (if the model is in the perturbative regime), at low energies there is intrinsically a further length-scale in the problem: the Fermi-wavelength λ_F. In the region where electrons barely crest the QPC (at a conductance of about $0.8G_Q$), the Fermi-wavelength in the center of the QPC is of the same order as l_x. However, it is straightforward to extract a reasonable idea of the precise value of λ_F from the single-particle Green's function, while it is

[5] This length is extracted from the decay of the Gaussian in the ground state wave function $\psi(x) \sim \exp(-\frac{x^2}{2l_\mathrm{x}^2})$. There are different conventions for defining this length scale (e.g. $\psi(x) \sim \exp(-\frac{x^2}{l_\mathrm{x}^2})$). The common definitions differ by factors of $\sqrt{2}$.

[6] While we retain the same scale, the interpretation of the scale differs drastically: In the harmonic oscillator, the scale l_x is the characteristic spatial extent of the eigenfunctions. For the inverted parabolic potential (the QPC), it is the characteristic scale of oscillations of wave-functions at energies corresponding to the resonance.

A similar change of interpretation occurs for the energy: The energy of the oscillator is determined by the scale $\omega = \sqrt{k/m}$. Since we can solve the spectrum of the oscillator exactly, we also know the spectrum of the inverted parabolic potential. The spectrum can be thought of as having complex eigenvalues (when sending $k \to -k$ in $\omega = \sqrt{k/m}$, ω becomes imaginary). These complex eigenvalues physically correspond to resonances, whose energy is determined by the real part and whose width is determined by the imaginary part [LB06]. Physically, a well-defined resonance would have a width much smaller than the distance to the next energies. The resonances in the inverted parabolic potential all lie at the same energy. While we may still use the terminology of resonances typically employed when talking about complex eigenvalues, we must be aware that they do not constitute resonances in the sense of well-defined peaks in the transmission.

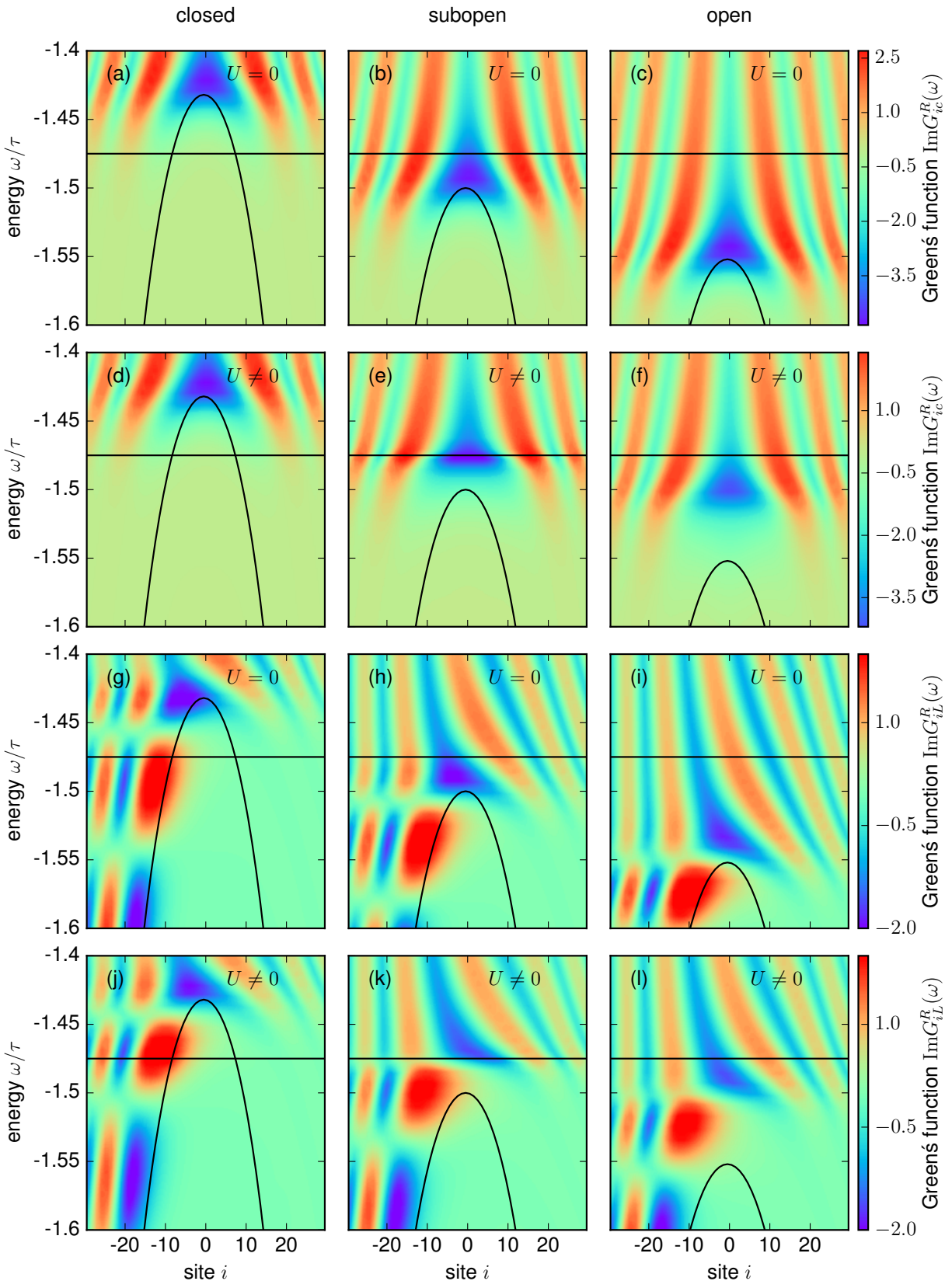

Figure 7.3: (a,b,c,d,e,f) The imaginary part of the Green's function $\mathrm{Re}G^R_{ci}(\omega)$ (colorscale) between the center of the QPC and site i as function of site and energy ω. (g,h,i,j,k,l) The imaginary part of the Green's function $\mathrm{Re}G^R_{Li}(\omega)$ (colorscale) between the left boundary of the QPC and site i as function of site and energy ω. (a,b,c,g,h,i) are non-interacting, (d,e,f,j,k,l) include interactions. The solid black line indicates the bare barrier.

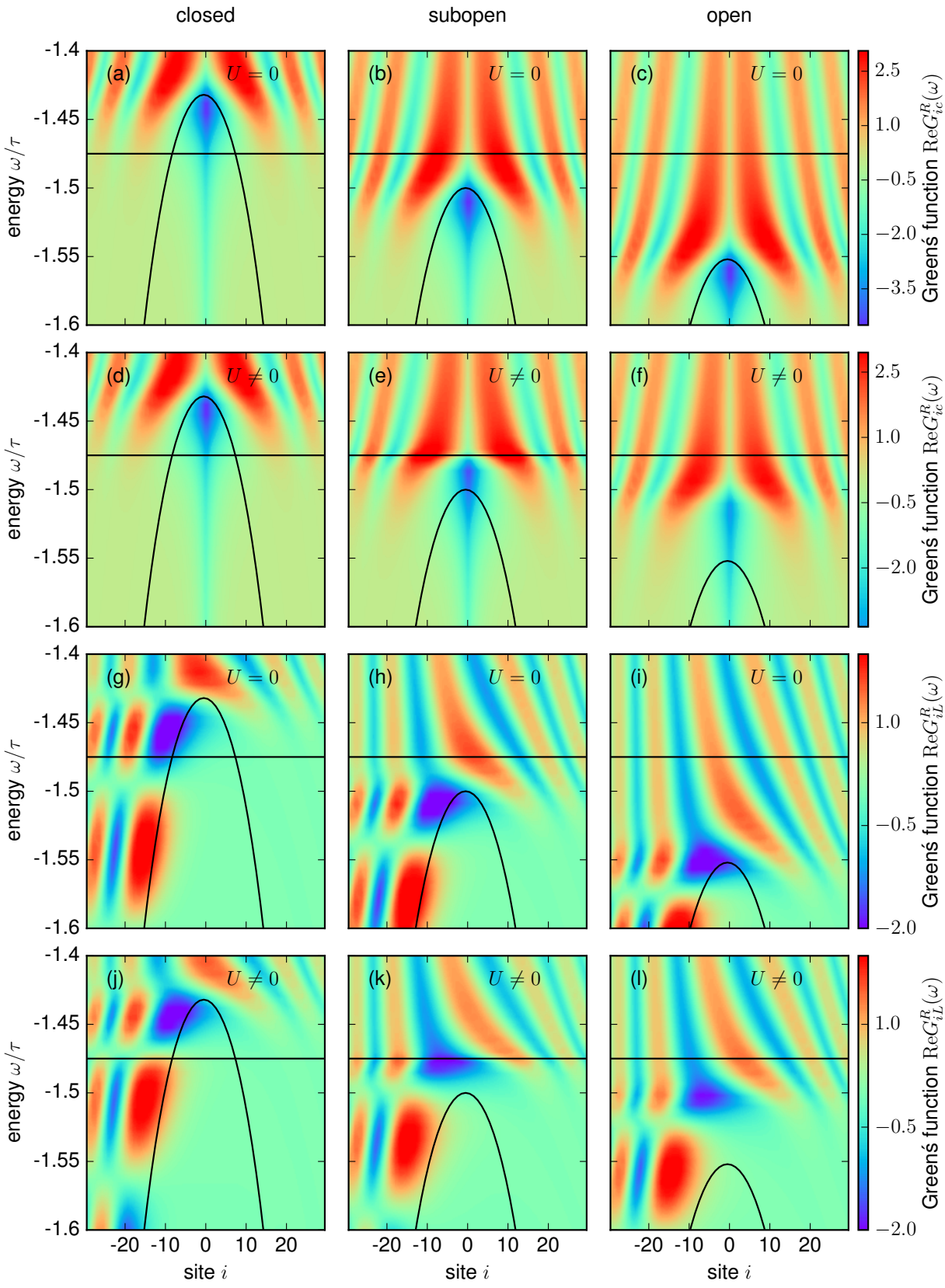

Figure 7.4: (a,b,c,d,e,f) The real part of the Green's function $\mathrm{Re}G^R_{ci}(\omega)$ (colorscale) between the center of the QPC and site i as function of site and energy ω. (g,h,i,j,k,l) The real part of the Green's function $\mathrm{Re}G^R_{Li}(\omega)$ (colorscale) between the left boundary of the QPC and site i as function of site and energy ω. (a,b,c,g,h,i) are non-interacting, (d,e,f,j,k,l) include interactions. The solid black line indicates the bare barrier.

somewhat more difficult to access the renormalized length l_{x}, because the renormalized barrier also depends on off-off-diagonal hopping elements, which are generated during the RG-flow.

Let us consider $\mathrm{Im}G^R(\omega = \mu)$. Fig. 7.3(a-f) shows $\mathrm{Im}G^R(\omega)_{ic}$, where c is the central site of the QPC. If we consider a fixed energy ω, we observe spatial oscillations, which we expect to occur with a spatial modulation determined by the corresponding wavelength λ.[7] We clearly see that the spatial modulation varies (i.e. λ varies), and the spatial oscillation is slower in the center (λ is larger in the center). This is in good agreement with the qualitative semi-classical idea that electrons in the center of the QPC are slower, leading to a smaller momentum and a larger wavelength. At higher energies, the local wavelength is shorter, as the electrons have more energy. At energies below the barrier, we observe hardly any features remaining. This absence of features below the barrier is related to the fact that we consider the Green's function between the center of the QPC and some other position: Far below the barrier, there are essentially no states (the LDOS is exponentially small in the distance between ω and the nominal barrier top underneath the barrier). Thus, any correlation function where we attempt to either add or remove an electron far below the barrier is extremely small (and not visible at all on the scale set by the correlation function in the (sub-)open regime).

In the non-interacting case [Fig. 7.3(a-c)], a change of the barrier height (V_{g}) merely shifts the structure explained previously. In the interacting case [Fig. 7.3(d-f)], a change of the barrier height (V_{g}) once more exhibits features of the Hartree-shift, pinning, and self-flattening: The energy below which features vanish (i.e. the energy below which Fig. 7.3(d-f) appears essentially mono-colored) is increased. As in the non-interacting case, this energy is slightly below the renormalized barrier top. The spatial extent of oscillations, i.e. the local Fermi wavelength, is enhanced as expected for a flatter barrier.

We observe that a precise definition of a local Fermi wavelength is tricky as significant modulation of the spatial oscillation length occurs within a single oscillation: Consider a subopen QPC at an energy $\omega = \mu$ (indicated by the black, horizontal line). In both the interacting and non-interacting case, we may attempt to define half of a Fermi-wavelength as the distance between two zeros. The distance between the two zeros closest to the center (one on the left, one on the right of the center) however is much larger than the distance between either of these zeros and the next zero (by a factor of about 2 in the interacting case). Since the length of an oscillation thus varies drastically within a single oscillation, we cannot simply define a clear $\lambda_F(x)$ in the same way we would if the potential were adiabatic. However, we may still compare any occurring spatial structure with a Fermi wavelength, we just have to consider the actual oscillations of G^R instead of a simple value for λ_F.

To recap: The *idea* of a local Fermi wavelength is valid, but the local Fermi wavelength varies quickly and we need to extract it directly from G^R.

We also note that the Fermi wavelength in the center of the QPC is such that half an oscillation covers the central region within $[-l_{\mathrm{x}}, l_{\mathrm{x}}]$. Thus, the shape of the barrier is highly relevant and the barrier may certainly not be treated as adiabatic (in the sense of "adiabatic" corresponding to "essentially constant over the typical scale probed by the excitations").

Let us now consider Fig. 7.3(g-l), which shows $\mathrm{Im}G^R(\omega)_{iL}$, where L is the left-most site of

[7] If the energy lies at the chemical potential, $\omega = \mu$, the corresponding wavelength is just the Fermi wavelength λ_F.

the QPC. Similarly to Fig. 7.3(a-f), we observe spatial modulations whose wavelength is reduced the higher the energy is. The wavelength is large at the barrier top, which again exhibits pinning, the Hartree-shift and self-flattening. We note that the local length scales are similar to the ones extracted with G^R_{ic}.

Compared with G^R_{ic} (Fig. 7.3(a-f)), G^R_{iL} (Fig. 7.3(g-l)) shows two further features: (i) at energies where transmission is small, there are strong oscillations on the left of the QPC, but no features on the right of the QPC; and (ii) the strong oscillations on left of a closed QPC exhibit an additional modulation with energy. Both of these features are easy to explain: If we consider excitations below the renormalized barrier top, the transmission is low (the tunneling amplitude is suppressed exponentially in the area underneath the potential). Thus, if we add an electron on the left of the barrier, it cannot efficiently propagate to the right of the barrier. In other words, the correlation function between left and right half of the central region is very small. If hardly any electrons are transmitted, then almost all electrons are reflected. At a given energy, the eigenfunctions of almost entirely reflected particles are – in good approximation – standing waves with a node at the barrier and a wavelength determined e.g. through WKB-type arguments. These eigenfunctions will exhibit (approximate) nodes at a specific point in space at some energies. If we hit an energy where the eigenfunction has an approximate node at the site L, we cannot excite this mode by adding or removing an electron at site L (or excite the mode only very weakly). Thus, at energies corresponding to this mode, the correlation function G^R_{iL} should approximately vanish, leading to a modulation of the spatial oscillations in the energy direction.

For completeness, Fig. 7.4 shows the real part of the Green's function, but is otherwise identical to Fig. 7.3. We observe the same features in the real part of the retarded Green's function as in the imaginary part. The reason for the similarity is simple: since $G^R(\omega)$ is analytic in the upper half plane and decays sufficiently fast, $G^R(\omega)$ satisfies the Kramers-Kronig relation connecting its real and imaginary parts. However, there is one additional feature in $\mathrm{Re}G^R_{iC}(\omega)$: a stripe at the center where $\mathrm{Re}G^R_{CC}(\omega)$ is almost zero for energies above the barrier and the modulus of $\mathrm{Re}G^R$ is large for energies below the barrier. This stripe can be understood by considering a single level of energy ϵ and width Γ. The real part of $G^R_{\text{single level}}(\omega)$ of such a single level is $\mathrm{Re}G^R_{\text{single level}}(\omega) \sim \frac{\omega-\epsilon}{(\omega-\epsilon)^2+\Gamma^2}$. So, if the energy ω hits the level, the real part of $G^R_{\text{single level}}$ vanishes, while the modulus of the real part takes its maximal value somewhat removed from the single level. Heuristically, in the band ω almost always hits a level, leading to a small on-site $\mathrm{Re}G^R$, while in the tunneling region there are almost no states to encounter, such that $|\mathrm{Re}G^R|$ becomes large and $\mathrm{Re}G^R$ becomes negative for energies below the level (the position of the "level" in the tunneling case is determined by the maximum of the LDOS).

7.4 One-particle S-matrix

The one-particle S-matrix links asymptotic one-particle states and is for our system given by [Tay12]

$$\mathcal{S}_{ab}(\omega) = \mathbb{1} - 2\pi i\rho\tau^2 \begin{pmatrix} G^R_{LL}(\omega) & G^R_{LR}(\omega) \\ G^R_{RL}(\omega) & G^R_{RR}(\omega) \end{pmatrix}, \tag{7.6}$$

where a, b take the values l(eft lead) and r(ight lead), and ρ is the density of states of the last lead site coupling to the system.[8] We would like to interpret the S-matrix according to

$$\mathcal{S}_{ab}(\omega) = \begin{pmatrix} R_L(\omega) & T_{LR}(\omega) \\ T_{RL}(\omega) & R_R(\omega) \end{pmatrix}, \tag{7.7}$$

where R and T denote reflection and transmission amplitudes. If all one-particle states are scattered into one-particle states, the one-particle S-matrix is unitary $SS^\dagger = 1$. In equilibrium, due to the parity-symmetry of our setup, we have $|T_{LR}| = |T_{RL}|$ and $|R_L| = |R_R|$. In equilibrium, the one-particle S-matrix is diagonalized by considering symmetric or antisymmetric wave-functions $(r, l \to \frac{1}{2}(r+l), \frac{1}{2}(r-l))$. If the one-particle S-matrix is unitary, then its eigenvalues must be of norm one, i.e. its eigenvalues λ_i may be represented as $\lambda_i = \exp(i\phi_i)$. ϕ_i is the symmetric or antisymmetric scattering phase.[9]

7.4.1 Loss of one-particle probability

Before we go into any details regarding the structure of the one-particle S-matrix, let us consider an incoming particle *at finite energy*.[10] At finite energy, there is the possibility of inelastic scattering: While one particle of energy ω comes in, we may have e.g. two particles and one hole of combined energy ω leave the system. This process is not part of the one-particle S-matrix given in Eq. (7.6). Since the one-particle S-matrix misses out on some final states, we do not expect it to be unitary. In fact, we would expect the operator norm of the S-matrix to be smaller than 1 (any normalized in-state is mapped to an out-state of at most the same norm; typically, the norm of the out-state is smaller than the norm of the in-state as not all physically possible out-states are contained in the out-states covered by this one-particle S-matrix).

Fig. 7.5 shows the norm of the deviation of the squared interacting single-particle S-matrix $|SS^\dagger - \mathbb{1}|$ from the identity as function of gate voltage and energy at zero temperature (Fig. 7.5(a)) and at finite temperature (Fig. 7.5(b)).[11] In the non-interacting case, only elastic scattering is possible. In other words, a single incoming particle at energy ω can only scatter into a single outgoing particle at energy ω. While the outgoing particle may be reflected or transmitted, the

[8] The assumptions that go into the derivation of Eq. (7.6) (in addition to the usual assumptions in scattering theory) are:

1. The system couples to two similar leads (both leads have the same spectrum and couple – apart from the position – to the system in the same manner).
2. There is a one-to-one correspondence between energy (frequency) ω and an asymptotic eigenstate within the lead.
3. Fermions are good degrees of freedom within the lead.

[9] Even if the one-particle S-matrix is not unitary, we will still refer to the appropriate phases as "scattering phases".

[10] By "finite energy", in this section we mean to say: Not at the chemical potential. While it is theoretically easy to postulate finite energy for the incoming electrons, experimentally it is much easier to go to either finite temperature or finite bias. The effects we describe here also appear in these situations.

[11] To be precise, we use the matrix 2-norm, which is equivalent to the modulus of the largest singular value of the matrix and the operator norm.

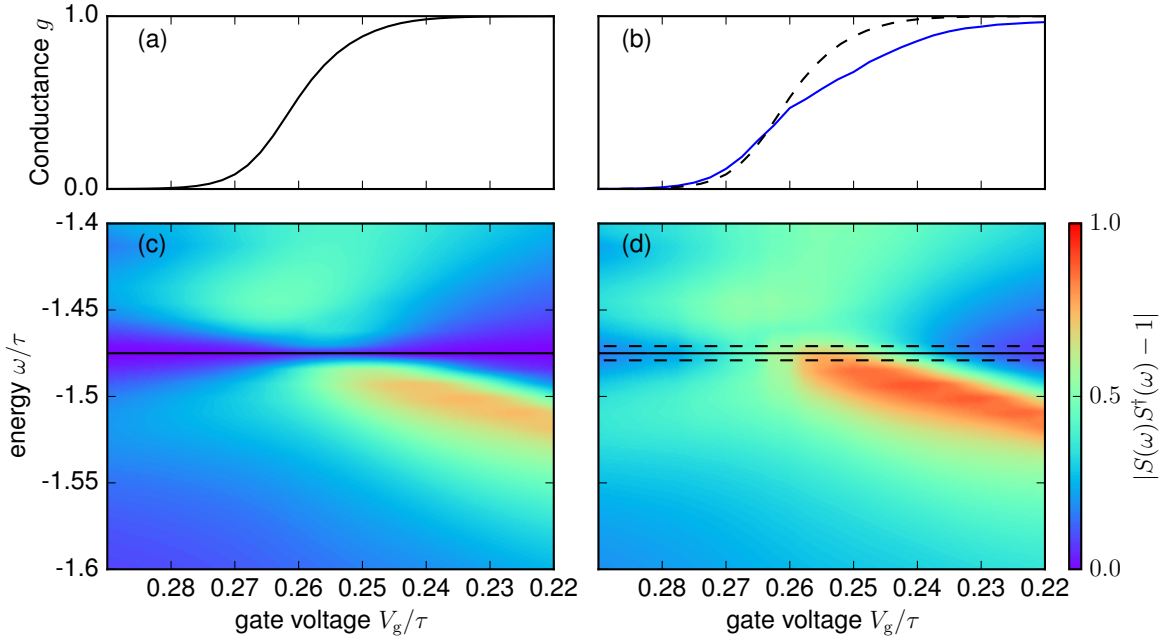

Figure 7.5: (a,b) The conductance as function of gate voltage for reference. Computed values at zero temperature are shown (a) as black solid line and (b) as black dashed line. Computed values at finite temperature are shown as blue curve in (b). (c,d) The norm of the deviation of the squared single-particle S-matrix from the identity matrix (colorscale) as function of gate voltage and energy; (c): zero temperature; (d): finite temperature. In the non-interacting case (not shown), particles cannot decay (decay happens by losing energy and exciting particle-hole-pairs) and the single particle S-matrix is unitary, i.e. $|S_{\mathrm{nonint}}S^\dagger_{\mathrm{nonint}}| = 1$. At zero temperature, electrons at the chemical potential (black line in c,d) do not decay (we are within a Fermi liquid, which is characterized by stable quasi-particle excitations at the chemical potential). At zero temperature, close to but not at the chemical potential, still no decay occurs. This means that the relevant physics has a reasonable chance of being captured by a static approximation. At finite temperature (d), the situation is drastically different: Even at the chemical potential (full black line; the dashed lines indicate $\mu \pm T$ to set the scale), single-particle physics is clearly insufficient to capture the full physics in the subopen region. Far in the closed or open region, the single particle excitations stabilize and the physics might be well-described by a static approximation.

single-particle S-matrix of a non-interacting system is unitary, $SS^\dagger = \mathbb{1}$.[12] In the interacting case, a single incoming electron may "decay" into an outgoing electron at a smaller energy and some number of electron-hole pairs (which may be split up; for example, if we inject a single electron from the left, a possible outgoing state would be two electrons exciting on the right and a hole moving to the left). Note that "smaller energy" should – in this context – be understood as "closer to the chemical potential". Since our system is in the perturbative regime, a single-electron excitation should be a good degree of freedom, i.e. at zero temperature an electron at the chemical potential should not decay into multi-particle states. This implies that at zero temperature the single-particle S-matrix should be unitary, which is clearly the case (consider the value of $|SS^\dagger - \mathbb{1}|$ at the chemical potential (black line) in Fig. 7.5(a)). We observe that there is indeed a narrow belt around the chemical potential in which the single-particle S-matrix is essentially unitary at zero temperature. It is reasonable to hope that the relevant physics within this belt could also be captured by a static approximation, in which the single-particle S-matrix is always unitary.[13] We observe that the size of the belt is significantly smaller during the conductance step (in particular in the subopen regime) than for a very open or closed QPC. This suggests that interaction effects beyond a Hartree-shift play an important role mainly during the conductance step.

The role of interactions beyond the Hartree-shift is well visible if we turn on a finite temperature (Fig. 7.5(b)). The temperature is indicated by dashed line (the dashed line represent $\omega = \mu \pm T$; the relevant physics should occur in an energy window of this order).[14] Of course, it is completely natural to expect that single-electron excitations at finite energy decay into multi-particle excitations. However, what is a priori unclear is the strength of this decay process. Considering Fig. 7.5, we observe that the single-particle S-matrix strongly deviates from a unitary matrix in the subopen regime, which leads us to conclude that inelastic processes (i.e. the decay of e.g. electrons into electrons and electron-hole pairs) are highly relevant.[15] It is thus of paramount importance that the approximation employed be able to capture these inelastic processes.

[12] We do not show a plot of this as $SS^\dagger = \mathbb{1}$ implies $|SS^\dagger - \mathbb{1}| = 0$ and thus the corresponding figure would be a mono-colored square.

[13] In a static approximation, the self-energy does not depend on energy. Since we would like to impose that electrons at the chemical potential are stable and do not decay in multi-particle processes, the self-energy at the chemical potential has to be real. A static approximation thus corresponds to a real self-energy, which renormalizes the effective potential and hopping (and thus reflection and transmission amplitudes), but does not lead to a violation of the unitarity of the single-particle S-matrix.

[14] To be slightly more precise: if the Fermi-Dirac distribution function is $n_F(\epsilon) = \frac{1}{1+\exp(\epsilon/T)}$, then the derivative of the distribution n_F is a peaked function, whose full width at half maximum is $2T\ln(3+\sqrt{8}) \approx 3.5T$. This window is almost twice as large as the window indicated by the dashed lines.

[15] Since the diagonal entries of $SS^\dagger$ correspond to sum of transmission and reflection probability ($|T|^2$ and $|R|^2$ respectively), as a rough estimate we may say that the deviation of $SS^\dagger$ from the identity corresponds to $1 - |R|^2 - |T|^2$, i.e. the probability of a particle to decay. While this is not true strictly speaking (the off-diagonal elements of $SS^\dagger$ may in principle be relevant), we have checked that for the system at hand the off-diagonal elements give a correction of at most $\sim 20\%$ (i.e. $|SS^\dagger - \mathbb{1}|$ and $|(SS^\dagger)_{11} - 1|$ differ by no more than $\sim 20\%$). We advise against strictly interpreting Fig. 7.5 as "percentage of single-particle excitations that decay", although the values shown are a reasonable estimate of the decay rate.

7.4.2 Phases of the S-matrix

There are at least four possibly interesting phases: The transmission and reflection phases, which may be measured for example in an interferometry experiment, and the symmetric and antisymmetric phase, which split the problem according to the $\mathbb{Z}_2$ parity symmetry. As we will see in Sec. 7.4.3, the transmission phase can also be used to determine the traversal time at a given energy ω.

Fig. 7.6 shows the four phases as functions of gate voltage and energy. As the QPC is opened (or energy increased), the transmission phase grows (which can already be understood in a WKB-type approximation: the corresponding wave-function has a larger kinetic energy and thus oscillates more quickly, leading to a larger phase $\delta \sim ikx$). A feature of the reflection phase at the chemical potential (the chemical potential is indicated by a black line) at a very open QPC may be disregarded, as the reflection probability is very small.[16] We emphasize that in contrast to a quantum dot, both symmetric and anti-symmetric phase (Fig. 7.6(a,b)) matter and change non-trivially.

In the interacting case (Fig. 7.6(e-h)), we observe a slow-down of phase growth as we open the QPC (which we can qualitatively understand through the Hartree-shift of the barrier). This slow-down of phase growth leads to a slow-down of the relevant physics.

7.4.3 Traversal time

It is useful to classify processes by the time-scales on which they occur. For the QPC, there is an eminently useful timescale: the traversal time, i.e. the time a particle spends within the QPC. In this section we wish to give some more details on the traversal time explained in chapter 6.

To be slightly more precise: We are interested in the time it takes a low-energy excitation (an electron close to the chemical potential) to traverse the QPC. From this last statement it is clear that we cannot simply compute the correlation function between a particle on the left and a particle on the right of the system as a function of frequency and Fourier-transform that, i.e. $G^R_{LR}(t)$ does not give the correct time-scale as it involves all energies, while we are interested in the low energy degrees of freedom only.

A solution was given by Wigner in [Wig55]. We reproduce the solution of [Wig55] in this section for convenience. Consider the time-evolution of a minimal wave-packet, consisting of two eigenstates close in energy (a single eigenstate will asymptotically [far in the leads] be a plane wave, and cannot be thought of as localized):

$$\psi_{\text{in}}(x,t) = \mathcal{N}\left(\exp(i(k-\delta k)x - i(\omega-\delta\omega)t) + \exp(i(k+\delta k)x - i(\omega+\delta\omega)t)\right), \tag{7.8}$$

where we have formed a superposition of the eigenstates at energies $\omega - \delta\omega$ and $\omega + \delta\omega$ (we will assume $\delta\omega$ to be infinitesimally small). $\mathcal{N}$ is required for the normalization of the wave-function. The form Eq. (7.8) of ψ_{in} is valid for x deep in the leads. ψ_{in} is "localized" at the position where the phases of its constituent eigenfunctions agree:

$$i(k-\delta k)x - i(\omega-\delta\omega)t = i(k+\delta k)x - i(\omega+\delta\omega)t$$

[16] If the modulus of a complex number is very small, its phase may fluctuate wildly without large effect.

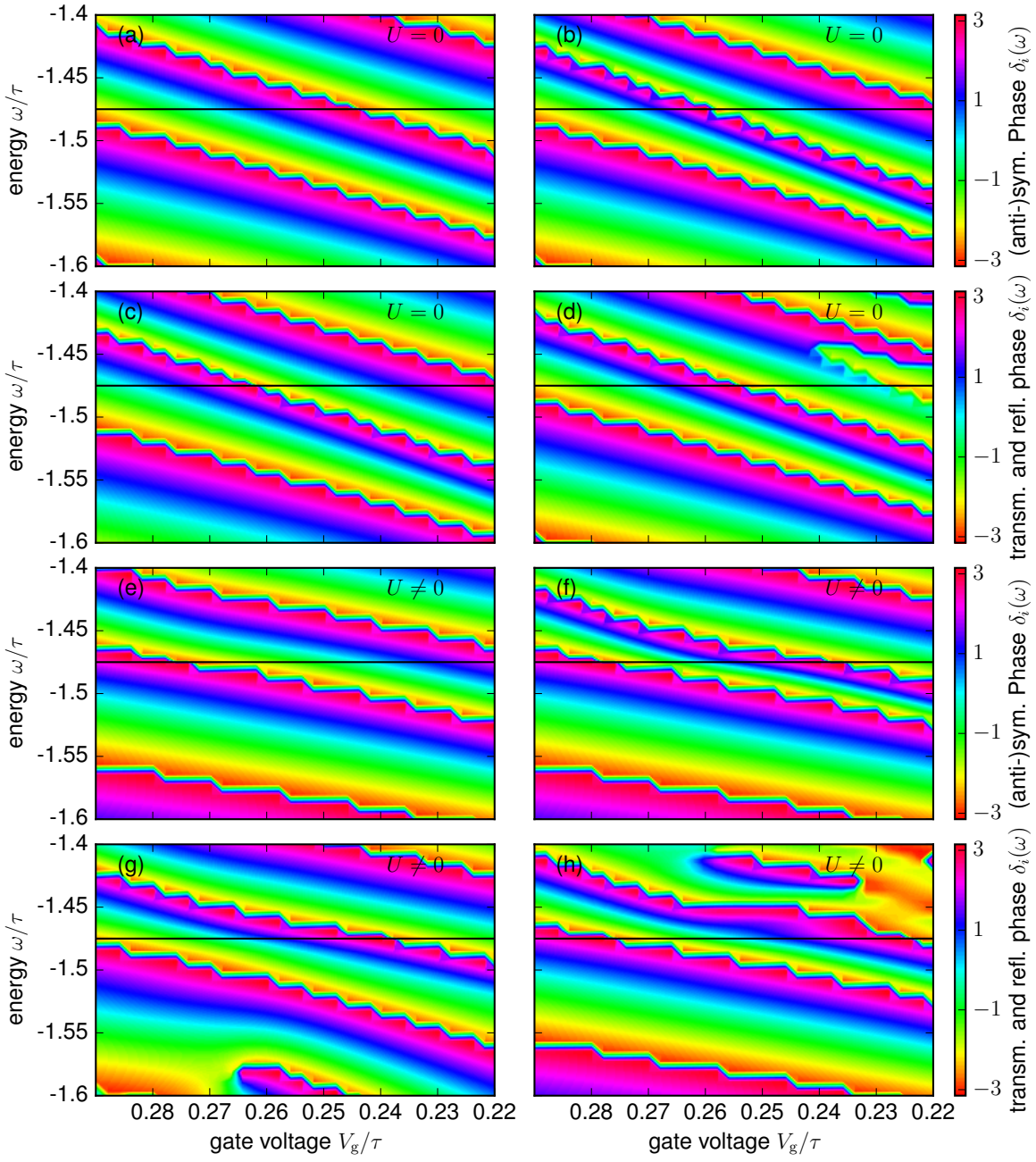

Figure 7.6: The phases of (a-d) the non-interacting and (e-h) the interacting single-particle S-matrix (colorscale) as function of gate voltage and energy ω: (a,e) antisymmetric phase, (b,f) symmetric phase, (c,g) transmission phase, and (d,h) reflection phase. The chemical potential is indicated by the solid black line. Note that in the non-interacting case, the position of the chemical potential is irrelevant.

$$\begin{aligned}
&\Rightarrow 0 = -2\delta k x + 2\delta\omega t \\
&\Rightarrow x = \frac{\delta\omega}{\delta k} t = v_{\text{group}} t.
\end{aligned} \tag{7.9}$$

Given conservation of energy, the outgoing transmitted wave-function is of the form

$$\begin{aligned}
\psi_{\text{trans}}(x,t) = \tilde{\mathcal{N}} \big(&\exp(i(k-\delta k)x - i(\omega-\delta\omega)t + 2i(\eta-\delta\eta)) \\
&+ \exp(i(k+\delta k)x - i(\omega+\delta\omega)t + 2i(\eta+\delta\eta))\big),
\end{aligned} \tag{7.10}$$

where we have used that asymptotically the momentum is in a one-to-one relation with the energy. We have introduced the transmission phase shift η ($\eta + \delta\eta$) at energy ω ($\omega + \delta\omega$). $\tilde{\mathcal{N}}$ is the normalization. Note that ψ_{trans} contains only the transmitted part of the wave-function. As such, its norm is $|T|^2 \leq 1$, where T is the transmission amplitude. The transmitted wavefunction is "localized" at

$$\begin{aligned}
&i(k-\delta k)x - i(\omega-\delta\omega)t + 2i(\eta-\delta\eta) = i(k+\delta k)x - i(\omega+\delta\omega)t + 2i(\eta+\delta\eta) \\
&\Rightarrow (-\delta k)x + \delta\omega t - 2\delta\eta = +\delta k x - \delta\omega t + 2\delta\eta \\
&\Rightarrow x = \frac{\delta\omega}{\delta k} t - 2\frac{\delta\eta}{\delta k} = v_{\text{group}} t - 2 v_{\text{group}} \partial_\omega \eta.
\end{aligned} \tag{7.11}$$

If we define the traversal time at energy ω as the time required to go from the left to the right of the system (traversing the length Δx), we see that the traversal time t_{trav} is given by

$$t_{\text{trav}}(\omega) = \frac{\Delta x}{v_{\text{group}}} + 2\partial_\omega \eta(\omega). \tag{7.12}$$

In the case we consider here, the scattering phase η is due to both the QPC potential and the interactions. Note that the traversal time t_{trav} manifestly depends on the choice of "left" and "right" end of the system. For example, if we were to move what we call the left-most site of the central region further into the lead, the traversal time would trivially increase as Δx grows. However, in the case we consider here, the slow-down due to the potential and the interactions is sufficiently large that it dominates the trivial $\frac{\Delta x}{v_{\text{group}}}$ part for reasonable choices of Δx.[17]

We also note that the traversal time depends only on the *phase* acquired when traversing the system, not the transmission probability itself. The reason is that we answer the question: Given that a particle of energy ω passed through the system, how long did it take? Figures of the traversal time must be read accordingly: The traversal time of particles at energies where very few particles are transmitted at all, even though it takes a well-defined value, is physically mostly irrelevant.[18]

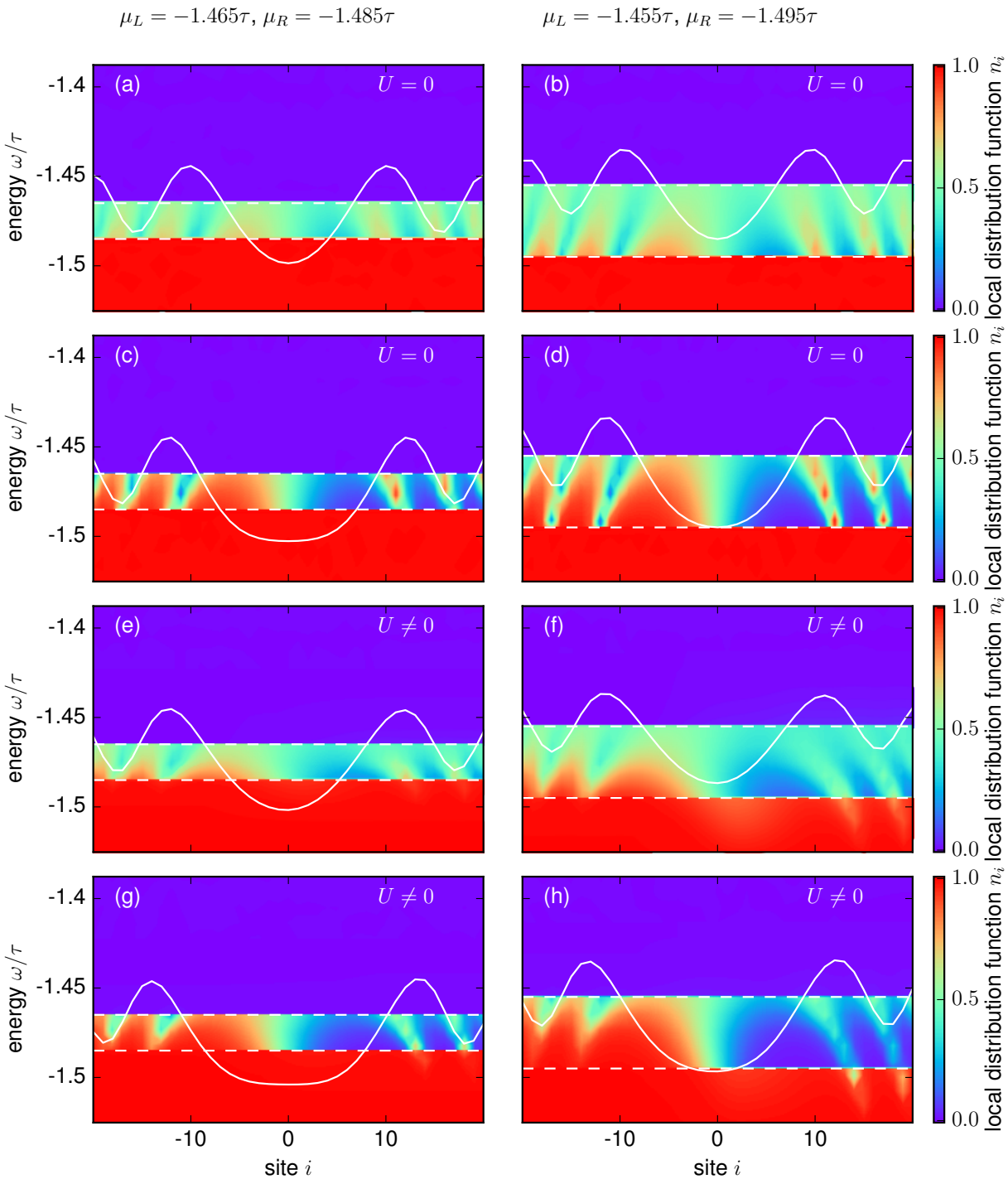

Figure 7.7: The local distribution function (color scale) of (a-d) a non-interacting and (e-h) an interacting QPC as function of position (site) and energy ω at zero temperature. The QPC in the upper row (a,b,e,f) is more open (conductance $G \approx 0.9G_Q$) than the QPC in the lower row (c,d,g,h; $G \approx 0.2G_Q$). In the right column (b,d,f,h) the bias is larger than in the left column (a,c,e,g). Apart from two clear discontinuities at the chemical potentials (the chemical potentials are indicated by dashed white lines), we observe an oscillatory pattern within the bias window. The length scale of this oscillatory features fits well with the length scale extracted from the single-particle dynamics (i.e. the Friedel oscillations). In white we show $\mathrm{Im}G_{ci}(\omega = \mu_L)$ (scaled by 0.01 and shifted such that $\mathrm{Im}G_{ci}(\omega = \mu_L) = 0$ lies at μ_L).

7.5 Effective distribution function

Finally, let us take a short look at an out-of-equilibrium property: the local distribution function.[19] Having defined a local distribution function n_i (see e.g. Sec. 5.3), let us first figure out what we expect:

(a) The local distribution function should exhibit sharp features at the leads' chemical potentials, which are smeared out on a scale set by the temperature.

(b) If we consider a closed QPC, the local distribution to the left (right) of the barrier should be essentially the distribution function of the left (right) lead.

(c) If the QPC is (sub-)open, the local distribution function should interpolate between the distribution function of the left and right leads.

As a corollary of (b) and (c), it follows that the distribution function outside of the window set by the temperature-smeared bias window should be either zero (for energies larger than the window) or one (for energies smaller than the window).

The local distribution function of two different non-interacting QPCs at zero temperature is shown in Fig. 7.7(a-d).

Let us check if the local distribution function in the non-interacting case is in accordance with our expectations:

(a) In Fig. (7.7)(a-d), we show the the left and right chemical potentials as dashed white lines. We see that for energies larger than the bias window, the local distribution function is zero, while it is one for energies below the bias window. Only within the bias window does the distribution function show any other structure. The transition between the in- and outside of the bias-window is abrupt.

(b) If we consider the more closed QPC (Fig. 7.7(c,d)), we see that the local distribution function to the left (right) of the barrier is somewhat similar to the distribution function of the left (right) lead (which is a step function). However, there are relevant corrections: We observe clear oscillatory features. The length scale associated with these oscillations is the same as the scale of Friedel-oscillations (which may be read off from the Green's function, whose imaginary part is shown as a white curve).

(c) If we go to a somewhat more open QPC (Fig. 7.7(a,b)), we see that the oscillations are less pronounced and the local distribution function $n_i \approx \frac{1}{2}\left(n_L + n_R\right)$ is well approximated by a (roughly equal weight) average over the leads' distribution functions.

[17] For the choice of left- and rightmost site as shown in the plots of this section, the scattering contribution $\partial_\omega \eta$ to the traversal time is larger than the "trivial" background contribution $\frac{\Delta x}{v_{\text{group}}}$ by a factor of about 5 at the chemical potential in the subopen region.

[18] For more on the traversal time, see chapter 6.

[19] Recall that for a non-equilibrium QPC we use a total of 41 sites.

We observe further that the local distribution function of a non-interacting QPC is bounded by zero and one, which is heartening.[20]

Let us now turn on interactions (Fig. 7.7(e-h)).

The first change that comes to mind is that the QPCs look more closed (i.e. the local distribution function shows a stronger dependence on position). This is easily explained by a first-order effect (Hartree shift): The electrons repel each other, such that any electron density (which is non-negligible in a somewhat open QPC) leads to an enhancement of the effective barrier. This effect is also seen in a reduction of the conductance as interactions are turned on.

The second change is particularly visible at large bias on the right hand side of the QPC: some of the oscillatory structure seems to bleed outside of the bias window (e.g. at $i = 34$, $\omega = -1.5$ in Fig. 7.7(h)). Since an interacting system generically mixes single-particle states of different energies, this bleeding is not necessarily surprising.

There is one invisible problem: the local distribution function in the interacting system at certain points takes values outside of the interval $[0, 1]$. We do not know if this is an error of the method (fRG) or in fact a generic feature of the chosen definition of n_i.

Comment: As a final remark, we note that there are many possible ways to define a local distribution function. For example, we could

(i) take the general equation $G^K = G^R F - F G^A$, and solve it for F.[21] We then extract a local distribution function by considering only the diagonal part of F.

(ii) take the general equation $G^K = G^R F - F G^A$, solve it for F, and then average the solution over some distances. Basically, we rewrite F_{ij} in center of mass coordinates as $\tilde{F}_{\frac{1}{2}(i+j),\frac{1}{2}(i-j)}$ and average over $\frac{1}{2}(i-j)$. The idea behind stems from a hydrodynamic intuition: We separate the system into slow and fast modes (fluctuating on long and short length scales) and average over the fast modes.

(iii) take the general equation $G^K = G^R F - F G^A$, solve it for F, and then average the solution over some distances with a non-trivial weight associated with each distance induced by the structure of the system. Basically, we rewrite F_{ij} in center of mass coordinates as $\tilde{F}_{\frac{1}{2}(i+j),\frac{1}{2}(i-j)}$ and average over $\frac{1}{2}(i-j)$ with the weight $\mathrm{Im}G^R_{i,j}/\mathrm{Im}G^R\frac{1}{2}(i+j),\frac{1}{2}(i+j)$. The idea is the same as previously.

The explicit form of the local distribution function is sensitive to the method chosen. However, the basic features explained here (the local distribution function is non-trivial mainly within the

[20] It is actually easy to prove that in a non-interacting system at zero temperature the local distribution outside of the bias window is zero or one, as appropriate. The main input lies in the fact that a non-interacting system does not mix single-particle states. In other words, if we consider a state at some energy ω, the distribution of this state depends only on the occupation of states at the same energy ω in the leads. However, the occupation of states with energies outside of the bias window is identical to the occupation of these states in equilibrium, with a chemical potential somewhere in the bias window. Thus, the local distribution function outside of the bias window has to be identical with an equilibrium distribution function with a chemical potential somewhere within the bias window. We have already seen that for an equilibrium setup the local distribution function is the equilibrium distribution function. Note that this argument does not constrain the local distribution function inside of the bias window.

[21] An equation of the form $AX + XA^\dagger + Q = 0$ with Hermitian matrices X and Q (the matrices A and Q are known, X is sought after) is known in control theory as Lyapunov-equation. It is a linear equation in X and may thus be solved trivially.

bias window, it has oscillatory structures following the Friedel-oscillations, and is dominated by an average over the distribution functions of the leads) are robust under a change of method.

Chapter 8

Specifics of the implementation

In this chapter, we explain the specific tricks and useful simplifications we employ when solving the QPC with Keldysh-fRG. As explained previously, we consider a perturbative truncation (we set the three-particle vertex and all higher vertices to zero) and approximate the two-particle vertex by a channel decomposition.[1]

8.1 Generic

The Keldysh-fRG equations exhibit two numerically costly parts: solving a high-dimensional ODE and performing integrals over frequencies. While both of these problems may be addressed by standard algorithms, it is usually possible to aid the algorithms with system-specific input. As algorithms we use a sixth-order Runge-Kutta algorithm with adaptive step-size to solve the ODE and a Gaussian quadrature algorithm based on Patterson sets (both implemented by Florian Bauer and Jan Heyder) to solve the ODE and perform the integrals.

8.1.1 ODE-Flow

It is useful to consider a flow not in Λ, but rather in some function $f(\Lambda)$ in order to help the predictor (the predictor guesses the size of the next step) as much as possible. If we flow directly in Λ as introduced in [JPS10a] (and used in [SBv17]), the usual predictor fails to accurately adapt the step-size. The reason lies in the different scales of the problem: If Λ is very large (compared to the band-width in the leads, which in our model is 4τ) the physics is dominated by the artificial leads with hybridization $\sim \Lambda$ and large steps may be used. In order to resolve the finer structures on the scale of the band-width (and later on, on the scale of the curvature or the width of the LDOS maximum) much smaller steps are needed. In other words, the system behaves drastically different at $\Lambda \gg$ band width, at $\Lambda \lesssim$ band width, and at $\Lambda \lesssim \Omega_x$. Since these constitute different scales, it is very difficult for the generic predictor to adapt correctly. However, if we use a $\log$, we transform a change in scale to a linear change, which is much

[1] Since this chapter deals mainly with the numerical implementation, we label the sites from 1 to N (with N odd). The central site thus is at $\frac{N+1}{2}$.

easier to predict. To be specific, we use

$$x = \log\left(\frac{\Lambda}{1+\Lambda}\right) \tag{8.1}$$

as flow parameter. From $\Lambda \in [0, \infty)$, we get $x \in (-\infty, 0)$. In practice, it is sufficient to flow from $x = -10^{-6}$ ($\Lambda \approx 10^6$) to $x = -20$ ($\Lambda \approx 2 \cdot 10^{-9}$).

Note that this substitution has to be compensated by a measure term w

$$\partial_\Lambda = w(x)\partial_x = \frac{(1-\exp(x))^2}{\exp(x)}\partial_x. \tag{8.2}$$

We remark that this weight has to be accounted for when determining the accuracy with which internal operations are performed. It is easiest to absorb this weight for example in the single-scale propagator and to then compute all expressions with a fixed accuracy.

8.1.2 Integrals over frequencies

Since our flow parameter is chosen such that the single-scale propagator does not exhibit δ-like features, we actually do have to compute integrals over frequencies (as explained e.g. in [JPS10a], a sharp single-scale propagator will lead to the violation of either causality or FDTs). There are multiple difficulties and nontrivial tricks associated with these integrals:

1. The integrals cover the full frequency axis. Numerically integrating over $\omega \in (-\infty, \infty)$ is not possible. However, we may mathematically substitute $u = f(\omega)$ with $u \in (-a, a)$ instead. We will give the explicit substitution later on. For now, we simply note that for our choice of the flow parameter the single-scale propagator decays as $1/\omega^2$ for large ω (and thus all integrands decay at least this quickly).

2. The integrals range over divergent points. At small values of Λ, the Green's function at the edge of the central region, the single-scale propagator, and the leads' Green's functions gain a $1/\sqrt{\omega - \text{band edge}}$ singularity (cut off at the scale Λ). While this singularity (or almost-singularity) is integrable, numerically such an integral is non-trivial. However, since we know of this singularity, we may avoid it by a suitable substitution.

   Thus, we have two issues which we want to solve via a clever substitution (the infinite range of integration and divergences of the integrand at finite frequencies).

   To obtain a useful substitution, we consider as example the integral

   $$I = \int_{\mathbb{R}} d\omega \frac{1}{\omega^2 + a^2}, \tag{8.3}$$

   with $a > 0$. Before we process this expression, let us split the integral into three parts, each of which has at most one problematic region:

   $$I = \underbrace{\int_{-\infty}^{-a} d\omega \frac{1}{\omega^2+a^2}}_{I_1} + \underbrace{\int_{-a}^{a} d\omega \frac{1}{\omega^2+a^2}}_{I_2} + \underbrace{\int_{a}^{\infty} d\omega \frac{1}{\omega^2+a^2}}_{I_3}. \tag{8.4}$$

Obviously, we encounter the "infinite integration range"-problem only in I_1 and I_3, and only at one end of the range of integration in each separate integral I_j. Let us now consider I_1 (we may treat I_3 analogously): We want to change I_1 to an integral over a finite range with a "simple" integrand, i.e. we want to pick $u(\omega)$ such that

$$I_1 = \int_{-1}^{b} du f(u), \tag{8.5}$$

where $f(u)$ is well-behaved everywhere and $u = -1$ corresponds to $\omega \to -\infty$. For concreteness, let us impose that $\lim_{u\to -1} f = \text{const}$. The problematic part of the integral stems from the $1/\omega^2$ behavior for large ω. For large ω, we thus have

$$\frac{d\omega}{\omega^2} \approx du \Rightarrow \omega^{-1} \approx -u + u_0, \tag{8.6}$$

with some offset u_0. We choose as substitution

$$u = -1 - \omega^{-1}. \tag{8.7}$$

Using the substitution Eq. (8.7), the integral I_1 becomes

$$I_1 = \int_{-1}^{-1+a^{-1}} du \frac{1}{1 + a^2(1+u)^2}, \tag{8.8}$$

which does not exhibit any problematic features. Note that by scaling initially, we could have put a in the integrand to any value we wanted, so we can achieve that the upper boundary remains fixed, i.e. $-1 + a^{-1} \stackrel{!}{=} a$. Any integral, where the analytical expression for the integral of the problematic part is known, can be put into a "nice" form by this procedure. It is even possible to introduce a sufficient number of free parameters to make the substitution continuous.

Of course, the substitution is not fully specified by fixing the asymptotics. In this work, we choose the substitution

$$\omega = \begin{cases} -2\tau\frac{(\tilde{y}+6)(1+\Lambda)}{(\tilde{y}+6)^2-1} - 6\tau, & \text{for } (\tilde{y} < -6) \\ -2\tau - \tau(\tilde{y}+2)^2/4, & \text{for } (-6 < \tilde{y} < -2) \\ \tau\tilde{y}\sqrt{\frac{4}{\tilde{y}^2} - \frac{(\tilde{y}^2-4)^2}{4\tilde{y}^2}}, & \text{for } (-2 < \tilde{y} < 2) \\ 2\tau + \tau(\tilde{y}-2)^2/4, & \text{for } (2 < \tilde{y} < 6) \\ -2\tau\frac{(\tilde{y}-6)(1+\Lambda)}{(\tilde{y}-6)^2-1} + 6\tau, & \text{for } (6 < \tilde{y}), \end{cases} \tag{8.9}$$

where $\tilde{y} = y/\tau \in (-7, 7)$. For convenience, $\omega = \pm 6\tau$, $\omega = \pm 2\tau$, and $\omega = 0$ are mapped to $y = \pm 6\tau$, $y = \pm 2\tau$, and $y = 0$, respectively. Futhermore, the substitution is antisymmetric, i.e. $\omega(-y) = -\omega(y)$.

Apart from the considerations just explained, at the outer regions $\tilde{y} < -6$ and $\tilde{y} > 6$, we have scaled ω by $1 + \Lambda$. The idea behind this scaling is simple: If we compress the

region $\omega \in (-\infty, -6\tau]$ to $y \in [-7\tau, -6\tau]$, then points "far away" from each other in ω get bunched closer together in y. At large values of Λ, the single-scale propagator shows characteristic structures at the scale Λ. If the substitution is insensitive to this fact, at large Λ all this structure is pressed into a very small region close to $y \approx -7\tau$. This implies that the integrand will change quickly close to $y \approx -7\tau$, which is generically problematic. However, since the integrand changes on the scale of Λ, by appropriate scaling the change becomes reasonably slow in the $\tilde{y}$ coordinates.

3. Computing the Green's function and the single-scale propagator is slow. Since the Green's function and the single-scale propagator are obtained by inverting a matrix, computing them takes a non-trivial amount of time. In itself, this time is relatively small. However, if this inversion needs be performed for each point at which the integrand is evaluated for each integral (the number of integrals at each step in the flow is proportional to the number of frequencies at which we compute the vertex and self-energy), the inversion is the slowest part of the computation of the integrand and highly relevant. One way out is to compute the Green's function and the single-scale propagator at a finite, but large number of frequencies beforehand and to then interpolate whenever they are required. The interpolation itself comes with a different set of problems:

   (a) Interpolation method: A priori, it is not clear how to interpolate. Given a sufficiently dense set of points, the method should become irrelevant, provided it does not produce severe artifacts. We pick a large number of frequencies (on the order of 30,000) and interpolate linearly in the substituted region (i.e. in $\tilde{y}$).

   (b) Behavior outside of interpolation range: The value the interpolation should return at frequencies larger/smaller than the largest/smallest point at which the function is known is a priori undefined. Since we need different behavior for G, S, and for the vertex (for G and S it is useful to return zero, while the vertex should return its value at the largest/smallest point [corresponding to the static contribution]), we avoid this issue by ensuring that we have all of these objects at sufficiently large/small frequencies for G and S to already be essentially zero (up to our accuracy). We may thus return the value of the largest/smallest known point.

   (c) Order of operations: Given that we use a substitution which leads to large peaks in the measure (e.g. when we map an infinite region to a finite region), generically even a very dense set of points might not be sufficiently dense if we incorporate the measure. It turns out that it is most practical to define a $\tilde{S} = wS$, where w is the measure and S "lives" on the substituted frequencies, and to interpolate $\tilde{S}$. As a consequence, we have to ensure that we shift all integrands such that S is evaluated at the frequency of integration, i.e.

   $$\int d\omega A(\omega) S(\omega + \omega_0) = \int d\omega A(\omega - \omega_0) S(\omega) = \int dy A(\omega(y) - \omega_0) \tilde{S}(y), \tag{8.10}$$

   for some function A.

   (d) Diverging points: At some frequencies S (or the measure times S) might diverge (e.g. at the band edge). The divergent point itself can obviously not be used for the

interpolation. In order to ensure a good interpolation, we thus add points very close to critical frequencies ω_c (at $\omega = \omega_c \pm \Delta \approx \omega_c \pm 10{-}12$).

4. The integrands exhibit multiple structures (local sharp peaks or dips), at possibly different scales. The integrands appearing in either the bubbles (flow of the vertex) or the self-energy are non-trivial in frequency space. The performance of some integrators can be enhanced by using knowledge of the structures appearing. Before we go into the integrands themselves, let us recall how we expect the single-scale propagator S to look: At large frequencies, S^R decays as $1/\omega^2$. The scale for this decay is set by $\max(\tau, \Lambda)$. At smaller frequencies, the behavior depends on the spatial position: Close to the band edges, S^R exhibits (at small Λ) a $1/\sqrt{\omega - \text{band edge}}$-divergence (cut off by Λ). At the center of the QPC, there is a similar divergence at the effective band edge ($\sim$top of the barrier), which gets cut off by either Ω_x or Λ. S^K exhibits (at low temperature) an additional sharp feature at the leads' chemical potentials (at zero temperature, this feature is a jump; at finite temperature T, the jump is smeared on the scale T). The structure of G is similar to that of S. If we now consider a bubble, e.g.

$$\int d\epsilon G(\Omega - \epsilon) S(\epsilon), \tag{8.11}$$

where G and S have various different Keldysh indices, we see that the integrand has sharp features at

$$\epsilon = \begin{cases} \pm 2\tau & (\text{band edges of } S, \text{ smeared by } \Lambda), \\ \Omega \pm 2\tau & (\text{band edges of } G, \text{ smeared by } \Lambda), \\ \pm(2\tau - V_g) & (\text{effective band edges of } S \text{ in the center, smeared by } \Lambda \text{ or } \Omega_x), \\ \Omega \pm (2\tau - V_g) & (\text{effective band edges of } G \text{ in the center, smeared by } \Lambda \text{ or } \Omega_x), \\ \mu & (\text{chemical potential of the leads in } S, \text{ smeared by temperature}), \\ \Omega - \mu & (\text{chemical potential of the leads in } G, \text{ smeared by temperature}), \end{cases} \tag{8.12}$$

Using the substitution explained previously, another sharp feature at $\epsilon \approx \pm\Lambda$ (and $\epsilon \approx \Omega \pm \Lambda$) can appear in the substituted integrand at large Λ. Since the substitution is continuous but not differentiable, the measure exhibits jumps, such that we additionally obtain features at $\epsilon = \pm 6\tau$ (and $\epsilon = \Omega \pm 6\tau$).

As a result of the bubble-integrals, the vertex contributions themselves exhibit sharp features at certain frequencies, in particular at 2μ for b_P and at 0 for b_X and b_D. These features enter in the integrals required to obtain the flow of the self-energy.

Before we move on, a further comment regarding the structure of the integrands is in order: Even though the QPC is "nice" in the sense that it is clear beforehand at which frequencies (roughly) the density of states becomes large (it follows the renormalized QPC potential), we might consider systems with sharper and less known frequency structure, for example a quantum dot (modeled by a trapping potential) or a disordered system. At large values of the flow parameter Λ used here, we do not expect these sharp structures to play a crucial role, as every

structure in frequency space is smeared out by the artificial leads to have a width of order $\gtrsim \Lambda$. As the flow parameter Λ approaches zero, these structures become sharper and – hopefully – settle at their actual width and position. While the non-interacting system might give an indication of the position of these structures, if the structures are sharper than the Hartree-shift (if they are so narrow that the overlap between the fully interacting level and the bare level is small), the positions determined by the non-interacting model become bad guesses. However, physically, we expect that these sharp levels smoothly appear or disappear with Λ. It would thus be possible to find them at largish values of Λ and to track their position throughout the flow (clearly, it is *not* valid to simply miss these structures with the integrator). A more ambitious version of the tracking might try to automatically adapt the discretization of the frequency axis to the new level positions. In the case of the QPC this additional tracking is not necessary.

8.1.3 Choice of frequencies

Since we are able to solve the system at only a finite number of frequencies (or: In order to work on a computer, we need to represent each function of frequency with a finite basis. In this work, we use a discrete set of frequencies and linearly interpolate), we need to pick a "good" set of frequencies. The majority of frequencies should lie sufficiently dense at the relevant energies. We thus linearly discretize the frequencies within $[-4\tau, 4\tau]$, using roughly two thirds of the available frequencies, and use the remaining frequencies to discretize the large-frequency part with exponential spacing. We aim at a largest frequency of about 10^8. In general, we wish to ensure that certain frequencies are present (e.g. the self-energy at the chemical potential). We thus add the additional frequencies μ, 2μ (for the P-channel), 0 (for the X- and D-channel), and at finite temperature T we add additional frequencies within a window of about $10T$ around these frequencies. We have checked that the results agree with a more dense discretization, i.e. more frequencies.

8.1.4 Parallelization

The problem at hand lends itself to a simple, yet very effective parallelization scheme: First off, we note that by far the largest part of the run-time of the program is spent on computing internal integrals (i.e. computing the bubbles Eq. (4.38),(4.39), or the integral over frequencies in the flow of the self-energy Eq. (4.37a)). Fortunately, the structure of the equations is such that the results of one internal integral may be computed independently of the results of all other internal integrals. It thus seems intuitive to parallelize the code on the level of the external frequencies (e.g. the frequency Π flowing through a bubble) and possibly also external spatial indices. Since we use ~ 1500 frequencies, and about 8 cores for production, a reasonable speed-up is achieved by implementing multi-threading on the level of the external frequencies.

As an example, consider the flow of the P-channel. At any given frequency Π, we have to compute the P-bubble at this frequency and then multiply the result by the corresponding part of the vertex. We thus put each frequency Π into a separate thread, leading to ~ 1500 threads. If each of these threads has its own local memory for the bubble, there is no danger of the threads contaminating each others memory. On the other hand, we have tested that the interpolation is sufficiently fast that there is no relevant locking associated with reading out

the Green's function and the single-scale propagator required for the bubble. We use OMP to parallelize the ~ 1500 threads (each of which is associated with an external frequency Π).

We remark that on 8 cores we achieve a speed-up of the program by a factor of about 6 to 7, while the bubble actually speeds up by a factor of almost 8. The difference is due to non-parallelized pieces of the code, e.g. the ODE-solver.

8.1.5 Other flow parameters

In the derivations so far, we have used two properties of the single-scale propagator: The retarded component as function of frequency is analytical in the upper half plane, and in equilibrium FDTs are respected throughout the flow. While this restricts the choice of flow parameters to exclude the simple sharp cut-offs along the (real or imaginary) frequency axis (which violate causality) or thermodynamic quantities (as a flow in the temperature T or the chemical potential μ will destroy FDTs), other flow parameters remain in principle valid. For example, if we were to flow in the gate voltage V_g and store the self-energy and vertex during the solution of the ODE, we would obtain a full conductance curve at once. Since this would constitute a large reduction in computational cost, it is a very enticing prospect.

As we are unable to solve the interacting system for any value of V_g (or more general: some barrier shape) exactly, we first need to obtain a starting self-energy and vertex for some potential through an approximate scheme (recall that our leads are non-interacting, while there are interactions in the central region. Thus, not even bosonization would necessarily help.). Since we are already using fRG, we could use our usual flow parameter (the artificial leads), to generate the vertex and self-energy for some barrier and then use this as initial value for a flow generated by changing V_g.

While the idea seems promising, in practice it is not feasible: The flow along a very small change of V_g (significantly less than Ω_x) actually takes a time longer than the equivalent flow of removing the artificial leads. In fact, the loss in time is such that a reasonable resolution of the conductance curve is achieved much more quickly by simply computing a large number of points with the flow utilizing the artificial leads. We suspect that the reason for the comparative slowness of the V_g-flow lies in the sharp LDOS-features which are highly sensitive to V_g. While the LDOS actually is pinned, the non-interacting LDOS is not. This means that the self-energy has to compensate by shifting a peak. This shift is of the same order as the width of the peak. Shifting a peak by its width – when considered at a given frequency – looks like a large change in the function. A large change in a function over a small change in a parameter usually is hard for an ODE-solver to do. Since the effects of changing the Hamiltonian are visible at all energies, we do not even gain the benefit of skimping on the integrals over frequencies.

To summarize: While different flow parameters are an enticing idea, the physical flow parameters we have tried (temperature and gate voltage) did not work out in practice.

8.1.6 Katanin's flow

The violation of charge conservation is a severe drawback of fRG. The simplest improvement may be achieved by a modified flow proposed by Katanin [Kat04]. In the modified flow, the derivative of the self-energy is calculated just as in the usual fRG flow. However, in the

derivative of the vertex, the single-scale propagator $S = G(\dot{G}_0^{-1})G$ is replaced by $S = -\dot{G} = G(\dot{G}_0^{-1})G - G\dot{\Sigma}G$, where $\dot{\Sigma}$ (the derivative of the self-energy) has already been computed using the usual single-scale propagator. In other words, the flow equations are (compare Eqs. (4.25) and (4.26))

$$\dot{\gamma}^1_{1'1} = S_{22'}\gamma^2_{1'2';12}, \tag{8.13}$$

$$\begin{aligned}\dot{\gamma}^2_{1'2';12} = -\dot{G}_{33'}\big(&\gamma^3_{1'2'3';123} - \gamma^2_{3'4;12}G_{4'4}\gamma^2_{1'2';4'3} - \gamma^2_{1'3';14}G_{44'}\gamma^2_{2'4';23} \\ &+\gamma^2_{2'3';14}G_{44'}\gamma^2_{1'4';23} + \gamma^2_{1'3';24}G_{44'}\gamma^2_{2'4';13} - \gamma^2_{2'3';24}G_{44'}\gamma^2_{1'4';13}\big)\,.\end{aligned} \tag{8.14}$$

This modification leads to a slight improvement in the fulfillment of Ward-identities belonging to conservation of electric charge.

While the violation of these Ward-identities is a severe issue, the Katanin flow does not help with the QPC. If we use the modified flow Eqs. (8.13) and (8.14), the ODE only converges at interaction strengths that are too weak for our purposes.

8.2 The QPC – Narrowing the band

Treating an homogeneous system on a computer entails a subtle issue: We would like to work in real space, to easier represent the inhomogeneity. Working on a computer, it seems natural to discretize the space. However, on a lattice, the dispersion is altered such that the spectrum of the Hamiltonian has the form of bands and is bounded from above and below. If we now turn on a potential energy in the form of $\sum_i V_i c_i^\dagger c_i$, the band is deformed. The deformation is such that states close to the upper band edge get pushed above the leads' upper band edge (assuming that V_i is non-negative and vanishes in the leads). Consequently, in a non-interacting system, these states will have infinite lifetime and be very sharp in frequency-space (in fact, they will correspond to δ-functions [or – for more mathematically minded readers – form the discrete part of the spectrum, which otherwise is continuous]). Of course, these states have to be taken into account correctly and consistently. Numerically, keeping track of very sharp features is expensive and tedious. Physically, we do not expect a large impact from states at the upper band edge. In fact, they should not matter for the qualitative behavior of the low-energy physics at all. We may thus ask: is there a way to simulate a potential which avoids these long-lived states?

The answer was given in [HBSvD17]: Through a discretization that is non-constant we can modify the upper band edge while keeping the lower band edge approximately invariant.

Here, we follow a slightly different argument and streamline the process somewhat: As an ansatz, let us return to the continuous system and consider the quantum-mechanical Hamiltonian

$$H = -\alpha(x)\partial_x^2. \tag{8.15}$$

The Hamiltonian Eq. (8.15) describes a system which upon discretization directly translates into a system with a position-dependent hopping. We will show that the spectrum of such a Hamiltonian is identical to the spectrum of a Hamiltonian with only a potential energy (for the argument here, we use units where the mass is $\frac{1}{2}$). We start by considering the time-independent

Schrödinger equation:

$$E\psi(x) = H\psi(x) = -\alpha(x)\partial_x^2\psi(x). \tag{8.16}$$

We now change coordinates from x to $y(x)$:

$$E\phi(y) = \left[-\alpha(x)\partial_x^2 y\partial_y - \alpha(\partial_x y)^2\partial_y^2\right]\phi(y), \quad \psi(x) = \phi(y(x)). \tag{8.17}$$

We choose $y(x)$ such that the prefactor of ∂_y^2 is minus one:

$$\partial_x y = \frac{1}{\sqrt{\alpha(x)}} \Rightarrow E\phi(y) = \left[\frac{\alpha'(x)}{2\sqrt{\alpha(x)}}\partial_y - \partial_y^2\right]\phi(y). \tag{8.18}$$

If we change from $\alpha(x)$ to $\gamma(y(x)) = \alpha(x)$, we obtain

$$\partial_x\alpha = (\sqrt{\gamma})^{-1}\,\partial_y\gamma \Rightarrow E\phi(y) = \left[\frac{\gamma'(y)}{2\gamma(y)}\partial_y - \partial_y^2\right]\phi(y). \tag{8.19}$$

Upon making the ansatz $\phi(y) = \exp(\beta(y))\rho(y)$, the Schrödinger equation becomes

$$E\rho(y) = \left[-\partial_y^2 + \left(-2\beta'(y) + \frac{\gamma'(y)}{2\gamma(y)}\right)\partial_y + \frac{\gamma'(y)}{2\gamma(y)}\beta'(y) - \beta''(y)\right]\rho(y). \tag{8.20}$$

Choosing $\beta' = \gamma'/(4\gamma)$, we obtain

$$E\rho(y) = \underbrace{\left[-\partial_y^2 + 2\beta'(y)^2 - \beta''(y)\right]}_{=H^\alpha_{\rm pot}}\rho(y). \tag{8.21}$$

In order to get a better idea of what happens here, let us consider

$$\alpha(x) = \alpha_0 - x^2/l^2 = \alpha_0 - \tilde{x}^2, \tag{8.22}$$

where we introduce some length scale l and use a tilde to denote a quantity measured in units of this length scale l. For this α, we obtain for a suitable choice of integration constants $\tilde{y} = \arctan\left[\frac{\tilde{x}}{\sqrt{\alpha_0-\tilde{x}^2}}\right]$, $\beta(y) = \frac{1}{4}\log\frac{\alpha_0}{1+\tan^2(\tilde{y})}$, and thus

$$\begin{aligned} H^\alpha_{\rm pot} &= -\partial_y^2 + \frac{1}{l^2}\left[\frac{3}{4} - \frac{1}{4}\cos(2\tilde{y})\right]\sec^2(\tilde{y}) \\ &\approx -\partial_y^2 + \frac{1}{l^2}\left[\frac{1}{2} + \tilde{y}^2\right], \end{aligned} \tag{8.23}$$

where we expanded in $\tilde{y}$. Thus, a quadratic barrier in $H^\alpha_{\rm pot}$ has the same spectrum as a quadratically space-dependent mass (note that the curvatures differ). Close to the center of the barrier the change of coordinates is merely a rescaling which can easily be taken into account (and corresponds to the difference in curvatures). If the relevant physics occurs in a spatial region close to the center of the barrier (of size $\lesssim l$), we may clearly choose either the Hamiltonian Eq. (8.21) or the Hamiltonian Eq. (8.15).

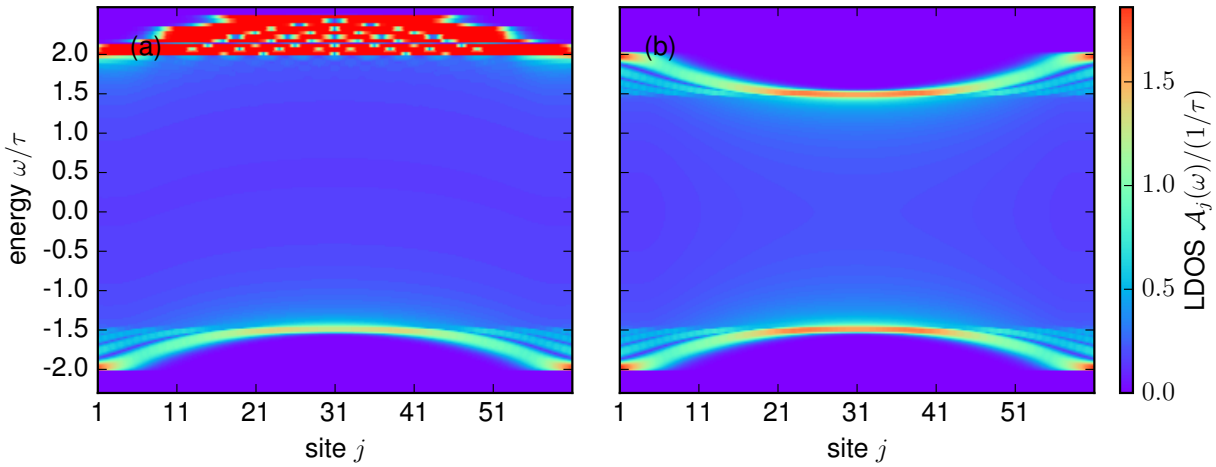

Figure 8.1: The local density of states (color scale) of a non-interacting QPC as function of position (site) and energy ω (for the non-interacting system the LDOS is independent of temperature and chemical potential). The maximum of the QPC potential is at site $i = 31$. (a) shows the LDOS of a QPC with an on-site potential, (b) with a narrowed band. We observe that the height of the LDOS peak at the center of the QPC close to the lower band edge is different [which we associate with a different curvature, c.f. Eq. (8.23)]. Further, if we turn on only an on-site potential, there appear stable states above the leads' upper band edge (red horizontal lines in (a) at frequencies larger than then 2τ). These states become visible only because we have introduced an artificial on-site broadening of 10^{-3} (in both plots). It is numerically quite tedious to treat these stable states. The discrete LDOS at the lower band edge differs because a step of size 1 in $\tilde{x}$- or in $\tilde{y}$-coordinates corresponds to a different physical length in the continuum description. However, since we use the LDOS to extract the curvature and compare observables only within the same model, the difference is irrelevant for us.

However, if we perform a naïve discretization, the Hamiltonians Eq. (8.21) and Eq. (8.15) differ substantially: The Hamiltonian with only a kinetic energy Eq. (8.15) leads to a space-dependent hopping, while the Hamiltonian with potential energy, Eq. (8.21), leads to constant hopping but an on-site energy. In the case of space-dependent hopping only, the upper band edge is pushed inwards (the potential is mimicked by shrinking the band width), leading to no bound states outside of the leads' spectrum, while in the case of an on-site potential only states outside of the leads' spectrum with infinite lifetime appear. Numerically, we choose to discretize Eq. (8.15), thus avoiding the problematic states at the upper band edge.[2]

Fig. 8.1 shows the effect of the two different Hamiltonians/discretizations: instead of introducing an on-site potential (whose LDOS is shown in Fig. 8.1(a)), we vary the hopping from site to site (whose LDOS is shown in Fig. 8.1(a)). Qualitatively, the lower band edge looks the same, while the upper band edge is deformed in a such a way that states with infinite lifetime

[2] It is clear that we could have chose any other mix of kinetic and potential energy by using a different choice of y and β. In fact, this is done in [HBSvD17], where both a potential energy and a spatially dependent hopping are employed.

are removed from the system.

8.3 Non-equilibrium Flow: The distribution function of the artificial leads

When the system is in a non-equilibrium situation, some further complications arise. The most severe complication is related to the fact that fRG is a non-conserving approximation, i.e. fRG violates the Ward-identities related to $U(1)$ charge conservation (e.g. Ref. [Kat04]). This manifests in the fact that the current in our approximation differs from bond to bond (c.f. the end of Sec. 8.3).

A subtle consequence of this spatial variation of the current is felt already during the flow: In order to specify the flow, we need to assign a distribution function to the artificial leads. Of course, in an exact solution of the full flow, this assignment is irrelevant at the end. During each point in flow (at any finite Λ) however, the system behaves differently depending on this assignment.

In equilibrium, we pick for each artificial lead the Fermi-Dirac distribution with chemical potential and temperature set by the values we want for the physical leads, as otherwise the system would not be in equilibrium at finite Λ. In a non-equilibrium situation, the choice of distribution function for the artificial leads is not a priori clear. It turns out that the choice is highly relevant for the results, given our approximation. While a strong dependence on a parameter that should – ideally – be completely irrelevant can be seen as a clear sign to distrust the results, we can view this dependence as a chance to pick the optimal value for the parameter. Of course, we need to exercise extreme caution when interpreting results obtained in this way.

In order to optimize the distribution function of the artificial leads, what is a good rationale? We want to minimize the impact of the artificial leads. The main effect of a badly chosen distribution function is to siphon particles from or inject particles into the system. If we can minimize the flow of particles between the artificial leads and the system, this should reduce artifacts due to our approximation. The flow of particles between the system and the artificial leads at a given site j is determined by the local distribution function, c.f. Sec. 7.5. So, if we pick a distribution function for the artificial lead that mimicks the local distribution function, (naïvely) no particles can enter or leave the system through the artificial leads.

While this idea is good, there are some challenges and questions that need to be addressed:

1. Can we even impose an arbitrary distribution function on the artificial leads?
2. What effect does this modification have on the flow equations themselves?
3. How do we compute the distribution function?
4. What is a good implementation?
5. Does it work? Is it useful?

Let us address these issues in order:

1. We can indeed impose an arbitrary distribution on the artificial leads. While this may at first glance seem trivial, let us recall a important facet of the artificial leads: There is a sensible physical system, with which we may associate with our generating functional even at finite Λ. This statement has far-reaching consequences. Mainly, we may use the fact that we describe a sensible physical system at finite Λ to generate a large set of constraints. For example, it is by no means necessary for the Green's function to have the correct analytical properties or satisfy the FDT in equilibrium during the flow. However, if the Green's function does, we have both an additional simple check and a guarantee that our approximations do not destroy this property. Various simplifications we have used no longer hold if the system at finite Λ is completely arbitrary.

   Now, it is well-known that a fermionic system will – in equilibrium – have a distribution function given by the Fermi-Dirac distribution. However, if we consider the derivation, then this statement is only true if at least some interaction exists (which is the case for any *real* system). On the other hand, it is straightforward to show that non-interacting fermions may be distributed with whatever distribution function we wish (e.g. [SCG+15]).[3]

2. Let us recall that the flow equations as presented here are valid if we modify *only* the quadratic part of the action. Since the artificial leads are non-interacting, the distribution function of the artificial leads enters only in the Keldysh component of the inverse bare Green's function, i.e. in the quadratic part of the action. So, the fRG equations as used here remain – in their general form – valid. We just have to take into account the fact that the explicit form of the single-scale propagator S and the Green's functions G will depend on the form of the local distribution functions.[4]

3. In order to compute the local distribution function n_i at given value of the flow parameter, we solve the (linear in n_i) set of equations (Eq. (8.24a) is simply the definition of the Keldysh component of the Green's function spelled out, and Eq. (8.24b) is the defining equation of the local distribution function, c.f. Sec. 5.3, 7.5)

$$\begin{aligned} G^K_{il}(\Lambda,\omega) = {} & G^R_{ij}(\Lambda,\omega)\left(\Sigma_{\mathrm{U}}{}^K(\Lambda,\omega)\right)_{jk} G^A_{kl}(\Lambda,\omega) \\ & + G^R_{ij}(\Lambda,\omega)\left(\sum_{\alpha=L,R}(1-2n_\alpha(\Lambda,\omega))\left(\Sigma_{\mathrm{lead}_\alpha}{}^R(\Lambda,\omega)-\Sigma_{\mathrm{lead}_\alpha}{}^A(\Lambda,\omega)\right)\right)_{jk} G^A_{kl}(\Lambda,\omega) \\ & + G^R_{ij}\left(\sum_{\alpha=1}^{N}(1-2n_\alpha(\Lambda,\omega))\left(\Sigma_{\mathrm{art.lead}_\alpha}{}^R(\Lambda,\omega)-\Sigma_{\mathrm{art.lead}_\alpha}{}^A(\Lambda,\omega)\right)\right)_{jk} G^A_{kl}(\Lambda,\omega), \end{aligned} \tag{8.24a}$$

$$G^K_{jj}(\Lambda,\omega) = (1-2n_j(\Lambda,\omega))\left(G^R_{jj}(\Lambda,\omega)-G^A_{jj}(\Lambda,\omega)\right). \tag{8.24b}$$

[3] If there are no interactions, non-interacting eigenenergies will never mix. A given occupation of a non-interacting eigenstate will remain (as does the occupation of *any* eigenstate). If we adiabatically turn on interactions, they will mix the eigenstates, leaving only one stable distribution (the Fermi-Dirac distribution). The simplest way to see this is from the kinetic equation. If the scattering term vanishes, *any* distribution is a valid solution.

[4] We will be more explicit regarding the form of S and G later on (c.f. Eqs. (8.24b),(8.28), and (8.30)).

The artificial leads contribute to both $\Sigma_{\text{lead}\,L/R}$ (through the artificial leads coupled to the physical lead sites) and to $\Sigma_{\text{art.lead}_i}$ (by directly coupling to these sites). G^R and G^A can be computed without knowledge of the local distribution function

$$G^R(\Lambda,\omega) = \frac{1}{\omega - H_0 - {\Sigma_{\text{U}}}^R(\Lambda,\omega) - {\Sigma_{\text{lead}}}^R(\Lambda,\omega) - {\Sigma_{\text{art.lead}}}^R(\Lambda,\omega)}; \quad G^A = G^{R\dagger}. \tag{8.25}$$

In order to solve Eq. (8.24), we rewrite it as

$$\begin{aligned}\sum_k \underbrace{\left(G^R_{jk}\delta_{jk} - G^A_{jk}\delta_{jk}\right)}_{=A_{jk}}(1-2n_k) = \underbrace{\left(G^R{\Sigma_{\text{U}}}^K G^A\right)_{jj} + \sum_{\beta=L,R}(1-2n_\beta)G^R_{j\beta}\left({\Sigma_{\text{lead}}}^R_{\beta\beta} - {\Sigma_{\text{lead}}}^A_{\beta\beta}\right)G^A_{\beta j}}_{=B_j} \\ + \underbrace{\sum_{k=1}^{N}\left(G^R_{jk}\left({\Sigma_{\text{art.lead}}}^R_{kk} - {\Sigma_{\text{art.lead}}}^A_{kk}\right)G^A_{kj}\right)}_{=\tilde{A}_{jk}}(1-2n_k)\end{aligned} \tag{8.26}$$

to obtain

$$1 - 2n_k = \left(A - \tilde{A}\right)^{-1}_{kj} B_j. \tag{8.27}$$

We note that B does *not* depend on the local distribution function, as it only contains the distribution functions of the isolated leads which we assume to be fixed to two (possibly different) Fermi-Dirac functions. We further note that the local distribution function does in fact depend on the self-energy Σ (in particular, on Σ_{U}) (in principle, by changing Σ, we can go from an open to a closed QPC, which exhibit drastically different distribution functions).

Since Σ depends explicitly on Λ, it is to be expected that the local distribution function n_i depends on Λ. This dependence on Λ is highly relevant, as it implies that the derivative of the local distribution function influences the Keldysh component of the single-scale propagator S.

4. The Keldysh component of the single-scale propagator is given by (c.f. Eq. (4.48))

$$\begin{aligned}S^K(\omega) &= \left(GG_0^{-1}\partial_\Lambda G_0 G_0^{-1} G\right)^K \\ &= -\left(G\partial_\Lambda G_0^{-1} G\right)^K \\ &= -G^R\left(\partial_\Lambda G_0^{-1K}\right)G^A - G^K\left(\partial_\Lambda G_0^{-1A}\right)G^A - G^R\left(\partial_\Lambda G_0^{-1R}\right)G^K,\end{aligned} \tag{8.28}$$

where G_{0K}^{-1} contains the local distribution function through

$${\Sigma_{\text{art.lead}}}^K_{jj} = (1-2n_j)\left({\Sigma_{\text{art.lead}}}^R_{jj} - {\Sigma_{\text{art.lead}}}^A_{jj}\right), \tag{8.29}$$

as we suppose that the (isolated physical and isolated artificial) leads are independently equilibrated and only couple to one site each. We have

$$\left(\partial_\Lambda G_{0K}^{-1}\right)_{ij} = \delta_{ij}\left((1-2n_i)i - 2i\Lambda\partial_\Lambda n_i\right) + \sum_{\beta=L,R} \delta_{i\beta}\delta_{j\beta}(1-2n_\beta)\partial_\Lambda\left(\Sigma_{\text{lead}}{}_\beta^R - \Sigma_{\text{lead}}{}_\beta^A\right). \tag{8.30}$$

At each step of the ODE, G is known (allowing us to compute n_i via Eq. (8.27)), as well as $\partial_\Lambda\Sigma_{\text{lead}}$ (we know Σ_{lead} for all Λs analytically, c.f. Eq. (S9) of [SBv17]). Thus, in order to determine the single-scale propagator S, we still need to obtain the derivative of the local distribution function, $\partial_\Lambda n_i$. However, if we just take the derivative of Eq. (8.27), this derivative contains terms of the form $\frac{d}{d\Lambda}\Sigma_{\text{U}}$. To determine $\frac{d}{d\Lambda}\Sigma_{\text{U}}$, which is given by the fRG-flow equations, we require the single-scale propagator S. If we want to enforce the absence of currents between the system and the artificial leads at all values of the flow parameter Λ, we thus need to solve a self-consistent integral equation (the derivative of the self-energy is obtained from the single-scale propagator by performing an integral). This is numerically not feasible.

Instead of solving a self-consistent equation at each step of the flow, we may pursue a different approach: We flow with some distribution function $n_i(\Lambda,\omega)$. During the flow, we compute the local distribution function $n_i^{\text{new}}(\Lambda,\omega)$, according to Eq. (8.27). In other words, using the self-energy obtained with n_i, we determine the n_i^{new} at which no current would flow between the system and the artificial leads. After the flow, we use n_i^{new} as guess for n_i and iterate this procedure, until the final self-energy has converged. In practice, this is roughly the case after 1 to 3 iterations, depending on the quality of the first guess. A good first guess (which we use throughout) is the local distribution function $n_i(\Lambda,\omega)$ obtained for a non-interacting system.

In this scheme (iterate the full flow until convergence is achieved), there are non-trivial questions: how to obtain smooth data for n_i as a function of Λ, and how to compute the derivative $\partial_\Lambda n_i$. While we may easily obtain somewhat smooth data by interpolating the distribution function, it turns out that it is particularly useful to interpolate the data not in Λ, but in a substituted space. For convenience, this substituted space corresponds to the data obtained from the substitution used in the flow, Eq. (8.1). The reasoning is the same as the one behind the substitution: The system (and with it the local distribution function) behaves differently at different *scales*, making an exponential scale particularly useful. The second question, how to compute the derivative of the local distribution function, allows for two naïve answers: Analytically, by expressing the derivative of the local distribution function through the Green's functions G, the single-scale propagator S, and the derivative of the self-energy $\partial_\Lambda\Sigma$; or numerically, by numerically differentiating the interpolated local distribution function. Since we require the derivative of the local distribution function at arbitrary values of the flow parameter Λ, we would need to interpolate the analytically computed points. It turns out in practice that the numerical derivative actually works better, because the interpolation of the analytical expression is difficult.[5]

[5] Essentially, what we require most is *internal consistency* between the Green's function G and the single-scale

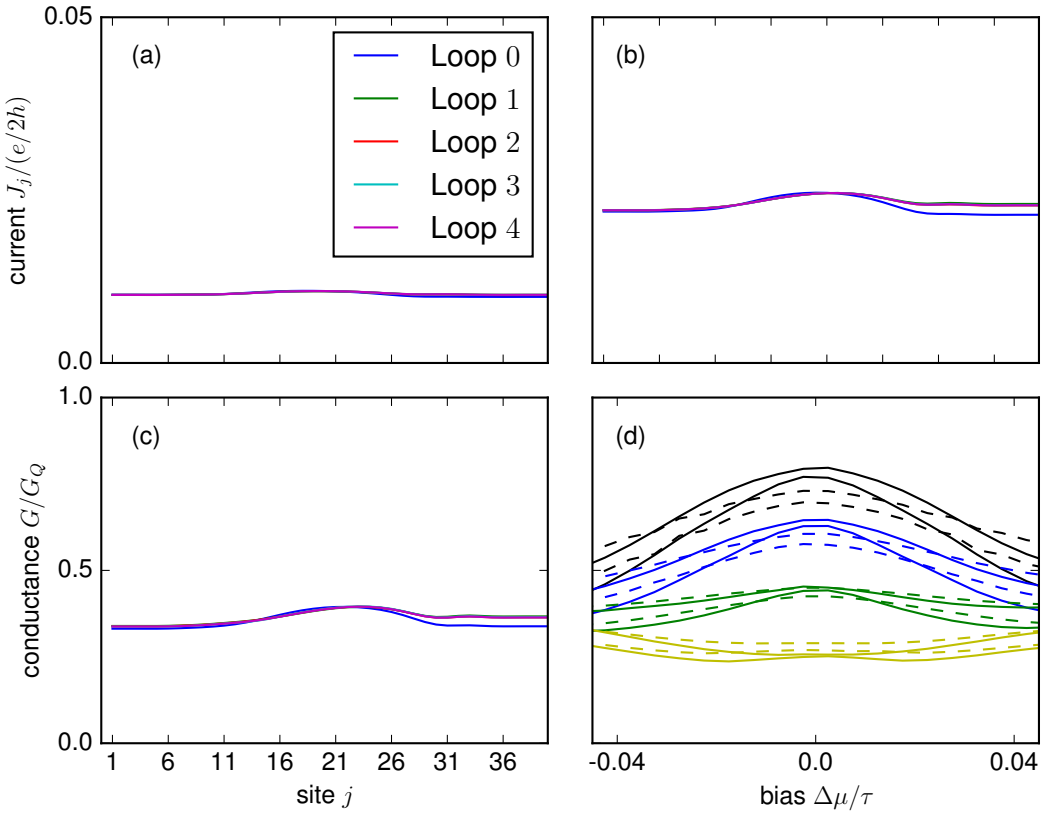

Figure 8.2: Current (a,b) and conductance (c,d) as function of site (a,b,c) or bias voltage (d) at different iterations (a,b,c) or gate voltages (d). (a,b) show the site-resolved current density $J_j = j_{jj+1}$ (c.f. Eq. (5.26)) at a fixed gate voltage ($V_g = 0.26\tau$) and different bias ($\Delta\mu = 0.024\tau$ in (a) and $\Delta\mu = 0.06\tau$ in (b)). We see that at large bias at least one iteration is required. (c) shows the site-resolved conductance at $V_g = 0.26\tau$ and $\Delta\mu = 0.024\tau$ (corresponding to the derivative of (a) w.r.t. to bias). We see that even minuscule changes in the current from site to site lead to "large" changes in the conductance, due to the numerical derivative. (d) shows the minimal and maximal values from the set of all site-resolved conductance values at different gate voltages (full, colored lines) and voltage biases (horizontal axis). All conductance curves are taken at the final iteration and computed by numerically differentiating the current. The dashed lines indicate the data at finite temperature $T = 0.005\tau$. While we clearly see a zero-bias peak in the full green curve (whose conductance at zero bias is $g < 0.5$), we do not have the accuracy to talk about the absence or presence of a zero-bias peak in the yellow curve. We remark that we do not observe any indication of the side-peaks observed experimentally (c.f. Fig. 2.4(a,d)). As we increase the temperature, the zero-bias anomaly is flattened (green curves), in qualitative agreement with experiment (c.f. Fig. 2.4(b)). The vanishing of the zero-bias anomaly in experiment at large conductance $g \gtrsim 0.5$, which we do not see at all, may be related to the side-peaks dominating the conductance-curve. In experiment, the conductance at zero bias is decreased significantly in the sub-open region, which we see as well.

5. Finally, let us take a look at the results (Fig. 8.2). When we consider the site-resolved conductance (i.e. the derivative of the local current density Eq. (5.26) w.r.t. the applied bias voltage $\Delta\mu$), we see that at least one iteration is required to converge the results.[6] The final conductance curves, Fig. 8.2(d), show a zero-bias anomaly at zero temperature (the zero-bias anomaly is the reduction of conductance as a small, finite bias is applied at conductances below $0.5G_Q$; the zero-bias anomaly is visible in the green and yellow curves). Further, Fig. 8.2(d) shows the onset of the $0.3G_Q$ plateau at large bias. An explanation of the $0.3G_Q$ plateau at large bias was given in [IZ09], based on the self-consistent Hartree-approximation (which – as a static approximation – misses out on inelastic processes but nonetheless seems sufficient to capture the important physics here): As the bias is increased, the effective barrier grows, leading to a reduction of the plateau from the non-interacting value of $0.5G_Q$ to some smaller value in the range of $0.3G_Q$. Clearly, our data is insufficient to capture more than the mere existence of the zero-bias peak. For example, we cannot reliably extract the curvature, even at zero bias, and cannot even claim to observe the existence of a zero bias peak at a conductance of $g \lesssim 0.3$. However, we do observe that the zero-bias anomaly seems to have a tendency to vanish as temperature is increased (dashed curves in Fig. 8.2(d)).

   Experimentally, the zero bias peak also vanishes at large conductances $g \gtrsim 0.5$ at finite temperature. While we do not observe this behavior, we may speculate that it is related to the presence (absence) of the side-peaks in experiment (our data): If we just add large peaks at a finite bias, which are mainly unaffected by temperature, then the reduction of the conductance at zero bias alone might be sufficient to remove the zero-bias peak at large conductance $g \gtrsim 0.5$.

8.4 Non-equilibrium Flow: Restricting the frequencies: Effective equilibrium

A further trick we may employ is based on the FDT: In equilibrium, we are only required to compute the retarded components of the self-energy and of each channel. In general, for a non-equilibrium setup, we have to compute the Keldysh component for the self-energy and each channel as well. However, in the perturbative regime, at energies far away from the bias

propagator S. We need to ensure that $S \sim \partial_\Lambda G|_{\Sigma=const}$. This is ensured by taking the numerical derivative (or by taking the analytical derivative of the interpolation object [if the interpolation is done by fitting some set of functions, the derivative of these functions is usually known analytically]). Evaluating the analytical derivative and then interpolating is more prone to violating the relation $S \sim \partial_\Lambda G|_{\Sigma=const}$. The numerical derivative is much more forgiving and thus works better with fewer data points.

[6] We remark that all conductance curves shown in Fig. 8.2 are computed by numerically differentiating the current. The numerical differentiation is performed through a minimization procedure, following [Cha11]. The results using other numerical derivatives are similar. Interestingly, the results based on the analytical derivative Eq. (5.38) are compatible but show larger error bars. We speculate that in general observables requiring the n-particle vertex are worse in fRG than observables requiring only the $m < n$-particle vertex. For example, in equilbrium the current is identical zero. So, the Ward identity of the form $\langle \partial j \rangle = 0$ is satisfied exactly. However, the more complicated Ward identity Eq. (5.25) is satisfied only to order U^2.

window, effectively an FDT should be restored.[7]

We argue that the Keldysh components need only be computed explicitly within essentially the bias window (enlarged by the appropriate thermal smearing), while at all other energies we may use the FDT. We will prove that $\dot{G}$ satisfies a FDT for frequencies sufficiently far away from the bias window, with exponentially small corrections. To be precise, we will show: Assuming that G satisfies a FDT for energies $\omega \notin [\mu - \epsilon, \mu + \epsilon]$, and the vertex accordingly for $\Pi \notin [2\mu - \epsilon^P, 2\mu + \epsilon^P]$, $X \notin [-\epsilon^X, +\epsilon^X]$, $\Delta \notin [-\epsilon^D, +\epsilon^D]$, with the epsilons being of order of the temperature, this assumption remains valid during the flow with exponential accuracy, where the temperature sets the decay. We note that the ϵ's grow during the flow. However, in practice, for systems where the truncation employed here is valid (i.e. perturbative systems), this growth of the FDT-violating regions is slow, such that it is sufficient to compute the vertex and the self-energy fully in only a narrow window, while large frequencies may be computed using the FDT.

The amount of time saved is determined approximately as one half times the ratio of the frequencies where the FDT is employed to all frequencies.[8]

8.4.1 Self-energy

To prove the assertion, let us first consider the flow of the self-energy in equilibrium. The bare interaction only leads to a real part of Σ^R and does not contribute to Σ^K. Thus, its contribution is clearly in accordance with our claim. Next, we focus on the part containing the X-Vertex (the other channels may be proven analogously):

$$\dot{\Sigma}^R(\omega) \sim i \int d\omega' S^K(\omega') a^X(\omega' - \omega) + S^R(\omega') b^X(\omega' - \omega), \tag{8.31}$$

$$\dot{\Sigma}^K(\omega) \sim i \int d\omega' S^R(\omega') a^X(\omega' - \omega) + S^A(\omega') a^{X\dagger}(\omega' - \omega) + S^K(\omega') b^X(\omega' - \omega). \tag{8.32}$$

In equilibrium, we have

$$\dot{\Sigma}^K(\omega) = (1 - 2n_F(\omega))(\dot{\Sigma}^R - \dot{\Sigma}^A) = \tanh\left(\frac{\omega - \mu}{2T}\right)(\dot{\Sigma}^R - \dot{\Sigma}^A) \tag{8.33}$$

If we use the modified flow equations

$$\dot{\Sigma}^R(\omega) \sim i \int d\omega' S^K(\omega') a^X(\omega' - \omega) + S^R(\omega') b^X(\omega' - \omega), \tag{8.34}$$

$$\dot{\Sigma}^K(\omega) \sim i \int d\omega' S^R(\omega') a^X(\omega' - \omega) + S^A(\omega') a^{X\dagger}(\omega' - \omega) + S^K(\omega') b^X(\omega' - \omega)$$

[7] This statement essentially boils down to: at energies far away from the bias window, $G^K = \pm(G^R - G^A)$ and similarly for the vertex, as the distribution functions approach one or zero.

[8] The calculation time of say the P-channel is $N_\Pi\,(t_a + t_b)$, where N_Π is the number of frequencies used to represent the P-channel and t_a (t_b) is the time required to compute the contribution to a_p (b_p). We have roughly $t_a = t_b$, as the majority of the run-time is spent on the integrals over frequencies and we may reuse the integral computed for a_p in b_p, which thus requires only one new integral to be computed for b_p. Since at least half of the frequencies used in the discretization lie outside of a somewhat enlarged bias-window, we save around 25% in run-time.

$$- S^R(\omega')a^{X\dagger}(\omega'-\omega) - S^A(\omega')a^X(\omega'-\omega), \tag{8.35}$$

then the FDT actually holds even without the integral (i.e. for each value of ω'). Note that we have merely added zero in the flow of the Keldysh component. In general (i.e. out of equilibrium), let us define $S^K_{FDT} := (1-2n_F)(S^R - S^A)$ and $\delta S^K := S^K - S^K_{FDT}$ (and analogously b^X_{FDT} and δb^X). We then have

$$\dot{\Sigma}^R(\omega) \sim i\int d\omega'(\delta S^K + S^K_{FDT})(\omega')a^X(\omega'-\omega) + S^R(\omega')(\delta b^X + b^X_{FDT})(\omega'-\omega), \tag{8.36}$$

$$\begin{aligned}\dot{\Sigma}^K(\omega) \sim i\int d\omega' & S^R(\omega')a^X(\omega'-\omega) + S^A(\omega')a^{X\dagger}(\omega'-\omega) \\ & + (\delta S^K + S^K_{FDT})(\omega')(\delta b^X + b^X_{FDT})(\omega'-\omega) - S^R(\omega')a^{X\dagger}(\omega'-\omega) - S^A(\omega')a^X(\omega'-\omega),\end{aligned} \tag{8.37}$$

If δS^K and δb^X are zero, these satisfy the FDT. Thus, the violation $\delta\dot{\Sigma} = \dot{\Sigma}^K - (1-2n_F)(\dot{\Sigma}^R - \dot{\Sigma}^A)$ of the FDT is given by

$$\begin{aligned}\delta\dot{\Sigma}(\omega) \sim i\int & d\omega'\delta S^K(\omega')(\delta b^X + b^X_{FDT})(\omega'-\omega) + S^K_{FDT}(\omega')\delta b^X(\omega'-\omega) \\ & - \tanh((\omega-\mu)/2T)\delta S^K(\omega')(a^X - a^{X\dagger})(\omega'-\omega) \\ & - \tanh((\omega-\mu)/2T)(S^R - S^A)(\omega')\delta b^X(\omega'-\omega) \\ \sim i\int & d\omega'\delta S^K(\omega')(\delta b^X - \coth(./2T)(a^X - a^{X\dagger}))(\omega'-\omega) \\ & + \tanh((\omega'-\mu)/2T)(S^R - S^A)(\omega')\delta b^X(\omega'-\omega) \\ & - \tanh((\omega-\mu)/2T)\delta S^K(\omega')(a^X - a^{X\dagger})(\omega'-\omega) \\ & - \tanh((\omega-\mu)/2T)(S^R - S^A)(\omega')\delta b^X(\omega'-\omega)\end{aligned} \tag{8.38}$$

The assumptions basically state that $\delta S^K(\omega \notin [\mu-\epsilon, \mu+\epsilon]) = 0$ and $\delta b^X(\omega \notin [-\epsilon^X, +\epsilon^X]) = 0$. We see that under these assumptions

$$\delta\dot{\Sigma}(\omega \notin [\mu-\epsilon, \mu+\epsilon]) = 0, \tag{8.39}$$

with exponential accuracy. The scale is clearly given by the temperature.

8.4.2 Vertex

We now check if the same holds for the flow of the vertex. Consider the schematic flow equation in the X-channel (once again, the other channels can be proven analogously)

$$\begin{aligned}\dot{a}^{X\dagger}(X) &= \left(U + a^{X\dagger}(X)\right)\left(I^{ph}_{qc|cc}(X) + I^{ph}_{cc|cq}(X)\right)\left(U + a^{X\dagger}(X)\right), \\ \dot{a}^X(X) &= \left(U + a^X(X)\right)\left(I^{ph}_{cc|qc}(X) + I^{ph}_{cq|cc}(X)\right)\left(U + a^X(X)\right),\end{aligned} \tag{8.40}$$

$$\dot{b}^X(X) = \left(U + a^{X\dagger}(X)\right)\left(I^{ph}_{cc|cc}(X) + I^{ph}_{qc|cq}(X) + I^{ph}_{cq|qc}(X)\right)\left(U + a^X(X)\right)$$

$$+\left(U+a^{X\dagger}(X)\right)\left(I^{ph}_{qc|cc}(X)+I^{ph}_{cc|cq}(X)\right)b^X(X)$$
$$+b^X(X)\left(I^{ph}_{cq|cc}(X)+I^{ph}_{cc|qc}(X)\right)\left(U+a^X(X)\right) \tag{8.41}$$

Consider X sufficiently far away from zero. Noting that $I^{ph}_{qq|cc}(X)=0=I^{ph}_{cc|qq}(X)$, we may modify the flow of b^X to

$$\begin{aligned}\dot{b}^X(X)=&\left(U+a^{X\dagger}(X)\right)\left(I^{ph}_{cc|cc}(X)+I^{ph}_{qc|cq}(X)+I^{ph}_{cq|qc}(X)-I^{ph}_{qq|cc}(X)-I^{ph}_{cc|qq}(X)\right)\left(U+a^X(X)\right)\\&+\left(U+a^{X\dagger}(X)\right)\left(I^{ph}_{qc|cc}(X)+I^{ph}_{cc|cq}(X)\right)b^X(X)\\&+b^X(X)\left(I^{ph}_{cq|cc}(X)+I^{ph}_{cc|qc}(X)\right)\left(U+a^X(X)\right)\end{aligned} \tag{8.42}$$

We may compute the difference

$$\begin{aligned}&\dot{b}^X(X)+\coth(X/2T)(\dot{a}^X-\dot{a}^{X\dagger})(X)\\&\quad=\left(U+a^{X\dagger}(X)\right)\left(I^{ph}_{cc|cc}(X)+I^{ph}_{qc|cq}(X)+I^{ph}_{cq|qc}(X)-I^{ph}_{qq|cc}(X)-I^{ph}_{cc|qq}(X)\right)\left(U+a^X(X)\right)\\&\quad+\left(U+a^{X\dagger}(X)\right)\left(I^{ph}_{qc|cc}(X)+I^{ph}_{cc|cq}(X)\right)b^X(X)\\&\quad+b^X(X)\left(I^{ph}_{cq|cc}(X)+I^{ph}_{cc|qc}(X)\right)\left(U+a^X(X)\right)\\&\quad+\coth(X/2T)\left(U+a^X(X)\right)\left(I^{ph}_{cc|qc}(X)+I^{ph}_{cq|cc}(X)\right)\left(U+a^X(X)\right)\\&\quad-\coth(X/2T)\left(U+a^{X\dagger}(X)\right)\left(I^{ph}_{qc|cc}(X)+I^{ph}_{cc|cq}(X)\right)\left(U+a^{X\dagger}(X)\right),\end{aligned} \tag{8.43}$$

and use the FDT for b^X (which is valid by assumption for X sufficiently far away from zero) to obtain:

$$\begin{aligned}&\dot{b}^X(X)+\coth(X/2T)(\dot{a}^X-\dot{a}^{X\dagger})(X)\\&\quad=\left(U+a^{X\dagger}(X)\right)\Big(I^{ph}_{cc|cc}(X)+I^{ph}_{qc|cq}(X)+I^{ph}_{cq|qc}(X)-I^{ph}_{qq|cc}(X)-I^{ph}_{cc|qq}(X)\\&\qquad-\coth(X/2T)\left(I^{ph}_{qc|cc}(X)+I^{ph}_{cc|cq}(X)-I^{ph}_{cc|qc}(X)-I^{ph}_{cq|cc}(X)\right)\Big)\left(U+a^X(X)\right).\end{aligned} \tag{8.44}$$

Explicitly writing the bubbles, we have to show that the following term vanishes with exponential accuracy:

$$\begin{aligned}&I^{ph}_{cc|cc}(X)+I^{ph}_{qc|cq}(X)+I^{ph}_{cq|qc}(X)-\coth(X/2T)\left(I^{ph}_{qc|cc}(X)+I^{ph}_{cc|cq}(X)-I^{ph}_{cc|qc}(X)-I^{ph}_{cq|cc}(X)\right)\\&\sim i\int d\omega'\,\big[G^K(-X/2+\omega')S^K(X/2+\omega')+S^K(-X/2+\omega')G^K(X/2+\omega')\\&\qquad+G^A(-X/2+\omega')S^R(X/2+\omega')+S^A(-X/2+\omega')G^R(X/2+\omega')\\&\qquad+G^R(-X/2+\omega')S^A(X/2+\omega')+S^R(-X/2+\omega')G^A(X/2+\omega')\end{aligned}$$

$$
\begin{aligned}
&- G^R(-X/2+\omega')S^R(X/2+\omega') - S^R(-X/2+\omega')G^R(X/2+\omega') \\
&- G^A(-X/2+\omega')S^A(X/2+\omega') - S^A(-X/2+\omega')G^A(X/2+\omega') \\
&- \coth(X/2T)\left[G^A(-X/2+\omega')S^K(X/2+\omega') + S^A(-X/2+\omega')G^K(X/2+\omega')\right. \\
&+G^K(-X/2+\omega')S^R(X/2+\omega') + S^K(-X/2+\omega')G^R(X/2+\omega') \\
&-G^R(-X/2+\omega')S^K(X/2+\omega') - S^R(-X/2+\omega')G^K(X/2+\omega') \\
&\left.-G^K(-X/2+\omega')S^A(X/2+\omega') - S^K(-X/2+\omega')G^A(X/2+\omega')\right]\Big] \qquad (8.45)
\end{aligned}
$$

This vanishes in equilibrium for each value of ω' separately. As before, we introduce $G^K = G^K_{FDT} + \delta G^K$ and we only need to consider terms $\sim \delta G^K, \sim \delta S^K, \sim \delta S^K \delta G^K$. For now, let us focus on the first terms of each line (GS and not SG). For X sufficiently far away from zero, there are two problematic frequencies $\omega' \approx \mu \pm X/2$. Consider first $\omega' \approx \mu + X/2$. Then, $\delta G^K \neq 0$, but $\delta S^K = 0$ with exponential accuracy. The problematic terms multiplying δG^K are:

$$
\begin{aligned}
&\delta G^K(-X/2+\omega')\left[S^K_{FDT}(X/2+\omega') - \coth(X/2T)S^R(X/2+\omega') + \coth(X/2T)S^A(X/2+\omega')\right] \\
&\quad = \delta G^K(\mu)\left[\tanh(X/2T)\left(S^R(X+\mu) - S^A(X+\mu)\right)\right. \\
&\qquad\qquad \left. - \coth(X/2T)\left(S^R(X+\mu) - S^A(X+\mu)\right)\right], \qquad (8.46)
\end{aligned}
$$

where the frequency argument μ means "close to μ". The terms Eq. (8.46) thus vanish with exponential accuracy. It is easy to see that the same happens for all other dangerous terms.

We have thus proven the theorem. We have numerically checked that the growth of the ϵ's is not severe by comparing the results obtained with and without the simplification of an effective FDT.

8.5 Checks

It is of paramount importance to check the correctness of one's implementation. To facilitate future modifications of the code, we give a short list of relevant checks that may be performed. Not all of these checks apply for every system. However, they all are relevant for the system at hand.

(i) If the self-energy Σ is set to zero, then the relation $\partial_\Lambda G = S$ must hold. This is used to confirm the consistency of G and S.

(ii) If the self-energy does not flow and the channels do not mix, each channel must satisfy an RPA-type equation. To be precise: The flow-equation $\dot{\gamma}_P = \gamma_P B_P \gamma_P$, where γ_P denotes the P-channel contribution to the vertex, and B_P the P-bubble in the flow, with initial condition $\gamma_P = U$, is solved by $\gamma_P = U\frac{1}{1-B_b U}$, where B_b is half of the P-bubble consisting only of Green's functions. Similar results hold for the X- and D-channel.

(iii) For most flow-parameters, discrete symmetries remain intact during the flow. In the case considered here, in equilibrium, the system respects left-right parity and symmetry under exchange of positions.

(iv) Continuous symmetries of the generating functional are usually not respected by fRG. However, the fRG flow is usually exact up to some order of the interaction. The violation of Ward-identities derived from the continuous symmetry thus has to scale as the first order that is not fully taken into account. Here, the continuous symmetry is a global $U(1)$ symmetry: $\psi \to \exp(i\alpha)\psi$, whose Ward-identity corresponds to charge conservation. Since the flow scheme used in this work is exact up to order (including) U^2, the Ward-identities following from charge conservation are only violated to third order in U. The scaling may be checked by considering small values of U. Note that as U is decreased the accuracy of all internal calculations has to be increased to reach sufficient resolution to actually observe a U^3 behavior, as the numerical error already starts at order U^1.

(v) Fundamental analytical properties are conserved for certain flow parameters. The hybridization flow used here conserves the analytic properties of Σ^R and the a's (Reminder: Σ^R, a^P, a^{X*}, and a^D are analytic in the upper half plane). To check analyticity in the upper half plane of a function f, one may check if the Kramers-Kronig relation

$$\mathrm{Re}(f(\Omega)) = \frac{1}{\pi}\mathcal{P}\int d\omega \frac{\mathrm{Im}(f(\omega))}{\omega - \Omega}, \tag{8.47}$$

with $\mathcal{P}$ denoting the principal value, is satisfied. Note that the static contribution (the value of f at infinity) has to be subtracted first.

Equivalently, we could check that the Fourier-transformed function $f(t)$ vanishes for times smaller than zero.[9]

(vi) The LDOS is normalized, i.e. $\int d\omega \frac{-\mathrm{Im}G^R_{ii}(\omega)_{ii}}{\pi} = 1$.

(vii) If fluctuation-dissipation theorems are not explicitly used, they should be satisfied throughout the flow (for the flow parameter used here).

(viii) For Fermi-liquids at $T = 0$: $\mathrm{Im}\Sigma(\mu) = 0$; at $T > 0$, but small: $\mathrm{Im}\Sigma(\mu) < 0$.[10]

(ix) For Fermi-liquids at $T = 0$: $\mathrm{Im}\Sigma(\omega = \mu \pm \epsilon) < 0$, where ϵ is a small number.

(x) For Fermi-liquids at $T = 0$ and small, finite bias: $\mathrm{Im}\Sigma(\omega = (\mu_L + \mu_R)/2) < 0$.

[9] Recall that analyticity in the upper half plane in frequency space is equivalent to "retardation", which means that the function follows a specific causality structure: it vanishes if events occur in the wrong order, i.e. it is zero for $t < 0$.

[10] Usually, Fermi-liquid properties are derived for a homogeneous system, where we would consider the self-energy at the Fermi-momentum. However, for the system at hand, a Fermi-liquid description of the low-energy degrees of freedom is valid. In this case, when we write statements like $\mathrm{Im}\Sigma(\omega) = \ldots$, we mean $\mathrm{Im}\Sigma_{ii}(\omega) = \ldots$, i.e. we refer to a single site. While we do not know of any rigorous proofs of these statements, they should nevertheless work out. We note however that we cannot say e.g. that $\mathrm{Im}\Sigma_{ij}(\omega)$ has specific properties. This is similar to an observation about the Green's function: $\mathrm{Im}G^R_{ii}$ has to be negative (it can be interpreted as a density of states), while $\mathrm{Im}G^R_{ij}$ may have arbitrary sign.

In equilibrium, at $T = 0$ however the special statement $\mathrm{Im}\Sigma_{ij}(\mu) = 0$ is true in our approximation. This can be straightforwardly shown from the flow equations.

(xi) The single-particle transmission probability P_T should be between 0 and 1. In equilibrium, at zero temperature and at $\omega = \mu$, P_T, together with the single-particle reflection probability P_R should add up to 1. Both probabilities are the squared moduli of the reflection and transmission amplitudes r and t respectively. The amplitudes may be read of from the single-particle S-matrix

$$S(\omega) = 1 - 2\pi i \tau \rho \begin{pmatrix} G^R_{-N,-N}(\omega) & G^R_{-N,N}(\omega) \\ G^R_{N,-N}(\omega) & G^R_{N,N}(\omega) \end{pmatrix} = \begin{pmatrix} r & t \\ t^* & r \end{pmatrix}, \tag{8.48}$$

where τ is the hopping between the leads and the system and ρ is the density of states at the edge of the leads in the absence of the central part of the system. If energy is available, i.e. either $\omega \neq \mu$ or $T \neq 0$ or $V_{sd} \neq 0$, the single-particle S-matrix is not unitary (as the single-particle S-matrix does not include processes of the type: electron $\rightarrow$ two electrons and one hole). Consequently, we expect (and actually observe numerically) $P_R + P_T < 1$ (c.f. Fig. 7.5).

Chapter 9

Publication: Low energy properties of the Kondo chain in the RKKY regime

This chapter deals with physics and methods unrelated to the methods and physics explained in the rest of the thesis. We consider a one-dimensional system of electrons with approximately linear dispersion, in contact with a spin disorder. Physically, we imagine for example a one-dimensional wire on top of an impure insulator with magnetic impurities, or the edge of an impure insulator.

It was shown in [TY15] that such a system, if we neglect the interactions of the electrons amongst themselves, and assume an anisotropic coupling between the spins and the electrons, can lead to helical modes as low-energy degrees of freedom (in the case of easy-plane anisotropy).[1] The helical modes are distinguished by their velocity, i.e. the particles associated with one helicity travel with a velocity v_1, while the particles associated with the other helicity travel with the velocity $v_2 \ll v_1$. The emergence of helical modes is due to a spontaneous $\mathbb{Z}_2$ symmetry breaking. It is important to emphasize that *both* helicities are present as gapless excitations, which is in contrast to earlier results, e.g. [BSL09, KSYL13]

In the work presented here, we further explain the details of [TY15] and extend the study of [TY15] to include electron-electron interactions and we compute the order-parameter of the symmetry breaking through the spin correlation functions.

The calculations necessary for these extensions are all due to Dennis Schimmel.

[1] A helical mode is carried by spinful charged particles. The spin of the particles is directly linked to the direction the particle travels in. For example, an electron of spin up traveling to the right has a specific helicity, which is the same helicity as an electron of spin down traveling to the left, but opposite to the helicity of an electron of spin up traveling to the left.

New Journal of Physics
The open access journal at the forefront of physics

Deutsche Physikalische Gesellschaft DPG
IOP Institute of Physics

Published in partnership with: Deutsche Physikalische Gesellschaft and the Institute of Physics

OPEN ACCESS

RECEIVED
23 December 2015

REVISED
4 March 2016

ACCEPTED FOR PUBLICATION
5 April 2016

PUBLISHED
3 May 2016

PAPER

Low energy properties of the Kondo chain in the RKKY regime

D H Schimmel[1], **A M Tsvelik**[2,4] **and O M Yevtushenko**[1,3]

[1] Ludwig Maximilians University, Arnold Sommerfeld Center and Center for Nano-Science, Munich, D-80333, Germany
[2] Condensed Matter Physics and Material Sciences Division, Brookhaven National Laboratory, Upton, NY 11973-5000, USA
[3] Institute for Theoretical Physics, Universität Erlangen-Nürnberg, Staudtstrasse 7, D-91058 Erlangen, Germany
[4] Author to whom any correspondence should be addressed.

E-mail: tsvelik@gmail.com

Keywords: helical symmetry, ideal protected transport, Kondo chain, RKKY

Abstract

We study the Kondo chain in the regime of high spin concentration where the low energy physics is dominated by the Ruderman–Kittel–Kasuya–Yosida interaction. As has been recently shown (Tsvelik and Yevtushenko 2015 *Phys. Rev. Lett.* **115** 216402), this model has two phases with drastically different transport properties depending on the anisotropy of the exchange interaction. In particular, the helical symmetry of the fermions is spontaneously broken when the anisotropy is of the easy plane type. This leads to a parametrical suppression of the localization effects. In the present paper we substantially extend the previous theory, in particular, by analyzing a competition of forward- and backward- scattering, including into the theory short range electron interactions and calculating spin correlation functions. We discuss applicability of our theory and possible experiments which could support the theoretical findings.

1. Introduction

The Kondo chain (KC) is one of the archetypal models for interacting low-dimensional systems which has been intensively studied during the past two decades [1–11]. It consists of band electrons on a one-dimensional lattice which interact with localized magnetic moments; electron–electron interactions can also be included in the consideration [1, 2, 5, 9, 12]. The KC is not exactly solvable, nevertheless, a lot is known about it both from numerical and analytical studies [1, 6–9]. In particular, ground state properties are known from DMRG for the isotropic point [13].

One possible realization of KC is a cleaved edge overgrowth GaAs quantum wire doped with magnetic ions. Such quantum wires were manufactured a long time ago [14, 15] and have been successfully used to study one-dimensional strongly correlated physics (see, for example, [16, 17]). Functionalizing them with dynamical magnetic impurities could yield an experimental realization of the KC. As another possible platform for KC one may use carbon nanotubes functionalized with magnetic ions or molecules containing magnetic ions (possible realizations can be found in [18–20]). Alternatively one may search for quasi one-dimensional structures with coexisting localized and delocalized electrons in bulk materials. The theory predicts that in iron-based ladder materials some of the iron d-orbitals are localized and some are itinerant [21–23]. The issue is to find such crystal structures where the ladders would be sufficiently isolated from each other to prevent three-dimensional ordering (three-dimensional ordering seems to occur in $BaFe_2Se_3$ [24]).

It has been recently shown by two of us that the KC may display a rather nontrivial physics in the anisotropic regime away from half-filling in the case of dense spins when the Ruderman–Kittel–Kasuya–Yosida (RKKY) exchange interaction dominates the Kondo screening [25]. We considered an anisotropic exchange interaction with the anisotropy of the XXZ-type. Then there are two phases with different low-energy properties, namely, the easy axis (EA) phase and the easy plane (EP) one. In the EA phase, all single fermion excitations are gapped. The charge transport is carried by collective excitations which can be easily pinned by ever present potential disorder. The situation is drastically different in the EP phase. The minimum of the ground state energy corresponds to the helical spin configuration with wave vector $2k_F$ (k_F being the Fermi wave vector) which opens a gap in the spectrum of the

fermions of a particular helicity while the electrons having the other (opposite) helicity remain gapless. We remind the readers that the helicity is defined as $\mathrm{sgn}(v)\,\mathrm{sgn}(\sigma)$, where v and σ the the electron velocity and its spin, respectively. This corresponds to the spontaneous breaking of the discreet $\mathbb{Z}_2$ helical symmetry. If the potential disorder is added to the phase with the broken symmetry a single-particle backscattering is prohibited either by spin conservation (for electrons with the same helicity) or by the gap in one of the helical sectors (for electrons with different helicity). This is similar to the absence of the single-particle back-scattering of edge modes in time-reversal invariant topological insulators [5, 26–32] and results in suppression of localization effects. The latter can appear only due to collective effects resulting in a parametrically large localization radius. In other words, ballistic charge transport in the EP phase has a partial symmetry protection which is removed either in very long samples or if the spin $U(1)$ symmetry is broken. This is also similar to the symmetry protection of the edge transport in 2d topological insulators: transport is ideal if time-reversal symmetry and spin $U(1)$ symmetry are present. However, it can be suppressed in a long sample due to spontaneously broken time-reversal symmetry [33, 34].

In the present paper, we continue to study the KC in the RKKY regime where the low energy physics is governed by the fermionic gaps. We aim to explain in more details the results of [25] and to substantially extend the theory, in particular, by analyzing the role of forward scattering (i.e., of the Kondo physics), by taking into account the short range electron interactions and by calculating the spin correlation functions.

Similar ideas to those presented here were already pursued in [2], where the emergence of helical order was recognized. In contrast to [2] we take into account the dynamics of the lattice spins whose presence substantially modifies the low-energy theory.

The Hamiltonian of the KC on a lattice is

$$\mathcal{H} = \mathcal{H}_0 + \mathcal{H}_{\mathrm{int}} = \sum_i [t c^\dagger_{i+1} c_i + \mathrm{h.c.}] + \sum_a \sum_{j\in M} J^a S^a_j c^\dagger_j \sigma^a c_j,\ a = x, y, z; \tag{1}$$

where t is the hopping matrix element, $c_i^{(\dagger)}$ annihilates (creates) an electron at site i, $\boldsymbol{S}_i$ is a local spin of magnitude s, σ^a is a Pauli matrix, and M constitutes a subset of all lattice sites. J denotes the interaction strength between the impurities and the electrons. We distinguish J_z and $J_x = J_y =: J_\perp$. Short range interactions between the electrons will be added later in section 4.4. The dynamics of a chain of spins will be added in section 2. We will be interested in the case of dense magnetic impurities, $\rho_s\,\xi_0 \gg 1/L_K$ (with the impurity density ρ_s and the single-impurity Kondo length L_K), when the effects of the electron-induced exchange can take predominance over the Kondo screening. The paper is organized as follows: we first introduce a convenient representation of the impurity spins in section 2. Necessary conditions for the RKKY regime are then discussed in section 3. The gap is studied in section 4. In section 5 we compute the conductance and analyze the effects of spinless disorder. The spin-spin correlation functions are given in section 6.

2. Formulation of the low energy theory

To develop a low energy description of the KC model (1) we have to single out slow modes and integrate over the fast ones. As the first step, we need to find a convenient representation of the spins such that it will be easy to separate the low and high energy degrees of freedom.

2.1. Separation of scales in the spin sector

Consider first a single spin. It is described by the Wess–Zumino term in the action [35]

$$S_{\mathrm{WZ}} = \mathrm{i}\int_0^1 \mathrm{d}u \int_0^\beta \mathrm{d}\tau \frac{s}{8\pi}\epsilon^{\mu\nu}\boldsymbol{n}\cdot(\partial_\mu \boldsymbol{n}\times\partial_\nu \boldsymbol{n}), \tag{2}$$

where $\boldsymbol{n}$ is the direction of the spin, u is an auxiliary coordinate, which together with τ parametrizes a disk. Multiple spins require a summation over spins and can be described by introducing a (dimensionless) spin density ρ_s

$$\sum_{\mathrm{impurities}} S_{\mathrm{WZ}} \to S = \int \mathrm{d}x \frac{\rho_s}{\xi_0} S_{\mathrm{WZ}}, \tag{3}$$

where ξ_0 is the underlying lattice constant for the spins.

Usually, two angular variables are used in parametrizing the spin $\mathbf{S} = s\{\sin(\theta)\cos(\psi), \sin(\theta)\sin(\psi), \cos(\theta)\}$:

$$\mathcal{L}_{\mathrm{WZ}}[\theta, \psi] = \frac{\mathrm{i}s\rho_s}{\xi_0}\cos\theta\partial_\tau\psi, \tag{4}$$

where we have neglected boundary contributions (topological terms).

The form of the Lagrangian equation (4) makes it difficult to separate fast and slow variables, since the angles θ and ψ contain both fast and slow modes. We need to find a different representation of the spin Berry phase, which will allow us to separate the fast and the slow modes explicitly. We first observe that the expression

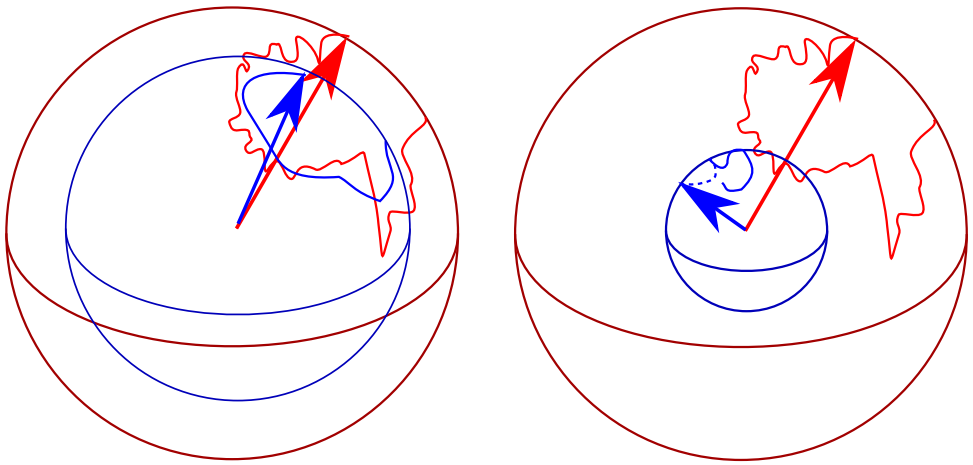

Figure 1. The fast (red) and slow (blue) spin trajectories as a function of time. The slow spin is shorter, since it is the fast spin averaged over some short timescale. The left panel shows the slow modes in the case of a free spin, in the right panel the spin physics is dominated by the interaction mediated by the backscattering electrons. In the latter case, the slow mode is orthogonal to the fast trajectory.

equation (4) can be obtained by considering a coordinate system comoving with the spin. Namely, we choose an orthnormal basis $\{\boldsymbol{e}_1, \boldsymbol{e}_2, \boldsymbol{e}_3\}$ at time $\tau = 0$ and assume that this coordinate system is comoving with the spin such that $s_i^e := (\boldsymbol{S}, \boldsymbol{e}_i)$ is independent of τ. Then it is easy to check that the following expression reproduces (4):

$$\mathcal{L}_{\mathrm{WZ}}[\theta, \psi] = -\frac{\mathrm{i}\rho_s}{2\xi_0}(\mathbf{S}, \mathbf{e}_i)(\mathbf{e}_j, \partial_\tau \mathbf{e}_k)\epsilon_{ijk}. \tag{5}$$

The check of equation (5) can be done by choosing the explicit parametrization

$$\mathbf{e}_1 = \{-\cos(\theta)\cos(\psi), -\cos(\theta)\sin(\psi), \sin(\theta)\}, \tag{6a}$$

$$\mathbf{e}_2 = \{\sin(\psi), -\cos(\psi), 0\}, \tag{6b}$$

$$\mathbf{e}_3 = \{\sin(\theta)\cos(\psi), \sin(\theta)\sin(\psi), \cos(\theta)\} = \boldsymbol{S}/s, \tag{6c}$$

with $\boldsymbol{S} \| \mathbf{e}_3$ and inserting equation (6) into equation (5). A specific choice of the basis $\mathbf{e}_{2,3}$ is not important since $\mathcal{L}_{\mathrm{WZ}}$ in the form equation (5) is manifestly covariant under both a rotation in x, y, z, and a change of basis $\{\mathbf{e}_i\}$.

In path integral quantization, we thus sum over all paths described by $\theta(x, \tau)$ and $\psi(x, \tau)$. The measure is given by $\mathcal{D}\{\Omega\} = \sin\theta \mathcal{D}\{\theta\}\mathcal{D}\{\psi\}$.

Let us now consider two superimposed spin motions: the actual trajectory considered in the path integral, and its slow component (figure 1). We already have the Wess–Zumino term for the actual trajectory. If we want to use equation (5) for the slow component, we need to introduce a second set of basis vectors which is comoving with the slow component. This doubles the number of angles, but we assume a separation of scales: of the four angles, two will be fast and two will be slow. Thus, there will be no double counting of modes which justifies our approach. A convenient choice for the slow basis is given by the rotation of the actual trajectory (figure 2)

$$\boldsymbol{e}_1' = -\sin(\alpha_\parallel)[\cos(\alpha_\perp)\mathbf{e}_1 + \sin(\alpha_\perp)\mathbf{e}_2] + \cos(\alpha_\parallel)\mathbf{e}_3, \tag{7a}$$

$$\boldsymbol{e}_2' = \sin(\alpha_\perp)\mathbf{e}_1 - \cos(\alpha_\perp)\mathbf{e}_2, \tag{7b}$$

$$\boldsymbol{e}_3' = \cos(\alpha_\parallel)[\cos(\alpha_\perp)\mathbf{e}_1 + \sin(\alpha_\perp)\mathbf{e}_2] + \sin(\alpha_\parallel)\mathbf{e}_3. \tag{7c}$$

The total path-integral measure now consists of the four angles: $\mathcal{D}\{\Omega_S, \Omega_{S'}\} = \cos\alpha_\parallel \sin\theta \mathcal{D}\{\theta\}\mathcal{D}\{\psi\}\mathcal{D}\{\alpha_\parallel\}\mathcal{D}\{\alpha_\perp\}$, which will be the product of the measures for fast and slow modes.

Now we can describe the dynamics of the slow modes, which is given by the slow Wess–Zumino term: we pick the bases such that $\mathbf{S} \| \mathbf{e}_3$ and $\mathbf{S}_{\mathrm{slow}} \| \mathbf{e}_3'$. The dynamics of the slow modes are then obtained by using equation (5) with the full spin $\mathbf{S}$ and the slow basis $\mathbf{e}_3'$:

$$S_{\mathrm{WZ}}^{\mathrm{slow}} = = \mathrm{i}s\rho_s\xi_0^{-1}\int \mathrm{d}x \int \mathrm{d}t \sin(\alpha_\parallel)[\partial_\tau\alpha_\perp + \cos(\theta)\partial_\tau\psi]. \tag{8}$$

The dynamics is that of the basis $\{\boldsymbol{e}_1', \boldsymbol{e}_2', \boldsymbol{e}_3'\}$ (i.e. of the slow spin), whereas the overall scale is that of the actual trajectory projected onto the slow component. This projection may be viewed as a renormalization of the length of the spin's slow component.

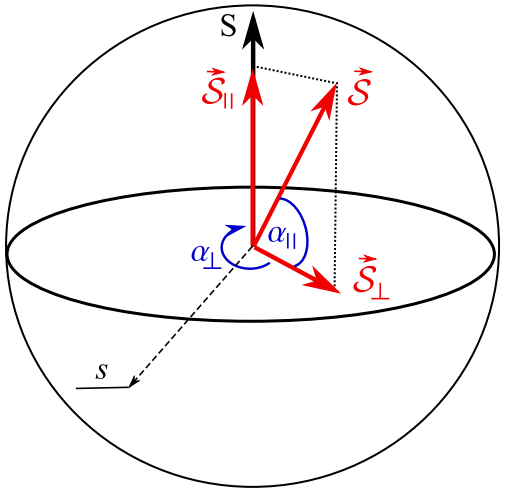

Figure 2. The parametrization of a spin by the angles θ, ψ, $\alpha_{\perp}$, $\alpha_{||}$.

2.2. The interaction between the spins and the fermions

The low-energy fermion modes are obtained by linearizing the spectrum and expanding the operators $\hat{c}$ in smooth chiral modes $\hat{R}_{\sigma}$, $\hat{L}_{\sigma}$

$$\hat{c}_{\uparrow\downarrow}(n) = \mathrm{e}^{-\mathrm{i}k_{\mathrm{F}}\xi_0 n}\hat{R}_{\uparrow\downarrow}(x) + \mathrm{e}^{\mathrm{i}k_{\mathrm{F}}\xi_0 n}\hat{L}_{\uparrow\downarrow}(x), \;\; x = n\xi_0. \tag{9}$$

The Lagrangian density of the band electrons becomes

$$\mathcal{L}_{\mathrm{e}} = \Psi^{\dagger}[(\hat{I}\otimes\hat{I})\partial_{\tau} - \mathrm{i}(\hat{I}\otimes\hat{\tau}^{z})v_{\mathrm{F}}\partial_{x}]\Psi. \tag{10}$$

The first space in the tensor product is the spin one, the Pauli matrices $\hat{\tau}^{a}$ act in the chiral space; $\hat{I} = \mathrm{diag}(1,\,1)$; $v_{\mathrm{F}} = 2t\xi_0\sin(k_{\mathrm{F}}\xi_0)$ is the Fermi velocity; $\Psi^{\mathrm{T}} = (R_{\uparrow},\,R_{\downarrow},\,L_{\uparrow},\,L_{\downarrow})$ is the four-component fermionic spinor field. If the electron interaction is taken into account, it is more convenient to use the bosonized Lagrangian density

$$\mathcal{L}_{\mathrm{e}} = -\sum_{\rho=\mathrm{c,s}}\left\{\frac{\mathrm{i}}{\pi}\partial_x\Theta_{\rho}\partial_{\tau}\Phi_{\rho} - \frac{1}{2\pi}\left[u_{\rho}K_{\rho}(\partial_x\Theta_{\rho})^2 + \frac{u_{\rho}}{K_{\rho}}(\partial_x\Phi_{\rho})^2\right]\right\}, \tag{11}$$

where K_{ρ} is the Luttinger paramter; u_{ρ} the renormalized Fermi velocity; and we have used the bosonization identity

$$\psi_{r\sigma} = \frac{1}{\sqrt{2\pi\xi_0}}U_{\sigma}\mathrm{e}^{-\mathrm{i}rk_{\mathrm{F}}x}\mathrm{e}^{-\frac{\mathrm{i}}{\sqrt{2}}[r\Phi_{\mathrm{c}}-\Theta_{\mathrm{c}}+\sigma(r\Phi_{\mathrm{s}}-\Theta_{\mathrm{s}})]}. \tag{12}$$

Φ_{c} (Φ_{s}) and Θ_{c} (Θ_{s}) are dual bosonic fields belonging to the charge (spin) sector, r distinguishes right- and left-moving modes, σ is the spin projection and U_{σ} are Klein factors. One can introduce spin and charge sources to determine how the low energy degrees of freedom couple to external perturbations:

$$\mathcal{L}_{\mathrm{source}} = h_{\mathrm{c}}(\rho_{\mathrm{c}}^{R} + \rho_{\mathrm{c}}^{L}) + h_{\mathrm{s}}(\rho_{\mathrm{s}}^{R} - \rho_{\mathrm{s}}^{L}) = -\frac{\sqrt{2}\,h_{\mathrm{c}}}{\pi}\partial_x\Phi_{\mathrm{c}} + \frac{\sqrt{2}\,h_{\mathrm{s}}}{\pi}\partial_x\Theta_{\mathrm{s}}, \tag{13}$$

here $\rho_{\mathrm{c/s}}^{R/L} = \rho_{\uparrow}^{R/L} \pm \rho_{\downarrow}^{R/L}$ is the charge/spin density of the right-/left-moving electrons. The spin source is included for purely illustrative purposes. We will combine the fermionic and bosonic description, selecting the one which is most convenient for the given caculations.

Now consider the electron-spin interactions $\mathcal{H}_{\mathrm{int}}$. We will explicitely distinguish forward and backward scattering since they give rise to different physics. The slow part of the backscattering term is (see appendix)

$$\mathcal{L}_{\mathrm{int}}^{(\mathrm{sl,\,bs})} = \frac{s\cos(\alpha_{||})\rho_{\mathrm{s}}}{2}R^{\dagger}\left\{J_{\perp}\left[\mathrm{e}^{\mathrm{i}\psi}\sin^2\left(\frac{\theta}{2}\right)\hat{\sigma}^{-} - \mathrm{e}^{-\mathrm{i}\psi}\cos^2\left(\frac{\theta}{2}\right)\hat{\sigma}^{+}\right] + 2J_z\sin(\theta)\hat{\sigma}^{z}\right\}L\mathrm{e}^{-\mathrm{i}\alpha} + \mathrm{h.c.}, \tag{14}$$

where $\alpha = \alpha_{\perp} - 2k_{\mathrm{F}}x$ and we have introduced the spin-flip operator $S_{\pm} = S_x \pm \mathrm{i}S_y$.

For the forward scattering, we obtain

$$\mathcal{L}_{\rm int}^{\rm (sl,\,fs)} = \frac{s\sin(\alpha_\parallel)\rho_{\rm s}}{2} R^\dagger \{J_\perp^{\rm f}\sin\theta\,[{\rm e}^{{\rm i}\psi}\sigma^- + {\rm e}^{-{\rm i}\psi}\sigma^+] + 2J_z^{\rm f}\cos\theta\sigma^z\}R + (R\to L) \tag{15}$$

3. Renormalization of forward versus backward scattering coupling constants

Equations (14) and (15) describe two competing phenomena: forward scattering tends towards Kondo-type physics, backward scattering opens a gap (see section 4). Both phenomena are distinct and mutually exclusive. If backscattering is dominant, then the emerging gap will cut the RG and suppress forward scattering. If forward scattering dominates, the formation of Kondo-singlett prevents the gap from opening [7]. We will focus on the physics related to the gaps. Therefore, we have to identify conditions under which the backscattering terms are more important. To determine the dominant term, we consider a first loop RG.

Let us consider the bosonized free electrons, equation (11). They constitute two Luttinger liquids, describing a spin density wave (SDW) and a charge density wave (CDW). If there is no electron–electron interaction, then $K_{\rm s} = K_{\rm c} = 1$. A weak, short range, spin independent repulsion between electrons changes $K_{\rm c}$ to $K_{\rm c} \lesssim 1$, but leaves $K_{\rm s}$ untouched.

The RG equations for the couplings read as (see appendix B):

$$\partial_l J_z^{\rm f} = -J_z^{\rm f},\ \ \partial_l J_\perp^{\rm f} = \left[\tfrac{1}{2}\left(K_{\rm s} + \tfrac{1}{K_{\rm s}}\right) - 2\right]J_\perp^{\rm f}, \tag{16}$$

$$\partial_l J_z^{\rm b} = \left[\tfrac{1}{2}(K_{\rm s}+K_{\rm c}) - 2\right]J_z^{\rm b},\ \partial_l J_\perp^{\rm b} = \left[\tfrac{1}{2}\left(K_{\rm c} + \tfrac{1}{K_{\rm s}}\right) - 2\right]J_\perp^{\rm b}, \tag{17}$$

where l parametrizes an energy cutoff Λ' via $\Lambda' = \exp(l)\Lambda$. The flow differs from that of single Kondo impurity because we consider a *dense array* of impurities. All of these terms are relevant, if $K_{\rm c}$ and $K_{\rm s}$ are close to 1. Assuming weak, short range, spin independent repulsion (i.e. $K_{\rm c} \lesssim 1$, and $K_{\rm s} = 1$), we see that the backward scattering terms flow faster in the RG-flow from high to low energies than forward scattering ones, i.e. the terms $\sim J^{\rm b}$ can dominate.

Let us assume that an impurity scatters anisotropically in spin space ($J_z \neq J_\perp$), but there is no difference between the electrons' directions ($J_{\rm bare}^{\rm f} = J_{\rm bare}^{\rm b}$). Then, simple scaling shows that backward scattering becomes relevant prior to forward scattering. The scattering will remain anisotropic and the strength of the anisotropy is dictated by the inital conditions (J_z versus $J_\perp$ at the beginning of the flow).

Weak, short range, spin dependent electron–electron interactions do not change the picture and backscattering dominates, provided that $|K_{\rm s} - 1| < |K_{\rm c} - 1|$. However, if the spin dependent electron–electron interactions are attractive (repulsive), they will drive the flow towards dominantly spin-flip (spin-conserving) backscattering.

Thus, we conclude that the gap physics dominates if there is a weak, repulsive, spin-independent electron–electron interaction. From now on, we consider this regime and neglect $J^{\rm f}$. We note that it is well-known that for large spins the Kondo-temperature is small [36]. Thus, for sufficiently large spins we can conclude without an explicit RG analysis that the gap physics will dominate.

4. Effects of backward scattering

We now focus on effects generated by backscattering. If the spin configuration is fixed, the backscattering terms act like mass terms for the fermions. This modifies the dispersion relations, as shown in figure 3. The ground state energy of single component massive fermions with mass m differs from that of gapless fermions by

$$\Delta E = -\frac{\xi_0}{2\pi v_{\rm F}} m^2 \ln(t/|m|) + \mathcal{O}(m^2). \tag{18}$$

To minimize the ground state energy, one thus has to maximize the gaps. Depending on the relative values of J^z and $J^\perp$ this leads to different ground state spin configurations and different physics.

4.1. EA anisotropy, $J_z \gg J_\perp$

Let us consider $J_z \gg J_\perp$. It is convenient to remove the phases α and ψ from the interaction equation (14). This can be done by the transformation of the fermion fields

$$R_\uparrow \to {\rm e}^{-{\rm i}\psi/2-{\rm i}\alpha/2}R_\uparrow,\quad R_\downarrow \to {\rm e}^{{\rm i}\psi/2-{\rm i}\alpha/2}R_\downarrow,\quad L_\uparrow \to {\rm e}^{-{\rm i}\psi/2+{\rm i}\alpha/2}L_\uparrow,\quad L_\downarrow \to {\rm e}^{{\rm i}\psi/2+{\rm i}\alpha/2}L_\downarrow, \tag{19}$$

which is anomalous. The anomaly is the well-known Tomonaga–Luttinger anomaly; its contribution to the Lagrangian is [37]

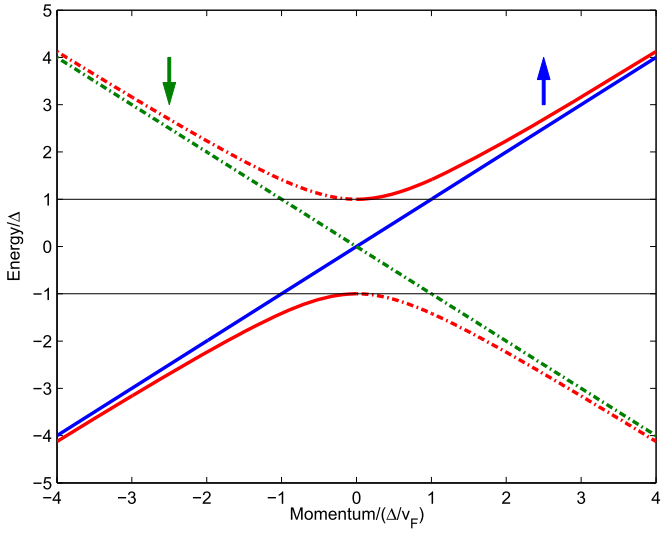

Figure 3. The dispersion of helical modes. Blue and green lines correspond to particles and holes of the first helical sector. For helical particles the direction is in one-to-one correspondes with their spin. Upon opening a gap Δ, the dispersion changes to the red curve.

$$\sum_{\sqrt{2}\Phi=\alpha,\psi} \mathcal{L}_{\mathrm{TL}}[\Phi, v_{\mathrm{F}}] = \sum_{\sqrt{2}\Phi=\alpha,\psi} \frac{1}{2\pi v_{\mathrm{F}}}[(\partial_\tau \Phi)^2 + (v_{\mathrm{F}}\partial_x \Phi)^2]. \tag{20}$$

This result may also be obtained from Abelian bosonization [38] (see the appendix C)[4]. We have neglected coupling between the charge (spin) density and the field α (ψ). This mixing is generically of the form

$$\mathcal{L}_{\mathrm{mixing}} \sim \mathrm{i}\partial_\tau \alpha(\rho_L - \rho_R)_{\mathrm{c}} + u\partial_x \alpha(\rho_L + \rho_R)_{\mathrm{c}} + \mathrm{i}\partial_\tau \psi(\rho_L + \rho_R)_{\mathrm{s}} + u\partial_x \psi(\rho_L - \rho_R)_{\mathrm{s}}, \tag{21}$$

where ρ_r stands for a density of left-/right-moving ($r = L$ and $r = R$) electrons and u is their velocity. Once the electrons become gapped, the low-energy degrees of freedom cannot excite density fluctuations. With this accuracy, in the low energy theory we can neglect derivatives of the electron densities.

The full Lagrangian is thus

$$\mathcal{L}^{(\mathrm{sl})} \simeq \mathcal{L}_{\mathrm{e}} + \mathcal{L}^{(\mathrm{sl})}_{\mathrm{int}}|_{\alpha,\psi=0} + \sum_{\sqrt{2}\Phi=\alpha,\psi} \mathcal{L}_{\mathrm{TL}}(\Phi, v_{\mathrm{F}}) + \mathcal{L}_{\mathrm{WZ}}; \tag{22}$$

Here $\mathcal{L}^{(\mathrm{sl})}_{\mathrm{int}}$ is only the backward scattering part $\mathcal{L}^{(\mathrm{sl,bs})}_{\mathrm{int}}$, equation (14). After the transformation equation (19), the sources now couple to the phases Φ_{c} and Θ_{s} and the angles

$$\mathcal{L}_{\mathrm{source}} = -\frac{h_{\mathrm{c}}}{\pi}\partial_x \alpha - \frac{h_{\mathrm{s}}}{\pi}\partial_x \psi - \frac{\sqrt{2}\,h_{\mathrm{c}}}{\pi}\partial_x \Phi_{\mathrm{c}} + \frac{\sqrt{2}\,h_{\mathrm{s}}}{\pi}\partial_x \Theta_{\mathrm{s}}. \tag{23}$$

$\mathcal{L}^{(\mathrm{sl})}_{\mathrm{int}}$ in equation (22) is a mass term. The masses for fixed spin variables are given by

$$m_{\pm}^2 = \frac{(s\cos\alpha_{\parallel}\rho_{\mathrm{s}})^2}{4}\left(\sqrt{(J_{\perp}^{\mathrm{b}})^2\cos^2\theta + (J_z^{\mathrm{b}})^2\sin^2\theta} \pm J_{\perp}^{\mathrm{b}}\right)^2. \tag{24}$$

In the case of $J_z \gg J_\perp$ the gap is always large (of order J_z) and it is maximized for $\theta = \pi/2$ and $\alpha_{\parallel} = 0$.

Since all fermions are gapped we may neglect their coupling to external sources, provided we restrict ourselves to energies below the gap. We now integrate out the fermions under this assumption, i.e. we will consider correlation functions on length scales larger than the coherence length v_{F}/m. Since the original normalization of the path integral was with respect to gapless fermions, the effective Lagrangian is now changed by the fermionic ground state energy equation (18). The total Lagrangian reads as

$$\mathcal{L}^{(\mathrm{sl})} \simeq -\frac{\Delta E}{\xi_0} + \sum_{\sqrt{2}\Phi=\alpha,\psi} \mathcal{L}_{\mathrm{TL}}(\Phi, v_{\mathrm{F}}) + \mathcal{L}_{\mathrm{WZ}}, \tag{25}$$

where we also have assumed that fluctations of the angles θ and $\alpha_{\parallel}$ are small, such that the angles are close to their ground state values. ΔE is a function of the angles, see equations (18) and (24). Expanding equation (25) in $\theta' = \theta - \pi/2$ and $\alpha_{\parallel}$, we obtain

[4] We use the conventions from [39].

$$\mathcal{L}^{(\mathrm{sl})}_{(\mathrm{ea})} = \sum_{\sqrt{2}\,\Phi=\alpha,\psi} \mathcal{L}_{\mathrm{TL}}(\Phi,\, v_{\mathrm{F}}) + \underbrace{a\{[(J^{\mathrm{b}}_z)^2 - (J^{\mathrm{b}}_\perp)^2](\theta')^2 + [(J^{\mathrm{b}}_z)^2 + (J^{\mathrm{b}}_\perp)^2](\alpha_\parallel)^2\}}_{\mathcal{L}_{\mathrm{gs}}} + \mathrm{i}s\rho_{\mathrm{s}}\xi_0^{-1}\alpha_\parallel(\partial_\tau\alpha), \tag{26}$$

where $a = \log(t/J)(s\rho_{\mathrm{s}})^2/4\pi v_{\mathrm{F}}$, and we do not distinguish between the J's in the log. We will further assume for now that $\partial_\tau\psi$ is small, such that the cross-term $\alpha_\parallel\theta'\partial_\tau\psi$ is a higher order contribution. This will be verified below. $\mathcal{L}_{\mathrm{gs}}$ in equation (26) is the mass term for θ' and $\alpha_\parallel$, which shows that the assumption of small θ' and $\alpha_\parallel$ is consistent.

Now we perform the integrals over $\alpha_\parallel$ and θ' and obtain

$$\mathcal{L}^{(\mathrm{sl})}_{(\mathrm{ea})} = \sum_{\sqrt{2}\,\Phi=\alpha,\psi} \mathcal{L}_{\mathrm{TL}}(\Phi,\, v_{\mathrm{F}}) + \frac{(s\rho_{\mathrm{s}}\xi_0^{-1})^2}{4a((J^{\mathrm{b}}_z)^2 + (J^{\mathrm{b}}_\perp)^2)}(\partial_\tau\alpha)^2. \tag{27}$$

Note that ψ and α remain gapless, justifying the previous approximation of small $\partial_\tau\psi$. Thus, two angular modes are fast (θ and $\alpha_\parallel$) and two are slow (α and ψ), as we expected.

Equation (27) is the action of two $U(1)$-symmetric Luttinger liquids with a charge mode, α, and a spin mode, ψ

$$\mathcal{L}_{\mathrm{ea}} = \frac{1}{2}\mathcal{L}_{\mathrm{TL}}(\psi,\, v_{\mathrm{F}}) + \frac{1}{K_\alpha}\mathcal{L}_{\mathrm{TL}}(\alpha,\, v_\alpha). \tag{28}$$

The two phases couple to different sources: α to charges and ψ to spins. The slow mode α has a renormalized velocity and Luttinger parameter

$$\frac{v_\alpha}{v_{\mathrm{F}}} = \frac{K_\alpha}{2} \simeq \xi_0\frac{\sqrt{J_z^2 + J_\perp^2}}{\pi v_{\mathrm{F}}}\sqrt{\log(t/J)} \ll 1, \tag{29}$$

where we used that the band width is the largest energy scale (i.e. $v_{\mathrm{F}}/\xi_0 \gg J$) in the last inequality. This severly affects the charge transport, which is mediated by α.

4.2. Breaking the $\mathbb{Z}_2$ symmetry

We have demonstrated that for $J_z \gg J_\perp$, all fermionic modes have approximately the same gap $\sim J_z$. Approaching the $SU(2)$ symmtric point, the mass m_- shrinks until it would reach zero at $J_z = J_\perp$. In terms of the EA picture, some fermions (two helical modes) become light and their contribution encompasses large fluctuations on top of their ground state energy. We explicitely assumed that the fluctuations around the ground state are small. Therefore, our approach is no longer valid for $m_- \to 0$.

For now, let us consider the other limit $J_z \ll J_\perp$. We will see that this parameter regime behaves in a way qualitatively different to $J_z \gg J_\perp$. The order parameter distinguishing the phases is discussed in section 6. The vanishing of the gap for $J_z \to J_\perp$, the spontaneous symmetry breaking for $J_z \ll J_\perp$ and the presence of an order parameter all strongly suggest the presence of a quantum phase transition, although its theoretical description is missing.

4.3. EP anisotropy, $J_z \ll J_\perp$

Let us put for simplicity $J_z \to 0$. Then, it is convenient to express equation (14) through helical modes

$$\mathcal{L}^{(h_1)}_{\mathrm{bs}} = s\cos\alpha_\parallel\rho_{\mathrm{s}}[J_\perp R^\dagger_\uparrow \cos^2(\theta/2)\mathrm{e}^{-\mathrm{i}(\psi+\alpha)}L_\downarrow + \mathrm{h.c.}], \tag{30}$$

$$\mathcal{L}^{(h_2)}_{\mathrm{bs}} = -s\cos\alpha_\parallel\rho_{\mathrm{s}}[J_\perp R^\dagger_\downarrow \sin^2(\theta/2)\mathrm{e}^{\mathrm{i}(\psi-\alpha)}L_\uparrow + \mathrm{h.c.}]. \tag{31}$$

Clearly, the interesting points are $\theta = 0,\ \pi$ and $\theta = \pi/2$. If $\theta = \pi/2$, then the effective $J_\perp$ is reduced by a factor of $\cos^2\pi/4 = \sin^2\pi/4 = \frac{1}{2}$ relative to the effective $J_\perp$ of a single gapped helical sector at $\theta = 0,\ \pi$. Since the ground state energy equation (18) of a helical sectors with the gap m_i is

$$\Delta E_{\mathrm{hel}} = -\frac{\xi_0}{2\pi v_{\mathrm{F}}}m_i^2\ln(t/|m_i|) + \mathcal{O}(m_i^2), \quad m_i \sim J_\perp, \tag{32}$$

the ground state of a single gapped sector of twice the mass has a lower energy than that of two equally gapped helical sectors. Thus, it is energetically favorable to spontaneously break the $\mathbb{Z}_2$ symmetry between different helical sectors. The two ground states are labelled by $\theta = 0$ and $\theta = \pi$.

Let us choose $\theta = 0$. Then, the first helical sector equation (30) becomes gapped, while the second sector equation (31) is gapless. Now, the angle $\alpha - \psi$ does not enter the action if fluctuations of θ are set to zero. It enters (in the leading order in θ) only via the combination

$$\mathcal{L} \supset \underbrace{-s\cos\alpha_\parallel\rho_{\mathrm{s}}J_\perp\frac{\theta^2}{4}\mathrm{e}^{-\mathrm{i}(\alpha-\psi)}R^\dagger_\downarrow L_\uparrow + \mathrm{h.c.}}_{\mathcal{L}^{(H2)}_{\mathrm{bs}}} + \underbrace{\mathrm{i}s\rho_{\mathrm{s}}\xi_0^{-1}\sin(\alpha_\parallel)\frac{\theta^2}{2}\partial_\tau\alpha}_{\mathcal{L}^{\mathrm{slow}}_{\mathrm{WZ}}}. \tag{33}$$

The last summand is (for $\alpha_\parallel \approx 0$) beyond our accuracy and will be neglected. The influence of the first two summands may be estimated by integrating over $R_\downarrow$ and $L_\uparrow$. The resulting expression is

$$\mathcal{L} \supset \mathrm{Tr}\log\left[\begin{pmatrix} \mathrm{i}\omega + v_\mathrm{F}k & 0 \\ 0 & \mathrm{i}\omega - v_\mathrm{F}k \end{pmatrix}^{-1}\begin{pmatrix} \mathrm{i}\omega + v_\mathrm{F}k & s\cos\alpha_\parallel\rho_\mathrm{s}J_\perp\frac{\theta^2}{4}\mathrm{e}^{-\mathrm{i}(\alpha-\psi)} \\ s\cos\alpha_\parallel\rho_\mathrm{s}J_\perp\frac{\theta^2}{4}\mathrm{e}^{\mathrm{i}(\alpha-\psi)} & \mathrm{i}\omega - v_\mathrm{F}k \end{pmatrix}\right]. \tag{34}$$

The off-diagonal parts will enter only starting at the second order of the expansion of the log, thus $\alpha - \psi$ only enters with a prefactor of $J_\perp^2\theta^4$, which is smaller than our accuracy and has to be neglected. Under this assumption, the angle α can be shifted to $\alpha - \psi$, thus eliminating one angular variable, as the Wess–Zumino term equation (8) also depends only on $\alpha + \psi$ to leading order in θ and $\alpha_\parallel$. It is easiest to eliminate α by bosonizing the modes coupled to the spins, and shifting[5]

$$\Theta_\mathrm{s} \to \Theta_\mathrm{s} - \sqrt{2}\,\alpha/4, \quad \Phi_\mathrm{c} \to \Phi_\mathrm{c} + \sqrt{2}\,\alpha/4. \tag{35}$$

The shift needs to be in both spin and charge sectors such that all charge conserving fermionic bilinears of the gapless sector remain unaffected. This is a consequence of the helical nature of the sectors and means that α will couple to both spin and charge sources:

$$\mathcal{L}_\mathrm{source} \supset -\frac{h_\mathrm{c}}{2\pi}\partial_x\alpha - \frac{h_\mathrm{s}}{2\pi}\partial_x\alpha, \tag{36}$$

where we did not write the coupling of the sources to the fermions. Next, we integrate out the gapped helical sector. The ground state energy contribution from this is

$$\Delta E = -\frac{\xi_0}{2\pi v_\mathrm{F}}m^2\ln(t/|m|) + \mathcal{O}(m^2), \tag{37}$$

where $m^2 = \frac{1}{2}\left(s\rho_\mathrm{s}\cos\alpha_\parallel\cos\frac{\theta}{2}J_\perp\right)^2$. The ground state energy equation (37) is minimized for $\alpha_\parallel = 0$ (we remind that $\theta \approx 0$). We expand ΔE to second order in $\alpha_\parallel$ and θ and obtain

$$\Delta E \approx -(s\rho_\mathrm{s})^2\frac{\xi_0}{4\pi v_\mathrm{F}}\log(t/J_\perp)J_\perp^2[(\theta/2)^2 + (\alpha_\parallel)^2]. \tag{38}$$

Thus, θ and $\alpha_\parallel$ are high-energy modes, which confirms the consistency of our approach in the EP phase. We can integrate out the fast variables and obtain

$$\mathcal{L}_\mathrm{ep} = R_\downarrow^\dagger G_R^{-1}R_\downarrow + L_\uparrow^\dagger G_L^{-1}L_\uparrow + \frac{1}{K'_\alpha}\mathcal{L}_\mathrm{TL}(\alpha, v'_\alpha), \tag{39}$$

where

$$\frac{v'_\alpha}{v_\mathrm{F}} = \frac{K'_\alpha}{4} = \frac{\xi_0 J_\perp}{2\pi v_\mathrm{F}}\sqrt{\log(t/J_\perp)} \ll 1, \tag{40}$$

and $G_{R/L}^{-1} = \partial_\tau \mp \mathrm{i}v_\mathrm{F}\partial_x$ is the inverse Green's function of free helical fermions. Upon bosonization, the gapless helical fermions become a helical Luttinger liquid:

$$\mathcal{L} = \mathcal{L}_\mathrm{TL}(\Phi^{H1}, v_\mathrm{F}) + \frac{1}{K'_\alpha}\mathcal{L}_\mathrm{TL}(\alpha, v_\alpha). \tag{41}$$

Thus, the low energy physics is described by two $U(1)$ Luttinger liquids, just as in the EA case. However, the Luttinger liquids are now helical modes and they differ from the EA case in the way they couple to external sources (see equation (36)).

4.4. The effects of electron interactions

In the discussion of the EA and EP cases, we have neglected the effects of electron interactions. However, we used interactions to find the regime where the gap physics dominates Kondo physics. To fill this gap, we investigate the effects of interactions on the results of sections 4.1 and 4.3.

In the presence of interactions, K_s and/or K_c acquire values different from one. This changes the effect of the transformation equation (19) in the EA case. These transformations now induce terms of the form

$$\mathcal{L} \supset \frac{1}{2\sqrt{2}\,\pi}\left(\frac{u_\mathrm{c}}{K_\mathrm{c}}\partial_x\alpha\partial_x\Phi_\mathrm{c} - u_\mathrm{s}K_\mathrm{s}\partial_x\psi\partial_x\Theta_\mathrm{s}\right). \tag{42}$$

Since all the fermions become massive, these terms may be dropped (see discussion following equation (21)). The other effect of interactions is a renormalization of the gap m (equation (24)). This is simply a renormalization of the parameters appearing in equation (26), which we will neglect for now.

[5] The same may be done in the EA case, as explained in appendix C.

In the EP case, the situation is different, because one helical branch remains gapless. If $K_s \neq 1/K_c$, the Luttinger parameter and the velocity of a helical sector (e.g. $R_\downarrow$ and $L_\uparrow$ as one sector) are changed to

$$\tilde{K} = \sqrt{\frac{u_c K_c + \frac{u_s}{K_s}}{\frac{u_c}{K_c} + u_s K_s}}, \quad \tilde{u} = \frac{1}{2}\sqrt{u_c^2 + u_s^2 + u_c u_s K_c K_s + \frac{u_c u_s}{K_c K_s}}, \tag{43}$$

yielding the free part of the Lagrangian

$$\mathcal{L}_{h_i} = -\frac{\mathrm{i}}{\pi}\partial_x \Theta_{h_i}\partial_\tau \Phi_{h_i} + \frac{1}{2\pi}\left(\tilde{u}\tilde{K}(\partial_x \Theta_{h_i})^2 + \frac{\tilde{u}}{\tilde{K}}(\partial_x \Phi_{h_i})^2\right). \tag{44}$$

Here, Φ_{h_i} is the bosonic field belonging to a given helical sector. The helical sectors h_1 (consisting of $R_\uparrow$ and $L_\downarrow$) and h_2 (consisting of $R_\downarrow$ and $L_\uparrow$) couple as

$$\mathcal{L}_{h-h} = \frac{1}{2\pi}\left\{\left(u_c K_c - \frac{u_s}{K_s}\right)(\partial_x \Theta_{h_2}\partial_x \Theta_{h_1}) + \left(\frac{u_c}{K_c} - u_s K_s\right)(\partial_x \Phi_{h_2}\partial_x \Phi_{h_1})\right\} \tag{45}$$

The transformation equation (35) thus adds to the Lagrangian the new part

$$\delta\mathcal{L} = \frac{1}{4\pi}\left(\frac{u_c}{K_c} - u_s K_s\right)(\partial_x \Phi_{h_2}\partial_x \alpha) + \mathcal{O}(\partial\alpha\partial\Phi_{h_1}, \partial\alpha\partial\Theta_{h_1}), \tag{46}$$

where Φ_{h_2} is the bosonic field belonging to the gapless (helical) fermionic modes. Dropping once more couplings of the derivative of the density of a gapped fermion (from the first helical sector) to gapless modes, the total low-energy Lagrangian $\mathcal{L}_{ep}$ from equation (39) is modified only by $\delta\mathcal{L}$ in equation (46)[6]:

$$\mathcal{L}_{ep}^{int} = \mathcal{L}_{h_2} + \frac{1}{K'_\alpha}\mathcal{L}_{TL}(\alpha, v'_\alpha) + \delta\mathcal{L}. \tag{47}$$

This expression can be analyzed by rediagonalizing it in field space. To do so, first integrate out Θ_{h_2}. This yields

$$\mathcal{L}_{ep}^{int} = \frac{1}{2\pi}\frac{1}{\tilde{u}\tilde{K}}(\partial_\tau \Phi_{h_2})^2 + \frac{1}{2\pi}\frac{\tilde{u}}{\tilde{K}}(\partial_x \Phi_{h_2})^2 + \frac{1}{2\pi}\left(\frac{1}{K'_\alpha}(\partial_\tau \alpha)^2 + \frac{1}{K'_\alpha}(v'_\alpha \partial_x \alpha)^2\right) + \frac{1}{4\pi}\left(\frac{u_c}{K_c} - u_s K_s\right)\partial_x \alpha \partial_x \Phi_{h_2}. \tag{48}$$

Next, we redefine the fields α and Φ_{h_2} such that the temporal derivatives have the same prefactor:

$$\alpha \to \sqrt{K'_\alpha}\,\alpha, \quad \Phi_{h_2} \to \sqrt{\tilde{u}\tilde{K}}\,\Phi_{h_2}. \tag{49}$$

This leads to

$$\mathcal{L}_{ep}^{int} = \frac{1}{2\pi}(\partial_\tau \Phi_{h_2})^2 + \frac{1}{2\pi}\tilde{u}^2(\partial_x \Phi_{h_2})^2 + \frac{1}{2\pi}(\partial_\tau \alpha)^2 + \frac{1}{2\pi}(v'_\alpha \partial_x \alpha)^2 + \delta\partial_x \alpha \partial_x \Phi_{h_2}, \tag{50}$$

where we have defined $\delta = \frac{1}{2\pi}\sqrt{\tilde{u}\tilde{K}K'_\alpha}\left(\frac{u_c}{K_c} - u_s K_s\right)$. Diagonalizing this leads to two new gapless particles with dispersion

$$\omega^2 = \tfrac{1}{2}(\tilde{u}^2 + v_\alpha^2 \pm \sqrt{(\tilde{u}^2 + v_\alpha^2)^2 + 4\delta^2})k^2. \tag{51}$$

Note that the remaining two degrees of freedom remain gapless. Interactions thus destroy the purely helical nature of low-energy excitations, but they cannot gap these exctiations.

4.5. Suppression of forward scattering

We have seen that dominant backscattering leads to a vacuum structure where $\alpha_\parallel \approx 0$. The forward scattering terms however are proportional to $\sin \alpha_\parallel$, equation (15). This confirms the suppression of their contribution once the gap is opened and examplifies our previous claim that Kondo physics and the gap physics are mutually exclusive.

5. Density–density correlation functions and disorder

5.1. Density–density correlation functions

We have shown that both the cases of EA and EP anistropy are described by two $U(1)$ Lutttinger liquids. However, the fields have different physical meaning as evinced by their coupling to external source. Their

[6] And a new effective Luttinger parameter and velocity, see equation (43).

difference can be seen from various correlation functions. Let us at first consider the density–density correlation function

$$\mathcal{C} = \langle \rho_c(1)\rho_c(2)\rangle = \frac{\delta^2 \log Z[h_c]}{\delta h_c(1)\delta h_c(2)}|_{h_c=0}, \tag{52}$$

where ρ_c is the electron density and $Z[h_c]$ is the generating functional in the presence of the source h_c. In general, there are several contributions to $\mathcal{C}$, including those from gapped and gapless excitations. Even if the fermionic modes become gapped, there still is a contribution from collective electron and spin modes to long range density–density correlation functions. This can be seen from the fact that some low energy degrees of freedom (EA: α; EP α and one helical fermion) couple to h_c. In Fourier space, the correlation functions are

$$\mathcal{C}_{ea}(\omega, q) = \left(\frac{q}{\pi}\right)^2 \langle \alpha^*\alpha\rangle, \tag{53}$$

$$\mathcal{C}_{ep}(\omega, q) = \left(\frac{q}{\pi}\right)^2 (\langle \Phi_H^*\Phi_H\rangle + \langle \alpha^*\alpha\rangle/4). \tag{54}$$

Using the corresponding low energy effective actions equations (28) and (39), this yields

$$\mathcal{C}_{ea}(\omega, q) = \frac{q^2 K_\alpha v_\alpha^2 \xi_0^{-2}}{\pi(\omega^2 + (v_\alpha q)^2)}, \tag{55}$$

$$\mathcal{C}_{ep}(\omega, q) = \frac{q^2}{\pi}\left(\frac{v_F^2\xi_0^{-2}}{\omega^2 + (v_F q)^2} + \frac{1}{4}\frac{K'_\alpha v'^2_\alpha \xi_0^{-2}}{\omega^2 + (v'_\alpha q)^2}\right). \tag{56}$$

Equations (55) and (56) correspond to ideal metallic transport. The small Luttinger parameter of the bosonic modes (K_α, $K'_\alpha \ll 1$) reflects the coupling of the spin waves to the gapped fermions and leads to a reduced Drude weight [33].

5.2. The role of potential disorder

Let us investigate how potential disorder affects charge transport. We add a weak random potential

$$V_{dis} = g(x)\Psi^\dagger(I \otimes \tau^+)\Psi + \text{h.c.}, \tag{57}$$

where $g(x)$ is the smooth $2k_F$ component of the scalar random potential. Note that we have dropped quickly oscillating modes, just as for the spin impurities. If the disorder itself is distributed according to the Gaussion orthogonal ensemble, then its $2k_F$ component has a Gaussian unitary distribution. Thus the function g is drawn from a Gaussian unitary ensemble (GUE). We use $\langle g(x)\rangle = 0$ and $\langle g^*(x)g(y)\rangle = 2\mathcal{D}\delta(x-y)$. We assume that the potential disorder is sufficiently weak, such that it does not influence the high energy physics. The precise meaning of this statement will be specified later.

As first step, we integrate the disorder exactly by using the replica trick. Upon disorder-averaging we obtain

$$S_{dis} = \sum_{i,j}\int dx \int d\{\tau_{1,2}\}\mathcal{D}[(R^\dagger_{\uparrow i}L_{\uparrow i} + (\uparrow \leftrightarrow \downarrow))(x,\tau_1)(L^\dagger_{\uparrow j}R_{\uparrow j} + (\uparrow \leftrightarrow \downarrow))(x,\tau_2)], \tag{58}$$

where i, j are replica indices. The remainder of the action is diagonal in replica space.

To understand the effect of S_{dis} on transport we now have to integrate out the massive modes. Recall that this involves first a shift of the fermionic fields (equation (19))[7]:

$$S_{dis} = \int dx \int d\{\tau_{1,2}\}\mathcal{D}[(R^\dagger_{\uparrow i}L_{\uparrow i}e^{i\alpha_i} + (\uparrow \leftrightarrow \downarrow))(x,\tau_1)(L^\dagger_{\uparrow j}R_{\uparrow j}e^{-i\alpha_j} + (\uparrow \leftrightarrow \downarrow))(x,\tau_2)], \tag{59}$$

where the gapped and gapless modes now are cleanly separated in the rest of the action (with our accuracy). Thus, it is easy to integrate out the gapped modes. We treat S_{dis} perturbatively, obtaining an expansion in the parameter $\frac{\mathcal{D}}{v_F m} \ll 1$ (weak disorder).

In the EA case, all fermions are gapped and the only gapless mode appearing in $\mathcal{L}_{dis}$ is the charge mode α. In the EP case only the fermions with a given helicity (e.g. $R_\uparrow$ and $L_\downarrow$) become gapped and the disorder mixes the two helical Luttinger liquids (α and the fermions of the non-gapped helicity). It is convenient to treat EA and EP separately.

5.2.1. Easy axis

We start with the EA case, and put $J_\perp = 0$. For transparency, we choose the fermionic spin-dependent mass $m_{ea}(\uparrow/\downarrow) = \pm m$. The matrix Green's function for the fermions with a given spin reads:

[7] In EP, the shift leads to the same result after absorbing ψ in α.

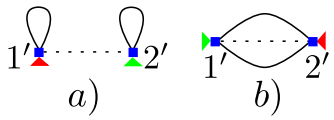

Figure 4. First order diagrams $O(\mathcal{D}^1)$ for the EA phase. Red (green) triangles denote $e^{i\alpha/2}$ ($e^{-i\alpha/2}$) with arguments of either the 1st or the 2nd vertex; dashed lines are the disorder correlation functions, solid lines stand for Green's functions of the massive fermions.

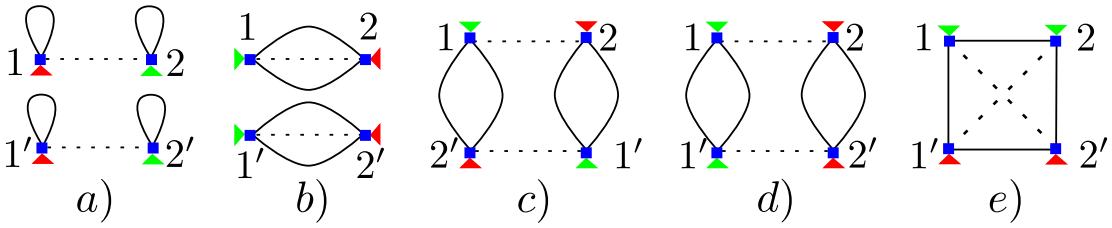

Figure 5. A relevant subset of the EA diagrams. Notations are explained in the caption of figure 4. (a) and (b) Class (ii), diconnected contributions. (c) Class (iii), red and green triangles are merged through a massive propagator. (d) Class (iv), we omit the diagram with crossed disorder lines. (e) Class (v), we omit the diagram with non-crossed disorder lines. Note that green and red triangles are connected by a massive propagator.

$$\hat{G}_m(\sigma) = ((G_R^{(0)})^{-1}(G_L^{(0)})^{-1} - m_{\rm ea}(\sigma)^2)^{-1}\begin{pmatrix} (G_L^{(0)})^{-1} & -m_{\rm ea}(\sigma) \\ -m_{\rm ea}(\sigma) & (G_R^{(0)})^{-1} \end{pmatrix}; \tag{60}$$

where $G_{R,L}^{(0)}$ are the Green's functions of free chiral particles. It is important that $\hat{G}_m$ is short ranged and it decays beyond the time scale $1/m_{\rm ea}$ (or beyond the coherence length $\xi_{\rm ea} \equiv v_f/m_{\rm ea}$). This implies in particular that two slow operators connected by a massive propagator form a single local operator on length- and timescales large compared to the inverse gap.

Leading terms are given by $\langle S_{\rm dis}\rangle_m$ where brackets mean that the massive fermions are integrated out. The corresponding diagrams are shown in figure 4. It is easy to check that the diagrams from figure 4(a) cancel out after summation over spin indices because $m_{\rm ea}(\uparrow) = -m_{\rm ea}(\downarrow)$. The diagrams from figure 4(b) are trivial since $\hat{G}_m$ is diagonal in the replica space and the spin phase α is smooth on the scale $1/m_{\rm ea}$; therefore

$$e^{i\alpha[1]}e^{-i\alpha[2]} \simeq e^{i\alpha[1]-i\alpha[1]} = 1, \tag{61}$$

with some small gradient corrections which are unable to yield pinning. Here we denoted $\alpha[j] \coloneqq \alpha(x_1, \tau_1)$.

Sub-leading terms of the order of $\frac{\mathcal{D}^2}{v_F m}$ are given by $\langle S_{\rm dis}S_{\rm dis}\rangle$. To be explicit, we need to compute

$$\begin{aligned}\langle S_{\rm dis}S_{\rm dis}\rangle_{\rm EA} = \mathcal{D}^2\Big\langle \int {\rm d}\{x, x'; \tau_{1,2}, \tau'_{1,2}\} \\ \times [(R^\dagger_{\uparrow i}L_{\uparrow i}e^{i\alpha_i} + (\uparrow \leftrightarrow \downarrow))(x,\tau_1)(L^\dagger_{\uparrow j}R_{\uparrow j}e^{-i\alpha_j} + (\uparrow \leftrightarrow \downarrow))(x,\tau_2)] \\ \times [(R^\dagger_{\uparrow k}L_{\uparrow k}e^{i\alpha_k} + (\uparrow \leftrightarrow \downarrow))(x',\tau'_1)(L^\dagger_{\uparrow l}R_{\uparrow l}e^{-i\alpha_l} + (\uparrow \leftrightarrow \downarrow))(x',\tau'_2)]\Big\rangle_{\rm EA}.\end{aligned} \tag{62}$$

In order to pin the CDW (the field α), an operator evaluating α at different times (i.e. times further apart than $1/m_{\rm ea}$) has to survive. The correlation function $\langle S_{\rm dis}S_{\rm dis}\rangle_{\rm EA}$ contains various possible contractions, most of which are unable to generate pinning:

(i) Contractions involving two fermionic creation or annihilation operators: they vanish due to the structure of the fermionic Green's function, which does not allow for propagation of Cooper pairs.

(ii) Contractions which simplify to two copies of the first order contribution (see figures 5(a), (b)): they do not generate backscattering, as shown above.

(iii) Contractions of fermions at (x, τ_1) with fermions at (x', τ'_2) and of fermions at (x, τ_2) with fermions at (x', τ'_1), with no contractions between (x, τ_1) and (x', τ'_1) (figure 5(c)): in these contractions—due to the short range nature of the fermions' Green'(s) functions—$e^{i\alpha}$ fuses with $e^{-i\alpha}$ at the same position and time (at an accuracy of $1/m$), and thus generate only derivatives of α, which are unable to pin the CDW.

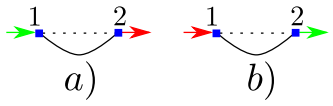

Figure 6. Two typical examples of first order diagrams $O(\mathcal{D}^1)$ for the EP phase. Red (green) arrows denote the product of smooth fields L, R with $e^{i\alpha/2}$ ($e^{-i\alpha/2}$). The smooth fields L, R are taken from the non-gapped helical sector.

(iv) Contractions of fermions at (x, τ_1) with fermions at (x', τ_1') and of fermions at (x, τ_2) with fermions at (x', τ_2'), with no contractions between (x, τ_1) and (x', τ_2') (figure 5(d)): these contractions all give the same result and are able to generate pinning.

(v) Contractions between all positions and times (figure 5(e)): this sets all positions and times (and replica indices) of the CDW equal to each other (with accuracy $1/m$), such that again only derivatives of the field α survive.

We calculate only one typical diagram which survives after all summations and is able to generate pinning (type (iv)). An example of such a diagram is shown in figure 5(d). All other diagrams of class (iv) yield identical results. The sign of the mass does not matter as there is an even number of propagators for each species.

Neglecting unimportant numerical factors, the analytical expression for the diagram from figure 5(d) reads as:

$$D_{\mathrm{ea}}^{(2)} \propto \mathcal{D}^2 \sum_{i,j} \int \mathrm{d}\{x, x'; \tau_{1,2}, \tau_{1,2}'\}\, e^{2i(\alpha_i[\mathbf{1}]-\alpha_j[\mathbf{2}])} [\hat{G}_m(\mathbf{1}, \mathbf{1}')]_{1,2} \times [\hat{G}_m(\mathbf{1}', \mathbf{1})]_{1,2} [\hat{G}_m(\mathbf{2}, \mathbf{2}')]_{1,2} [\hat{G}_m(\mathbf{2}', \mathbf{2})]_{1,2}. \tag{63}$$

Here, we have taken into account that the diagonal structure of $\hat{G}_m$ results in $i = k$; $j = l$ and fused together slow spin phases, for instance: $\alpha[\mathbf{1}] + \alpha[\mathbf{1}'] \simeq 2\alpha[\mathbf{1}]$. Now we note that $\hat{G}_m(\mathbf{1}, \mathbf{1}') = \hat{G}_m(\mathbf{1} - \mathbf{1}')$ and integrate over all primed variables:

$$D_{\mathrm{ea}}^{(2)} \propto \frac{\tilde{\mathcal{D}}_0}{\xi_{\mathrm{ea}}^2} \sum_{i,j} \int \mathrm{d}\{x; \tau_{1,2}\}\, e^{i(\alpha_i[\mathbf{1}]-\alpha_j[\mathbf{2}])}; \quad \tilde{\mathcal{D}}_0 \equiv \mathcal{D}\left(\frac{\mathcal{D}}{v_{\mathrm{F}} m_{\mathrm{ea}}}\right). \tag{64}$$

The structure of equation (64) corresponds to the non-local Sine-Gordon model which appears in the theory of the usual disordered TLL [39]. The effective disorder strength $\tilde{\mathcal{D}}$ is renormalized and obeys the well-known RG equation [40]:

$$\mathrm{EA}: \partial_{\log} \log(\tilde{\mathcal{D}}) = 3 - 2K_\alpha \simeq 3, \quad \tilde{\mathcal{D}}(\xi_{\mathrm{ea}}) = \tilde{\mathcal{D}}_0; \tag{65}$$

the second equality of equation (65) has been obtained by using equation (29).

Note that the effective strength of the disorder is suppressed compared to free fermions by an additional factor of $\mathcal{D}/(v_{\mathrm{F}} m)$. However, the operator is more relevant than for free fermions, as $K_\alpha^{(\mathrm{EA})} \ll 1$.

5.2.2. Easy plane

Let us now turn to the EP case. We start again from the leading diagrams generated by $\langle S_{\mathrm{dis}} \rangle$. The principal difference of the EP phase from the EA one is that the matrix Green's function, equation (60), corresponds now to the massive fermions with a given helicity. This changes the structure of the first order diagram, see figure 6. All these diagrams correspond to forward-scattering of the massless helical fermions and they contain only small gradients of the phase α, see equation (61) and its explanation. Thus, the leading diagrams are trivial and they cannot yield localization, the sub-leading diagrams must be considered.

There are several categories of sub-leading diagrams:

(i) Contractions involving two creation or annihilation operators: they are identically zero.

(ii) Contractions which correspond to two copies of the leading diagrams (figure 7(a)): they do not lead to backscattering and cannot pin the charge transport.

(iii) Contractions of fermions at (x, τ_1) with fermions at (x', τ_2') and of fermions at (x, τ_2) with fermions at (x', τ_1'), with no contractions between (x, τ_1) and (x', τ_1') (the second part—excluding certain contractions—is trivial, as there is only one massive fermion at each vertex) (figure 7(b)): these contractions—due to the short range nature of the fermions' Green's function—combine $e^{i\alpha}$ with $e^{-i\alpha}$ at the same position and time (at an accuracy of $1/m$), and thus generate only derivatives of α, which are unable to pin the CDW.

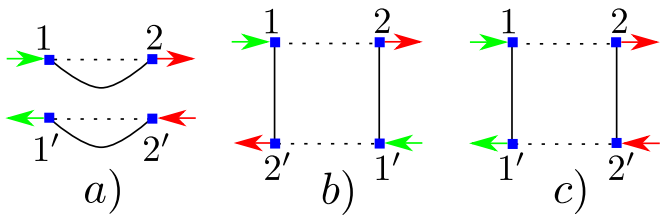

Figure 7. A relevant subset of the EP diagrams. Notations are explained in the caption of figure 6. (a) Class (ii), diconnected contributions. (b) Class (iii), red and green arrows are merged through a massive propagator. We omit the diagram with crossed disorder lines. Note that green and red arrows are connected by a massive propagator. (c) Class (iv), we omit the diagram with crossed disorder lines.

(iv) Contractions of fermions at (x, τ_1) with fermions at (x', τ_1') and of fermions at (x, τ_2) with fermions at (x', τ_2'), with no contractions between (x, τ_1) and (x', τ_2') (the second condition is again trivially satisifed) (figure 7(c)). These contractions all give the same result and are able to generate pinning.

The only relevant diagrams are those of class (iv), which all yield the same result. We will compute one of these diagrams (figure 7(c)). Neglecting unimportant numerical factors, the analytical expression for the diagram from figure 7(c) reads as:

$$D_{\rm ep}^{(2)} \propto \mathcal{D}^2 \sum_{i,j} \int \mathrm{d}\{x, x'; \tau_{1,2}, \tau_{1,2}'\} \mathrm{e}^{\mathrm{i}(\alpha_i[\mathbf{1}]-\alpha_j[\mathbf{2}])} L_{\downarrow j}^\dagger[\mathbf{2}] R_{\uparrow i}^\dagger[\mathbf{1}] L_{\downarrow i}[\mathbf{1}] R_{\uparrow j}[\mathbf{2}] [\hat{G}_m(\mathbf{1}, \mathbf{1}')]_{1,2} [\hat{G}_m(\mathbf{2}, \mathbf{2}')]_{1,2}; \quad (66)$$

see explanations after equation (63) and note the m must be substituted for $m_{\rm ea}(\sigma)$ in $\hat{G}_m$. Calculating integrals over all primed variables, we find:

$$D_{\rm ep}^{(2)} \propto \bar{\mathcal{D}}_0 \sum_{i,j} \int \mathrm{d}\{x; \tau_{1,2}\} \mathrm{e}^{\mathrm{i}(\alpha_i[\mathbf{1}]-\alpha_j[\mathbf{2}])} L_{\downarrow j}^\dagger[\mathbf{2}] R_{\uparrow i}^\dagger[\mathbf{1}] L_{\downarrow i}[\mathbf{1}] R_{\uparrow j}[\mathbf{2}], \quad \bar{\mathcal{D}}_0 \equiv \mathcal{D}\left(\frac{\mathcal{D}}{v_{\rm F} m}\right). \quad (67)$$

This equation also can be reduced to the form of equation (64) if remaining fermions are bosonized and we explicitly single out new CDWs and SDWs. However, the RG equation for $\bar{\mathcal{D}}$ can be obtained without such a complicated procedure with the help of the power counting. Firstly we note that the scaling dimension of each back-scattering term in equation (67), $L^\dagger R$ and $R^\dagger L$, is 1. The anomalous dimension of each exponential, $\mathrm{e}^{\pm \mathrm{i}\alpha}$, is $K_\alpha' \ll 1$. The normal dimension in equation (67) is 3 which comes from three-fold integral. Combining these dimensions together and neglecting small K_α', we find

$$\mathrm{EP}: \partial_{\log} \log(\bar{\mathcal{D}}) = 3 - 2 \times 1 + O(K_\alpha) \simeq 1; \quad \bar{\mathcal{D}}(\xi_{\rm ep}) = \bar{\mathcal{D}}_0, \ \xi_{\rm ep} = v_{\rm F}/m. \quad (68)$$

Note that while the scaling of the disorder strength is the same as for free fermions, but the effective strength (the starting value of the flow) is reduced parametrically by a factor of $\mathcal{D}/(v_{\rm F} m) \ll 1$.

5.2.3. Localization radius

We now can find the localization radius for both phases, EA and EP. The solution of the RG equations, equations (65) and (68), reads as

$$\tilde{\mathcal{D}}(x) = \tilde{\mathcal{D}}_0 \left(\frac{x}{\xi_{\rm ea}}\right)^3, \quad \bar{\mathcal{D}}(x) = \bar{\mathcal{D}}_0 \frac{x}{\xi_{\rm ep}}; \quad (69)$$

with $\xi_{\rm ep} = v_{\rm F}/m$. The localization radius is defined as a scale on which the renormalized disorder becomes of the order of the cut-off:

$$\tilde{\mathcal{D}}(L_{\rm ea}^{\rm (loc)}) = K_\alpha v_\alpha^2/\xi_{\rm ea} \sim K_\alpha^3 v_{\rm F}^2/\xi_{\rm ea}; \quad \bar{\mathcal{D}}(L_{\rm ep}^{\rm (loc)}) = v_{\rm F}^2/\xi_{\rm ep}. \quad (70)$$

The additional small factor K_α in the equation for $L_{\rm ea}^{\rm (loc)}$ can be justified with the help of the standard optimization procedure [39] where $L^{\rm (loc)}$ is defined as a spatial scale on which the typical potential energy of the disorder becomes equal to the energy governed by the term $\propto(\partial_x \alpha)^2$ in the Lagrangian $\mathcal{L}_{\rm ea}$, equation (28).

Definitions equation (70) result in

$$L_{\rm ea}^{\rm (loc)} \sim \xi_{\rm ea} K_\alpha \left(\frac{v_{\rm F}^2}{\xi_{\rm ea} \tilde{\mathcal{D}}_0}\right)^{1/3} \sim \xi_{\rm ea} K_\alpha \left(\frac{v_{\rm F} m_{\rm ea}}{\mathcal{D}}\right)^{2/3}; \quad L_{\rm ep}^{\rm (loc)} \sim \frac{v_{\rm F}^2}{\bar{\mathcal{D}}_0} \sim \xi_{\rm ep} \left(\frac{v_{\rm F} m}{\mathcal{D}}\right)^2. \quad (71)$$

Assuming $\xi_{ea} \sim \xi_{ep}$ and $m_{ea} \sim m$, we obtain

$$\frac{L_{ea}^{(loc)}}{L_{ep}^{(loc)}} \sim K_\alpha \left(\frac{\mathcal{D}}{v_F m}\right)^{4/3} \ll 1. \tag{72}$$

This demonstrates that the strong suppression of localization can occur in the EP phase where the helical symmetry is broken.

We note that the scaling exponent of $\tilde{\mathcal{D}}(x)$ is the same as in the case of non-interacting 1d fermions but suppression of localization in the EP phase is reflected by the additional large factor $v_F m/\mathcal{D}$ in the expression for the localization radius $L_{ep}^{(loc)}$. We further note that unlike for free fermions our flow starts at the correlation length v_F/m, not at the lattice constant ξ_0. However, for characteristic length scales $\xi_0 < l < \xi_{ea/ep}$, the mass is not relevant and the flow of our system mimics that of free fermions in the absence spinful impurities. The flow only begins to differ at $l \approx \xi_{ea/ep}$, such that we should compare to free fermions with a cutoff $\xi_{ea/ep}$.

5.2.4. Alternative approach to disorder

In this section we present an alternative approach which confirms the previous results on disorder. The main idea is to integrate out the massive modes before averaging over disorder. We will focus on the main steps and neglect unimportant prefactors. Let us start again at equation (57). In the EA case, we perform a shift $\Phi_c \to \Phi_c - \alpha/\sqrt{2}$. This shift leads to

$$V_{dis}^{ea} = g(x) e^{i\alpha} \Psi^\dagger (I \otimes \tau^+) \Psi + \text{h.c.}, \tag{73}$$

such that the field α couples to the potential disorder. Let us integrate out the massive fermions. The leading term (in powers of the disorder) in the Lagrangian is then

$$L_{dis} \sim \tfrac{1}{\xi_0} \int dx \, [g_{eff}(x) e^{i2\alpha} + \text{h.c.}], \tag{74}$$

where we introduced the non-Gaussian effective disorder

$$g_{eff}(x) \sim \frac{1}{2v_F} \int dy g(x + y/2) g(x - y/2) e^{-m|y|/v_F}; \tag{75}$$

the exponential stems from real space Green's function of fermions with mass m[8]. Equation (75) is valid for large distances $y \gg v_F/m$.

In the EP case, before integrating out the massive fermions, we shift their phase Φ_c by $\sqrt{2}\,\alpha/4$:

$$V_{dis}^{ep} = \int dx \, [g(x) e^{i\alpha/2} R_\uparrow^\dagger L_\uparrow + g(x) e^{i\alpha/2} R_\downarrow^\dagger L_\downarrow + \text{h.c.}]. \tag{76}$$

Each term describes a coupling of a gapped fermion from the first helical sector with a gapless one from the second helical sector and with a low-energy angle α. Upon integrating out the gapped fermions, the disorder generates the following contribution to the low energy effective Lagrangian:

$$\mathcal{L}_{dis}^{(H2)} \supset \int dx \, [g_{eff}(x) R_\downarrow^\dagger e^{i\alpha} L_\uparrow + \text{h.c.}], \tag{77}$$

where $g_{eff}(x)$ is of the form of equation (75)[9].

Thus, both in EA and EP, we obtain gapless particles coupled to an effective disorder.

To order $\frac{\mathcal{D}}{v_F m}$, only the first and second moment of the distribution function of g_{eff} contribute (see appendix E). This is equivalent to the statement that the non-Gaussianities of the distribution of g_{eff} are irrelevant in our approximation.

The leading order contributions of the effective disorder to the localization may then be estimated similarly to the diagrammatic approach. Upon integrating over the disorder (and assuming it is a Gaussian distribution), we obtain

$$S_{dis} \sim \sum_{i,j} \int d\tau d\tau' dx \frac{\mathcal{D}^2}{v_F m} \mathcal{O}_i(x, \tau) \mathcal{O}_j^\dagger(x, \tau'), \tag{78}$$

where the operator $\mathcal{O}$ is given by

$$\text{EA}: \ \mathcal{O}_i(x, \tau) = \frac{1}{\xi_0} e^{i2\alpha_i(x,\tau)}, \tag{79}$$

[8] Note that equation (74) corresponds to figures 5(c) and (d): the fermionic lines are contracted to a single point and the two disorder lines are merged into one line corresponding to g_{eff}.

[9] Equation (77) corresponds to contracting the internal fermion lines in figures 7(b) and (c), and then merging the two disorder lines into a single lines described by g_{eff}.

$$\text{EP}: \ \mathcal{O}_i(x,\tau) = e^{i\alpha_i} R^{\dagger}_{i,\downarrow} L_{i,\uparrow}. \tag{80}$$

This yields the same scaling and, thus, the same localization radius equation (71) as in the diagrammatic approach.

The advantage of this approach is that the order of approximations follows the ordering of the relevant energy scales. We first eliminate the highest energy (m) and only then approach the much smaller pinning energy. The price is the non-Gaussianity of the effective disorder. However, since higher moments of the effective disorder are suppressed by additional factors of $\frac{\mathcal{D}}{v_F m}$, the non-Gaussianities only enter in higher orders that we do not consider here.

6. Spin correlation functions and order parameter

Let us consider the spin correlators $\langle S^a(1) S^b(2)\rangle$ and see which correlation function reflects the broken $\mathbb{Z}_2$ symmetry.

Before computing the correlators, we note the following: the low energy physics of both phases is captured by two uncorrelated $U(1)$ Luttinger liquids and by a set of fast angles. The slow component of the spins (in the basis where $S_{\text{slow}} \| e_3'$) depends on the angles via

$$S^x/s = -\cos\alpha_\parallel \cos\alpha_\perp \cos\theta\cos\psi + \cos\alpha_\parallel \sin\alpha_\perp \sin\psi + \sin\alpha_\parallel \sin\theta\cos\psi; \tag{81a}$$

$$S^y/s = -\cos\alpha_\parallel \cos\alpha_\perp \cos\theta\sin\psi - \cos\alpha_\parallel \sin\alpha_\perp \cos\psi + \sin\alpha_\parallel \sin\theta\sin\psi; \tag{81b}$$

$$S^z/s = \cos\alpha_\parallel \cos\alpha_\perp \sin\theta + \sin\alpha_\parallel \cos\theta. \tag{81c}$$

The effective low energy physics is generated at $\alpha_\parallel \approx 0$. Therefore, equation (81) simplifies to

$$S^x/s = -\cos\alpha_\perp \cos\theta\cos\psi + \sin\alpha_\perp \sin\psi; \tag{82a}$$

$$S^y/s = -\cos\alpha_\perp \cos\theta\sin\psi - \sin\alpha_\perp \cos\psi; \tag{82b}$$

$$S^z/s = \cos\alpha_\perp \sin\theta; \tag{82c}$$

where we neglect fast fluctuations of $\alpha_\parallel$ around its ground state value. We will also need the correlation functions (for large distances) in a Luttinger liquid described by the field ρ with Luttinger parameter K and velocity v:

$$\langle \sin(\rho(x_1) \pm \rho(x_2))\rangle = 0; \quad \langle \cos(\rho(x_1) + \rho(x_2))\rangle = 0; \ \langle \sin(\rho(x_1))\cos(\rho(x_2))\rangle = 0; \tag{83a}$$

$$\langle \sin(\rho(x_1))\sin(\rho(x_2))\rangle = \langle \cos(\rho(x_1))\cos(\rho(x_2))\rangle = \tfrac{1}{2}\langle \cos(\rho(x_1) - \rho(x_2))\rangle = \frac{\xi_0^{K/2}}{[(v\tau + \xi_0)^2 + x^2]^{K/4}}. \tag{83b}$$

Here, $\langle \cos(\rho(x_1) + \rho(x_2))\rangle = 0$ due to 'electroneutrality' [39].

6.1. Spin correlation functions; EA

In the case of the EA anisotropy, the physics at energies smaller that $J_z - J_\perp$ is governed by $\theta \approx \pi/2$ (fast fluctuations are again neglected). At these energies the spin components become

$$S^x/s = \sin\alpha_\perp \sin\psi, \ \ S^y/s = -\sin\alpha_\perp \cos\psi, \ \ S^z/s = \cos\alpha_\perp. \tag{84}$$

Then the transverse spin correlators are given by

$$\langle S^x(1) S^x(2)\rangle/s^2 = \langle S^y(1) S^y(2)\rangle/s^2 = \langle (\sin\alpha_\perp \sin\psi)(1)(\sin\alpha_\perp \sin\psi)(2)\rangle + \mathcal{O}(\theta - \pi/2, \alpha_\parallel), \tag{85}$$

where (j) denotes (τ_j, x_j). Since ψ and α are not correlated, the correlation function factorizes. The correlation function of the $\alpha_\perp$ component can be written as

$$\langle \sin\alpha_\perp(1)\sin\alpha_\perp(2)\rangle = -\tfrac{1}{2}[\langle \cos(2k_F(x_1 + x_2) + \alpha(1) + \alpha(2))\rangle - \langle \cos(2k_F(x_1 - x_2) + \alpha(1) - \alpha(2))\rangle]. \tag{86}$$

Combining equations (86) and (83) leads to

$$\langle S^x(1) S^x(2)\rangle/s^2 = \tfrac{1}{4}\cos[2k_F(x_1 - x_2)]\langle \cos(\alpha(1) - \alpha(2))\rangle \langle \cos(\psi(1) - \psi(2))\rangle = \cos(2k_F x)\left(\frac{\xi_0}{\sqrt{(\tau v_\alpha)^2 + x^2}}\right)^{\frac{K_\alpha}{2}} \left(\frac{\xi_0}{\sqrt{(\tau v_F)^2 + x^2}}\right)^{\frac{1}{2}}, \tag{87}$$

where we introduced $x = x_1 - x_2$ and $\tau = \tau_1 - \tau_2$. The transverse spin correlation function of x and y components is

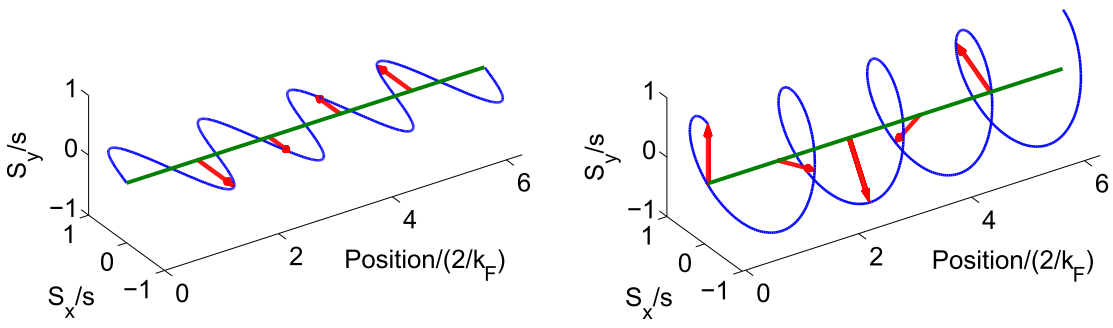

Figure 8. A travelling spin wave in the EA (left) and EP (right) setup. Since S^x and S^y in the EA case are uncorrelated to leading order, we only show one contribution.

$$\langle S^x(1)S^y(2)\rangle/s^2 \sim f(\alpha_\perp)\langle \sin\psi(1)\cos\psi(2)\rangle = 0. \tag{88}$$

Equation (88) shows that there is no spin rotation in xy-plane, see figure 8. In particular, this implies that the Fourier-transform of the dynamical in-plane spin susceptibility

$$\langle S^+(1)S^-(2)\rangle/s^2 = 2\langle S^x(1)S^x(2)\rangle/s^2, \tag{89}$$

has peaks both at $2k_F$ and $-2k_F$.

The correlators of S^z spin components are given by

$$\begin{aligned}\langle S^z(1)S^z(2)\rangle/s^2 &= \langle(\cos\alpha_\perp)(1)(\cos\alpha_\perp)(2)\rangle + \mathcal{O}(\theta-\pi/2,\,\alpha_\parallel)\\ &= \cos(2k_Fx)\left(\frac{\xi_0}{\sqrt{(\tau v)^2+x^2}}\right)^{\frac{K_\alpha}{2}}.\end{aligned} \tag{90}$$

They decay more slowly than the transverse spin correlator equation (88) because the S_z component couples more strongly to the localized electrons. The correlation function between the axis and the plane $\langle S^zS^x\rangle$ vanishes. Thus, all cross-correlation functions are zero in the EA case.

6.2. Spin correlation functions; EP

In the case of the EP, the asymptotics of the spin correlation functions are determined by $\theta \approx 0$, or $\theta \approx \pi$. Let us choose $\theta = 0$. Then the spin operators become

$$S^x/s = -\cos\alpha_\perp\cos\psi + \sin\alpha_\perp\sin\psi = -\cos(\alpha_\perp+\psi); \tag{91}$$

$$S^y/s = -\cos\alpha_\perp\sin\psi - \sin\alpha_\perp\cos\psi = -\sin(\alpha_\perp+\psi); \tag{92}$$

$$S^z/s = 0. \tag{93}$$

In our notations: $\alpha_\perp = 2k_Fx + \alpha$ and $\alpha \to \alpha - \psi$ in the EP case. Thus, the transverse spin correlation function reads as

$$\begin{aligned}\langle S^x(1)S^x(2)\rangle/s^2 &= \langle[\cos(2k_Fx+\alpha)](1)[\cos(2k_Fx+\alpha)](2)\rangle\\ &= \cos(2k_Fx)\left(\frac{\xi_0}{\sqrt{(\tau v'_\alpha)^2+x^2}}\right)^{K'_\alpha/2}.\end{aligned} \tag{94}$$

Due to $SO(2)$-symmetry in the x–y-plane, this is the same as the $\langle S^yS^y\rangle$ correlation function. The transverse spin rotation correlation function is

$$\langle S^x(1)S^y(2)\rangle/s^2 = \sin(2k_Fx)\left(\frac{\xi_0}{\sqrt{(\tau v'_\alpha)^2+x^2}}\right)^{K'_\alpha/2}. \tag{95}$$

Equation (95) reveals the spin rotation (helical configuration) in the EP case, see figure 8. Contrary to the EA case, the Fourier transform of the dynamical in-plane spin susceptibility

$$\langle S^+(1)S^-(2)\rangle/s^2 = 2(\langle S^x(1)S^x(2)\rangle - \mathrm{i}\langle S^xS^y\rangle)/s^2 = \exp(-\mathrm{i}2k_Fx)\left(\frac{\xi_0}{\sqrt{(\tau v'_\alpha)^2+x^2}}\right)^{K'_\alpha/2} \tag{96}$$

has a peak only at $2k_F$. The longitudinal spin correlator $\langle S^zS^z\rangle$ is zero in our accuracy (at fixed $\theta = 0$, $\alpha_\parallel = 0$).

6.3. Order parameter

We have shown that the low energy spin excitations of the EA case are planar spin oscillations, whereas in the EP case the spins form a helix, see figure 8.

The transverse spin correlation function $\langle S^x(1)S^y(2)\rangle$, which reflects rotations of the spins, is zero in the non-helical phase (EA), but nonvanishing in the helical one (EP). Thus we suggest to use it as an order parameter. In analogy with antiferromagnetic ordering [41], we define the two-point order parameter

$$\mathcal{A}_c = \epsilon_{abc}\langle S^a(1)S^b(1+\xi_0)\rangle, \tag{97}$$

which is non-vanishing only in the helical phase, where there is a low-energy helical mode propagating within the dense chain of the magnetic impurities.

7. Conclusion

Low-energy properties of an anisotropic KC away from half-filling are governed either by the Kondo screening or by the RKKY interaction generated by the backscattering of electrons on the spins. The latter process becomes dominant when the concentration of the spins is sufficiently large and when the repulsive electron–electron interactions are sufficiently strong. Then the RKKY interaction opens a gap in the quasiparticle spectrum, equation (24), which further suppresses the Kondo screening. Depending on the anisotropy of the exchange interaction, the backscattering processes may either lead to a formation of the CDWs and the SDWs (EA anisotropy), equation (28), or generate the helical low energy modes (EP anisotropy), equation (41). The appearence of such modes is related to spontaneous breking of the $\mathbb{Z}_2$(helical)-symmetry. We have shown that the order parameter characterizing the corresponding quantum phase transition is the average of the vector product of neighboring spins $\mathcal{A}_c = \epsilon_{abc}\langle S^a(1)S^b(1+\xi_0)\rangle$. The helical nature of the modes is also manifest in the asymmetry between the $+2k_F$ and $-2k_F$ peaks in the in-plane spin susceptibility $\langle S^+S^-\rangle$, equation (96). The ideal charge transport supported by the gapless helical modes is robust: it remains ballistic even if a weak random potential of static impurities is present. This protection requires the spin the $U(1)$ symmetry and exists up to the parametrically large scale, see equation (71). We have shown that short-range electron–electron interactions mix the two helical sectors, but cannot gap out any low-energy modes, such that for weak interactions the qualitative description in terms of the helical modes remains valid.

Even though the helical modes may be reminiscent of the edge modes of topological insulators, we emphasize that, in our case, they are generated by the many-body interactions in one spacial dimension. Experimentally, the helical modes could be detected in samples exhibiting one-dimensional structure with spin impurities. As we have discussed in Introduction, promising candidates are ladder-type Fe-selenides, where almost completely filled bands of electrons might serve as spin impurities [21], or single-wall carbon nanotubes functionalized by magnetic ions [18]. Since the advent of the cleaved edge overgrowth method [42], quantum wires on the edge of GaAs heterostructures are also viable candidates.

Usually, one cannot control the anisotropy of real materials. Therefore, one needs an experimental evidence that the charge transport in a given system with the dense array of the Kondo impurities is supported by modes with a broken helical symmetry. The cleanest signature could be provided by the local spin susceptibility (equations (89) and (96)), which clearly provides a smoking gun signature for the helical order. The local spin susceptibility may be experimentally accessible through nitrogen-vacancy based STM measurements if the Kondo array is made as a one-dimensional wire [43].

Another experimental signature of the helical phase is frequency-resolved charge transport. We remind the readers that in our model the charge is carried either by the collective mode α (EA), or by the collective mode α and the helical fermion (EP) with the velocity of the α-excitations being always small (equations (29) and (40)). If a sufficiently clean sample of a finite size is adiabatically connected to leads, its dc conductance remains ideal, $2e^2/h$ [44]. However, the frequency resolved conductance is expected to show a substantial decrease at $\omega_c \sim 1/t_{\rm Th}^{(\alpha)}$; where $t_{\rm Th}^{(\alpha)} \sim L/v_\alpha$ is the Thouless time associated with the mode α. Since the α-modes are very slow ω_c is small. For frequencies larger than ω_c, the slow collective modes cannot contribute and the conductance drops either to zero (EA) or to e^2/h (EP). The latter jump would confirm that the system is in the helical phase which is robust against localization effects.

A similar transition could also be detected at $\omega = 0$ in the temperature dependence of the conductance. We expect that at finite temperature domains of different helicity develop. At temperatures above the energy of a domain-wall ($T > E_{\rm domain\ wall}$) the quasiparticles do not contribute to the dc transport any longer and a crossover of the conductance from $2e^2/h$ to e^2/h is expected with increasing T. Hence, the T-dependence of the conductance at very small temperatures (possibly less than 5 mK reached in [45]) should be studied.

In order to check that the reduction of the conductance is related to the presence of the localized spins, one may repeating the measurements on samples where the magnetic atoms are not present. If the spin-spin

interaction is important the presence or absence of the additional localized spins will have a strong influence on the conductance. Finally, we have shown that the helical transport is partially protected from localization effects. This means that the conductance will not change even if the sample length becomes longer than the mean-free path of the material.

The theory of the frequency and temperature dependent conductance of the KC requires further theoretical work.

Acknowledgments

AMT acknowledges the hospitality of Ludwig Maximilians University where part of this work was done. AMT was supported by the US Department of Energy (DOE), Division of Materials Science, under Contract No. DE-AC02-98CH10886. OMYe acknowledges support from the DFG through SFB TR-12, and the Cluster of Excellence, Nanosystems Initiative Munich. DHS is supported through by the DFG through the Excellence Cluster Nanosystems Initiative Munich, SFB/TR 12 and SFB 631. We are grateful to Vladimir Yudson and Igor Yurkevich for useful discussions.

Appendix A. Derivation of the low-energy Lagrangian

In this section we give a short derivation of the form of the electron-spin interactions in terms of the fast and slow angular variables ($\alpha_\parallel$, $\alpha_\perp$, θ, and ψ). Thus, consider the interaction term

$$H_{\rm int} = \sum_m J_a\, \hat{c}_m^\dagger\, \hat{\sigma}^a \hat{S}^a(m)\, \hat{c}_m. \tag{A1}$$

Using the representation of the fermions in terms of left- and rightmovers, equation (9), this term splits into forward and backward scattering contributions

$$H_{\rm int} = H_{\rm forward} + H_{\rm backward}, \tag{A2}$$

$$H_{\rm forward} = \sum_m J_a^{\rm f}\, \hat{R}_m^\dagger\, \hat{\sigma}^a \hat{S}^a(m)\, \hat{R}_m + \sum_m J_a^{\rm f}\, \hat{L}_m^\dagger\, \hat{\sigma}^a \hat{S}^a(m)\, \hat{L}_m, \tag{A3}$$

$$H_{\rm backward} = +\sum_m J_a^{\rm b} e^{2ik_{\rm F}x}\, \hat{R}_m^\dagger\, \hat{\sigma}^a \hat{S}^a(m)\, \hat{L}_m + \sum_m J_a^{\rm b} e^{-2ik_{\rm F}x}\, \hat{L}_m^\dagger\, \hat{\sigma}^a \hat{S}^a(m)\, \hat{R}_m, \tag{A4}$$

where the superscript f (b) denotes forward (backward) scattering contributions. Using the low-energy spin $S_{\rm LE} \| \boldsymbol{e}_3'$ and taking the dense impurity limit, we obtain

$$\begin{aligned}\mathcal{L}_{\rm int}^{\rm (bs)} = s\rho_{\rm s} e^{2ik_{\rm F}x} R^\dagger \Big\{ \tfrac{J_\perp^{\rm b}}{2} [&+ e^{i\nu\psi}(-\cos\alpha_\parallel \cos\alpha_\perp \cos\theta - i\cos\alpha_\parallel \sin\alpha_\perp + \sin\alpha_\parallel \sin\theta)\hat{\sigma}^- \\ &+ e^{-i\psi}(-\cos\alpha_\parallel \cos\alpha_\perp \cos\theta + i\cos\alpha_\parallel \sin\alpha_\perp + \sin\alpha_\parallel \sin\theta)\hat{\sigma}^+] \\ &+ J_z^{\rm b}\hat{\sigma}_z(\sin\alpha_\parallel \cos\theta + \cos\alpha_\parallel \cos\alpha_\perp \sin\theta)\Big\} L + {\rm h.c.}.\end{aligned} \tag{A5}$$

This expresses the back-scattering part of the electron-spin interaction in terms of the angular variables and the fermions. To obtain the low-energy part, we first shift $\alpha_\perp \to \alpha(x) + 2k_{\rm F}x$. Then, neglecting all quickly oscillating terms ($\sim e^{4ik_{\rm F}x}$), equation (A5) reduces to

$$\begin{aligned}\mathcal{L}_{\rm int}^{\rm (sl)\,(bs)} = \frac{s\cos(\alpha_\parallel)\rho_{\rm s}}{2} R^\dagger \left\{ J_\perp \left[e^{i\psi} \sin^2\left(\frac{\theta}{2}\right)\hat{\sigma}^- - e^{-i\psi}\cos^2\left(\frac{\theta}{2}\right)\hat{\sigma}^+ \right] + J_z \sin(\theta)\hat{\sigma}^z \right\} L e^{-i\alpha} \\ + {\rm h.c.}; \quad \tilde{s} \equiv s\cos(\alpha_\parallel).\end{aligned} \tag{A6}$$

The forward-scattering part of the action is obtained by following the same procedure with $H_{\rm forward}$:

$$\mathcal{L}_{\rm int}^{\rm (sl)\,(fs)} = \frac{s\sin(\alpha_\parallel)\rho_{\rm s}}{2} R^\dagger \{ J_\perp^{\rm f} \sin\theta [e^{i\psi}\sigma^- + e^{-i\psi}\sigma^+] + 2J_z^{\rm f}\cos\theta\sigma^z \} R + (R \to L). \tag{A7}$$

Appendix B. Bosonization and the RG equations

Here we briefly remind readers of the bosonization identity used throughout, and the derivation of the RG equations. We only derive one RG equation explicitely, but the other RG equations may be obtained by the same procedure.

The bosonization formula is

$$\Psi_{r\sigma} = \frac{1}{\sqrt{2\pi\alpha}} U_\sigma \mathrm{e}^{-\mathrm{i}rk_\mathrm{F}x} \mathrm{e}^{-\frac{1}{\sqrt{2}}\mathrm{i}[r\Phi_\mathrm{c}-\Theta_\mathrm{c}+\sigma(r\Phi_\mathrm{s}-\Theta_\mathrm{s})]}, \tag{B1}$$

where Φ_c (Φ_s) and Θ_c (Θ_s) are dual fields belonging to the charge (spin) density wave, r distinguishes right- and left-moving and σ is the spin. The Klein factors U_σ are real coordinate independent fermionic operators obeying the anticommutation relations $\{U_\sigma, U_{\sigma'}\} = \delta_{\sigma,\sigma'}$.

After bosonization equation (B1), the electron-spin interaction contains the terms

$$\begin{aligned}
\mathcal{L}_z^\mathrm{f} &:= J_z^\mathrm{f} S_z (R^\dagger \sigma_z R + L^\dagger \sigma_z L) = -\sqrt{2} S_z \frac{J_z^\mathrm{f}}{\pi} \partial_x \Phi_\mathrm{s}, \\
\mathcal{L}_-^\mathrm{f} &:= J_\perp^\mathrm{f} S_- (R^\dagger \sigma_+ R + L^\dagger \sigma_+ L) = S_- \frac{J_\perp^\mathrm{f}}{\pi\xi_0} \exp(-\sqrt{2}\,\mathrm{i}\Theta_\mathrm{s})(\exp(\sqrt{2}\,\mathrm{i}\Phi_\mathrm{s}) + \exp(-\sqrt{2}\,\mathrm{i}\Phi_\mathrm{s})), \\
\mathcal{L}_+^\mathrm{f} &:= J_\perp^\mathrm{f} S_+ (R^\dagger \sigma_- R + L^\dagger \sigma_- L) = S_+ \frac{J_\perp^\mathrm{f}}{\pi\xi_0} \exp(\sqrt{2}\,\mathrm{i}\Theta_\mathrm{s})(\exp(-\sqrt{2}\,\mathrm{i}\Phi_\mathrm{s}) + \exp(\sqrt{2}\,\mathrm{i}\Phi_\mathrm{s})), \\
\mathcal{L}_z^\mathrm{b} &:= J_z^\mathrm{b} S_z (R^\dagger \sigma_z L + L^\dagger \sigma_z R) = S_z \frac{J_z^\mathrm{f}}{2\pi\xi_0} \exp(-2\mathrm{i}k_\mathrm{F}x) \exp(\sqrt{2}\,\mathrm{i}\Phi_\mathrm{c})(\exp(\sqrt{2}\,\mathrm{i}\Phi_\mathrm{s}) - \exp(-\sqrt{2}\,\mathrm{i}\Phi_\mathrm{s})) + \mathrm{h.c.}, \\
\mathcal{L}_-^\mathrm{b} &:= J_\perp^\mathrm{b} (S_- R^\dagger \sigma_+ L + S_+ L^\dagger \sigma_- R) = S_- \frac{J_\perp^\mathrm{f}}{\pi\xi_0} \exp(-2\mathrm{i}k_\mathrm{F}x) \exp(\sqrt{2}\,\mathrm{i}(\Phi_\mathrm{c} - \Theta_\mathrm{s})) + \mathrm{h.c.}, \\
\mathcal{L}_+^\mathrm{b} &:= J_\perp^\mathrm{b} (S_+ R^\dagger \sigma_- L + S_- L^\dagger \sigma_+ R) = S_+ \frac{J_\perp^\mathrm{f}}{\pi\xi_0} \exp(-2\mathrm{i}k_\mathrm{F}x) \exp(\sqrt{2}\,\mathrm{i}(\Phi_\mathrm{c} + \Theta_\mathrm{s})) + \mathrm{h.c.}.
\end{aligned} \tag{B2}$$

The flow of the coupling constants is obtained by integrating out high energy modes. To do so, one must split Φ_α, Θ_α and S_β into fast (superscript $>$) and slow (superscript $<$) modes:

$$\Phi_\alpha = \Phi_\alpha^< + \Phi_\alpha^>, \quad \Theta_\alpha = \Theta_\alpha^< + \Theta_\alpha^>, \quad S_\beta = S_\beta^< + S_\beta^>. \tag{B3}$$

The measure of the path integral splits into fast and slow modes as well. We then perform the integral over the fast modes in a perturbative series in J and reexponentiate the result. The first order in J leads to the one-loop RG equations. As in the bosonization treatment of the Kondo impurity, we will treat the spins as constant during the RG flow. Thus, we need to compute

$$\int \mathcal{D}\{\Phi, \Theta\} \exp\left(-S_\mathrm{LL}[\Phi, \Theta] - \int \mathrm{d}\tau \mathrm{d}x J_a S_a f_a(\Phi, \Theta)\right), \tag{B4}$$

where S_LL is the Luttinger liquid action for Φ and Θ and f_a is a function which can be read off from (B2). Note that there is space–time UV cutoff ξ_0 (or equivalently an energy–momentum cutoff Λ). Let us consider as an example the term proportional to J_z^b:

$$\begin{aligned}
&\int \mathcal{D}\{\Phi^>, \Theta^>\} \exp(-S_\mathrm{LL}[\Phi^>, \Theta^>]) \int \mathrm{d}\tau \mathrm{d}x J_z^\mathrm{b} S_z^< f_z^\mathrm{b}(\Phi^> + \Phi^<, \Theta^> + \Theta^<) \\
&= \int \mathrm{d}\tau \mathrm{d}x J_z^\mathrm{b} S_z^< \int \mathcal{D}\{\Phi^>, \Theta^>\} \exp(-S_\mathrm{LL}[\Phi^>, \Theta^>]) \frac{1}{2\pi\xi_0} \exp(-2\mathrm{i}k_\mathrm{F}x) \exp(\sqrt{2}\,\mathrm{i}(\Phi_\mathrm{c}^> + \Phi_\mathrm{c}^<)) \\
&\quad \times (\exp(\sqrt{2}\,\mathrm{i}(\Phi_\mathrm{s}^> + \Phi_\mathrm{s}^<)) - \exp(-\sqrt{2}\,\mathrm{i}(\Phi_\mathrm{s}^> + \Phi_\mathrm{s}^<))) + \mathrm{h.c.}
\end{aligned} \tag{B5}$$

The components $\Phi^>$ ($\Theta^>$) and $\Phi^<$ ($\Theta^<$) are of high and low energy, such that the energy of $\Phi^>$ ($\Theta^>$) lies in the interval $[\Lambda', \Lambda]$. Using the equalities $\langle \mathrm{e}^{\sqrt{2}\,\mathrm{i}\Phi_\mathrm{s}^>} \rangle_> = (\Lambda'/\Lambda)^{K_\mathrm{s}/2}$ and $\langle \mathrm{e}^{\sqrt{2}\,\mathrm{i}\Theta_\mathrm{s}^>} \rangle_> = (\Lambda'/\Lambda)^{1/(2K_\mathrm{s})}$, we can perform the average over fast modes. This yields

$$\begin{aligned}
&\int \mathcal{D}\{\Phi^>, \Theta^>\} \exp(-S_\mathrm{LL}[\Phi^>, \Theta^>]) \int \mathrm{d}\tau \mathrm{d}x J_z^\mathrm{b} S_z^< f_z^\mathrm{b}(\Phi^> + \Phi^<, \Theta^> + \Theta^<) \\
&= \int \mathrm{d}\tau \mathrm{d}x J_z^\mathrm{b} S_z^< \left(\frac{\Lambda'}{\Lambda}\right)^{\frac{1}{2}(K_\mathrm{s}+K_\mathrm{c})} f_z^\mathrm{b}(\Phi^<, \Theta^<).
\end{aligned} \tag{B6}$$

Since the cutoff was changed from Λ' to Λ, we need to rescale x and τ to recover the original expression. Reexponentiating (B6) yields

$$J_z^\mathrm{b}(\Lambda') = J_z^\mathrm{b}(\Lambda) \left(\frac{\Lambda'}{\Lambda}\right)^{\frac{1}{2}(K_\mathrm{s}+K_\mathrm{c})-2}. \tag{B7}$$

The RG equation is obtained expressing equation (B7) as a differential equation in the parametrization $\Lambda' = \Lambda \mathrm{e}^{-l-dl}$, where dl is an infinitesimal number:

$$\partial_l J_z^{\rm b} = \left[\tfrac{1}{2}(K_{\rm s}+K_{\rm c})-2\right]J_z^{\rm b}. \tag{B8}$$

Appendix C. The shift of the angles in the EA case

We present a short, alternative derivation of the action after the shift eliminiating the angles α and ψ from the interaction vertices, equation (22). This proof is based on abelian bosonization. Upon bosonization, equation (B1), the free part of the Lagrangian are a spin and charge Tomonaga–Luttinger liquid:

$$\mathcal{L} = \mathcal{L}_{\rm TL,dual}[\Phi_{\rm c},\Theta_{\rm c}] + \mathcal{L}_{\rm TL,dual}[\Phi_{\rm s},\Theta_{\rm s}], \tag{C1}$$

with

$$\mathcal{L}_{\rm TL,dual}[\Phi_a,\Theta_a] = -\frac{\rm i}{\pi}\partial_x\Theta_a\partial_\tau\Phi_a + \frac{1}{2\pi}\left(uK(\partial_x\Theta_a)^2 + \frac{u}{K}(\partial_x\Phi_a)^2\right). \tag{C2}$$

We use a description in terms of fields Φ and their duals Θ. The shift equation (19) is in bosonic language

$$\Phi_{\rm c} \to \Phi_{\rm c} + \alpha/\sqrt{2},\ \Theta_{\rm s} \to \Theta_{\rm s} - \psi/\sqrt{2}. \tag{C3}$$

Performing this shift also in the Tomonaga–Luttinger liquid equation (C1), we obtain the new terms of the form

$$\mathcal{L}_{\rm mixing} \sim -{\rm i}\partial_\tau\alpha\partial_x\Theta_{\rm c} - \partial_x\alpha\partial_x\Phi_{\rm c} - {\rm i}\partial_\tau\psi\partial_x\Phi_x - \partial_x\psi\partial_x\Theta_{\rm s}. \tag{C4}$$

and terms of the type

$$\mathcal{L}_{\rm TL,dual}[\alpha/\sqrt{2},\Theta_{\rm c}] + \mathcal{L}_{\rm TL,dual}[\Phi_{\rm s},\psi/\sqrt{2}]. \tag{C5}$$

Since after bosonization spatial derivatives of $\Phi_{\rm c/s}$ ($\Theta_{\rm c/s}$) correspond to the charge/spin density (current), equation (C4) contains precisely the terms of equation (21), and may be neglected by the same arguments. After averaging over the dual fields $\Theta_{\rm c}$ and $\Phi_{\rm s}$, equation (C5) is the same as the Tomonaga–Luttinger anomaly equation (20). We thus have obtained the same expression as in the main text, without explicitely using the Tomonaga–Luttinger anomaly.

Appendix D. Accounting for interactions

In this section we show how to obtain equation (47). We start from the bosonized Lagrangian of interacting electrons

$$\mathcal{L} = -\frac{\rm i}{\pi}\partial_x\Theta_{\rm c}\partial_\tau\Phi_{\rm c} + \frac{1}{2\pi}\left(u_{\rm c}K_{\rm c}(\partial_x\Theta_{\rm c})^2 + \frac{u_{\rm c}}{K_{\rm c}}(\partial_x\Phi_{\rm c})^2\right) - \frac{\rm i}{\pi}\partial_x\Theta_{\rm s}\partial_\tau\Phi_{\rm s} + \frac{1}{2\pi}\left(u_{\rm s}K_{\rm s}(\partial_x\Theta_{\rm s})^2 + \frac{u_{\rm s}}{K_{\rm s}}(\partial_x\Phi_{\rm s})^2\right). \tag{D1}$$

In order to rewrite equation (D1) in terms of helical fields, we define

$$\Phi_{h_1} = \tfrac{1}{\sqrt{2}}(\Phi_{\rm c}-\Theta_{\rm s}),\quad \Theta_{h_1} = \tfrac{1}{\sqrt{2}}(\Theta_{\rm c}-\Phi_{\rm s}), \tag{D2a}$$

$$\Phi_{h_2} = \tfrac{1}{\sqrt{2}}(\Phi_{\rm c}+\Theta_{\rm s}),\quad \Theta_{h_2} = \tfrac{1}{\sqrt{2}}(\Theta_{\rm c}+\Phi_{\rm s}). \tag{D2b}$$

This choice stems from the identities

$$\begin{aligned}\rho_\downarrow^R &= \frac{\sqrt{2}}{\pi}\partial_x(\Theta_{\rm c}-\Phi_{\rm c}-(\Theta_{\rm s}-\Phi_{\rm s})),\\ \rho_\uparrow^L &= \frac{\sqrt{2}}{\pi}\partial_x(-\Theta_{\rm c}-\Phi_{\rm c}-\Theta_{\rm s}-\Phi_{\rm s}).\end{aligned} \tag{D3}$$

If there are no particles of one specific helical sector (e.g. $R_\downarrow$ and $L_\uparrow$), then both of these densities should vanish. This is guaranteed if there are no fluctuations in Φ_{h2} and Θ_{h2}. Thus, the fields Φ_{h2} and Θ_{h2} correspond to the helical sector containing $R_\downarrow$ and $L_\uparrow$.

Inserting equation (D2*a*) into equation (D1), we obtain

$$\begin{aligned}2\mathcal{L} =& -\tfrac{\rm i}{\pi}\partial_x(\Theta_{h_1}+\Theta_{h_2})\partial_\tau(\Phi_{h_1}+\Phi_{h_2}) + \tfrac{1}{2\pi}\left(u_{\rm c}K_{\rm c}(\partial_x(\Theta_{h_1}+\Theta_{h_2}))^2 + \tfrac{u_{\rm c}}{K_{\rm c}}(\partial_x(\Phi_{h_1}+\Phi_{h_2}))^2\right)\\ &-\tfrac{\rm i}{\pi}\partial_x(-\Phi_{h_1}+\Phi_{h_2})\partial_\tau(-\Theta_{h_1}+\Theta_{h_2}) + \tfrac{1}{2\pi}\left(u_{\rm s}K_{\rm s}(\partial_x(-\Phi_{h_1}+\Phi_{h_2}))^2 + \tfrac{u_{\rm s}}{K_{\rm s}}(\partial_x(-\Theta_{h_1}+\Theta_{h_2}))^2\right)\end{aligned} \tag{D4}$$

$$= -2\tfrac{\mathrm{i}}{\pi}\partial_x(\Theta_{h_1})\partial_\tau(\Phi_{h_1}) + \tfrac{1}{2\pi}\left(\left(u_\mathrm{c}K_\mathrm{c} + \tfrac{u_\mathrm{s}}{K_\mathrm{s}}\right)(\partial_x\Theta_{h_1})^2 + \left(\tfrac{u_\mathrm{c}}{K_\mathrm{c}} + u_\mathrm{s}K_\mathrm{s}\right)(\partial_x\Phi_{h_1})^2\right)$$
$$- 2\tfrac{\mathrm{i}}{\pi}\partial_x(\Theta_{h_2})\partial_\tau(\Phi_{h_2}) + \tfrac{1}{2\pi}\left(\left(u_\mathrm{c}K_\mathrm{c} + \tfrac{u_\mathrm{s}}{K_\mathrm{s}}\right)(\partial_x\Theta_{h_2})^2 + \left(\tfrac{u_\mathrm{c}}{K_\mathrm{c}} + u_\mathrm{s}K_\mathrm{s}\right)(\partial_x\Phi_{h_2})^2\right)$$
$$+ \tfrac{1}{2\pi}\left(2\left(u_\mathrm{c}K_\mathrm{c} - \tfrac{u_\mathrm{s}}{K_\mathrm{s}}\right)\partial_x\Theta_{h_2}\partial_x\Theta_{h_1} + 2\left(\tfrac{u_\mathrm{c}}{K_\mathrm{c}} - u_\mathrm{s}K_\mathrm{s}\right)\partial_x\Phi_{h_2}\partial_x\Phi_{h_1}\right). \tag{D5}$$

The shift equation (35), which keeps the second helical sector invariant, corresponds to $\Phi_{h_1} \to \Phi_{h_1} + \alpha/2$. After neglecting couplings between gapless modes and derivatives of the first helical sector, we find in addition to the free part $\mathcal{L}_\mathrm{TL}$ of α

$$\mathcal{L} = -\tfrac{\mathrm{i}}{\pi}\partial_x\Theta_{h_1}\partial_\tau\Phi_{h_1} + \tfrac{1}{4\pi}\left(\left(u_\mathrm{c}K_\mathrm{c} + \tfrac{u_\mathrm{s}}{K_\mathrm{s}}\right)(\partial_x\Theta_{h_1})^2 + \left(\tfrac{u_\mathrm{c}}{K_\mathrm{c}} + u_\mathrm{s}K_\mathrm{s}\right)(\partial_x\Phi_{h_1})^2\right)$$
$$- \tfrac{\mathrm{i}}{\pi}\partial_x\Theta_{h_2}\partial_\tau\Phi_{h_2} + \tfrac{1}{4\pi}\left(\left(u_\mathrm{c}K_\mathrm{c} + \tfrac{u_\mathrm{s}}{K_\mathrm{s}}\right)(\partial_x\Theta_{h_2})^2 + \left(\tfrac{u_\mathrm{c}}{K_\mathrm{c}} + u_\mathrm{s}K_\mathrm{s}\right)(\partial_x\Phi_{h_2})^2\right)$$
$$+ \tfrac{1}{2\pi}\left(\tfrac{u_\mathrm{c}}{K_\mathrm{c}} - u_\mathrm{s}K_\mathrm{s}\right)\partial_x\Phi_{h_2}\partial_x\alpha. \tag{D6}$$

Introducing

$$\tilde{K} = \sqrt{\frac{u_\mathrm{c}K_\mathrm{c} + \frac{u_\mathrm{s}}{K_\mathrm{s}}}{\frac{u_\mathrm{c}}{K_\mathrm{c}} + u_\mathrm{s}K_\mathrm{s}}}, \quad \tilde{u} = \frac{1}{4}\sqrt{u_\mathrm{c}^2 + u_\mathrm{s}^2 + u_\mathrm{c}u_\mathrm{s}K_\mathrm{c}K_\mathrm{s} + \frac{u_\mathrm{c}u_\mathrm{s}}{K_\mathrm{c}K_\mathrm{s}}}, \tag{D7}$$

equation (D6) may be written as

$$\mathcal{L} = -\tfrac{\mathrm{i}}{\pi}\partial_x\Theta_{h_1}\partial_\tau\Phi_{h_1} + \tfrac{1}{2\pi}\left(\tilde{u}\tilde{K}(\partial_x\Theta_{h_1})^2 + \tilde{u}\tfrac{1}{\tilde{K}}(\partial_x\Phi_{h_1})^2\right)$$
$$- \tfrac{\mathrm{i}}{\pi}\partial_x\Theta_{h_2}\partial_\tau\Phi_{h_2} + \tfrac{1}{2\pi}\left(\tilde{u}\tilde{K}(\partial_x\Theta_{h_2})^2 + \tilde{u}\tfrac{1}{\tilde{K}}(\partial_x\Phi_{h_2})^2\right)$$
$$+ \tfrac{1}{2\pi}\left(\tfrac{u_\mathrm{c}}{K_\mathrm{c}} - u_\mathrm{s}K_\mathrm{s}\right)\partial_x\Phi_{h_2}\partial_x\alpha. \tag{D8}$$

Appendix E. Non-Gaussianities in the effective disorder

In this appendix, we demonstrate that the higher moments of the effective disorder g_eff distribution function in the alternative approach to disorder are of higher order in $\frac{\mathcal{D}}{v_\mathrm{F}m} \ll 1$. Thus, in our accuracy, we may safely neglect the non-Gaussianities of the effective disorder.

We have assumed that the distribution of the $2k_\mathrm{F}$ Fourier components of the original disorder potential is Gaussian, however the distribution of $g_\mathrm{eff}(x)$ is not Gaussian. To investigate the effect of the non-Gaussianity of the distribution function of the effective disorder g_eff, we consider its moments. The first moment is zero:

$$\langle g_\mathrm{eff}(x)\rangle_\mathrm{dis} \sim \left\langle \frac{1}{v_\mathrm{F}}\int \mathrm{d}y g(x + y/2)g(x - y/2)\mathrm{e}^{-m|y|/v_\mathrm{F}}\right\rangle_\mathrm{dis} = 0, \tag{E1}$$

because g is distributed according to the GUE. The second moment is given by

$$\langle g_\mathrm{eff}(x)g_\mathrm{eff}(x')\rangle_\mathrm{dis} \sim \left\langle \frac{1}{v_\mathrm{F}^2}\int \mathrm{d}y\mathrm{d}\tilde{y} g(x + y/2)g(x - y/2)g(x' + \tilde{y}/2)g(x' - \tilde{y}/2)\mathrm{e}^{-m(|y|+|\tilde{y}|)/v_\mathrm{F}}\right\rangle_\mathrm{dis} = 0, \tag{E2}$$

and

$$\begin{aligned}\langle g_\mathrm{eff}(x)g^*_\mathrm{eff}(x')\rangle_\mathrm{dis} &\sim \tfrac{1}{v_\mathrm{F}^2}\left\langle \int \mathrm{d}y\mathrm{d}\tilde{y}\ g(x + y/2)g(x - y/2)g^*(x' + \tilde{y}/2)g^*(x' - \tilde{y}/2)\mathrm{e}^{-m(|y|+|\tilde{y}|)/v_\mathrm{F}}\right\rangle_\mathrm{dis}\\ &\sim \frac{\mathcal{D}^2}{v_\mathrm{F}^2}\int \mathrm{d}y\mathrm{d}\tilde{y}(\delta(x + y/2 - x' + \tilde{y}/2)\delta(x - y/2 - x' - \tilde{y}/2)\\ &\qquad + \delta(x + y/2 - x' - \tilde{y}/2)\delta(x - y/2 - x' + \tilde{y}/2))\mathrm{e}^{-m(|y|+|\tilde{y}|)/v_\mathrm{F}}\\ &\sim \tfrac{\mathcal{D}^2}{v_\mathrm{F}m}\delta(x - x').\end{aligned} \tag{E3}$$

Higher moments contain additional contractions, reflecting the non-Gaussianity of the distribution of g_eff. As an example, consider the fourth moment

$$\langle g_{\rm eff}(x)g_{\rm eff}(y)g^*_{\rm eff}(z)g^*_{\rm eff}(w)\rangle_{\rm dis} \sim \frac{1}{\nu_{\rm F}^4}\Big\langle \int {\rm d}x'{\rm d}y'{\rm d}z'{\rm d}w'\; g(x+x'/2)g(x-x'/2)g(y+y'/2)g(y-y'/2) \times g^*(z+z'/2)g^*(z-z'/2)g^*(w+w'/2)g^*(w-w'/2) \times {\rm e}^{-m(|x'|+|y'|+|z'|+|w'|)/\nu_{\rm F}}\Big\rangle_{\rm dis}. \tag{E4}$$

There are two distinct kinds of contractions: Gaussian ones (contracting e.g. $\langle g(x+x'/2)g^*(z+z'/2)\rangle$, $\langle g(x-x'/2)g^*(z-z'/2)\rangle$, $\langle g(y+y'/2)g^*(w+w'/2)\rangle$, and $\langle g(y-y'/2)g^*(w-w'/2)\rangle$) and non-Gaussian ones, e.g. contracting $\langle g(x-x'/2)g^*(z-z'/2)\rangle$, $\langle g(x+x'/2)g^*(w+w'/2)\rangle$, $\langle g(y+y'/2)g^*(z+z'/2)\rangle$, and $\langle g(y-y'/2)g^*(w-w'/2)\rangle$. The latter yields:

$$\begin{aligned}\langle g_{\rm eff}(x)g_{\rm eff}(y)g^*_{\rm eff}(z)g^*_{\rm eff}(w)\rangle_{\rm dis} &\supset \frac{\mathcal{D}^4}{\nu_{\rm F}^4}\int {\rm d}x'{\rm d}y'{\rm d}z'{\rm d}w'\delta(x-x'/2-z+z'/2)\delta(x+x'/2-w-w'/2)\\ &\quad\times\delta(y+y'/2-z-z'/2)\delta(y-y'/2-w+w'/2)\\ &\quad\times{\rm e}^{-m(|x'|+|y'|+|z'|+|w'|)/\nu_{\rm F}}\\ &\sim \frac{\mathcal{D}^4}{\nu_{\rm F}^4}\int {\rm d}x'{\rm d}y'{\rm d}z'{\rm d}w'\delta(z'-y+x-y'/2-x'/2)\delta(w'-x\\ &\quad+y-y'/2-x'/2)\\ &\quad\times\delta(x'-2w+2z-y')\delta(z+w-x-y)\\ &\quad\times{\rm e}^{-m(|x'|+|y'|+|z'|+|w'|)/\nu_{\rm F}}\\ &\sim \frac{\mathcal{D}^4}{\nu_{\rm F}^4}\delta(z+w-x-y)\int {\rm d}y'{\rm e}^{-m(|2w-2z+y'|+|y'|+|y'-2z+2y|+|2w-2y+y'|)/\nu_{\rm F}}.\end{aligned} \tag{E5}$$

In addition to the phase space factor of $\nu_{\rm F}/m$, we obtain an exponential suppression of lengths $(w-z)$ etc larger than $\nu_{\rm F}/m$. The leading order for large distances may be extracted by formally taking the limit $m\to\infty$. The exponential may then be approximated by a δ-function: $\delta(x)=\lim_{m\to\infty}(m/\nu_{\rm F})\exp(-m|x|/\nu_{\rm F})$. Note that in the case of multiple terms in the exponent some of them might be spurious, i.e. $\exp(-m(|x|+|x|)/\nu_{\rm F})\sim(\nu_{\rm F}/m)\delta(x)$. Taking this into account the large-distance limit of equation (E5) leads to

$$\langle g_{\rm eff}(x)g_{\rm eff}(y)g^*_{\rm eff}(z)g^*_{\rm eff}(w)\rangle_{\rm dis} \sim \frac{\mathcal{D}^4}{\nu_{\rm F}^4}\delta(z+w-x-y)\frac{\nu_{\rm F}^3}{m^3}\delta(z-w)\delta(y-w). \tag{E6}$$

Higher moments are suppressed in a similar fashion. Thus, we have proven that the non-Gaussian contributions are supressed by at least the factor $\frac{\mathcal{D}^2}{(\nu_{\rm F}m)^2}$.

References

[1] Gulácsi M 2004 *Adv. Phys.* **53** 769
[2] Braunecker B, Simon P and Loss D 2009 *Phys. Rev.* B **80** 165119
[3] Klinovaja J, Stano P, Yazdani A and Loss D 2013 *Phys. Rev. Lett.* **111** 186805
[4] Gulacsi M 2004 *Adv. Phys.* **53** 769
[5] Maciejko J 2012 *Phys. Rev.* B **85** 245108
[6] Tsunetsugu H, Sigrist M and Ueda K 1997 *Rev. Mod. Phys.* **69** 809
[7] Zachar O, Kivelson S A and Emery V J 1996 *Phys. Rev. Lett.* **77** 1342
[8] Honner G and Gulacsi M 1997 *Phys. Rev. Lett.* **78** 2180
[9] Novais E, Miranda E, Castro Neto A H and Cabrera G G 2002a *Phys. Rev.* B **66** 174409
[10] Novais E, Miranda E, Castro Neto A H and Cabrera G G 2002b *Phys. Rev. Lett.* **88** 217201
[11] Shibata N, Ishii C and Ueda K 1995 *Phys. Rev.* B **51** 3626
[12] White S R and Affleck I 1996 *Phys. Rev.* B **54** 9862
[13] Juozapavicius A, McCulloch I P, Gulacsi M and Rosengren A 2002 *Phil. Mag.* B **82** 1211
[14] Pfeiffer L, Strmer H, Baldwin K, West K, Goi A, Pinczuk A, Ashoori R, Dignam M and Wegscheider W 1993 *J. Cryst. Growth* **127** 849
[15] Wegscheider W, Kang W, Pfeiffer L, West K, Stormer H and Baldwin K 1994 *Solid-State Electron.* **37** 547
[16] Tarucha S, Honda T and Saku T 1995 *Solid State Commun.* **94** 413
[17] Maslov D L 1995 *Phys. Rev.* B **52** R14368
[18] Simon F, Kramberger C, Pfeiffer R, Kuzmany H, Zólyomi V, Kürti J, Singer P M and Alloul H 2005 *Phys. Rev. Lett.* **95** 017401
[19] Rmmeli M H *et al* 2007 *J. Phys. Chem.* C **111** 4094
[20] Churchill H O H, Bestwick A J, Harlow J W, Kuemmeth F, Marcos D, Stwertka C H, Watson S K and Marcus C M 2009 *Nat. Phys.* **5** 321
[21] Rincón J, Moreo A, Alvarez G and Dagotto E 2014 *Phys. Rev. Lett.* **112** 106405
[22] Caron J M, Neilson J R, Miller D C, Llobet A and McQueen T M 2011 *Phys. Rev.* B **84** 180409
[23] Luo Q *et al* 2013 *Phys. Rev.* B **87** 024404
[24] Nambu Y *et al* 2012 *Phys. Rev.* B **85** 064413
[25] Tsvelik A M and Yevtushenko O M 2015 *Phys. Rev. Lett.* **115** 216402
[26] Moore J E and Balents L 2007 *Phys. Rev.* B **75** 121306(R)
[27] Maciejko J, Liu C, Oreg Y, Qi X L, Wu C and Zhang S C 2009 *Phys. Rev. Lett.* **102** 256803

[28] Roy R 2009 *Phys. Rev.* B **79** 195321
[29] Xu C and Moore J E 2006 *Phys. Rev.* B **73** 045322
[30] Franz M and Molenkamp L 2013 *Topological Insulators* (Amsterdam: Elsevier)
[31] Kurita M, Yamaji Y and Imada M 2015 arXiv:1511.02532
[32] Kawakami T and Hu X 2016 *J. Phys. Soc. Jpn.* **85** 013701
[33] Altshuler B L, Aleiner I L and Yudson V I 2013 *Phys. Rev. Lett.* **111** 086401
[34] Yevtushenko O M, Wugalter A, Yudson V I and Altshuler B L 2015 *EPL* **112** 57003
[35] Tsvelik A M 2003 *Quantum Field Theory in Condensed Matter Physics* (Cambridge: Cambridge University Press)
[36] Schrieffer J R 1967 *J. Appl. Phys.* **38** 1143
[37] Grishin A, Yurkevich I V and Lerner I V 2004 *Phys. Rev.* B **69** 165108
[38] Gogolin A O, Nersesyan A A and Tsvelik A M 1998 *Bosonization and Strongly Correlated Systems* (Cambridge: Cambridge University Press)
[39] Giamarchi T 2004 *Quantum Physics in One Dimension* (Oxford: Clarendon, Oxford University Press)
[40] Giamarchi T and Schulz H J 1988 *Phys. Rev.* B **37** 325
[41] Fradkin E 2013 *Field Theories of Condensed Matter Physics* (Cambridge: Cambridge University Press)
[42] Pfeiffer L, Yacoby A, Stormer H, Baldwin K, Hasen J, Pinczuk A, Wegscheider W and West K 1997 *Microelectron. J.* **28** 817
[43] Stano P, Klinovaja J, Yacoby A and Loss D 2013 *Phys. Rev.* B **88** 045441
[44] Maslov D L and Stone M 1995 *Phys. Rev.* B **52** R5539(R)
[45] Scheller C P, Liu T-M, Barak G, Yacoby A, Pfeiffer L N, West K W and Zumbühl D M 2014 *Phys. Rev. Lett.* **112** 066801

Chapter 10

Conclusion and outlook

In this work, we have extended the fRG treatment of a QPC from Matsubara [BHS+13, BHvD14, HBS+14, HBS+15] to real frequencies on the Keldysh contour. With this new treatment, we were able to unify two major competitors for the explanation of the 0.7-anomaly: spontaneous spin polarization and Kondo-like physics due to a localized state. We achieved this unification by showing that the spin noise within the QPC is slow and spin-locked, i.e. the spins fluctuate slowly and are co-oriented over a large region. Since the spin excitations are not frozen, a fully dynamical treatment is essential to extract and compare timescales (c.f. chapters 6 and 7).

As further consistency checks of the model in equilibrium in future one could compute the shot noise [DZM+06] or the spin drag.[1]

Even though the results at finite bias are at best preliminary, and significant improvement is still required, we have undertaken the first steps to extending the numerical code to non-equilibrium situations. Chapter 8 deals with some of the tricks which in future may help to push Keldysh-fRG to a reliable treatment of extended out-of-equilibrium systems.

In particular in a non-equilibrium situation, the QPC still offers enticing puzzles: While we qualitatively observe a zero-bias anomaly, we see no indication of the side-peaks generically measured in experiment, remnants of which also appear in measurements of the thermopower.[2] So far, no satisfactory explanation of these side-peaks has been given. It is an interesting question if either an enhanced feedback and channel structure (for ideas on this see [Wei14, HS09]), a modification of the flow (e.g. by taking into account more diagrams [Kv17]), or even the inclusion of long-range interactions would lead to the emergence of these side-peaks.

In a somewhat different ansatz, the fRG code that currently exists may be used to attempt the solution of other problems. For example, an application of the equilibrium Keldysh fRG

[1] Let us assume that we are able to apply a bias for up and down electrons separately. At small changes in the bias, we may write

$$\begin{pmatrix} \delta J_\uparrow \\ \delta J_\downarrow \end{pmatrix} = \begin{pmatrix} G_{\uparrow\uparrow} & G_{\uparrow\downarrow} \\ G_{\downarrow\uparrow} & G_{\downarrow\downarrow} \end{pmatrix} \begin{pmatrix} \delta\mu_\uparrow \\ \delta\mu_\downarrow \end{pmatrix}, \tag{10.1}$$

where J_σ denotes the current of particles with spin σ and δJ_σ is the change in this spin-resolved current upon the change of the bias for the spin τ by $\delta\mu_\tau$. $G_{\sigma\bar{\sigma}}$ (with $\bar{\sigma}$ denoting the spin opposite to the spin σ) is the spin drag. In a non-interacting model $G_{\sigma\bar{\sigma}}$ is manifestly zero.

[2] The thermo-power is the change in current if a temperature-bias is applied.

code to the problem of many-body-localization is currently under investigation. While the program is in principle able to handle a generic one-dimensional system of electrons with short-range interactions, it may become necessary to implement further improvements. Aside from the Katanin flow (Sec. 8.1.6), it might be necessary to improve the ODE-solver. A promising ansatz is to project the solution after each Runge-Kutta step onto a set satisfying the Ward-identity (see [ACR94] for a possible algorithm).[3]

In the context of the Kondo chain, it is interesting to follow in the footsteps of topological insulators, certain of which exhibit helical edge modes. From a theoretical and experimental perspective, one may cannibalize the literature dealing with these systems and research the extent to which the results change between the topological insulators and the Kondo chain. For example, inducing a superconducting gap through a proximity-effect may lead to interesting topological physics.

[3] The improvement of the ODE-solver was not necessary for the QPC, as we obtain good agreement with DMRG results even with a simple ODE-solver. However, in other contexts it might be of paramount importance to respect the Ward-identities better than the program does at the moment.

Bibliography

[AB59] Y. Aharonov and D. Bohm. Significance of electromagnetic potentials in the quantum theory. *Phys. Rev.*, 115:485–491, Aug 1959.

[AB92] P. Aurenche and T. Becherrawy. A Comparison of the real time and the imaginary time formalisms of finite temperature field theory for 2, 3, and 4 point Green's functions. *Nucl. Phys.*, B379:259–303, 1992.

[ACR94] Uri M. Ascher, Hongsheng Chin, and Sebastian Reich. Stabilization of daes and invariant manifolds. *Numerische Mathematik*, 67(2):131–149, Mar 1994.

[AEKM08] Sabine Andergassen, Tilman Enss, Christoph Karrasch, and Volker Meden. *A Gentle Introduction to the Functional Renormalization Group: The Kondo Effect in Quantum Dots*, pages 1–17. Springer Netherlands, Dordrecht, 2008.

[B̈88] M. Büttiker. Absence of backscattering in the quantum hall effect in multiprobe conductors. *Phys. Rev. B*, 38:9375–9389, Nov 1988.

[BHS+13] F. Bauer, J. Heyder, E. Schubert, D. Borowsky, D. Taubert, B. Bruognolo, D. Schuh, W. Wegscheider, J. von Delft, and S. Ludwig. Microscopic origin of the 0.7-anomaly in quantum point contacts. *Nature*, 501(7465):73–78, sep 2013.

[BHvD14] Florian Bauer, Jan Heyder, and Jan von Delft. Functional renormalization group approach for inhomogeneous interacting fermi systems. *Phys. Rev. B*, 89:045128, Jan 2014.

[BMF+16] B. Brun, F. Martins, S. Faniel, B. Hackens, A. Cavanna, C. Ulysse, A. Ouerghi, U. Gennser, D. Mailly, P. Simon, S. Huant, V. Bayot, M. Sanquer, and H. Sellier. Electron phase shift at the zero-bias anomaly of quantum point contacts. *Phys. Rev. Lett.*, 116:136801, Mar 2016.

[BSL09] Bernd Braunecker, Pascal Simon, and Daniel Loss. Nuclear magnetism and electron order in interacting one-dimensional conductors. *Phys. Rev. B*, 80:165119, Oct 2009.

[Cha11] Rick Chartrand. Numerical differentiation of noisy, nonsmooth data. *ISRN Applied Mathematics*, 2011, 2011.

[CLGG+02] S. M. Cronenwett, H. J. Lynch, D. Goldhaber-Gordon, L. P. Kouwenhoven, C. M. Marcus, K. Hirose, N. S. Wingreen, and V. Umansky. Low-temperature fate of the 0.7 structure in a point contact: A kondo-like correlated state in an open system. *Phys. Rev. Lett.*, 88(22):226805, May 2002.

[CSHY85] K.-c. Chou, Z.-b. Su, B.-l. Hao, and L. Yu. Equilibrium and nonequilibrium formalisms made unified. *physrep*, 118:1–131, February 1985.

[DZM+06] L. DiCarlo, Y. Zhang, D. T. McClure, D. J. Reilly, C. M. Marcus, L. N. Pfeiffer, and K. W. West. Shot-noise signatures of 0.7 structure and spin in a quantum point contact. *Phys. Rev. Lett.*, 97:036810, Jul 2006.

[FV63] R.P Feynman and F.L Vernon. The theory of a general quantum system interacting with a linear dissipative system. *Annals of Physics*, 24:118 – 173, 1963.

[Gia03] T. Giamarchi. *Quantum Physics in One Dimension*. International Series of Monographs on Physics. Clarendon Press, 2003.

[Hao81] B.-l. Hao. Closed time path Green's functions and nonlinear response theory. *Physica A Statistical Mechanics and its Applications*, 109:221–236, October 1981.

[HBS+14] J. Heyder, F. Bauer, E. Schubert, D. Borowsky, D. Taubert, B. Bruognolo, D. Schuh, W. Wegscheider, J. von Delft, and S. Ludwig. On the relation between the 0.7-anomaly and the kondo effect: Geometric crossover between a quantum point contact and a kondo quantum dot. 2014.

[HBS+15] Jan Heyder, Florian Bauer, Enrico Schubert, David Borowsky, Dieter Schuh, Werner Wegscheider, Jan von Delft, and Stefan Ludwig. Relation between the 0.7 anomaly and the kondo effect: Geometric crossover between a quantum point contact and a kondo quantum dot. *Phys. Rev. B*, 92:195401, Nov 2015. arXiv:1409.3415 [cond-mat.str-el].

[HBSvD17] Jan Heyder, Florian Bauer, Dennis Schimmel, and Jan von Delft. Derivation of oguri's linear conductance formula for interacting fermions within the keldysh formalism. *Phys. Rev. B*, 96:125141, Sep 2017.

[HS09] C. Husemann and M. Salmhofer. Efficient parametrization of the vertex function, Ω scheme, and the t, t' hubbard model at van hove filling. *Phys. Rev. B*, 79:195125, May 2009.

[ILK+13] M. J. Iqbal, Roi Levy, E. J. Koop, J. B. Dekker, J. P. de Jong, J. H. M. van der Velde, D. Reuter, A. D. Wieck, Ramon Aguado, Yigal Meir, and C. H. van der Wal. Odd and even kondo effects from emergent localization in quantum point contacts. *Nature*, 501(7465):79–83, Sep 2013.

[IZ09] S. Ihnatsenka and I. V. Zozoulenko. Origin of the "0.25 anomaly" in the nonlinear conductance of a quantum point contact. *Phys. Rev. B*, 79:235313, Jun 2009.

[Jak10] Severin Georg Jakobs. *Functional renormalization group studies of quantum transport through mesoscopic systems*. PhD thesis, Aachen, 2010. Zsfassung in dt. und engl. Sprache; Aachen, Techn. Hochsch., Diss., 2009.

[JPS10a] Severin G. Jakobs, Mikhail Pletyukhov, and Herbert Schoeller. Nonequilibrium functional rg with frequency dependent vertex function - a study of the single impurity anderson model. *Phys. Rev. B*, 81:195109, 2010.

[JPS10b] Severin G Jakobs, Mikhail Pletyukhov, and Herbert Schoeller. Properties of multi-particle green's and vertex functions within keldysh formalism. *J. Phys. A: Math. and Theor.*, 43(10):103001, 2010.

[Kam11] Alex Kamenev. *Field Theory of Non-Equilibrium Systems*. Cambridge University Press, 2011.

[Kar10] C. Karrasch. The Functional Renormalization Group for Zero-Dimensional Quantum Systems in and out of Equilibrium. *ArXiv e-prints*, September 2010.

[Kat04] A. A. Katanin. Fulfillment of ward identities in the functional renormalization group approach. *Phys. Rev. B*, 70:115109, Sep 2004.

[KBH$^+$00] A. Kristensen, H. Bruus, A. E. Hansen, J. B. Jensen, P. E. Lindelof, C. J. Marckmann, J. Nygård, C. B. Sørensen, F. Beuscher, A. Forchel, and M. Michel. Bias and temperature dependence of the 0.7 conductance anomaly in quantum point contacts. *Phys. Rev. B*, 62:10950–10957, Oct 2000.

[Kel64] L. V. Keldysh. Diagram technique for nonequilibrium processes. *Zh. Eksp. Teor. Fiz.*, 47:1515–1527, 1964. [Sov. Phys. JETP20,1018(1965)].

[KEM06] C. Karrasch, T. Enss, and V. Meden. Functional renormalization group approach to transport through correlated quantum dots. *Phys. Rev. B*, 73(23):235337, 2006.

[KM05] C. L. Kane and E. J. Mele. Quantum spin hall effect in graphene. *Phys. Rev. Lett.*, 95:226801, Nov 2005.

[KSYL13] Jelena Klinovaja, Peter Stano, Ali Yazdani, and Daniel Loss. Topological superconductivity and majorana fermions in rkky systems. *Phys. Rev. Lett.*, 111:186805, Nov 2013.

[Kub57] Ryogo Kubo. Statistical-mechanical theory of irreversible processes. i. general theory and simple applications to magnetic and conduction problems. *Journal of the Physical Society of Japan*, 12(6):570–586, 1957.

[Kub66] R Kubo. The fluctuation-dissipation theorem. *Reports on Progress in Physics*, 29(1):255, 1966.

[Kv17] F. B. Kugler and J. von Delft. Multiloop functional renormalization group for general models. *ArXiv e-prints*, July 2017.

[Lan57] Rolf Landauer. Spatial variation of currents and fields due to localized scatterers in metallic conduction. *IBM Journal of Research and Development*, 1(3):223–231, 1957.

[Lan81] Rolf Landauer. Can a length of perfect conductor have a resistance? . *Physics Letters A*, 85(2):91–93, 1981.

[Lau81] R. B. Laughlin. Quantized hall conductivity in two dimensions. *Phys. Rev. B*, 23:5632–5633, May 1981.

[Lau83] R. B. Laughlin. Anomalous quantum hall effect: An incompressible quantum fluid with fractionally charged excitations. *Phys. Rev. Lett.*, 50:1395–1398, May 1983.

[LB06] Michel Le Bellac. *Quantum Physics*. Cambridge University Press, 2006.

[LW60] J. M. Luttinger and J. C. Ward. Ground-state energy of a many-fermion system. ii. *Phys. Rev.*, 118:1417–1427, Jun 1960.

[Mat04] K. A. Matveev. Conductance of a quantum wire at low electron density. *Phys. Rev. B*, 70(24):245319, Dec 2004.

[Mic11] A P Micolich. What lurks below the last plateau: experimental studies of the $0.7 \times 2e^2/h$ conductance anomaly in one-dimensional systems. *Journal of Physics: Condensed Matter*, 23(44):443201, 2011.

[MS59] Paul C. Martin and Julian Schwinger. Theory of many-particle systems. i. *Phys. Rev.*, 115:1342–1373, Sep 1959.

[MSH+12] W. Metzner, M. Salmhofer, C. Honerkamp, V. Meden, and K. Schönhammer. Functional renormalization group approach to correlated fermion systems. *Rev. Mod. Phys.*, 84:299, 2012.

[NO88] J.W. Negele and H. Orland. *Quantum many-particle systems*. Frontiers in physics. Addison-Wesley Pub. Co., 1988.

[Ogu01] Akira Oguri. Transmission probability for interacting electrons connected to reservoirs. *J. Phys. Soc. Jap.*, 70(9):2666–2681, 2001.

[RYF+10] Y. Ren, W. W. Yu, S. M. Frolov, J. A. Folk, and W. Wegscheider. Zero-bias anomaly of quantum point contacts in the low-conductance limit. *Phys. Rev. B*, 82:045313, 2010.

[SBv17] D. H. Schimmel, B. Bruognolo, and J. von Delft. Spin Fluctuations in the 0.7 Anomaly in Quantum Point Contacts. *Physical Review Letters*, 119(19):196401, November 2017.

[SCG+15] L. M. Sieberer, A. Chiocchetta, A. Gambassi, U. C. Täuber, and S. Diehl. Thermodynamic equilibrium as a symmetry of the schwinger-keldysh action. *Phys. Rev. B*, 92:134307, Oct 2015.

[SHT+11] L. W. Smith, A. R. Hamilton, K. J. Thomas, M. Pepper, I. Farrer, J. P. Griffiths, G. A. C. Jones, and D. A. Ritchie. Compressibility measurements of quasi-one-dimensional quantum wires. *Phys. Rev. Lett.*, 107:126801, Sep 2011.

[SL13] Alfredo X. Sánchez and Jean-Pierre Leburton. Temperature modulation of the transmission barrier in quantum point contacts. *Phys. Rev. B*, 88:075305, Aug 2013.

[SMS08] Sloggett, C., Milstein, A. I., and Sushkov, O. P. Correlated electron current and temperature dependence oftheconductance of a quantum point contact. *Eur. Phys. J. B*, 61(4):427–432, 2008.

[Sre07] Mark Srednicki. *Quantum Field Theory*. Cambridge University Press, 2007.

[Tay12] J.R. Taylor. *Scattering Theory: The Quantum Theory of Nonrelativistic Collisions*. Dover Books on Engineering. Dover Publications, 2012.

[TNA+98] K. J. Thomas, J. T. Nicholls, N. J. Appleyard, M. Y. Simmons, M. Pepper, D. R. Mace, W. R. Tribe, and D. A. Ritchie. Interaction effects in a one-dimensional constriction. *Phys. Rev. B*, 58:4846–4852, Aug 1998.

[TNS+96] K. J. Thomas, J. T. Nicholls, M. Y. Simmons, M. Pepper, D. R. Mace, and D. A. Ritchie. Possible spin polarization in a one-dimensional electron gas. *Phys. Rev. Lett.*, 77(1):135–138, Jul 1996.

[TY15] A. M. Tsvelik and O. M. Yevtushenko. Quantum phase transition and protected ideal transport in a kondo chain. *Phys. Rev. Lett.*, 115:216402, Nov 2015.

[vWvHB+88] B. J. van Wees, H. van Houten, C. W. J. Beenakker, J. G. Williamson, L. P. Kouwenhoven, D. van der Marel, and C. T. Foxon. Quantized conductance of point contacts in a two-dimensional electron gas. *Phys. Rev. Lett.*, 60:848–850, Feb 1988.

[WB98] Chuan-Kui Wang and K.-F. Berggren. Local spin polarization in ballistic quantum point contacts. *Phys. Rev. B*, 57(8):4552–4556, Feb 1998.

[WBvD17] Lukas Weidinger, Florian Bauer, and Jan von Delft. Functional renormalization group approach for inhomogeneous one-dimensional fermi systems with finite-ranged interactions. *Phys. Rev. B*, 95:035122, Jan 2017.

[Wei95] Steven Weinberg. *The Quantum Theory of Fields*, volume 1. Cambridge University Press, 1995.

[Wei96] Steven Weinberg. *The Quantum Theory of Fields*, volume 2. Cambridge University Press, 1996.

[Wei14] Lukas Weidinger. Longer ranged interactions in quantum point contacts. Master's thesis, Ludwig-Maximilians-Universität München, 2014.

[Wel05] H. Arthur Weldon. Thermal four-point functions with analytic extensions. *Phys. Rev. D*, 72:096005, Nov 2005.

[WH02] Enke Wang and Ulrich Heinz. Generalized fluctuation-dissipation theorem for nonlinear response functions. *Phys. Rev. D*, 66:025008, Jul 2002.

[Wig55] Eugene P. Wigner. Lower limit for the energy derivative of the scattering phase shift. *Phys. Rev.*, 98:145–147, Apr 1955.

[WWW52] G. C. Wick, A. S. Wightman, and E. P. Wigner. The intrinsic parity of elementary particles. *Phys. Rev.*, 88:101–105, Oct 1952.

[ZJ02] J. Zinn-Justin. *Quantum Field Theory and Critical Phenomena*. International series of monographs on physics. Clarendon Press, 2002.

Appendix: Explicit derivation of the flow of the P-channel

In order to obtain the flow-equations in the channel decomposition, we consider the vertex flow in Eq. (4.36). For the P-Channel, we only keep the part of the flow equation that is proportional to the P-bubble, Eq. (4.38). If we now insert the channel decomposition, Eq. (4.32), into the flow equation of the P-Channel, the first term in Eq. (4.36), we obtain

$$\partial_\Lambda \varphi^P_{1'2'|12}(\Pi) = \frac{1}{2}(\bar{v} + \varphi^P(\Pi) + \Phi^X + \Phi^D)_{1'2'|34} I^{pp}_{34|3'4'}(\Pi)(\bar{v} + \varphi^P(\Pi) + \Phi^X + \Phi^D)_{3'4'|12}, \quad (10.2)$$

where I^{pp} was defined in Eq. (4.38) The P-bubble has the properties

$$(I^{pp})^{ab|a'b'} = 0 \;\; if \;\; a = a' = q \;\; or \;\; b = b' = q, \quad (10.3)$$

(due to the fact that $G^{qq} = 0 = S^{qq}$) and

$$(I^{pp})^{qc|cq} = 0 = (I^{pp})^{cq|qc}. \quad (10.4)$$

(the integrand is analytical in the upper/lower half plane and decays as $1/\omega^3$). Note that an infinitesimal imaginary part is attached to ω, such that $I^{pp}_{cq|qc}$ is a scalar product of retarded and advanced functions. Further note that both properties depend on the choice of flow parameter. A *physical* flow-parameter will usually respect both properties. Under complex conjugation we have:

$$(I^{pp})^{ab|a'b'}_{(\sigma_1\sigma_2)(ij|kl)}(\omega) = -(-)^{a+a'+b+b'}(I^{pp})^{a'b'|ab}_{(\sigma_2\sigma_1)(kl|ij)}(\omega)^*. \quad (10.5)$$

To proceed, let us assume that the interchannel feedback is such that it mimicks a renormalization of the bare vertex, i.e. the feedback is on-site and occurs only with a Keldysh-structure that exhibits an odd number of q components. Thus, expanding the flow equation in its full glory, we obtain

$$\begin{aligned}
&\partial_\Lambda \left(\varphi^P\right)^{qq|cq}_{(\sigma\bar{\sigma})(ii|jj)}(\Pi) = \partial_\Lambda a^P_{(\sigma\bar{\sigma})(ij)}(\Pi)^* \\
&\quad = \frac{1}{2}\left(\varphi^P(\Pi)\right)^{qq|cc}_{(\sigma\bar{\sigma}|\sigma\bar{\sigma})(ii|kl)} I^{pp}_{cc|cc}(\Pi)_{(\sigma\bar{\sigma}|\sigma\bar{\sigma})(kl|mn)} \left(\bar{v} + \varphi^P(\Pi) + \frac{1}{2}U^X + \frac{1}{2}U^D\right)^{cc|cq}_{(\sigma\bar{\sigma}|\sigma\bar{\sigma})(mn|jj)} \\
&\quad + \frac{1}{2}\left(\varphi^P(\Pi)\right)^{qq|cc}_{(\sigma\bar{\sigma}|\sigma\bar{\sigma})(ii|kl)} I^{pp}_{cc|cq}(\Pi)_{(\sigma\bar{\sigma}|\sigma\bar{\sigma})(kl|mn)} \left(\varphi^P(\Pi)\right)^{cq|cq}_{(\sigma\bar{\sigma}|\sigma\bar{\sigma})(mn|jj)}
\end{aligned}$$

$$
\begin{aligned}
&+\frac{1}{2}\left(\varphi^P(\Pi)\right)^{qq|cc}_{(\sigma\bar{\sigma}|\sigma\bar{\sigma})(ii|kl)} I^{pp}_{cc|qc}(\Pi)_{(\sigma\bar{\sigma}|\sigma\bar{\sigma})(kl|mn)} \left(\varphi^P(\Pi)\right)^{qc|cq}_{(\sigma\bar{\sigma}|\sigma\bar{\sigma})(mn|jj)}\\
&+\frac{1}{2}\left(\bar{v}+\varphi^P(\Pi)+\frac{1}{2}U^X_+\frac{1}{2}U^D\right)^{qq|cq}_{(\sigma\bar{\sigma}|\sigma\bar{\sigma})(ii|kl)} I^{pp}_{cq|cc}(\Pi)_{(\sigma\bar{\sigma}|\sigma\bar{\sigma})(kl|mn)}\\
&\quad\times\left(\bar{v}+\varphi^P(\Pi)+\frac{1}{2}U^X+\frac{1}{2}U^D\right)^{cc|cq}_{(\sigma\bar{\sigma}|\sigma\bar{\sigma})(mn|jj)}\\
&+\frac{1}{2}\left(\bar{v}+\varphi^P(\Pi)+\frac{1}{2}U^X+\frac{1}{2}U^D\right)^{qq|qc}_{(\sigma\bar{\sigma}|\sigma\bar{\sigma})(ii|kl)} I^{pp}_{qc|cc}(\Pi)_{(\sigma\bar{\sigma}|\sigma\bar{\sigma})(kl|mn)}\\
&\quad\times\left(\bar{v}+\varphi^P(\Pi)+\frac{1}{2}U^X+\frac{1}{2}U^D\right)^{cc|cq}_{(\sigma\bar{\sigma}|\sigma\bar{\sigma})(mn|jj)}\\
&+\frac{1}{2}\left(\bar{v}+\varphi^P(\Pi)+\frac{1}{2}U^X+\frac{1}{2}U^D\right)^{qq|qc}_{(\sigma\bar{\sigma}|\sigma\bar{\sigma})(ii|kl)} I^{pp}_{qc|qc}(\Pi)_{(\sigma\bar{\sigma}|\sigma\bar{\sigma})(kl|mn)} \left(\varphi^P(\Pi)\right)^{qc|cq}_{(\sigma\bar{\sigma}|\sigma\bar{\sigma})(mn|jj)}\\
&+\frac{1}{2}\left(\bar{v}+\varphi^P(\Pi)+\frac{1}{2}U^X+\frac{1}{2}U^D\right)^{qq|cq}_{(\sigma\bar{\sigma}|\sigma\bar{\sigma})(ii|kl)} I^{pp}_{cq|cq}(\Pi)_{(\sigma\bar{\sigma}|\sigma\bar{\sigma})(kl|mn)} \left(\varphi^P(\Pi)\right)^{cq|cq}_{(\sigma\bar{\sigma}|\sigma\bar{\sigma})(mn|jj)}\\
&+\frac{1}{2}\left(\varphi^P(\Pi)\right)^{qq|cc}_{(\sigma\bar{\sigma}|\bar{\sigma}\sigma)(ii|kl)} I^{pp}_{cc|cc}(\Pi)_{(\bar{\sigma}\sigma|\bar{\sigma}\sigma)(kl|mn)} \left(\bar{v}+\varphi^P(\Pi)-\frac{1}{2}U^D-\frac{1}{2}U^X\right)^{cc|cq}_{(\bar{\sigma}\sigma|\sigma\bar{\sigma})(mn|jj)}\\
&+\frac{1}{2}\left(\varphi^P(\Pi)\right)^{qq|cc}_{(\sigma\bar{\sigma}|\bar{\sigma}\sigma)(ii|kl)} I^{pp}_{cc|cq}(\Pi)_{(\bar{\sigma}\sigma|\bar{\sigma}\sigma)(kl|mn)} \left(\varphi^P(\Pi)\right)^{cq|cq}_{(\bar{\sigma}\sigma|\sigma\bar{\sigma})(mn|jj)}\\
&+\frac{1}{2}\left(\varphi^P(\Pi)\right)^{qq|cc}_{(\sigma\bar{\sigma}|\bar{\sigma}\sigma)(ii|kl)} I^{pp}_{cc|qc}(\Pi)_{(\bar{\sigma}\sigma|\bar{\sigma}\sigma)(kl|mn)} \left(\varphi^P(\Pi)\right)^{qc|cq}_{(\bar{\sigma}\sigma|\sigma\bar{\sigma})(mn|jj)}\\
&+\frac{1}{2}\left(\bar{v}+\varphi^P(\Pi)-\frac{1}{2}U^D-\frac{1}{2}U^X\right)^{qq|cq}_{(\sigma\bar{\sigma}|\bar{\sigma}\sigma)(ii|kl)} I^{pp}_{cq|cc}(\Pi)_{(\bar{\sigma}\sigma|\bar{\sigma}\sigma)(kl|mn)}\\
&\quad\times\left(\bar{v}+\varphi^P(\Pi)+-\frac{1}{2}U^D-\frac{1}{2}U^X\right)^{cc|cq}_{(\bar{\sigma}\sigma|\sigma\bar{\sigma})(mn|jj)}\\
&+\frac{1}{2}\left(\bar{v}+\varphi^P(\Pi)-\frac{1}{2}U^D-\frac{1}{2}U^X\right)^{qq|qc}_{(\sigma\bar{\sigma}|\bar{\sigma}\sigma)(ii|kl)} I^{pp}_{qc|cc}(\Pi)_{(\bar{\sigma}\sigma|\bar{\sigma}\sigma)(kl|mn)}\\
&\quad\times\left(\bar{v}+\varphi^P(\Pi)-\frac{1}{2}U^D-\frac{1}{2}U^X\right)^{cc|cq}_{(\bar{\sigma}\sigma|\sigma\bar{\sigma})(mn|jj)}\\
&+\frac{1}{2}\left(\bar{v}+\varphi^P(\Pi)-\frac{1}{2}U^D-\frac{1}{2}U^X\right)^{qq|qc}_{(\sigma\bar{\sigma}|\bar{\sigma}\sigma)(ii|kl)} I^{pp}_{qc|qc}(\Pi)_{(\bar{\sigma}\sigma|\bar{\sigma}\sigma)(kl|mn)} \left(\varphi^P(\Pi)\right)^{qc|cq}_{(\bar{\sigma}\sigma|\sigma\bar{\sigma})(mn|jj)}\\
&+\frac{1}{2}\left(\bar{v}+\varphi^P(\Pi)-\frac{1}{2}U^D-\frac{1}{2}U^X\right)^{qq|cq}_{(\sigma\bar{\sigma}|\bar{\sigma}\sigma)(ii|kl)} I^{pp}_{cq|cq}(\Pi)_{(\bar{\sigma}\sigma|\bar{\sigma}\sigma)(kl|mn)} \left(\varphi^P(\Pi)\right)^{cq|cq}_{(\bar{\sigma}\sigma|\sigma\bar{\sigma})(mn|jj)}
\end{aligned}
\tag{10.6}
$$

where we have used that the $cc|cc$ component of the vertex vanishes. Inserting the representation Eq. (4.34a), we obtain

$$
\begin{aligned}
&\partial_\Lambda \left(\varphi^P\right)^{qq|cq}_{\sigma\bar{\sigma}}(\Pi) \\
&\quad= \frac{1}{2}\left(\frac{U}{2} + a^P(\Pi)^*_{(\sigma\bar{\sigma}|\sigma\bar{\sigma})(ki)} + \frac{1}{2}U^X_\Lambda + \frac{1}{2}U^D_\Lambda\right) I^{pp}_{cq|cc}(\Pi)_{(\sigma\bar{\sigma}|\sigma\bar{\sigma})(kk|mm)} \\
&\qquad\times \left(\frac{U}{2} + a^P(\Pi)^*_{(\sigma\bar{\sigma}|\sigma\bar{\sigma})(jm)} + \frac{1}{2}U^X_\Lambda + \frac{1}{2}U^D_\Lambda\right) \\
&\quad+ \frac{1}{2}\left(\frac{U}{2} + a^P(\Pi)^*_{(\sigma\bar{\sigma}|\sigma\bar{\sigma})(ki)} + \frac{1}{2}U^X_\Lambda + \frac{1}{2}U^D_\Lambda\right) I^{pp}_{qc|cc}(\Pi)_{(\sigma\bar{\sigma}|\sigma\bar{\sigma})(kk|mm)} \\
&\qquad\times \left(\frac{U}{2} + a^P(\Pi)^*_{(\sigma\bar{\sigma}|\sigma\bar{\sigma})(jm)} + \frac{1}{2}U^X_\Lambda + \frac{1}{2}U^D_\Lambda\right) \\
&\quad+ \frac{1}{2}\left(\frac{U}{2} + a^P(\Pi)^*_{(\sigma\bar{\sigma}|\sigma\bar{\sigma})(ki)} + \frac{1}{2}U^X_\Lambda + \frac{1}{2}U^D_\Lambda\right) I^{pp}_{qc|qc}(\Pi)_{(\sigma\bar{\sigma}|\sigma\bar{\sigma})(kk|mm)} \left(b^P(\Pi)\right)_{(\sigma\bar{\sigma}|\sigma\bar{\sigma})(mj)} \\
&\quad+ \frac{1}{2}\left(\frac{U}{2} + a^P(\Pi)^*_{(\sigma\bar{\sigma}|\sigma\bar{\sigma})(ki)} + \frac{1}{2}U^X_\Lambda + \frac{1}{2}U^D_\Lambda\right) I^{pp}_{cq|cq}(\Pi)_{(\sigma\bar{\sigma}|\sigma\bar{\sigma})(kk|mm)} \left(b^P(\Pi)\right)_{(\sigma\bar{\sigma}|\sigma\bar{\sigma})(mj)} \\
&\quad+ \frac{1}{2}\left(-\frac{U}{2} - a^P(\Pi)^*_{(\sigma\bar{\sigma}|\sigma\bar{\sigma})(ki)} - \frac{1}{2}U^D_\Lambda - \frac{1}{2}U^X_\Lambda\right) I^{pp}_{cq|cc}(\Pi)_{(\bar{\sigma}\sigma|\bar{\sigma}\sigma)(kk|mm)} \\
&\qquad\times \left(-\frac{U}{2} - a^P(\Pi)^*_{(\sigma\bar{\sigma}|\sigma\bar{\sigma})(jm)} - \frac{1}{2}U^D_\Lambda - \frac{1}{2}U^X_\Lambda\right) \\
&\quad+ \frac{1}{2}\left(-\frac{U}{2} - a^P(\Pi)^*_{(\sigma\bar{\sigma}|\sigma\bar{\sigma})(ki)} - \frac{1}{2}U^D_\Lambda - \frac{1}{2}U^X_\Lambda\right) I^{pp}_{qc|cc}(\Pi)_{(\bar{\sigma}\sigma|\bar{\sigma}\sigma)(kk|mm)} \\
&\qquad\times \left(-\frac{U}{2} - a^P(\Pi)^*_{(\sigma\bar{\sigma}|\sigma\bar{\sigma})(jm)} - \frac{1}{2}U^D_\Lambda - \frac{1}{2}U^X_\Lambda\right) \\
&\quad+ \frac{1}{2}\left(-\frac{U}{2} - a^P(\Pi)^*_{(\sigma\bar{\sigma}|\sigma\bar{\sigma})(ki)} - \frac{1}{2}U^D_\Lambda - \frac{1}{2}U^X_\Lambda\right) I^{pp}_{qc|qc}(\Pi)_{(\bar{\sigma}\sigma|\bar{\sigma}\sigma)(kk|mm)} \left(-b^P(\Pi)\right)_{(\sigma\bar{\sigma}|\sigma\bar{\sigma})(mj)} \\
&\quad+ \frac{1}{2}\left(-\frac{U}{2} - a^P(\Pi)^*_{(\sigma\bar{\sigma}|\sigma\bar{\sigma})(ik)} - \frac{1}{2}U^D_\Lambda - \frac{1}{2}U^X_\Lambda\right) I^{pp}_{cq|cq}(\Pi)_{(\bar{\sigma}\sigma|\bar{\sigma}\sigma)(kk|mm)} \left(-b^P(\Pi)\right)_{(\sigma\bar{\sigma}|\sigma\bar{\sigma})(mj)}
\end{aligned}
\tag{10.7}
$$

Using that $I_{cq|cq} = 0 = I_{qc|qc}$, we simplify to

$$
\begin{aligned}
&\partial_\Lambda \left(\varphi^P\right)^{qq|cq}_{\sigma\bar{\sigma}}(\Pi) \\
&\quad= \left(\frac{U}{2} + a^P(\Pi)^*_{(\sigma\bar{\sigma}|\sigma\bar{\sigma})(ki)} + \frac{1}{2}U^X_\Lambda + \frac{1}{2}U^D_\Lambda\right) I^{pp}_{cq|cc}(\Pi)_{(\sigma\bar{\sigma}|\sigma\bar{\sigma})(kk|mm)} \\
&\qquad\times \left(\frac{U}{2} + a^P(\Pi)^*_{(\sigma\bar{\sigma}|\sigma\bar{\sigma})(jm)} + \frac{1}{2}U^X_\Lambda + \frac{1}{2}U^D_\Lambda\right) \\
&\quad+ \left(\frac{U}{2} + a^P(\Pi)^*_{(\sigma\bar{\sigma}|\sigma\bar{\sigma})(ki)} + \frac{1}{2}U^X_\Lambda + \frac{1}{2}U^D_\Lambda\right) I^{pp}_{qc|cc}(\Pi)_{(\sigma\bar{\sigma}|\sigma\bar{\sigma})(kk|mm)} \\
&\qquad\times \left(\frac{U}{2} + a^P(\Pi)^*_{(\sigma\bar{\sigma}|\sigma\bar{\sigma})(jm)} + \frac{1}{2}U^X_\Lambda + \frac{1}{2}U^D_\Lambda\right)
\end{aligned}
\tag{10.8}
$$

$$= \left(\frac{U}{2} + a^P(\Pi)^*_{(\sigma\bar{\sigma}|\sigma\bar{\sigma})(ki)} + \frac{1}{2}U^X_\Lambda + \frac{1}{2}U^D_\Lambda\right)\left(I^{pp}_{cq|cc}(\Pi)_{(\sigma\bar{\sigma}|\sigma\bar{\sigma})(kk|mm)} + I^{pp}_{qc|cc}(\Pi)_{(\sigma\bar{\sigma}|\sigma\bar{\sigma})(kk|mm)}\right)$$
$$\times \left(\frac{U}{2} + a^P(\Pi)^*_{(\sigma\bar{\sigma}|\sigma\bar{\sigma})(jm)} + \frac{1}{2}U^X_\Lambda + \frac{1}{2}U^D_\Lambda\right), \tag{10.9}$$

which is just Eq. (4.40a).

Further, in the P-channel we need (where indices only refer to φ and I, not to the U's):

$$\begin{aligned}
&\partial_\Lambda \left(\varphi^P\right)^{cq|cq}_{(\sigma\bar{\sigma})(ii|jj)}(\Pi) = \partial_\Lambda b^P_{(\sigma\bar{\sigma})(ij)}(\Pi)\\
&= \frac{1}{2}\left(\frac{1}{2}U + \varphi^P(\Pi) + \frac{1}{2}U^X + \frac{1}{2}U^D\right)^{cq|cc}_{(\sigma\bar{\sigma}|\sigma\bar{\sigma})(ik)} I^{pp}_{cc|cc}(\Pi)_{(\sigma\bar{\sigma}|\sigma\bar{\sigma})(kk|mm)}\\
&\qquad\times\left(\frac{1}{2}U + \varphi^P(\Pi) + \frac{1}{2}U^X + \frac{1}{2}U^D\right)^{cc|cq}_{(\sigma\bar{\sigma}|\sigma\bar{\sigma})(mj)}\\
&+\frac{1}{2}\left(\varphi^P(\Pi)\right)^{cq|qc}_{(\sigma\bar{\sigma}|\sigma\bar{\sigma})(ik)} I^{pp}_{qc|cc}(\Pi)_{(\sigma\bar{\sigma}|\sigma\bar{\sigma})(kk|mm)}\left(\frac{1}{2}U + \varphi^P(\Pi) + \frac{1}{2}U^X + \frac{1}{2}U^D\right)^{cc|cq}_{(\sigma\bar{\sigma}|\sigma\bar{\sigma})(mj)}\\
&+\frac{1}{2}\left(\varphi^P(\Pi)\right)^{cq|cq}_{(\sigma\bar{\sigma}|\sigma\bar{\sigma})(ik)} I^{pp}_{cq|cc}(\Pi)_{(\sigma\bar{\sigma}|\sigma\bar{\sigma})(kk|mm)}\left(\frac{1}{2}U + \varphi^P(\Pi) + \frac{1}{2}U^X + \frac{1}{2}U^D\right)^{cc|cq}_{(\sigma\bar{\sigma}|\sigma\bar{\sigma})(mj)}\\
&+\frac{1}{2}\left(\frac{1}{2}U + \varphi^P(\Pi) + \frac{1}{2}U^X + \frac{1}{2}U^D\right)^{cq|cc}_{(\sigma\bar{\sigma}|\sigma\bar{\sigma})(ik)} I^{pp}_{cc|qc}(\Pi)_{(\sigma\bar{\sigma}|\sigma\bar{\sigma})(kk|mm)}\left(\varphi^P(\Pi)\right)^{qc|cq}_{(\sigma\bar{\sigma}|\sigma\bar{\sigma})(mj)}\\
&+\frac{1}{2}\left(\frac{1}{2}U + \varphi^P(\Pi) + \frac{1}{2}U^X + \frac{1}{2}U^D\right)^{cq|cc}_{(\sigma\bar{\sigma}|\sigma\bar{\sigma})(ik)} I^{pp}_{cc|cq}(\Pi)_{(\sigma\bar{\sigma}|\sigma\bar{\sigma})(kk|mm)}\left(\varphi^P(\Pi)\right)^{cq|cq}_{(\sigma\bar{\sigma}|\sigma\bar{\sigma})(mj)}\\
&+\frac{1}{2}\left(\varphi^P(\Pi)\right)^{cq|cq}_{(\sigma\bar{\sigma}|\sigma\bar{\sigma})(ik)} I^{pp}_{cq|qc}(\Pi)_{(\sigma\bar{\sigma}|\sigma\bar{\sigma})(kk|mm)}\left(\varphi^P(\Pi)\right)^{qc|cq}_{(\sigma\bar{\sigma}|\sigma\bar{\sigma})(mj)}\\
&+\frac{1}{2}\left(\varphi^P(\Pi)\right)^{cq|qc}_{(\sigma\bar{\sigma}|\sigma\bar{\sigma})(ik)} I^{pp}_{qc|cq}(\Pi)_{(\sigma\bar{\sigma}|\sigma\bar{\sigma})(kk|mm)}\left(\varphi^P(\Pi)\right)^{cq|cq}_{(\sigma\bar{\sigma}|\sigma\bar{\sigma})(mj)}\\
&+\frac{1}{2}\left(\frac{1}{2}U + \varphi^P(\Pi) + \frac{1}{2}U^X + \frac{1}{2}U^X\right)^{cq|qq}_{(\sigma\bar{\sigma}|\sigma\bar{\sigma})(ik)} I^{pp}_{qq|cc}(\Pi)_{(\sigma\bar{\sigma}|\sigma\bar{\sigma})(kk|mm)}\\
&\qquad\times\left(\frac{1}{2}U + \varphi^P(\Pi) + \frac{1}{2}U^X + \frac{1}{2}U^X\right)^{cc|cq}_{(\sigma\bar{\sigma}|\sigma\bar{\sigma})(mj)}\\
&+\frac{1}{2}\left(\frac{1}{2}U + \varphi^P(\Pi) + \frac{1}{2}U^X + \frac{1}{2}U^X\right)^{cq|cc}_{(\sigma\bar{\sigma}|\sigma\bar{\sigma})(ik)} I^{pp}_{cc|qq}(\Pi)_{(\sigma\bar{\sigma}|\sigma\bar{\sigma})(kk|mm)}\\
&\qquad\times\left(\frac{1}{2}U + \varphi^P(\Pi) + \frac{1}{2}U^X + \frac{1}{2}U^X\right)^{qq|cq}_{(\sigma\bar{\sigma}|\sigma\bar{\sigma})(mj)}\\
&+\frac{1}{2}\left(-\frac{1}{2}U + \varphi^P(\Pi) - \frac{1}{2}U^X - \frac{1}{2}U^D\right)^{cq|cc}_{(\sigma\bar{\sigma}|\bar{\sigma}\sigma)(ik)} I^{pp}_{cc|cc}(\Pi)_{(\bar{\sigma}\sigma|\bar{\sigma}\sigma)(kk|mm)}
\end{aligned}$$

$$
\begin{aligned}
&\times \left(-\frac{1}{2}U+\varphi^P(\Pi)-\frac{1}{2}U^X-\frac{1}{2}U^D\right)^{cc|cq}_{(\bar\sigma\sigma|\bar\sigma\sigma)(mj)}\\
&+\frac{1}{2}\left(\varphi^P(\Pi)\right)^{cq|qc}_{(\sigma\bar\sigma|\bar\sigma\sigma)(ik)} I^{pp}_{qc|cc}(\Pi)_{(\bar\sigma\sigma|\bar\sigma\sigma)(kk|mm)} \left(-\frac{1}{2}U+\varphi^P(\Pi)-\frac{1}{2}U^X-\frac{1}{2}U^D\right)^{cc|cq}_{(\bar\sigma\sigma|\sigma\bar\sigma)(mj)}\\
&+\frac{1}{2}\left(\varphi^P(\Pi)\right)^{cq|cq}_{(\sigma\bar\sigma|\bar\sigma\sigma)(ik)} I^{pp}_{cq|cc}(\Pi)_{(\bar\sigma\sigma|\bar\sigma\sigma)(kk|mm)} \left(-\frac{1}{2}U+\varphi^P(\Pi)-\frac{1}{2}U^X-\frac{1}{2}U^D\right)^{cc|cq}_{(\bar\sigma\sigma|\sigma\bar\sigma)(mj)}\\
&+\frac{1}{2}\left(-\frac{1}{2}U+\varphi^P(\Pi)-\frac{1}{2}U^X-\frac{1}{2}U^D\right)^{cq|cc}_{(\sigma\bar\sigma|\bar\sigma\sigma)(ik)} I^{pp}_{cc|qc}(\Pi)_{(\bar\sigma\sigma|\bar\sigma\sigma)(kk|mm)} \left(\varphi^P(\Pi)\right)^{qc|cq}_{(\bar\sigma\sigma|\sigma\bar\sigma)(mj)}\\
&+\frac{1}{2}\left(-\frac{1}{2}U+\varphi^P(\Pi)-\frac{1}{2}U^X-\frac{1}{2}U^D\right)^{cq|cc}_{(\sigma\bar\sigma|\bar\sigma\sigma)(ik)} I^{pp}_{cc|cq}(\Pi)_{(\bar\sigma\sigma|\bar\sigma\sigma)(kk|mm)} \left(\varphi^P(\Pi)\right)^{cq|cq}_{(\bar\sigma\sigma|\sigma\bar\sigma)(mj)}\\
&+\frac{1}{2}\left(\varphi^P(\Pi)\right)^{cq|cq}_{(\sigma\bar\sigma|\bar\sigma\sigma)(ik)} I^{pp}_{cq|qc}(\Pi)_{(\bar\sigma\sigma|\bar\sigma\sigma)(kk|mm)} \left(\varphi^P(\Pi)\right)^{qc|cq}_{(\bar\sigma\sigma|\sigma\bar\sigma)(mj)}\\
&+\frac{1}{2}\left(\varphi^P(\Pi)\right)^{cq|qc}_{(\sigma\bar\sigma|\bar\sigma\sigma)(ik)} I^{pp}_{qc|cq}(\Pi)_{(\bar\sigma\sigma|\bar\sigma\sigma)(kk|mm)} \left(\varphi^P(\Pi)\right)^{cq|cq}_{(\bar\sigma\sigma|\sigma\bar\sigma)(mj)}\\
&+\frac{1}{2}\left(-\frac{1}{2}U+\varphi^P(\Pi)-\frac{1}{2}U^X-\frac{1}{2}U^X\right)^{cq|qq}_{(\sigma\bar\sigma|\bar\sigma\sigma)(ik)} I^{pp}_{qq|cc}(\Pi)_{(\bar\sigma\sigma|\bar\sigma\sigma)(kk|mm)}\\
&\quad\times \left(-\frac{1}{2}U+\varphi^P(\Pi)-\frac{1}{2}U^X-\frac{1}{2}U^X\right)^{cc|cq}_{(\bar\sigma\sigma|\sigma\bar\sigma)(mj)}\\
&+\frac{1}{2}\left(-\frac{1}{2}U+\varphi^P(\Pi)-\frac{1}{2}U^X-\frac{1}{2}U^X\right)^{cq|cc}_{(\sigma\bar\sigma|\bar\sigma\sigma)(ik)} I^{pp}_{cc|qq}(\Pi)_{(\bar\sigma\sigma|\bar\sigma\sigma)(kk|mm)}\\
&\quad\times \left(-\frac{1}{2}U+\varphi^P(\Pi)-\frac{1}{2}U^X-\frac{1}{2}U^X\right)^{qq|cq}_{(\bar\sigma\sigma|\sigma\bar\sigma)(mj)}
\end{aligned}
\tag{10.10}
$$

$$
\begin{aligned}
&\partial_\Lambda \left(\varphi^P\right)^{cq|cq}_{(\sigma\bar\sigma)(ii|jj)}(\Pi) = \partial_\Lambda b^P_{(\sigma\bar\sigma)(ij)}(\Pi)\\
&\quad=\frac{1}{2}\left(\frac{1}{2}U+a^P_{(\sigma\bar\sigma)(ik)}(\Pi)+\frac{1}{2}U^X+\frac{1}{2}U^D\right) I^{pp}_{cc|cc}(\Pi)_{(\sigma\bar\sigma|\sigma\bar\sigma)(kk|mm)}\\
&\qquad\times\left(\frac{1}{2}U+a^{P*}_{(\sigma\bar\sigma)(jm)}(\Pi)+\frac{1}{2}U^X+\frac{1}{2}U^D\right)\\
&\quad+\frac{1}{2}\left(b^P(\Pi)\right)_{(\sigma\bar\sigma|\sigma\bar\sigma)(ik)} I^{pp}_{qc|cc}(\Pi)_{(\sigma\bar\sigma|\sigma\bar\sigma)(kk|mm)}\left(\frac{1}{2}U+a^{P*}_{(\sigma\bar\sigma)(jm)}(\Pi)+\frac{1}{2}U^X+\frac{1}{2}U^D\right)\\
&\quad+\frac{1}{2}\left(b^P_{(\sigma\bar\sigma)(ik)}(\Pi)\right)^{cq|cq} I^{pp}_{cq|cc}(\Pi)_{(\sigma\bar\sigma|\sigma\bar\sigma)(kk|mm)}\left(\frac{1}{2}U+a^{P*}_{(\sigma\bar\sigma)(jm)}(\Pi)+\frac{1}{2}U^X+\frac{1}{2}U^D\right)\\
&\quad+\frac{1}{2}\left(\frac{1}{2}U+a^P_{(\sigma\bar\sigma)(ik)}(\Pi)+\frac{1}{2}U^X+\frac{1}{2}U^D\right) I^{pp}_{cc|qc}(\Pi)_{(\sigma\bar\sigma|\sigma\bar\sigma)(kk|mm)}\left(b^P(\Pi)\right)_{(\sigma\bar\sigma)(mj)}
\end{aligned}
$$

$$
\begin{aligned}
&+\frac{1}{2}\left(\frac{1}{2}U+a^{P}_{(\sigma\bar{\sigma})(ik)}(\Pi)+\frac{1}{2}U^{X}+\frac{1}{2}U^{D}\right)I^{pp}_{cc|cq}(\Pi)_{(\sigma\bar{\sigma}|\sigma\bar{\sigma})(kk|mm)}\left(b^{P}(\Pi)\right)_{(\sigma\bar{\sigma})(mj)}\\
&+\frac{1}{2}\left(\frac{1}{2}U+a^{P}_{(\sigma\bar{\sigma})(ik)}(\Pi)+\frac{1}{2}U^{X}+\frac{1}{2}U^{X}\right)I^{pp}_{qq|cc}(\Pi)_{(\sigma\bar{\sigma}|\sigma\bar{\sigma})(kk|mm)}\\
&\quad\times\left(\frac{1}{2}U+a^{P*}_{(\sigma\bar{\sigma})(jm)}(\Pi)+\frac{1}{2}U^{X}+\frac{1}{2}U^{X}\right)\\
&+\frac{1}{2}\left(\frac{1}{2}U+a^{P}_{(\sigma\bar{\sigma})(ik)}(\Pi)+\frac{1}{2}U^{X}+\frac{1}{2}U^{X}\right)I^{pp}_{cc|qq}(\Pi)_{(\sigma\bar{\sigma}|\sigma\bar{\sigma})(kk|mm)}\\
&\quad\times\left(\frac{1}{2}U+a^{P*}_{(\sigma\bar{\sigma})(jm)}(\Pi)+\frac{1}{2}U^{X}+\frac{1}{2}U^{X}\right)\\
&+\frac{1}{2}\left(-\frac{1}{2}U-a^{P}_{(\sigma\bar{\sigma})(ik)}(\Pi)-\frac{1}{2}U^{X}-\frac{1}{2}U^{D}\right)I^{pp}_{cc|cc}(\Pi)_{(\sigma\bar{\sigma}|\sigma\bar{\sigma})(kk|mm)}\\
&\quad\times\left(-\frac{1}{2}U-a^{P*}_{(\sigma\bar{\sigma})(jm)}(\Pi)-\frac{1}{2}U^{X}-\frac{1}{2}U^{D}\right)\\
&+\frac{1}{2}\left(-b^{P}(\Pi)\right)_{(\sigma\bar{\sigma})(ik)}I^{pp}_{cq|cc}(\Pi)_{(\sigma\bar{\sigma}|\sigma\bar{\sigma})(kk|mm)}\left(-\frac{1}{2}U-a^{P*}_{(\sigma\bar{\sigma})(jm)}(\Pi)-\frac{1}{2}U^{X}-\frac{1}{2}U^{D}\right)\\
&+\frac{1}{2}\left(-b^{P}(\Pi)\right)_{(\sigma\bar{\sigma})(ik)}I^{pp}_{qc|cc}(\Pi)_{(\sigma\bar{\sigma}|\sigma\bar{\sigma})(kk|mm)}\left(-\frac{1}{2}U-a^{P*}_{(\sigma\bar{\sigma})(jm)}(\Pi)-\frac{1}{2}U^{X}-\frac{1}{2}U^{D}\right)\\
&+\frac{1}{2}\left(-\frac{1}{2}U-a^{P}_{(\sigma\bar{\sigma})(ik)}(\Pi)-\frac{1}{2}U^{X}-\frac{1}{2}U^{D}\right)I^{pp}_{cc|cq}(\Pi)_{(\sigma\bar{\sigma}|\sigma\bar{\sigma})(kk|mm)}\left(-b^{P}(\Pi)\right)_{(\sigma\bar{\sigma})(mj)}\\
&+\frac{1}{2}\left(-\frac{1}{2}U-a^{P}_{(\sigma\bar{\sigma})(ik)}(\Pi)-\frac{1}{2}U^{X}-\frac{1}{2}U^{D}\right)I^{pp}_{cc|qc}(\Pi)_{(\sigma\bar{\sigma}|\sigma\bar{\sigma})(kk|mm)}\left(-b^{P}(\Pi)\right)_{(\sigma\bar{\sigma})(mj)}\\
&+\frac{1}{2}\left(-\frac{1}{2}U-a^{P}_{(\sigma\bar{\sigma})(ik)}(\Pi)-\frac{1}{2}U^{X}-\frac{1}{2}U^{X}\right)I^{pp}_{qq|cc}(\Pi)_{(\sigma\bar{\sigma}|\sigma\bar{\sigma})(kk|mm)}\\
&\quad\times\left(-\frac{1}{2}U-a^{P*}_{(\sigma\bar{\sigma})(jm)}(\Pi)-\frac{1}{2}U^{X}-\frac{1}{2}U^{X}\right)\\
&+\frac{1}{2}\left(-\frac{1}{2}U-a^{P}_{(\sigma\bar{\sigma})(ik)}(\Pi)-\frac{1}{2}U^{X}-\frac{1}{2}U^{X}\right)I^{pp}_{cc|qq}(\Pi)_{(\sigma\bar{\sigma}|\sigma\bar{\sigma})(kk|mm)}\\
&\quad\times\left(-\frac{1}{2}U-a^{P*}_{(\sigma\bar{\sigma})(jm)}(\Pi)-\frac{1}{2}U^{X}-\frac{1}{2}U^{X}\right)
\end{aligned}
\tag{10.11}
$$

$$
\begin{aligned}
&\partial_{\Lambda}\left(\varphi^{P}\right)^{cq|cq}_{(\sigma\bar{\sigma})(ii|jj)}(\Pi)=\partial_{\Lambda}b^{P}_{(\sigma\bar{\sigma})(ij)}(\Pi)\\
&\quad=\left(\frac{1}{2}U+a^{P}_{(\sigma\bar{\sigma})(ik)}(\Pi)+\frac{1}{2}U^{X}+\frac{1}{2}U^{D}\right)I^{pp}_{cc|cc}(\Pi)_{(\sigma\bar{\sigma}|\sigma\bar{\sigma})(kk|mm)}\\
&\qquad\times\left(\frac{1}{2}U+a^{P*}_{(\sigma\bar{\sigma})(jm)}(\Pi)+\frac{1}{2}U^{X}+\frac{1}{2}U^{D}\right)\\
&\quad+\left(\frac{1}{2}U+a^{P}_{(\sigma\bar{\sigma})(ik)}(\Pi)+\frac{1}{2}U^{X}+\frac{1}{2}U^{X}\right)I^{pp}_{qq|cc}(\Pi)_{(\sigma\bar{\sigma}|\sigma\bar{\sigma})(kk|mm)}
\end{aligned}
$$

$$
\begin{aligned}
&\times \left(\frac{1}{2}U + a^{P*}_{(\sigma\bar{\sigma})(jm)}(\Pi) + \frac{1}{2}U^X + \frac{1}{2}U^X\right) \\
&+ \left(\frac{1}{2}U + a^{P}_{(\sigma\bar{\sigma})(ik)}(\Pi) + \frac{1}{2}U^X + \frac{1}{2}U^X\right) I^{pp}_{cc|qq}(\Pi)_{(\sigma\bar{\sigma}|\sigma\bar{\sigma})(kk|mm)} \\
&\times \left(\frac{1}{2}U + a^{P*}_{(\sigma\bar{\sigma})(jm)}(\Pi) + \frac{1}{2}U^X + \frac{1}{2}U^X\right) \\
&+ \left(b^P(\Pi)\right)_{(\sigma\bar{\sigma}|\sigma\bar{\sigma})(ik)} I^{pp}_{qc|cc}(\Pi)_{(\sigma\bar{\sigma}|\sigma\bar{\sigma})(kk|mm)} \left(\frac{1}{2}U + a^{P*}_{(\sigma\bar{\sigma})(jm)}(\Pi) + \frac{1}{2}U^X + \frac{1}{2}U^D\right) \\
&+ \left(b^{P}_{(\sigma\bar{\sigma})(ik)}(\Pi)\right)^{cq|cq} I^{pp}_{cq|cc}(\Pi)_{(\sigma\bar{\sigma}|\sigma\bar{\sigma})(kk|mm)} \left(\frac{1}{2}U + a^{P*}_{(\sigma\bar{\sigma})(jm)}(\Pi) + \frac{1}{2}U^X + \frac{1}{2}U^D\right) \\
&+ \left(\frac{1}{2}U + a^{P}_{(\sigma\bar{\sigma})(ik)}(\Pi) + \frac{1}{2}U^X + \frac{1}{2}U^D\right) I^{pp}_{cc|qc}(\Pi)_{(\sigma\bar{\sigma}|\sigma\bar{\sigma})(kk|mm)} \left(b^P(\Pi)\right)_{(\sigma\bar{\sigma})(mj)} \\
&+ \left(\frac{1}{2}U + a^{P}_{(\sigma\bar{\sigma})(ik)}(\Pi) + \frac{1}{2}U^X + \frac{1}{2}U^D\right) I^{pp}_{cc|cq}(\Pi)_{(\sigma\bar{\sigma}|\sigma\bar{\sigma})(kk|mm)} \left(b^P(\Pi)\right)_{(\sigma\bar{\sigma})(mj)} \\
&= \sum_{km} \Big[\left(\tfrac{1}{2}U_i\delta_{ik} + a^P(\Pi)^{(\sigma\bar{\sigma})}_{(ik)} + \tfrac{1}{2}U^{X\,(\sigma\bar{\sigma})}_{(ik)}\right) \left(I^{pp}_{cc|cc}(\Pi)^{(\sigma\bar{\sigma}|\sigma\bar{\sigma})}_{(kk|mm)} + I^{pp}_{qq|cc}(\Pi)^{(\sigma\bar{\sigma}|\sigma\bar{\sigma})}_{(kk|mm)} + I^{pp}_{cc|qq}(\Pi)^{(\sigma\bar{\sigma}|\sigma\bar{\sigma})}_{(kk|mm)}\right) \\
&\times \left(\tfrac{1}{2}U_j\delta_{jm} + a^{P*}(\Pi)^{(\sigma\bar{\sigma})}_{(jm)} + \tfrac{1}{2}U^{X\,(\sigma\bar{\sigma})}_{(jm)}\right) \\
&+ b^P(\Pi)^{(\sigma\bar{\sigma})}_{(ik)} \left(I^{pp}_{qc|cc}(\Pi)^{(\sigma\bar{\sigma}|\sigma\bar{\sigma})}_{(kk|mm)} + I^{pp}_{cq|cc}(\Pi)^{(\sigma\bar{\sigma}|\sigma\bar{\sigma})}_{(kk|mm)}\right) \left(\tfrac{1}{2}U_j\delta_{jm} + a^{P*}(\Pi)^{(\sigma\bar{\sigma})}_{(jm)} + \tfrac{1}{2}U^{X\,(\sigma\bar{\sigma})}_{(jm)}\right) \\
&+ \left(\tfrac{1}{2}U_i\delta_{ik} + a^P(\Pi)^{(\sigma\bar{\sigma})}_{(ik)} + \tfrac{1}{2}U^{X\,(\sigma\bar{\sigma})}_{(ik)}\right) \left(I^{pp}_{cc|qc}(\Pi)^{(\sigma\bar{\sigma}|\sigma\bar{\sigma})}_{(kk|mm)} + I^{pp}_{cc|cq}(\Pi)^{(\sigma\bar{\sigma}|\sigma\bar{\sigma})}_{(kk|mm)}\right) b^P(\Pi)^{(\sigma\bar{\sigma})}_{(mj)}\Big],
\end{aligned}
\tag{10.12}
$$

which is just Eq. (4.40d).

Acknowledgements

It is my great pleasure to extend warm thanks to my supervisor, Prof. Jan von Delft. I greatly appreciate his faith in his students' abilities, as well as his tenuous strive for detailed understanding. His continous drive and remarkable work ethic have been an astounding example.

Furthermore, I would like to thank my predecessors in the "business" of the 0.7-anomaly, Florian Bauer and Jan Heyder, for the great work and understanding they have bequeathed upon me. This work would have been impossible without their previous insights. I would also like to thank their collaborators Olga Goulko and Stefan Ludwig, for providing further input. Lukas Weidinger deserves special thanks for putting up with me and my code and his effort to continue to grow the Keldysh-fRG code. Discussions with all of these people have continously brought new understanding to me.

I sincerely thank Oleg Yevtushenko and Alexei Tsvelik for their work on the Kondo chain. While I am astounded by Alexei's ability to generate ideas, Oleg's fundamental understanding and clear, precise procedures have been a great help.

I extend my thanks to the members of the chairs von Delft, Schollwöck, and Hofmann for the great working atmosphere and for the many interesting discussion I have had with them throughout my Ph.D. Even if most of the discussions were not related to my project, I gained many physical insights from them. It is my pleasure to in particular thank Fabian Kugler, Hong-Hao Tu, Lode Pollet, Claudius Hubig, Cora Uhlemann, Michael Kopp, and Stefan Hofmann for putting up with my questions and providing answers.

Finally, I sincerely thank my parents, Gudrun and Jim, for their staunch support and unyielding faith in me. I would like to thank my extended family members (in particular including my godmother Uschi and uncle Volker) for providing moral support and some amount of entertainment.